Post-Tensioned Bridge Girder Anchorage Zone Enhancement with Fiber Reinforced Concrete (FRC)

Final Report

Submitted to

The Florida Department of Transportation
(FDOT Contract No. BDB14)

By

Kamal Tawfiq, Ph.D., P.E.
Brenda Robinson, Ph.D., P.E., C.G.C.

April 29, 2008

DISCLAIMER

The opinions, findings and conclusions expressed in this publication are those of the authors and do not necessarily reflects those of the State of Florida Department of Transportation

SI (MODERN METRIC) CONVERSION FACTORS

APPROXIMATE CONVERSIONS TO SI UNITS

SYMBOL	WHEN YOU KNOW	MULTIPLY BY	TO FIND	SYMBOL
LENGTH				
in	inches	25.4	millimeters	mm
ft	feet	0.305	meters	m
yd	yards	0.914	meters	m
mi	miles	1.61	kilometers	km

SYMBOL	WHEN YOU KNOW	MULTIPLY BY	TO FIND	SYMBOL
AREA				
in^2	square inches	645.2	square millimeters	mm^2
ft^2	square feet	0.093	square meters	m^2
yd^2	square yard	0.836	square meters	m^2
ac	acres	0.405	hectares	ha
mi^2	square miles	2.59	square kilometers	km^2

SYMBOL	WHEN YOU KNOW	MULTIPLY BY	TO FIND	SYMBOL
VOLUME				
fl oz	fluid ounces	29.57	milliliters	mL
gal	gallons	3.785	liters	L
ft^3	cubic feet	0.028	cubic meters	m^3
yd^3	cubic yards	0.765	cubic meters	m^3
NOTE: volumes greater than 1000 L shall be shown in m^3				

SYMBOL	WHEN YOU KNOW	MULTIPLY BY	TO FIND	SYMBOL
MASS				
oz	ounces	28.35	grams	g
lb	pounds	0.454	kilograms	kg
T	short tons (2000 lb)	0.907	megagrams (or "metric ton")	Mg (or "t")

SYMBOL	WHEN YOU KNOW	MULTIPLY BY	TO FIND	SYMBOL
TEMPERATURE (exact degrees)				
°F	Fahrenheit	5 (F-32)/9 or (F-32)/1.8	Celsius	°C

SYMBOL	WHEN YOU KNOW	MULTIPLY BY	TO FIND	SYMBOL
ILLUMINATION				
fc	foot-candles	10.76	lux	lx
fl	foot-Lamberts	3.426	$candela/m^2$	cd/m^2

SYMBOL	WHEN YOU KNOW	MULTIPLY BY	TO FIND	SYMBOL
FORCE and PRESSURE or STRESS				
lbf	poundforce	4.45	newtons	N
lbf/in^2	poundforce per square inch	6.89	kilopascals	kPa

APPROXIMATE CONVERSIONS TO SI UNITS

SYMBOL	WHEN YOU KNOW	MULTIPLY BY	TO FIND	SYMBOL
LENGTH				
mm	millimeters	0.039	inches	in
m	meters	3.28	feet	ft
m	meters	1.09	yards	yd

SYMBOL	WHEN YOU KNOW	MULTIPLY BY	TO FIND	SYMBOL
AREA				
mm^2	square millimeters	0.0016	square inches	in^2
m^2	square meters	10.764	square feet	ft^2
m^2	square meters	1.195	square yards	yd^2
ha	hectares	2.47	acres	ac

SYMBOL	WHEN YOU KNOW	MULTIPLY BY	TO FIND	SYMBOL
VOLUME				
mL	milliliters	0.034	fluid ounces	fl oz
L	liters	0.264	gallons	gal
m^3	cubic meters	35.314	cubic feet	ft^3
m^3	cubic meters	1.307	cubic yards	yd^3

SYMBOL	WHEN YOU KNOW	MULTIPLY BY	TO FIND	SYMBOL
MASS				
g	grams	0.035	ounces	oz
kg	kilograms	2.202	pounds	lb
Mg (or "t")	megagrams (or "metric ton")	1.103	short tons (2000 lb)	T

SYMBOL	WHEN YOU KNOW	MULTIPLY BY	TO FIND	SYMBOL
TEMPERATURE (exact degrees)				
°C	Celsius	1.8C+32	Fahrenheit	°F

SYMBOL	WHEN YOU KNOW	MULTIPLY BY	TO FIND	SYMBOL
ILLUMINATION				
lx	lx	lx	lx	lx
cd/m^2	cd/m^2	cd/m^2	cd/m^2	cd/m^2

SYMBOL	WHEN YOU KNOW	MULTIPLY BY	TO FIND	SYMBOL
FORCE and PRESSURE or STRESS				
N	newtons	0.225	pound force	lbf
kPa	kilopascals	0.145	pound force per square inch	lbf/in^2

*SI is the symbol for the International System of Units. Appropriate rounding should be made to comply with Section 4 of ASTM E380.

Technical Report Documentation Page

1- Report	2- Government Accession No.	3- Recipients Catalog No.
4- Title and Subtitle Post-Tensioned Bridge Girder Anchorage Zone Enhancement with Fiber Reinforced Concrete (FRC)		5- Report Date June 2, 2008 6- Performing Organization Code
7- Author's Kamal Tawfiq, and Brenda Robinson		8- Performing organization Report No.
9- Performing Organization Name and Address Florida A & M University Department of Civil and Environmental Engineering FAMU-FSU College of Engineering 2525 Pottsdamer Street Tallahassee, Florida 32312		10- Work Unit (TRAIS) 11-Contract or Grant No BDB14
12- Sponsoring Agency Name and Address Florida Department of Transportation 605 Suwannee Street Tallahassee, FL 32399-0450		13 Type of Contract and Period Covered Draft Final (August 2004-March 2008) 14 Sponsoring Agency Code

15. Supplementary Notes
Prepared in cooperation with the U.S. Department of Transportation

16. Abstract

The main objective of this research was to investigate the use of steel fiber reinforced concrete (SFRC) in post-tensioning (PT) anchorage zones of bridge girders. The purpose of using SFRC is to enhance the overall performance and to reduce the amount of steel rebar required in the anchorage zone. Reducing steel congestion in post-tensioning anchorage zones can improve the constructability of post-tensioned bridge elements. It was the intent of this investigation of the post-tensioning anchorage zone to consider both the behavior of the local zone and the general zone when steel fiber reinforced concrete is used. To achieve the objectives of this study, both experimental and analytical investigations were conducted aiming at reducing the amount of mild steel reinforcement required by the AASHTO code at the anchorage zone. The experimental part of the study involved laboratory testing of twenty-seven (27) samples representing typical anchorage zone dimensions in post-tensioned girders. The analytical study was conducted using non-linear finite element analysis in order to have a comprehensive stress analysis of the anchorage zones with and without fiber reinforcement and mild steel.

Comparison of experimental and analytical results showed that the addition of steel fibers could enhance the performance of post-tensioned anchorage zones and reduce the bursting and confinement mild reinforcement required in these zones. For anchorage specimens with b/h equals to 0.22 and 0.33, it was found that the addition of 0.5 percent steel fibers by volume was enough to decrease the mild steel reinforcement by 40 percent or more. Results from this investigation suggested that the addition of steel fibers to concrete post-tensioned anchorage zones may save labor cost and time but may not significantly change the overall project costs.

17. Key Words:	18. Distribution Statement		
post-tensioning, steel fiber, anchorage zone, prestress	No restriction. This report is available to the public through the National Technical Information Service, Springfield, VA 22161		
19. Security Classf. (of this report) Unclassified	20. Security Classf (of this page) Unclassified	21. No of Pages 251	22. Price

ACKNOWLEDGEMENTS

The research reported here was sponsored by the Florida Department of Transportation. Sincere thanks are due to Marc Ansley P.E., the State Structural Engineer, for his guidance, support, and encouragement. Special thanks to Dr. Nur Yazdani for initiating this research project. Thanks to the structural laboratory staff for helping in conducting the laboratory testing on the block samples.

EXECUTIVE SUMMARY

The main objective of this research was to investigate the use of steel fiber reinforced concrete (SFRC) in post-tensioning (PT) anchorage zones of bridge girders. The purpose of using SFRC is to enhance the overall performance and to reduce the amount of steel rebar required in the anchorage zone. Reducing steel congestion in post-tensioning anchorage zones can improve the constructability of post-tensioned bridge elements. It was the intent of this investigation of the post-tensioning anchorage zone to consider both the behavior of the local zone and the general zone when steel fiber reinforced concrete is used. To achieve the objectives of this study, both experimental and analytical investigations were conducted aimed at reducing the amount of mild steel reinforcement required by the AASHTO code in anchorage zone. The experimental part of the study involved laboratory testing of twenty-seven (27) specimens representing typical anchorage zone dimensions in post-tensioned girders. The analytical study was conducted using non-linear finite element analysis in order to have a comprehensive stress analysis of the anchorage zones with and without fiber reinforcement and mild steel.

Comparison of experimental and analytical results showed that the addition of steel fibers could enhance the performance of post-tensioned anchorage zones and reduce the bursting and confinement mild reinforcement required in these zones. For anchorage specimens with plate width/block width (b/h) ratios equal to 0.22 and 0.33, it was found that the addition of 0.5 percent steel fibers by volume was enough to decrease the mild steel reinforcement by 40 percent

or more. Results from this investigation suggested that the addition of steel fibers to concrete post-tensioned anchorage zones may save labor and time but may not significantly change the overall project costs.

This final report presents the work performed for the "Post-Tensioned Bridge Girder Anchorage Zone Enhancement with Fiber Reinforced Concrete (FRC)" Project from January, 2005 to December, 2007. All research tasks have been completed for the project and are discussed in chapters of this report as shown below.

Task 1: Background Information (Chapters 1 and 2)

Task 2: Test Matrix Set-Up (Chapter 3)

Task 3: Procurement of Materials (Chapters 4)

Task 4: Post-Tensioned Anchorage Zone Testing (Chapter 5)

Task 5: Theoretical Modeling (Chapter 4 and 6)

Task 6: Analysis of Results (Chapters 4, 5 and 6)

Task 7: Cost Comparison (Chapter 6)

Task 8: Recommendations to FDOT (Chapter 7)

TABLE OF CONTENTS

TABLE OF FIGURES

TABLE OF TABLES

CHAPTER 1

INTRODUCTION

1.1 Post-Tensioned Concrete

In reinforced concrete and prestressed concrete, steel reinforcement is used to resist the tensile forces and stresses in the concrete. In prestressed concrete, compression is introduced in concrete elements to increase load capacity and improve behavior. The beneficial effects of prestressing have lead to the development of long span structures, especially long span bridge structures.

There are two methods for prestressing concrete: pre-tensioning and post-tensioning. In pre-tensioning, prestressing steel (either rods or strands) are stressed (stretched), held in place, bonded to concrete which is cast after the steel is stressed, and released after the concrete reaches a specified strength. When the prestressing steel is released, compressive force is applied to the concrete. Typically, as long as the concrete strength is strong enough to withstand the compressive stresses that develop when the load is applied, pre-tensioning increases the tensile capacity of the structural member.

Fueled by the desire to erect bridges with longer clear spans and smaller cross-sections, engineers introduced design and construction innovations such as segmental box girder bridge

construction. In segmental box girder bridge construction, post-tensioning is used to connect individual bridge segments together to create bridge spans. In post-tensioning, concrete elements (i.e. bridge segments) are cast with embedded post-tensioning anchorage devices. When the segments are assembled, prestressing steel (most commonly steel strands) are threaded through the anchors and ducts, stressed and locked in place. As a result, large compressive forces are introduced in the bridge segments at and near the anchors. Figure 1-1 shows a drawing of a typical box girder bridge span which shows the post-tensioning tendons, duct and anchors. Figure 1-2. shows segmental box girder segments that are being erected by the balanced cantilever method. Visible in this figure are shear keys, ducts holes and deviation blocks which are some of the typical features of segmental box girders.

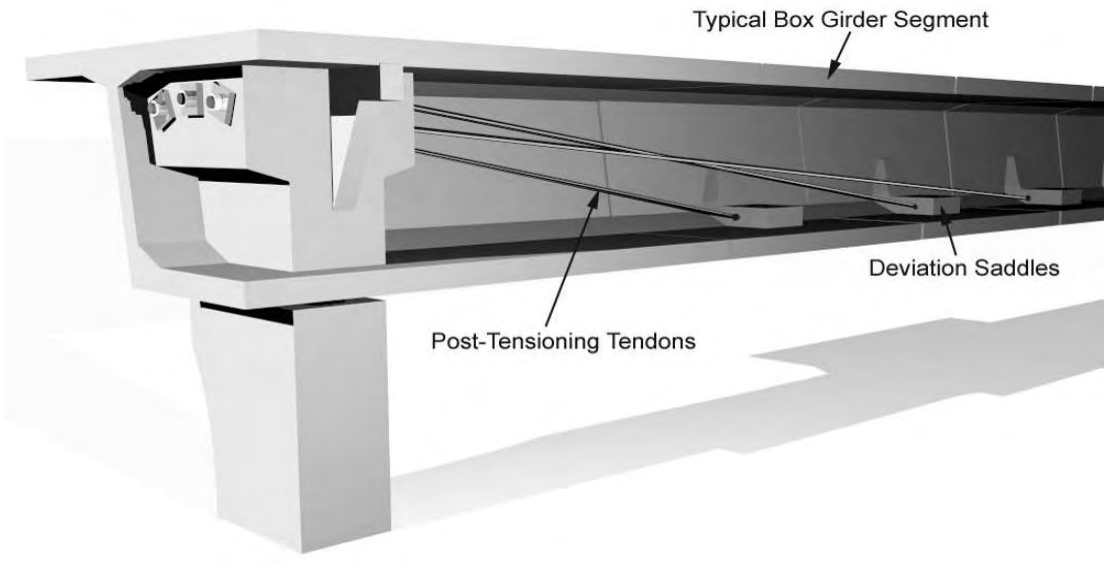

Figure 1-1: Segmental Box Girder Bridge

Figure 1-2: Segmental Box Girders

1.2 Anchorage Zone Details

Post-tensioning tendons transmit high compressive forces to concrete sections. Figure 1-3 shows stress paths that develop as a result of the post-tensioning force. As shown in Figure 1-3a, the concentrated post-tensioning force at the surface becomes nearly equivalent to a linearly distributed force along the members cross-section at a distance away from the load surface. The distance through which this load transformation takes place is called the "anchorage zone". In the 2007 LRFD Bridge Design Specifications, the American Association of State Highway Officials (AASHTO) considers the post-tensioned anchorage zone as two regions: the local zone and the general zone (AASHTO, 2007). According to AASHTO the local zone is in the immediate vicinity of the anchorage device.

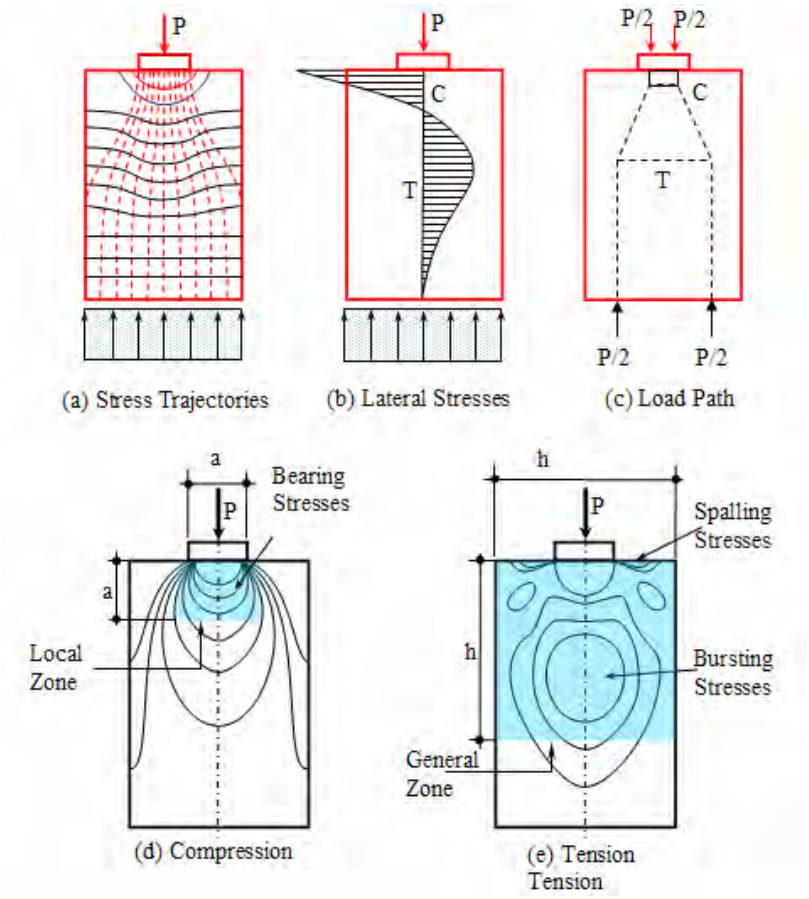

Figure 1-3: Stress distribution at the anchorage zone

The general zone is the area where the tensile stresses develop due to the spreading of the tensile force. For end anchorage zones, the transverse dimensions of the general zone may be taken as the length and width of the segment (or component) but not larger than the longitudinal dimension of the segment (or component). The length of the general zone shall be one to one and one half (1 to 1.5) times the greater of the transverse dimensions (AASHTO, 2007).

The lateral stress distribution which occurs in the anchorage zone is shown in Figure 1.3b. As shown, compressive lateral stresses develop in the vicinity of the anchor bearing plate. At a distance away from the anchor, lateral tensile stresses develop. These tensile stresses are

referred to as “bursting stresses”. Reinforcement must be provided to resist the bursting tensile stresses. Principal compressive and tensile stress contours for a post-tensioning anchorage zone are shown in Figure 1-3d and Figure 1-3e, respectively. Three critical stress regions which develop are shown in Figure 1-3d and Figure 1-3e. These are the locations of high bearing stresses, spalling stresses and bursting stresses.

The anchorage supplier is responsible for providing anchorage devices and information which complies with AASHTO requirements. The Engineer of Record is responsible for the overall design of the post-tensioning anchorage zone, both the general zone and the local zone. This responsibility includes the location of the tendons and anchorage devices, the reinforcement in the anchorage zone and the tendon stressing sequence. To provide adequate resistance for the large compressive forces at the anchors and the large tensile forces that develop at a distance ahead of the anchors, the post-tensioned anchorage zone must be properly designed and detailed.

1.3 Anchorage Zone Reinforcement

If the concrete dimensions are large enough surrounding the anchorage device, adequate confinement may be provided by the concrete. However, anchorage device suppliers typically provide spiral reinforcement in the local zone to provide the required confinement for high compressive stresses. Figure 1-4 is a cross-section of a bridge box girder segment that shows an example of a post-tensioning anchorage device (a VSL EC5-19 anchor) and some of the required steel reinforcement, including the spiral reinforcement in the vicinity of the anchor.

The AASHTO code list three methods that may be used to design the general zone: 1. strut-and-tie models, 2. refined elastic stress analyses, and 3. other approximate methods. Figure 1-3c, shows a simplified load path and force mechanism that may be used in a strut-and-tie model to design for the forces that develop in the anchorage zone. For approximate stress analysis and design, the AASHTO code provides equations for estimating compressive stresses, bursting forces and edge tension forces for members that satisfy certain geometric and other conditions.

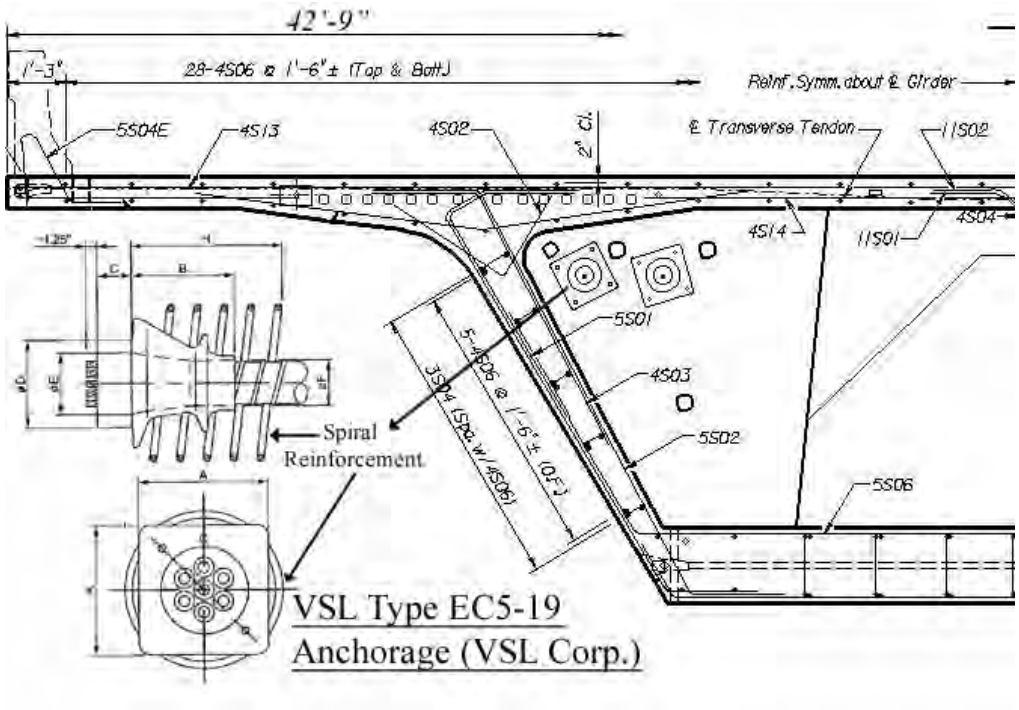

Figure 1-4: Example of a Special Anchorage Device (VSL Corp)

The approximate method equation for computing the bursting force takes into consideration the factored tendon force (P_u), the lateral dimension of the anchorage device (a), the lateral dimension of the cross section (h), and the inclination of the tendon force (a). When there is a single, straight, concentric tendon, the equation for the bursting force (T_{burst}) simplifies to the following:

$$T_{burst} = 0.25\ P_u\ (1- a/h) \qquad 1\text{-}1$$

It is the Engineer of Record's responsibility to design bursting reinforcement to resist the computed bursting force. Using a reinforcement allowable stress, f_s, and a bursting force, T_{burst}, the required area of steel, A_s, would be computed as follows:

$$A_s = T_{burst} / f_s \qquad 1\text{-}2$$

The AASHTO code requires that the bursting steel be distributed such that the distance from the centroid of the bursting force is equal to d_{burst}. When there is a single, straight, concentric tendon, d_{burst} is computed by the following equation:

$$d_{burst} = 0.5h \qquad 1\text{-}3$$

1.4 Problems with Anchorage Zones in Bridges

If the post-tensioned anchorage zone is not properly detailed and designed to withstand the forces and stresses which develop, failure of the anchorage zone can occur. If there is inadequate confinement reinforcement in the local zone (the vicinity immediately surrounding the anchorage device) cracking, crushing and spalling of concrete may occur. To prevent failure in the anchorage zone, non-prestressed (or mild steel) is used to resist the tensile stresses. Due to the large forces active in the anchorage zones much mild steel is required. Steel congestion in the area may lead to problems related to poor concrete consolidation.

1.5 Fiber Reinforced Concrete

Concrete is a material that is prone to cracking. Research has shown that adding fibers (steel or polymer fibers) helps to delay the development of cracks and to reduce the size of cracks that do develop (Khajuria et al, 1991). Since the 1960's steel fibers have been used in many construction applications including in shotcrete, precast concrete, concrete slabs, concrete floors and other applications (Vondran, 1991). Some of the beneficial effects of using fibers in concrete are enhancing tensile behavior; improving post crack resistance; increasing development/splice strength of reinforcement; increasing first-crack flexural strength and the post-cracking flexural stiffness; reducing instantaneous and long term deflections; restraining the creep of cement matrixes under axial compression; improving creep properties; reducing shrinkage of cement matrices; and reducing basic creep, shrinkage and total deformation (Tan et al, 1994).

1.6 Objectives of the Study

The main objective of this research was to investigate the use of steel fiber reinforced concrete (SFRC) in post-tensioning (PT) anchorage zones of bridge girders. The purpose of using SFRC is to enhance the overall performance and to reduce the amount of steel rebar required in the anchorage zone. Reducing steel congestion in post-tensioning anchorage zones can improve the constructability of post-tensioned bridge elements. Results from an investigation by Haroon (2003) showed that the use of SFRC improved the local zone capacity and provided a reduction in secondary mild reinforcement.

It was the intent of this study to consider both the behavior of the local zone and the general zone when steel fiber reinforced concrete is used. Also, It was desirable to implement a test program that considered material stress levels that are similar to those typically found in post-tensioned bridge members (such as concrete post-tensioned segmental box girders). To achieve the objectives of this study, both experimental and analytical investigations were conducted aiming at reducing the amount of mild steel reinforcement required by the AASHTO code at the anchorage zone. The experimental part of the study involved laboratory testing of twenty-seven (27) samples representing typical anchorage zone dimensions in post-tensioned girders. The analytical study was conducted using non-linear finite element analysis in order to have a comprehensive stress analysis of the anchorage zones with and without fiber reinforcement and mild steel reinforcement.

Inherent in the objective is the determination of the proper ratio of steel fibers that can be used without jeopardizing the constructability of the anchor zone. Meeting the objective of this study resulted in the development of a rational method to analyze and design the local and general zones reinforced with steel fibers.

CHAPTER 2

LITERATURE REVIEW AND RESEARCH METHODS

Sanders (1990), Stone (1983) and Haroon (2006), reported that failures of the anchorage zones of precast prestressed concrete girders are brittle in nature. This is the case even when failure is due to yielding of reinforcing steel. Thus, failure of the post-tensioned anchorage zone should be avoided. A well designed anchorage zone should safely transfer the tendon forces developed at ultimate loads such that if a failure occurs in the structures, it is a ductile failure away form the anchorage zone.

Haroon (2003) reported that, according to Breen et al (1994), cracking rather than complete failure occurs more frequently in the anchorage zone. Haroon suggests two reasons for this frequent occurrence; (1) the anchorage zone is inherently tough, and (2) when anchorage zone fails during construction, the anchorage zone is most likely repaired and not reported as a failure.

To resist tensile forces, a large volume of spiral and other reinforcement may be required at the end zones of a prestressed bridge girder. Reinforcement congestion in the anchorage zone may be a cause of poor concrete consolidation, resulting in failures caused by crushing of the concrete ahead of the anchor (Libby, 1976). As the volume of steel increases in the zone, the difficulty of placing the steel increases also. In addition, reinforcement components (i.e. anchorage devices and ducts) used in close proximity cause congestion in the anchorage zone. As a result, it

becomes difficult to place concrete, anchorages and post-tensioning ducts in the zone. It is labor intensive to produce and place secondary anchorage reinforcement. Fiber reinforced concrete (FRC) possesses better properties, such as tension, compression, shear, bond, flexural toughness and ductility than conventional concrete. Therefore, it may be possible to utilize FRC in the end zones of prestressed and post-tensioned bridge girders to reduce the amount of secondary reinforcement.

2.1 Fiber Reinforced Concrete

Fibers added to concrete could be metallic, polymeric or natural. The metallic fibers have high modulus and high strength. Their behavior is ductile. Polymeric fibers are strong and ductile but their modulus is relatively lower than cement composite. Therefore, the addition of polymeric fibers does not change modulus of elasticity, flexural strength, and compressive strength of concrete (Berke and Dallaire, 1994).

Fibers in concrete serve mainly three functions: 1) to increase toughness of the composite by providing energy absorption mechanism related to de-bonding and pull-out processes of the fiber bridging the cracks, 2) to increase ductility of the composite by permitting multiple cracking, 3) to increase strength of the composite by transferring stresses and loads across cracks. For fiber reinforced cementitious composites, load-deflection curves provide information concerning the effect of the fibers on the toughness of the composite and its crack control potential. The area under the load-deflection curve represents energy-absorbing capacity. The addition of steel fibers to concrete improves impact strength, toughness, flexural strength, fatigue strength, crack resistance and spall resistance (ACI, 2002).

Swamy and Al-Ta'an (1982) conducted research to determine the influence of fiber reinforcement on the deformation characteristics and ultimate strength in flexure of concrete beams. They tested fifteen (15) reinforced concrete beams. The test parameters included the fiber content by volume (0.0%, 0.5%, 1.0%) and the use of low carbon crimped steel fibers either throughout the beam depth or in the effective tension zone only. The researchers concluded that: (1) steel fibers are effective in resisting deformation at all stages of loading; (2) steel fibers inhibit crack growth and crack widening; (3) steel fiber reinforced beams showed significant inelastic deformation and ductility at failure; and (4) steel fibers have limited effect in increasing flexural strength of reinforced beams**.**

Bohra and Belaguru (1991) investigated the long term durability of nylon, polypropylene and polyester fibers in concrete. Specimens with 0.5% fibers (by volume) were stored in lime saturated water maintained at 50^{o} deg. C. Addition of fibers to the concrete mix resulted in reduction in slump. In addition, fibers contributed to approximately a 10% reduction in compressive strength. However, test results indicated that "all three fibers provided post-crack resistance." By measuring flexural toughness, the researches found that nylon and polypropylene fibers are durable in concrete. "Specimens with polyester fibers had lower indices after accelerated aging."

Vondran (1991) reported that steel fibers can have up to twice the modulus of rupture, shear strength, torsional strength, and fatigue endurance; up to 1.4 times the abrasion and erosion resistance; and up to 5 times the impact energy absorption of plain concrete. He also stated that

steel fibers make concrete tougher and more ductile and decrease permeability due to cracking by preventing microcracks from becoming working cracks.

Shaaban and Gesund (1993) investigated whether consolidation by rodding or vibrating influenced the compressive strength and split tensile strength of 6”x12” concrete cylinders containing steel fibers. Acknowledging the sample size was relatively small, the authors concluded that: 1. “SFRC cylinders tested in compression have essentially the same strength, whether consolidated by rodding or external vibration.” 2. “Split tensile tests for tensile strength show significant increases in tensile strength with the addition of steel fibers, and considerably more strength gain for vibrated specimens than for rodded specimens.” The authors state, “It also appeared that external vibration produced a more uniform distribution of fibers and fiber orientations.”

Chaallal et al (1996) conducted a study to compare the performance of steel fiber reinforced concrete (SFRC) wall/coupling beam joints under cyclic loading with the performance of conventional reinforced concrete (CRC) joints. The results of the research showed that the SFRC joint with reduced transverse reinforcement (hoops) performed relatively well. In particular, the researchers found that the SFRC specimens 1) dissipated 31 percent more energy than the CRC specimens, 2) improved bond and anchorage of reinforcement, 3) developed more closely spaced cracks, and 4) showed minimum spalling. The authors concluded that “the use of SFRC in seismic regions to enhance structural integrity and to ease steel congestion in plastic hinge regions is potentially viable.”

In 1996, the South Dakota (SD) Department of Transportation (DOT), the 3M Company, the Federal Highway Administration and other entities sponsored an open house in Pierre, South Dakota to introduce polyolefin fibers to transportation agencies, consultants, concrete suppliers and academicians. At dosage rates of up to 2% by volume, the addition of polyolefin fibers (2" long, 0.025" plastic fibers) to concrete was reported to increase concrete ductility, toughness and resistance to shrinkage and cracking. The South Dakota DOT had used polyolefin fibers in bridge deck overlays, bridge barriers, concrete paving and bridge deck replacement with good results.

Harajili and Salloukh (1997) investigated the effect of fibers on the development/splice strength of reinforcing bars. Using fifteen (15) beam specimens cast without transverse reinforcement in the constant moment region, differing amounts of tensile reinforcement and fibers (steel and polypropylene), the researcher tested the beams in flexure. There were six (6) major conclusions from the research: 1. "Hooked steel fibers considerably increases the development/splice strength of reinforcing bars in tension"; 2. Steel fibers are more effective in increasing development/splice strength than transverse reinforcement; 3. Using hooked bars results in more cracks around spliced bars, less growth of splitting cracks, substantial improvement in the ductility of bond failure; 4. Polypropylene fibers at 0.6% by volume improved the ductility of bond failure but were not as effective as steel fibers; 5. The bond strength ratio increases as the volume fraction of fibers increases, and 6. "Bond tests conducted using pullout specimens largely underestimate the effect of fibers on the splitting bond resistance of reinforcing bars in tension."

Bayasi, Gebham and Hill (2004) conducted research on reinforced concrete seismic beam-column joints. After testing six (6) beam-column joints, the researcher concluded that "addition of steel fibers to reinforced concrete seismic beam-column joints improves strength, ductility and toughness of joints. By using steel fibers, hoop spacing in the joint can be relaxed as steel fibers will have an effect similar to that of reinforcing steel." According to the recommendation, for exterior beam-column joints, steel fibers at a volume fraction of 2% can be used with a code hoop spacing increased by a factor of 2. For high seismic risk areas, it was recommended that in a SFRC joint, the hoop spacing could be increased by a factor of 1.5. In summarizing literature on beam-column joints published by other researchers from 1974 to 1992, the authors noted that the consistent findings were that joints reinforced with steel fibers had higher ultimate moment capacity, increased ductility, increased cumulative energy dissipation, improved ultimate rotation capacity, improved stiffness, less spalling, better confinement, better crack control, higher shear strength, increased tensile strength and increased bearing strength (Bayasi et al, 2004).

Tan et al (1994) investigated instantaneous and long-term deflection of steel fiber reinforced concrete beams. A total of fourteen (14) beams were tested: four to failure under third point loading and nine (9) under long term creep tests. Fiber content was varied from 0.55 to 2.0%. Two of the conclusions from the research were: "1. The inclusion of steel fibers was found to result in an increase in first-crack flexural strength and post-cracking flexural stiffness of reinforced concrete beams. 2. Both the instantaneous and long-term deflections of SFRC beams were smaller than comparable plain concrete beams."

2.2 Fiber Reinforcement in Prestressed Concrete

Wafa (1992) tested 18 axially prestressed and non-prestressed concrete beams subjected to torsion. The variables included prestressing levels and fiber volumes (0.0% to 2.0%). The researcher concluded that in torsion, "beams without fibers have practically no ductility and failure is sudden and violent. Addition of fiber beyond 1 percent [1%] increases ductility and torsional strength". However, for fiber volumes less than 1%, "there is practically no increase in the torsional strength".

Junior and Hanai (1999) tested nine (9) concrete beams to investigate the influence of steel and polypropylene fibers on shear performance of thin-walled I-beams with reduced shear reinforcement. Variables for the beams included prestressing, no prestressing, shear reinforcement ratios, amount and type of fibers. The authors found that fiber reinforcement contributed to more effective crack control and smaller deflections. For beams with stirrups, the presence of fibers resulted in increased shear strength after first cracking and decreased deflection. However, these beneficial effects did not occur in beams without stirrups. According to the authors, increases in strength in the fiber reinforced beams varied from 13% to 19%. One conclusion reached by the authors is that "the contributions of fibers can be considered equivalent to a fraction of the shear reinforcement" … which "confirms the possibility of an advantageous partial substitution of stirrups for fibers."

The authors made reference to ACI Committee 544 and work by Shah and Ouyang. Junior and Hanai stated, "The use of short fibers in concrete offers noticeable advantages such as limited cracking and increases toughness. It can also increase shear strength, allowing reduction of

stirrup reinforcement, and improved ductility and safety." Two of the main conclusions from the research related to fiber reinforcement were as follows: 1. "The addition of fibers does not increase the compressive strength of concrete, but it can increase tensile strength in some cases. The modulus of elasticity of concrete can be altered with the introduction of fibers"; 2. "Fiber effectiveness is higher in beams with stirrups. In all the fiber reinforced beams failure was more ductile and there was increased strength, always between 8 and 10 kN. The fibers can be considered as equivalent shear reinforcement. In this aspect, the advantages provided by steel and polypropylene fibers were similar, but the strain in the stirrups in steel fibers beams was smaller."

2.3 Post-Tensioned Anchorage Zones

The development of post-tensioning as one method of prestressing concrete occurred after 1923. Franz Dischinger designed the first prestressed concrete bridge which was built in Aue, Germany in 1937 (Hengprathanee, 2004). After the bridge at Aue was constructed, the Dywidag post-tensioning system was invented by Ulrich Finsterwalder in the 1940's (Hengprathanee, (2004). Since the 1940's, post-tensioning has been used in concrete bridges. The first use of post-tensioned concrete in the United States was in the Walnut Bridge which was constructed in Philadelphia in 1950 (Podolny and Muller, 1982). The Walnut Lane Bridge was a cast-in-place, post-tensioned bridge.

Concrete structural members are prestressed to increase their load carrying ability and improve their behavior under loading. Post-tensioning is one of two methods (pre-tensioning and post-tensioning) for prestressing concrete structural elements. In post-tensioning anchorage zones

high stresses develop due to the transfer of prestressing force through bearing plates and anchors. To prevent these stresses from causing splitting, bursting and cracking of the concrete in the anchorage zone, adequate detailing is required. This detailing includes provision of sufficient concrete volume and reinforcing steel in the high stress region. Design specifications, anchorage devices, and design experience are all important for successfully designing and detailing of anchorage zones.

In 1956, Huang wrote the following: "Although, the post-tensioning method for prestressing concrete structural members has been used by engineers for thirty years, literature concerning the end block stresses has been remarkably scarce. In 1946, Professor Mangel made probably the first publication dealing with the problem."

If Huang's statement is accurate, then the design and behavior of post-tensioning anchorage zones have been an area of concern for over 60 years. While some design guidance was provided by researchers such as Guyon, Morsch and Leonhardt, codified design procedures were lacking for a long period of time. The Post-Tensioning Institute first published its *Post-Tensioning Manual* in 1972. The American Association of State Transportation Officials (AASHTO) did not include post-tensioning anchorage design guidelines in its bridge design specifications until 1994 (Roberts-Wollman and Breen, 2000). This specification resulted from research conducted by Breen et al (1994) at the University of Texas at Austin.

Huang noted that although the end block (anchorage zone) problem was a three dimensional problem most of the existing methods for analyzing the end blocks treated the problem as two

dimensional by neglecting forces in the vertical direction. These often neglected forces included the beam support reaction, the dead and live load applied over the anchor block, the weight of the end block, and the vertical force of an inclined cable. In his investigation, Huang sought to consider the "actual" distribution of stresses in the end block by using experimental and analytical methods (Huang, 1956).

To complete his study, Huang instrumented and tested one post-tensioned beam and completed a two-dimensional numerical analysis. The test beam was modeled based upon a beam with a fifty (50) foot span. To represent the two end zones, a 9'-6" beam was instrumented, post-tensioned and loaded. The concrete compressive strength, f'c, of the beam was 6000 psi. Even though Huang's study was limited and problems developed with some of the strain gages, he noted that the existing methods for designing the end block gave "quite different" results from his experimental and analytical results. He compared his results to design methods proposed by Guyon, Mandel and others. Huang made four (4) conclusions: 1. For the end block, the optimum length-depth ratio is probably close to one; 2. To prevent failure in the end zone, vertical and horizontal reinforcement should be used for a distance of one end block length away from the load surface; 3. "The horizontal normal stress (parallel to the tendon)…may be assumed to follow a linear vertical distribution with sufficient accuracy, but laterally, its distribution is better approximated by a parabola; 4. While some of the other loads in the end zone can be neglected, "the reaction from the end support and the vertical shear at the juncture should be considered."

Saadoun (1980) completed a three dimensional photoelastic investigation of the end block. His investigation considered single and multiple anchorages, external and embedded ducts and end

blocks with and without ducts. In addition, he conducted tests on concrete end block models. Some of his conclusions were as follows:

- High sub-surface shears in the vicinity of the anchorage unit [device] initiate a punching shear type failure and the subsequent propagation of tensile cracks in a complex compression-tension stress field caused by wedging action of the concrete cone governs the failure of the end block"

- For external anchorage end blocks, the sub-surface shear stress reach a maximum value of three times the mean compression that occurs just beneath the edge of the loaded area

- All two-dimensional theoretical solutions underestimate the critical tensile stresses and forces and completely overlook the real significance of the high sub-surface shears in the immediate vicinity of the anchorage units

- The photoelastic methodology provides a realistic picture of the nature of magnitude and stress distribution and that the Poisson's ratio differential effect is small"

- Tensile zones were found in the corners of end blocks, the spalling zones and between the anchorage units

- One third of the load applied at the embedded anchorage unit was transmitted through shear tractions on the longitudinal surface of the anchorage unit. This leads to a reduction in the level of the maximum tensile stresses and forces

- The maximum transverse tensile forces for the embedded anchorage were only 65 to 70% of the corresponding values for the external anchorage units

Burdett's (1990) research included a comparison of existing codes and design guidelines for the design of anchorages zones. According to Burdett, most of the codes reviewed did not distinguish between the local and the general anchorage zones. However, the codes did limit the bearing stresses under the anchorage device and did give some estimate of the tensile bursting forces. Most formulas for bursting force that Burdett reviewed were in the form of :

$$F = K P (1 - a_1/a_2) \qquad 2.1$$

where F = the bursting force, K= a factor between 0.25 and 0.3, P = the tendon force, a_1 = the dimension of the anchorage device and, a_2 = the lateral dimension of the member. As reported by Burdett, Guyon proposed a linear approximation defined by the equation:

$$T_{burst} = 0.3P (1-a/h) \qquad 2.2$$

where P = the tension force, a= the dimension of the anchorage plate, and h= the depth of the section. In addition, Burdett noted that most of the design codes gave maximum values for the maximum tensile stress in the range of $0.5(f'_c)^{1/2}$ to $7.5(f'_c)^{1/2}$.

In addition to reviewing existing codes, Burdett conducted finite element analysis (FEA) of the anchorage zone and evaluated strut-and-tie (SNT) models of the zone. His findings included the following:

1. The bursting stresses obtained from the FEA, showed good agreement with other solutions;
2. The stress distribution was closest to the elastic solution obtained by Guyon;
3. Using a factor of 0.25 instead of 0.3 resulted in a better fit of the FEA results, but the values were smaller than the predicted values for plate sizes smaller than 0.15h;
4. Values of the spalling force obtained from the finite element analysis showed that the constant value for spalling forces equal to 4% of the applied load proposed by Guyon is conservative;
5. Stresses from the FEA are reliable and accurate;
6. The strut-and-tie Model results were in close agreement with the finite element method results.

The investigation conducted by Burdett was part of a comprehensive research program completed at the University of Texas at Austin to help improve the AASHTO specifications and provide design guidance for bridge post-tensioned anchorage zones. This research was sponsored by the Transportation Research Board's (TRB) National Cooperative Highway

Research Program. Other UTA researchers involved with this study included J. E. Breen, C. Roberts, D. Sanders and G. Wollman (Breen et al, 1994). As a result of this research program, the team proposed anchorage design specifications for AASHTO. These proposed specifications included practical design formulas for the tensile bursting force and for the location of the centroid of the tensile stresses:

$$T_{burst} = 0.25(1-a/h) + 0.5P\sin(\alpha) \qquad 2.3$$

$$d_{burst} = 0.5(h-2e) + 5\, e \sin(\alpha) \qquad 2.4$$

where P = the total factored tendon load, a= the lateral dimension of the anchorage device or group of devices, e = the eccentricity of the anchorage device or group of devices, h= the transverse dimension of the cross section, and α = the inclination of the resultant of the tendon or tendons with respect to the centerline of the member. In addition to the equations, the proposed specification, recommended the subdivision of the anchorage zone into a local zone and a general zone.

Roberts (1990) conducted research to examine acceptance test procedures for post-tensioning systems, to consider the performance of post-tensioned anchorage local zones and to propose specifications for design and construction of anchorage zones. Roberts conducted anchorage tests using several different testing procedures for acceptance of anchorage hardware. She evaluated four different testing procedures including the ones recommended by the following entities:

1. the European FIP code,

2. the Post-Tensioning Institute

3. the German DIN code and

4. the Austrian Code

As a result of load tests and evaluations of the existing codes, Roberts proposed a rectangular prism test block for the local zone. The cross-sectional dimensions of the block were to be related to the edge distance or minimum spacing of anchors (the smaller of the values) and the length of the block was to be two times the longer of the cross-sectional dimensions.

In addition, to proposing the test specimen, she proposed a procedure and criteria for acceptance. Some of her research conclusions were as follows:

1. "The primary parameters which affect the first cracking load are the tensile capacity of the concrete and the a/h ratio";
2. An increase in spiral diameter
    a) does not increase first cracking load,
    b) does not significantly decrease crack widths,
    c) does increase the ultimate load, and
    d) does increase the ultimate deformation capacity of the specimen.

In summary, Roberts states, "The behavior of the local zone is primarily a function of the A/A_b ratio, the area confined by the primary confining reinforcement, and the volumetric ratio of the reinforcing steel to the confined concrete. The interaction of these variables dictates the overall local zone behavior."

Sanders (1990) conducted a study to develop a generalized approach for the design and proper reinforcement of post-tensioned anchorage zones. He performed load tests and developed strut-and-tie model for the research. He performed experimental tests (load tests) on thirty-six (36) specimens representing different types of anchorage zones: zones with eccentric, concentric, multiple and inclined tendons. As a result of his work, he developed a modified strut-and-tie model which "more accurately represents the ultimate behavior and capacity of the anchorage zone" (Sanders ,1990). The results of his work were used to help develop the AASHTO specifications for post-tensioned anchorage zones.

Using finite element models, strut-and-tie models and experimental tests, Wollman (1992) investigated post-tensioned anchorage zones as a part of the research conducted at the University of Texas at Austin. Wollman concluded that both strut-and-tie models and finite element analysis can be safely used to design post-tensioned anchorage zones. According to Wollman, the strut-and-tie models gave conservative predictions for failure loads. Also, he concluded that the magnitude and location of bursting forces and bursting stresses are affected by the presence of reaction forces in the anchorage zones. However, the influence of the reaction forces is conservative and may be neglected for small tendon eccentricity and in the absence of flexural tensile stresses at the end of the anchorage zone (Wollman, 1992).

The Post-Tensioning Institute published a document entitled *Anchorage Zone Design* which was authored by Wollman and Robert-Wollman (2000). This publication provided post-tensioned anchorage zone design guidance and examples for design professionals.

Jo, Byun and Tae (2002) modeled the post-tensioned anchorage zone of a cable-stayed bridge. They used three-dimensional and two-dimensional finite element models to investigate the stress distribution in the anchorage zone. Study parameters included the cable inclination, the position of the anchor plate, the modeling methods and three-dimensional effects. Jo et al reported that Leonhardt provided an equation for computing the transverse tensile force, T, in 1964. The Leonhardt equation is as follows:

$$T = 0.3 \sum P (1-a/h)+0.5 \left| \sum P_u \sin \alpha \right| \qquad 2.5$$

where P = the maximum prestressing force due to post-tensioning, a=the anchor plate width, h = the member depth, P_u = the factored tendon force and α = the angle of inclination of the tendon force. As can be seen by comparison, this equation is very similar to the equation that is presented in the AASHTO design specifications for computing T_{burst}. Two of the conclusions made by Jo et al were as follows: 1. The inclination of the cable influences the stress distribution. The maximum bursting stress increases when the cable inclination angle becomes acute; 2. Since the three-dimensional analysis showed slightly less [stress] values for the anchorage [zone] than the two-dimensional analysis, for simplicity in analysis and safety in design, two-dimensional analysis can be used.

Haroon (2003) investigated the feasibility of using steel fibers to reduce the amount of steel reinforcement in post-tensioned anchorage zones. He performed material tests with concrete containing Xerox steel fibers, Dramix ZP305 steel and Harbourite H-330 synthetic fibers. For the material tests, Haroon considered fiber volume percentages of 0.5%, 0.75% and 1.0%. In

addition to the material test, Haroon performed AASHTO Special Anchorage Device Acceptance Tests for 12.5”x12.5”x25” concrete specimens cast with VSL EC 5-7 anchorages and Xerox and Dramix ZP305 steel fibers. In the test blocks Haroon used 0.75% and 1.0% fibers (by volume). Cyclic loading tests were performed on the test blocks to evaluate local anchorage zone reinforcement. Thirty-seven (37) anchorage test blocks with different amounts of spiral reinforcement, tie reinforcement and steel fiber reinforcement were tested. To help verify test results, Haroon performed a finite element analysis of the test block. As a result of his research, Haroon concluded that adding steel fibers increased the concrete 1) compressive strength, 2) tensile strength, 3) flexural first crack strength and 4) post-crack energy absorption capacity. Based upon his tests results, Haroon recommended that steel fiber reinforced concrete (SFRC) be used in the end zones of prestressed girders to reduce or eliminate secondary reinforcement (i.e. steel spirals and/or tie reinforcement). He stated, ”from the reinforcement congestion perspective, elimination of the spiral steel is more beneficial than the elimination or reduction of skin reinforcement [steel ties]”.

Hengprathanee (2004) used the DIANA finite element analysis program to conduct linear and nonlinear finite analyses of the post-tensioned anchorage zones. He considered the presence of a support reaction in the anchorage zone and post-tensioning tendons with different configurations (concentric, eccentric, inclined and inclined eccentric). In addition, he considered strut-and-tie models for design of anchorage zones. As a result of his research, Hengprathanee proposed a new approach for the design of non-rectangular anchorage zones. This new approach was based upon a modified version of the strut-and-tie model. For the reaction forces in the rectangular

anchorage zones, Hengrathanee proposed a modification to the AASHTO code equations for T_{burst} and d_{burst}.

$$T_{burst} = 0.25 \sum P_u (1-a/(h-2e))+0.4 \sum (P_u \sin \alpha) + R(0.25- 5 \sin \alpha) >= 0.125 \sum P_u \quad 2.6$$

$$d_{burst} = 0.5 (h -2e)+ 0.25a+0.25 (h-2e) \sin \alpha + (R /(\sum P_u)) (h -2e) (1.5-10 \sin \alpha) \quad 2.7$$

where T_{burst} = tensile force; P_u =factored tendon force; d_{burst} = the distance from the anchorage device to the centroid of the bursting force, T_{burst}; α = the lateral dimension of the anchorage; e= the eccentricity of the anchorage; h=the lateral dimension of the anchorage zone in the direction considered; a= the angle of inclination of the tendon force; and R= the reaction force applied at the bottom surface of the anchorage zone.

Johnson (2006) completed a finite element analysis model of a post-tensioned (PT) anchorage zone for one of the box girder anchor segments of the Mid-Bay Bridge which is located in Florida. The finite element model of the Mid-Bay Bridge segment was used to evaluate the size of PT anchorage test specimen for the experimental program and the percentage of steel fiber to use in the anchorage load test program for this study.

2.3.1 Post-Tensioning Systems

Two of the post-tensioning anchorage systems used in the United States of America are the VSL Post-Tensioning System and the Dywidag Post-tensioning System. The Dywidag System was developed in the 1940's. "The VSL Post-Tensioning Systems have been used throughout the world since 1956 (VSL Corporation, 1996)". While the two systems are similar, the anchorage

devices for each system are unique. Post-tensioned anchorages from these two systems are used in this research program. Specifications for the two systems are given in Chapter 5.

2.3.2 Stress Distribution for Post-Tensioning Anchorage Zones

Research has shown that a transverse bursting force develops in the anchorage zone a distance away for the end of a beam where the post-tensioning force is applied to the beam. This tensile force is transverse to the path of the tendon. The force must be resisted by steel reinforcement. The total area of steel that is required to resist this force can be computed by dividing the magnitude of the tensile force by the allowable stress of the reinforcement: $A_s = T/f_s$, where T is the tensile force, f_s is the allowable stress of the reinforcing steel and A_s equals the area of steel required to resist the bursting force. The area of the bearing plate of an anchorage device must be adequate to satisfy the AASHTO code requirements, including the concrete compressive stress limit of Section 5.10.9.6.2.

2.3.3 Post-Tensioned Anchorage Zones in AASHTO Design Specifications

According to the AASHTO code (2007), "anchorage and couplers are to develop at least 95% of the minimum specified ultimate strength of the prestressing steel without exceeding the anchorage set movement assumed for the design. Unbonded systems are also to pass a dynamic loading test." In addition, at critical sections, the strength required of bonded tendon can not exceed the resistance of the tendon assembly (anchorage or coupler). In Section 5.4.6, AASHTO provides guidelines for the size and alignment of ducts. The radius of curvature of tendon ducts in the anchorage areas shall not be less than 12.0 ft. "The size of the duct shall not exceed 0.4 times the least gross concrete thickness at the duct (AASHTO, 2007)."

Section 5.10.9 of the code defines anchorage zone dimensions for end anchorage zones and intermediate anchorage zones. The coded states that for design purposes the anchorage zone comprises two regions: the local zone and the general zone. The Engineer of Record is responsible for the design of the anchorage zone. Section 5.10.9.3.1 list three methods that may be used for the design of the general zone: 1. strut-and-tie models, 2. refined elastic stress analyses and 3. other approximate methods.

For certain conditions or limitations, the AASHTO code provides equations for estimating concrete compressive stresses, the location and magnitude of the bursting force, and the edge tension in post-tensioned anchorage zones in Section 5.10.9.6, Approximate Stress Analyses and Design. The AASHTO equations for the location and the magnitude of the bursting stresses are as follows:

$$T_{burst} = 0.25 \Sigma P_u (1-a/h) + 0.5 | \Sigma (P_u \sin \alpha) | \quad (2.8)$$

$$d_{burst} = 0.5(h-2e) + 5\, e \sin \alpha \quad (2.9)$$

In these equations, T_{burst} =tensile force (or bursting force) in the anchorage zone; P_u=factored tendon force; d_{burst} =the distance from the anchorage device to the centroid of the bursting force, T_{burst}; a = the lateral dimension of the anchorage; e=the eccentricity of the anchorage; h =the lateral dimension of the anchorage zone in the direction considered; α=the angle of inclination of the tendon. These equations were considered in the evaluation of the performance of the post-tensioned anchorage zone with steel fiber reinforced concrete (SFRC).

2.4 Research Methods

In the conduct of this research, the work performed included 1. testing materials; 2. load testing twenty-seven (27) anchorage specimens; 3. using the finite element method to model test specimens; 4. using empirical equations for computing forces and stresses; and 5) comparing all test, finite element results and empirical results. Compressive strength, tensile strength, flexural strength and modulus of elasticity tests were performed for concrete with and without steel fibers. The actual mix design used for this research project is similar to one recommended by the Florida Department of Transportation (FDOT) Materials Laboratory. This concrete mix was a high slump mix design. A 4000 psi concrete mix was used because this is the minimum concrete strength recommended by VSL, a post-tensioned anchorage manufacturer. For example, although VSL's literature states that "maximum prestressing force may be applied when concrete reaches a cylinder strength of 3500 psi", the VSL anchorage device dimensions are valid for a nominal concrete cylinder strength at 28 days of 4000 psi.

The three (3) fibers used in the research project were Dramix ZP305, Helix, and Novomesh 850. In the initial stages of this research project, Helix was a relatively new product consisting of "twisted polygon shaped high tensile steel wires" (Polytorx). Novomesh 850 is a combination of steel and polypropylene fiber blend.

To help determine the types and percentages of steel fiber that could improve the performance of the post-tensioned anchorage zone, material tests were performed. Tests were performed for plain concrete and for concrete containing each of the three fibers (Dramix, Helix and Novomesh). The fiber percentages used varied from 0.25% to 1.0% by volume. Based upon

research by Haroon (2003), a 1.0% fiber percentage was originally considered for use for each anchorage specimen. However, finite element analysis and material tests were performed before the load test specimens were cast. The fiber percentage selection was made as a result of considering 1) recommendations from the fiber manufacturers, 2) finite element analysis results, and 3) material test results. The dosage of 0.5% fiber by volume was selected for the fiber percentage (by volume) to use in the anchorage test specimens in this research program.

One (1) anchorage test specimen size was used in the load test program. The size of the anchorage test specimens was based upon the definition of the general post-tensioning anchorage zone and the AASHTO code. A review of several box girder bridges that have been constructed in the State of Florida was considered also. These bridges included the Santa Rosa Bay Bridge (BR# 580174), Choctawhatchee Bay Bridge (Mid-Bay, BR#570091), and SR-600 Bridge (BR# 790187 & 790188). However, the initial geometry of the proposed test specimen was based primarily upon two main sources of information: 1) the joint manufacturer's recommendations concerning minimum edge distances and minimum anchor spacing, and 2) the AASHTO code definitions of local and general post-tensioning zones and the geometry limitations for use of the AASHTO "Approximate Method" for designing post-tensioning anchorage zones.

The adequacy of the specimen size was verified twice by using finite element analyses. The first round of finite element analysis was done on a typical segment of MidBay Bridge where stresses at the PT anchorage zone were determined and compared with the anticipated stresses from the proposed laboratory test specimens. Also, the geometry and the boundary conditions of the tested specimen were obtained based on the distribution of the tensile stresses in the PT anchorage

zone. Another round of FEA was conducted after the completion of the laboratory testing program. This round was needed to compare the strain measurements from tested specimens with those predicted from the first round of FEA. Additionally, a parametric analysis was done to obtain a modified relationship for determining the bursting forces in PT anchorage zone when SFRC is used.

Section 5.10.9.6.1 of the 2007 AASHTO code lists conditions that must be true for stresses and forces to be estimated using the approximate stress analyses and design equations. One of the conditions stated in AASHTO Section 5.10.9.6.1 is that "the minimum edge distance of the anchorage in the main plane of the member is not less than 1.5 times the corresponding lateral dimension, "a", of the anchorage device." The size of the load test specimens used in this research was based upon having two (2) VSL EC 5-7 anchorage devices embedded in each specimen.

In this study, the stress distribution at the anchorage zone was investigated using ANSYS software program. Several models were produced to simulate the laboratory test samples. Using finite element analysis results, plots of transverse stresses were used to obtain transverse forces for specimens with different percentages of fiber and anchor plate to transverse depth ratios (a/h). Based upon empirical equations presented in the AASHTO code for post-tensioning anchorage zones, transverse tensile forces were calculated. The calculated forces were compared to the FEA results. In addition, compression and tension forces anticipated in the post-tensioning anchorage zone were computed using the strut-and-tie method. The transverse tensile forces calculated by the strut-and-tie method were compared to the test results and the finite element

results. Based upon the research, a new equation was proposed for computing the transverse tensile forces. This equation takes into consideration the percentage of steel fibers used in the concrete.

Chapter 3 discusses in detail the materials test program. Chapter 4 presents the anchorage test program parameters considered in casting twenty-seven (27) anchorage specimens and the laboratory load test results for each of the twenty-seven (27) load test specimens. Chapter 5 presents all the results from the testing program with descriptions of the behavior of each specimen during testing.. In Chapter 6, numerical calculations based upon the AASHTO code, experimental results, and finite element analysis results are compared with the laboratory test results. An approximate cost comparison for using reinforced concrete and fiber reinforced concrete in post-tensioned anchorage zones is also given in Chapter 6. Finally, Chapter 7 contains conclusions and recommendations resulting from the research program.

CHAPTER 3

MATERIALS TESTING

To help determine acceptable fibers and percentage of fibers to use in the anchorage load test program, extensive materials testing was performed. The materials test program considered a 4000 psi mix design, three (3) different fibers, and a range of fiber percentages: 0%, 0.25%, 0.33%, 0.5%, 0.75% and 1.0%. To investigate materials properties for the fiber reinforced concrete, compressive strength, tensile strength and flexural strength tests were conducted from "preliminary" concrete batches which were cast before anchor test specimens were cast. In addition to conducting material tests from the preliminary concrete batches, sixteen (16) 18" x 18" x 2.5" concrete slabs were cast to help evaluate cracking resistance.

In this chapter the materials used in the testing program are described. After the preliminary material tests were conducted, twenty-seven (27) anchor test specimens were cast. For these specimens, additional compressive strength, tensile strength and modulus of elasticity tests were performed. The material test results for the anchorage test specimens are included in this chapter. However, the selection of the geometry and the fiber contents of the anchorage test specimens are described in detail in Chapter 4. In Chapter 4, the load test results for the anchorage test specimens are presented and discussed.

3.1 Concrete Mix Design

A 4000 psi concrete mix was used because the minimum concrete strength recommended by one post-tensioned anchorage supplier (VSL) is 4000 psi. Recognizing that the inclusion of steel fibers in the concrete mix would result in a decrease in workability, a high slump concrete mix was selected. Thus the 4000 psi concrete mix design that was selected had 7 to 9 in slump. Detailed design mix is shown in Table 3-1.

Table 3-1: 4000 psi Concrete Mix Design

Specifications for Mix Design of f'c = 4000 psi. Slump 7-9 in, Air Content = 0 to 6.0%		
Component	Specification	1 y^3
Cement (lb)	Suwannee American (AASHTO M-85-Type II)	509
Coarse Aggregate (lb)	E. P. Jahna (57 SG, 2.53 SSD)	1638
Pine Aggregate (lb)	Crowder Sand (2.55 50, 2.64 SSD)	1092
Air Entrainment Admixture (oz)	AEA 92 Euclid (AASHTO M-154)	1.9
WPDA 64 Admixture (oz)	Eucon WP Euclid (AASHTO M-194 Type D)	45.6
Fly Ash (lb)	Boral (ASTM 0-618 Class F)	251
Water (gal (lb))	Potable	34.5 (287.5)

3.2 Material Tests

The three (3) fibers used in the research project are Dramix ZP305, Helix, and Novomesh 850. Dramix ZP305 (a steel fiber with bent ends) was used in earlier tests conducted by Haroon (2003). Helix is a product consisting of twisted polygon shaped high tensile steel wires. Novomesh 850 is a steel and polypropylene blend. Although a 1% fiber percentage was originally considered due to results of the research conducted by Haroon (2003), material test specimens were cast with different amounts of fibers (0.0%, 0.25%, 0.33%, 0.5%, 0.75% and

1.0% by volume). Figure 3-1 shows the three types of fibers used in this study. Table 3-2 describes the properties of these fibers

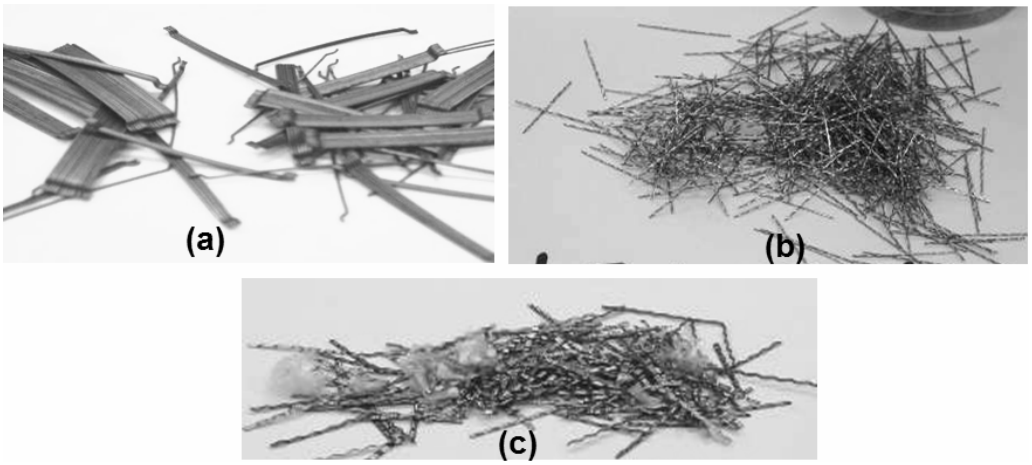

Figure 3-1 Steel Fiber (a) Dramix ZP305 (b) Helix (c) Novomesh 850

Table 3-2: Steel Fiber Information

Fiber Information						
Fiber	L (in)	Steel Dia.	Steel Aspect Ratio	Steel Tensile Strength	Deformation	Recommended Dosage Range and Recommended Concrete Slump
Dramix ZP305	1.18 in (30 mm)	0.02 in (0.55 mm)	55	Min. 145 ksi (1100 N/mm2)	Hooked ends	Less than 2% by Volume- Recommended maximum Dosage based upon 8 mm max aggregate size: 110 kg/m^3 (185 lb/y^3)
Helix	1 in	0.02 in	50		Twisted polygon shape	5 to 66 lb/CY ≈ 0.04% to 0.5%
Novomesh 850	1.5 in		34	140-180 ksi	Continuously Deformed Circular Segment	24 to 48 lb/CY ≈ 0.18% to 0.35%

3.3 Material Test Results for S1 and S2 Anchorage Specimens

A total of 27 batches of concrete were cast to investigate material properties prior to the casting of the anchorage test specimens. Ready-mix concrete was used in Concrete Batches 1 through 4. The ready-mix concrete was mixed and delivered to the FAMU-FSU College of Engineering by a ready mix vendor. Based upon the material test results and the finite element analysis, the size of the anchorage block specimens was decided. Finally, another 8 batches of concrete were mixed and 27 anchorage test specimens using 0.5% fibers by volume were then prepared for laboratory testing. Concurrently, cylindrical samples were prepared from the last 8 batches to determine the compressive strength and the split tensile strength of the concrete. Additional information about concrete mix design for the 35 batches is shown in Table 3-3 to Table 3-9.

Table 3-3: Concrete Batches 1 to 5

Batch Number	1	2	3	4	5
Batch Source	TRM	TRM	TRM	TRM	FAMU
Cast Date	2/28/06	3/1/06	3/2/06	3/3/06	4/18/06
Amount Made (yd^3)	2.5	1.0	2.0	2.0	0.18
Cement (lb)	1265	565	1105	1045	91.62
Coarse Aggregate (lb)	4450	2110	3440	3360	294.84
Fine Aggregate (lb)	2780	1110	2370	2240	197
Flyash (lb)	610	255	505	510	45.18
Euclid, Air Entrainment (ml)	5	91	3	3	10.3
Euclid, Water Reducer (ml)	228		182	182	246.3
Superplasticizer (ml)	0	0	0	0	0
Water	28 gal		19 gal	17 gal	51.75 lb
Water Cement Ratio (w/c)	.18		.15	.14	0.38
Slump Before Fiber (in)	7.5	5	7.5	7.0	9.5
Slump After Fiber (in)				4.5	
Fiber	Helix	Helix	Dramix	Novomesh	NONE
Specimens Cast	Plain	Plain	D.25	N.25	Plain
	H.25	H.75	D.36	N.36	
	H.36	H1.0	D.50	N.50	
	H.50	Beams	D.75	N.75	
		Slabs	D1.0	N1.0	

Table 3-4: Concrete Batches 6 To 10

Batch Number	6	7	8	9	10
Batch Source	FAMU	FAMU	FAMU	FAMU	FAMU
Cast Date	4/28/06	4/30/06	5/1/06	5/2/06	5/2/06
Amount Made (yd^3)	0.10	0.10	0.10	0.10	0.10
Cement (lb)	50.9	50.9	50.9	50.9	50.9
Coarse Aggregate (lb)	163.8	163.8	163.8	163.8	163.8
Fine Aggregate (lb)	109.2	109.2	109.2	109.2	109.2
Flyash (lb)	25.1	25.1	25.1	25.1	25.1
Euclid, Air Entrainment (ml)	6	6	6	6	6
Euclid, Water Reducer (ml)	135	135	135	0	0
Superplasticizer (ml)	0	0	0	450	450
Water (lb)	28.75	28.75	28.75	28.75	28.75
Water Cement Ratio (w/c)	0.38	0.38	0.38	0.38	0.38
Slump Before Fiber (in)		5.75	4.75	10.25	9
Slump After Fiber (in)	4.25	0.5	0.375	4.0	2.75
Fiber	Dramix	Helix	Novomesh	Dramix	Helix
Fiber (lb)	13.2	13.2	13.2	13.2	13.2
Specimens Cast	D1.0	H1.0	N1.0	D1.0	H1.0

Table 3-5: Concrete Batches 11 to 15

Batch Number	11	12	13	14	15
Batch Source	FAMU	FAMU	FAMU	FAMU	FAMU
Cast Date	5/3/06	5/3/06	5/4/06	5/5/06	5/5/06
Amount Made (yd^3)	0.10	0.10	0.10	0.10	0.10
Cement (lb)	50.9	50.9	50.9	50.9	50.9
Coarse Aggregate (lb)	163.8	163.8	163.8	163.8	163.8
Fine Aggregate (lb)	109.2	109.2	109.2	109.2	109.2
Flyash (lb)	25.1	25.1	25.1	25.1	25.1
Euclid, A. E. (ml)	6	6	6	6	6
Euclid, W. R. (ml)	0	0	0	0	0
Superplasticizer (ml)	650	450	550	450	225
Water (lb)	28.75	28.75	28.75	28.75	28.75
Water Cement Ratio (w/c)	0.38	0.38	0.38	0.38	0.38
Slump Before Fiber (in)	8.75	9.0	8.5	11	10.5
Slump After Fiber (in)	0.75	6.5	3.75	9.75	9
Fiber Type	Novomesh	Dramix	Helix	Novomesh	Novomesh
Fiber (lb)	13.2	6.6	6.6	6.6	4.8
Specimens Cast	N1.0	D.50	H.50	N.50	N.36

Table 3-6: Concrete Batches 16 To 20

Batch Number	16	17	18	19	20
Batch Source	FAMU	FAMU	FAMU	FAMU	FAMU
Cast Date	5/7/06	5/7/06	5/8/06	5/10/06	5/10/06
Amount Made (yd^3)	0.10	0.10	0.10	0.10	0.10
Cement (lb)	50.9	50.9	50.9	50.9	50.9
Coarse Aggregate (lb)	163.8	163.8	163.8	163.8	163.8
Fine Aggregate (lb)	109.2	109.2	109.2	109.2	109.2
Fly ash (lb)	25.1	25.1	25.1	25.1	25.1
Euclid, Air Entrainment (ml)	6	6	6	6	6
Euclid, Water Reducer (ml)	0	0	135	135	135
Superplasticizer (ml)	225	225	0	0	0
Water	28.75	28.75	28.75	28.75	28.75
Water Cement Ratio (w/c)	0.38	0.38	0.38	0.38	0.38
Slump Before Fiber (in)	10.25	10.75	10.25	9.5	8.75
Slump After Fiber (in)	9.5	10.5	8.5	7.0	5.75
Fiber	Helix	Dramix	Helix	Novomesh	Dramix
Fiber (lb)	4.8	4.8	9.9	9.9	9.9
Specimens Cast	H.36	D.36	H.75	N.75	D.75

Table 3-7: Concrete Batches 21 To 25

Batch Number	21	22	23	24	25
Batch Source	FAMU	FAMU	FAMU	FAMU	FAMU
Cast Date	5/12/06	5/12/06	5/12/06	5/16/06	5/16/06
Amount Made (yd^3)	0.10	0.10	0.10	0.10	0.10
Cement (lb)	50.9	50.9	50.9	50.9	50.9
Coarse Aggregate (lb)	163.8	163.8	163.8	163.8	163.8
Fine Aggregate (lb)	109.2	109.2	109.2	109.2	109.2
Flyash (lb)	25.1	25.1	25.1	25.1	25.1
Euclid, A. E. (ml)	6	6	6	6	6
Euclid, W.R. (ml)	135	135	135	135	135
Superplasticizer (ml)	0	0	0	0	0
Water	28.75	28.75	28.75	28.75	28.75
Water Cement Ratio (w/c)	0.38	0.38	0.38	0.38	0.38
Slump Before Fiber (in)	10.0	10.0	10.75	10.0	9.0
Slump After Fiber (in)	10.25	9.875	9.5	5.75	7.0
Fiber	Dramix	Novomesh	Helix	Novomesh	Helix
Fiber (lb)	3.3	3.3	3.3	13.2	13.2
Specimens Cast	D.25	N.25	H.25	N1.0	H1.0

Table 3-8: Concrete Batches 26 To 30

Batch Number	26	27	28	29	30
Batch Source	FAMU	FAMU	TRM	TRM	TRM
DOT Mix Number			03-1131	03-1131	03-1131
Cast Date	5/16/06	5/19/06	9/28/06	9/28/06	10/3/06
Amount Made (yd^3)	0.10	0.10	1.0	2.0	2.0
Cement (lb)	50.9	50.9	510	1018	1025
Coarse Aggregate (lb)	163.8	163.8	1690	3770	3320
Fine Aggregate (lb)	109.2	109.2	1125	2290	5570
Flyash (lb)	25.1	25.1	251	502	1525
Euclid, Air Entrainment	6 ml	6 ml	1 oz	3	3
Euclid, Water Reducer	135 ml	135 ml	92 oz	182 oz	182 oz
Superplasticizer (ml)	0	0			
Water (gal)	28.75lbs	28.75Lb	15 gal	51 gal	34 gal
Water Cement Ratio (w/c)	0.38	0.38	.25	0.42	0.28
Slump Delivery Ticket (in)			7	7	7
Slump at FAMU (in)	9.5	10.0			7.5
Fiber	NONE	NONE	NONE	Dramix	Helix
Fiber (lb)				132	132
Specimens Cast	Plain	Plain	S1 Test	S1 Test	S1 Test
			Plain	D.50	H.50

Table 3-9: Concrete Batches 31 To 35

Batch Number	31	32	33	34	35
Batch Source	TRM	TRM	TRM	TRM	TRM
DOT Mix Number	03-1131	03-116CIV	03-116CIV	03-116CIV	03-116CIV
Cast Date	10/3/06	1/16/07	1/16/07	1/17/07	1/17/07
Amount Made (yd^3)	2.0	1.00	2.00	2.00	2.00
Cement (lb)	1025	500	1005	1010	1015
Coarse Aggregate (lb)	3380	1660	2410	3290	4050
Fine Aggregate (lb)	2250	1120	1005	2250	2470
Flyash (lb)	502	235	405	535	490
Euclid, Air Entrainment (ml)	3	1	3	4	3
Euclid, Water Reducer (ml)	182 oz	44	90	90	90
Superplasticizer (ml)					
Water (gal)	41	12	32	37	33
Water Cement Ratio (w/c)					
Slump Before Fiber (in)	7	7	7	7	7
Slump After Fiber (in)	5.5	6.25	8.5	7.3	6.5
Fiber	Novomesh	None	Dramix	Helix	Novomesh
Fiber (lb)	132	0	132	132	132
Specimens Cast	S1 Test	S2 Test	S2 Test	S2 Test	S2 Test
	N0.5	Plain	D0.5	H0.5	N0.5

3.4 Comparison of Strength Properties with Other Studies

Based upon the preliminary material test results and the finite element modeling, the fiber percentage used for the test specimens was 0.5% for each of the three fibers. After the preliminary materials tests were completed, twenty-seven (27) anchorage test specimens were cast from concrete Batches 28 through 35 which were mixed and delivered by Trinity Materials, LLC. In the following figures and tables, materials test results are presented for the concrete cylinders cast from the thirteen (13) anchorage test specimens cast between September 28 and October 3, 2006 and the fourteen (14) anchorage test specimens cast in January 2007. From each concrete batch, approximately thirty (30) concrete cylinders were cast. From these cylinders, compressive strength tests and split tensile strength tests were performed.

3.4.1 Compressive and Tensile Strength Tests for S1 Specimens

The compressive strength test results are presented in Figure 3-2. The average 28 day compressive strengths for Plain, Dramix, Helix and Novomesh cylinders were 4846 psi, 4767 psi, 2848 psi, and 4305 psi, respectively. The low value for Helix cylinders may have been due in part to a batching error and an attempted correction made by Trinity Materials, LLC. This error resulted in a mix design for Helix specimens that contained much more fine aggregate and fly ash than were used in the other batches. At age 135 days, the compressive strength of the Helix cylinders was 3770 psi. The anchorage test specimens cast with Helix were tested at ages 145 days and 148 days. It should be noted that the 3770 is less than the concrete design strength of 4000 psi but it is greater than 3500 psi, the VSL allowable compressive strength for applying the maximum prestress force.

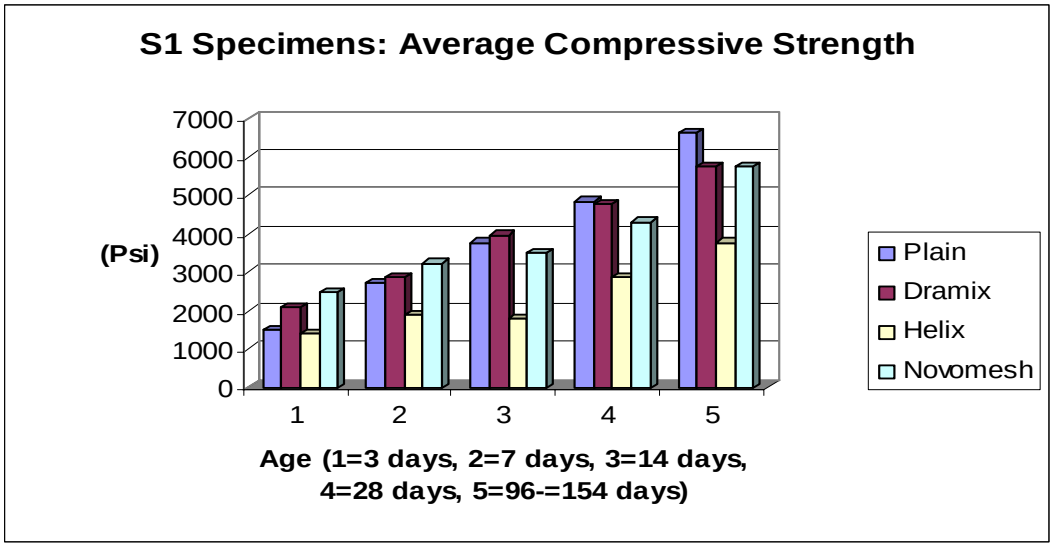

Figure 3-2: S1 Specimens Compressive Strength Results

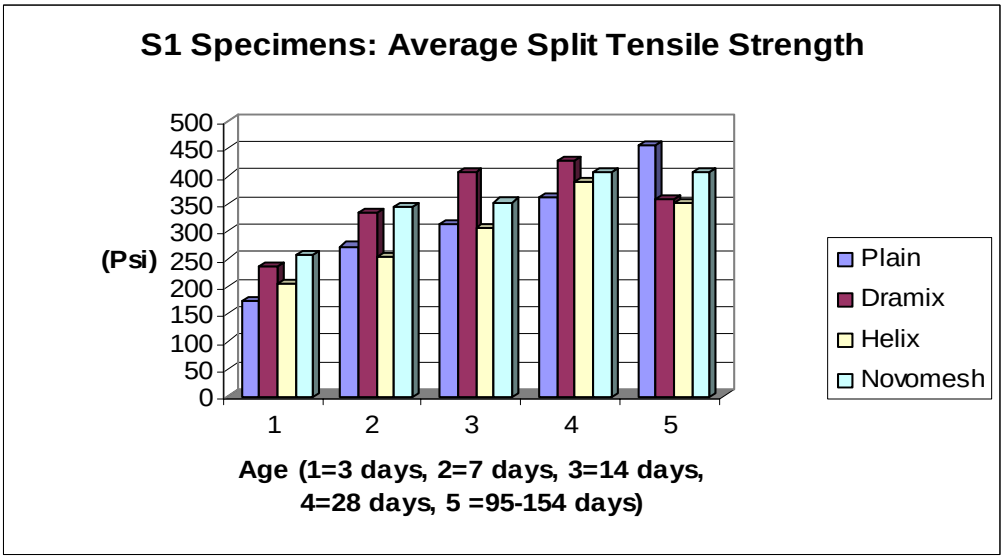

Figure 3-3: S1 Specimens Average Split Tensile Strength Results

The tensile strength test results are presented in Figure 3-3. The average 28 day split tensile strengths for Plain, Dramix, Helix and Novomesh cylinders were 362 psi, 427 psi, 389 psi, and

408 psi, respectively. The maximum split tensile strength (427 psi) was for the concrete made with 0.5% Dramix fibers. However, at age 95 days, the maximum split tensile strength measured was 359 psi for cylinders with 0.5% Dramix fibers. The 28 day compressive strength of the Helix cylinders was less than 3000 psi and over 33% less than that for the other cylinders. However, the 28 day tensile strength of the Helix cylinders was greater than that of the plain cylinders and within 10% of the tensile strengths of the Dramix and Novomesh cylinders.

3.4.2 Compressive and Tensile Strength Tests for S2 Specimens

The compressive strength test results are presented in a bar chart (Figure 3-4). The average 28 day compressive strengths for Plain, Dramix, Helix and Novomesh cylinders were 4212 psi, 3463 psi, 4550 psi, and 4127 psi, respectively. Thus, for the S2 specimens, the concrete batch for Dramix cylinders had the lowest compressive strength. In the concrete mix for the Dramix cylinders, less coarse aggregate, fine aggregate and fly ash were used than was specified in the design mix. However, at 56 days, the age when the anchorage specimens were tested, the compressive strength of the Dramix cylinders was 4200 psi, 5% higher than the concrete mix design strength.

The tensile strength test results are presented in Figure 3-5. The average 28 day tensile strengths for Plain, Dramix, Helix and Novomesh cylinders were 265 psi, 323 psi, 361 psi, and 410 psi, respectively. The maximum split tensile strength was for the Novomesh fiber reinforced concrete. Although the 28 day compressive strength of the Dramix cylinders was 17% less than that of the plain concrete cylinders, the 28 day tensile strength of the Dramix cylinders was about

21% greater than that of the plain concrete cylinders. Thus, the Dramix fibers enhanced the tensile strength of the concrete.

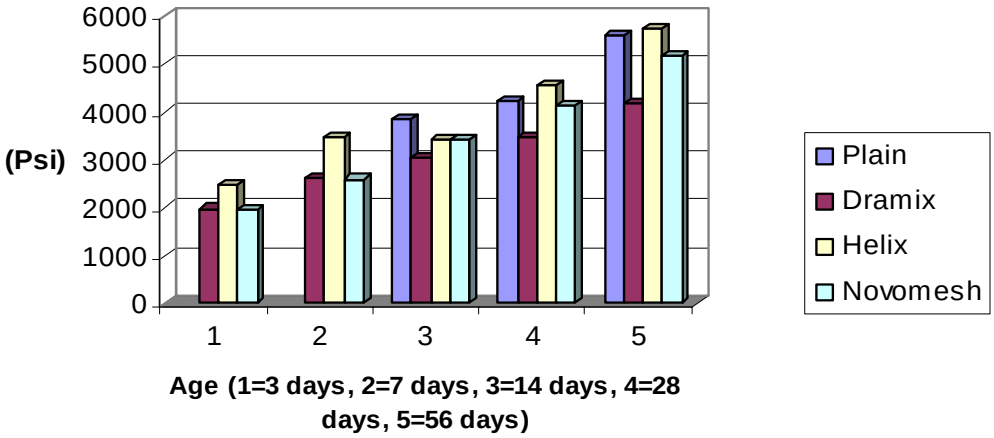

Figure 3-4: S2 Specimens Compressive Strength Results

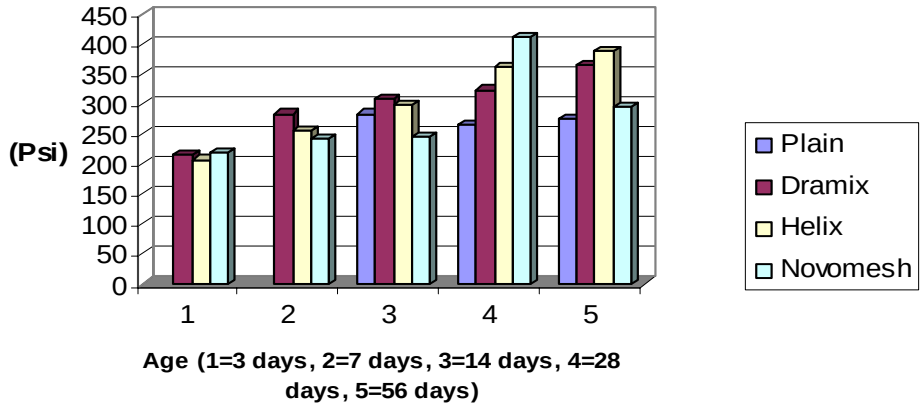

Figure 3-5: S2 Specimens Average Split Tensile Strength Results

3.4.3 Modulus of Elasticity Tests for S2 Specimens

Using concrete cylinders which remained after the compressive strength tests and tensile strength tests were completed for the S2 Specimens, modulus of elasticity tests were performed. The measured modulus of elasticity values are shown in Figure 3-6. Also shown in this figure are the

computed modulus values which result from using the AASHTO LRFD Bridge Design Specifications (2007) code equation (5.4.2.4.-1). As shown in the figure, for all cases except for cylinders with Helix fibers, the measured modulus is less than the AASHTO computed value. The modulus of elasticity for the Helix fiber reinforced concrete was 2% greater than the value computed using the AASHTO equation.

According to the AASHTO LRFD Bridge Design Specifications (2007), the Poisson's ratio can be assumed to be 0.2 if physical tests are not conducted. The measured values for Poisson's ratio were 0.21, 0.22, 0.23 and 0.25 for plain concrete, Dramix fiber concrete, Helix fiber concrete and Novomesh fiber concrete, respectively.

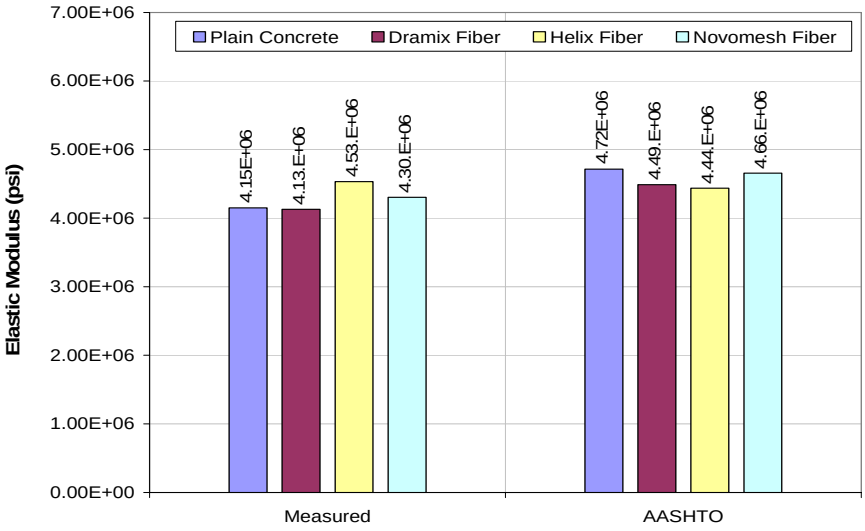

Figure 3-6: Measured vs. AASHTO Elastic Modulus for Concrete Samples

3.4.4 Modulus of Rupture Tests for S2 Specimens

Modulus of rupture tests were conducted for the concrete used to cast the S2 Anchorage Specimens. These flexure strength test results are presented in Figure 3-7. As shown in the

figure, the cylinders with 0.5% Helix fiber had the greatest modulus of rupture strength (f_r = 821 psi = 0.821 ksi). According to the AASHTO code commentary, research data by others show that most modulus of rupture values are between $0.24\sqrt{f'_c}$ to $0.37\sqrt{f'_c}$. For the Helix fiber reinforced concrete, the test value for the modulus of rupture was within the range computed (0.576 ksi to 0.888 ksi) by using the AASHTO code equations and f'_c = 5.757 ksi (at age 56 days). For the Novomesh fiber reinforced concrete, the test value for the modulus of rupture (0.755 ksi at age 69 days) was within the range computed (0.546 ksi to 0.842 ksi) by using the AASHTO code equations and f'_c = 5.179 ksi (at age 61 days). For the Dramix fiber reinforced concrete, the test value for the modulus of rupture (0.787 ksi at age 72 days) was higher than the range (0.492 ksi to 0.758 ksi) computed using the AASHTO code equations and f'_c = 4.200 ksi (at age 56 days). There was less than a 10% difference in high and low modulus of rupture test values for the three different fibers.

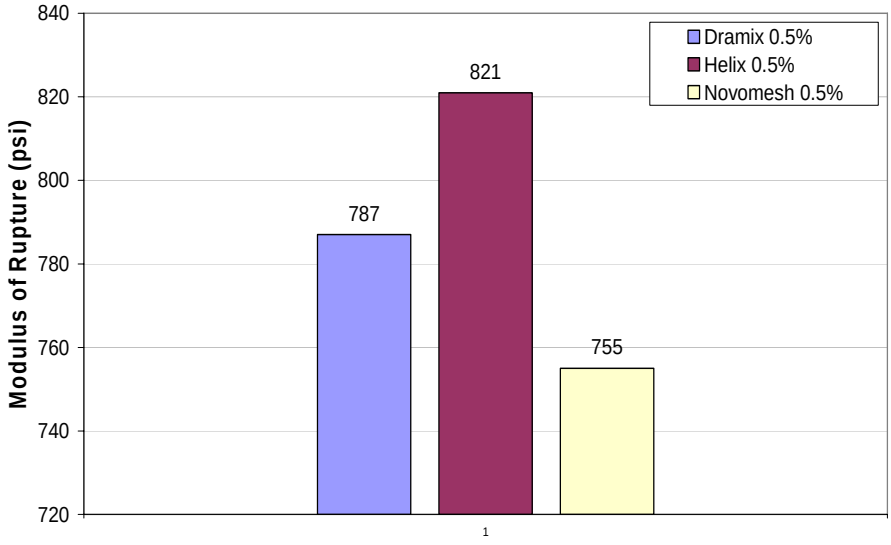

Figure 3-7: S2 Specimens Modulus of Rupture

3.5 Comparison of Strength Properties with Other Studies

To derive a meaningful comparison between the SFRC properties from specimens used in this study and with those reported in literature, it was decided to compare strength results at the 28 days period.

Figure 3-8 to Figure 3-16 present compressive strength (f'_c), split tensile strength (f'_t) and flexural strength (f_r) for the three types of steel fibers.

Figure 3-8 shows that SFRC with Dramix fiber exhibited variable values for the compressive strength. For this type of fiber, the trend was not clear for the effect of fiber content on the compressive strength values. An increase of 18.8% of the compressive strength was noticed when the percentage fiber increased from 0.25% to 1%. However, increasing the fiber content from 0.25% to 0.50% improved the compressive strength values by about 27%. SFRC Specimens with Helix fiber showed some reductions in the compressive strength values as compared with those obtained from plain concrete. It is possible that this reduction was due to the formation of lumps when the percentage of fiber increased. SFRC Specimens with Novomesh fiber followed the same trend as of Helix fiber.

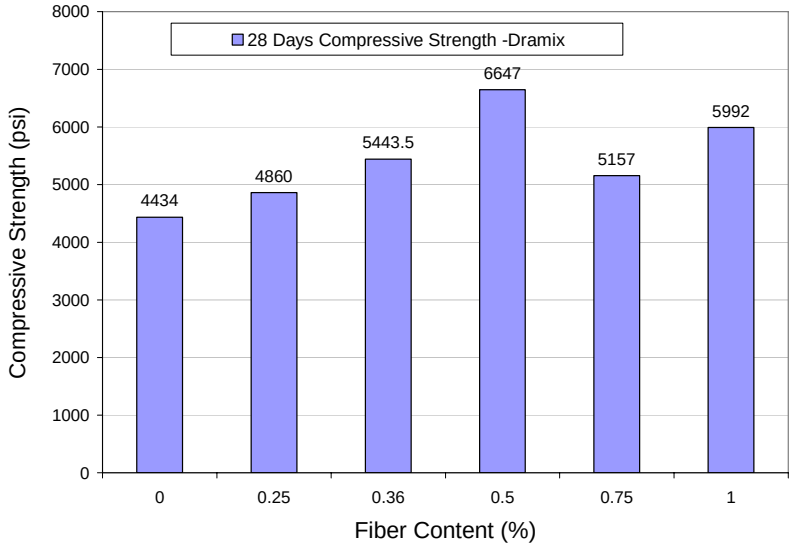

Figure 3-8: Compressive Strength of Dramix SFRC.

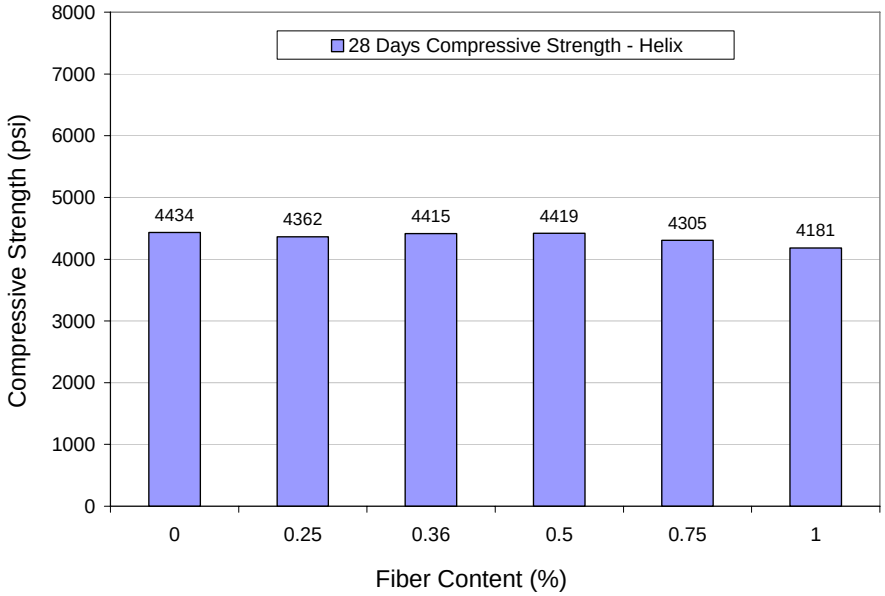

Figure 3-9: Compressive Strength of Helix SFRC.

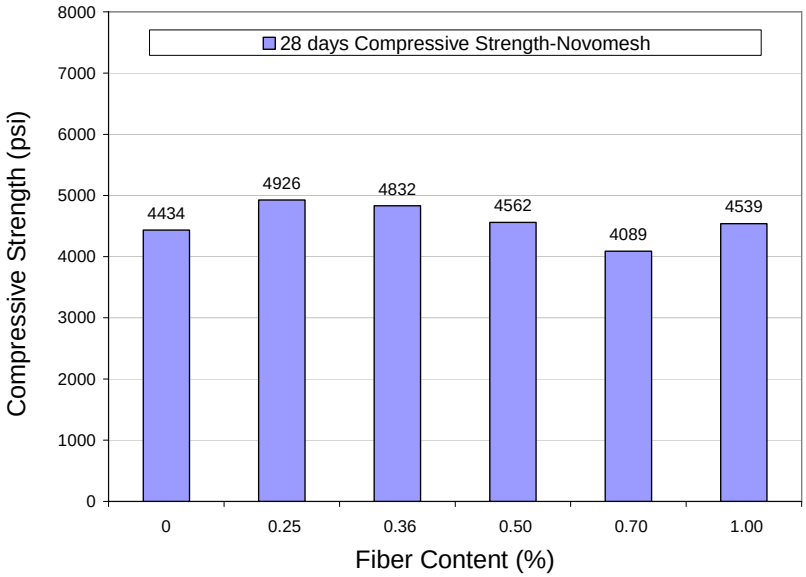

Figure 3-10: Compressive Strength of Novomesh SFRC.

Figure 3-11 to Figure 3-13 show the split tensile strength results of the three fibers used in this study. For specimens with Dramix and Helix fibers, the split tensile strength increased as the fiber content increased. SFRC with Novomesh fiber exhibited the same trend with exceptions for specimens with 0.36% and 0.5% fiber. At 0.5% steel fiber the specimens produced the same split tensile strength as for those with 1%.

The flexural strength values increased with the fiber content for Dramix SFRC. The other types of fibers did not show the same trend indicating that the increasing percentage of fiber may not appreciate the flexural strength of concrete.

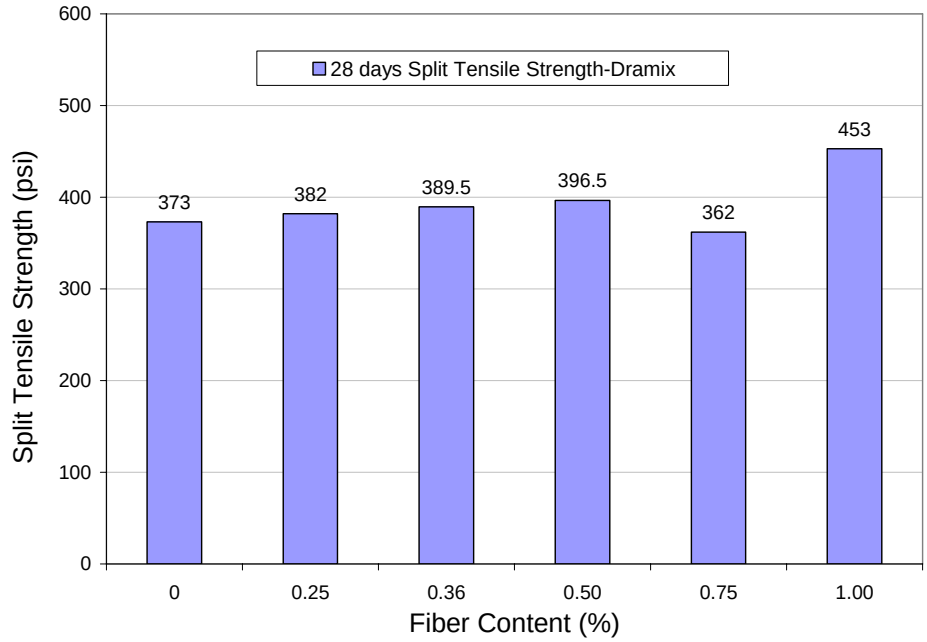

Figure 3-11: Split Tensile Strength of Dramix SFRC.

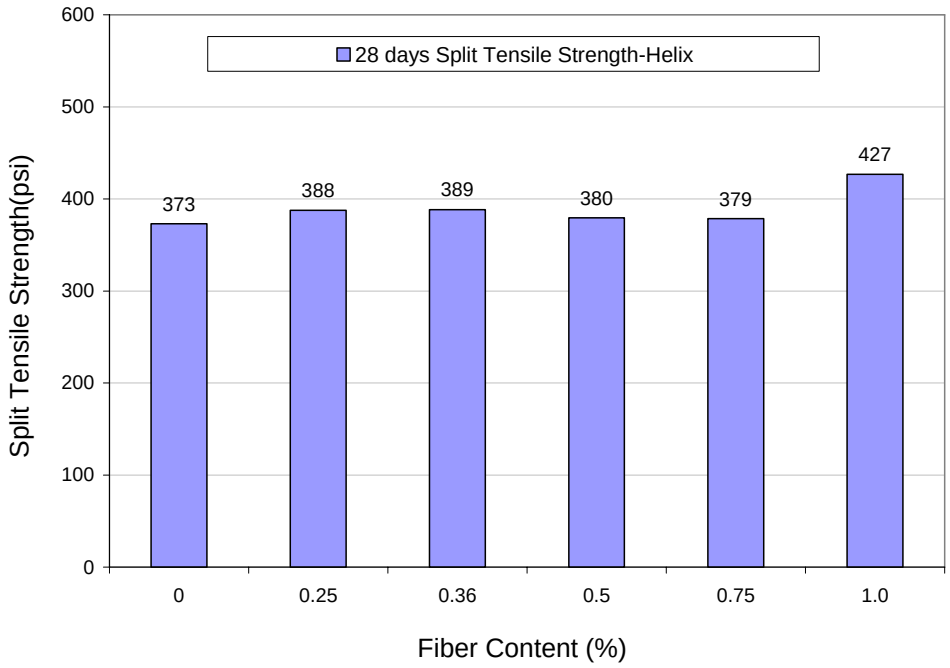

Figure 3-12: Split Tensile Strength of Helix SFRC.

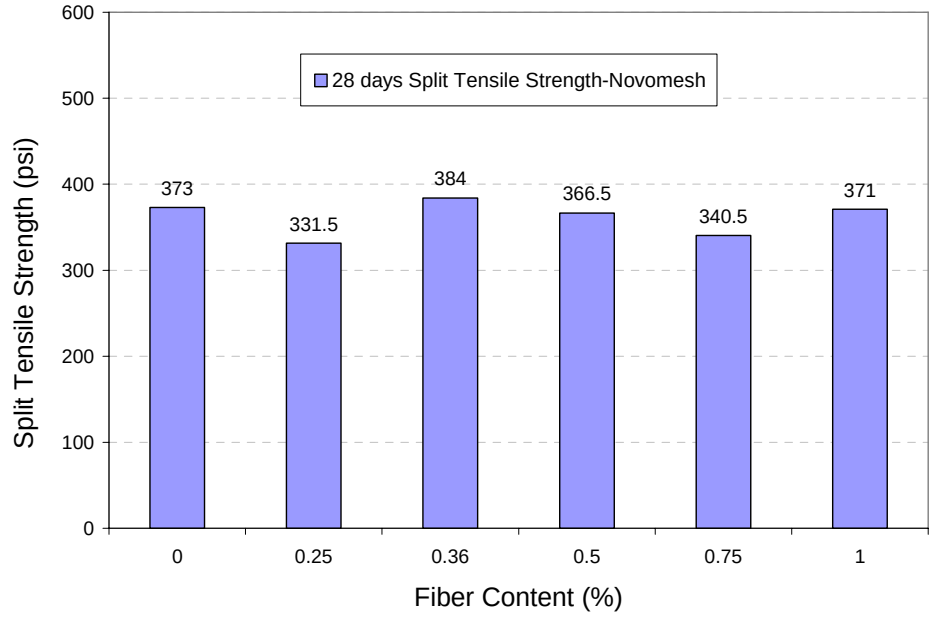

Figure 3-13: Split Tensile Strength of Novomesh SFRC.

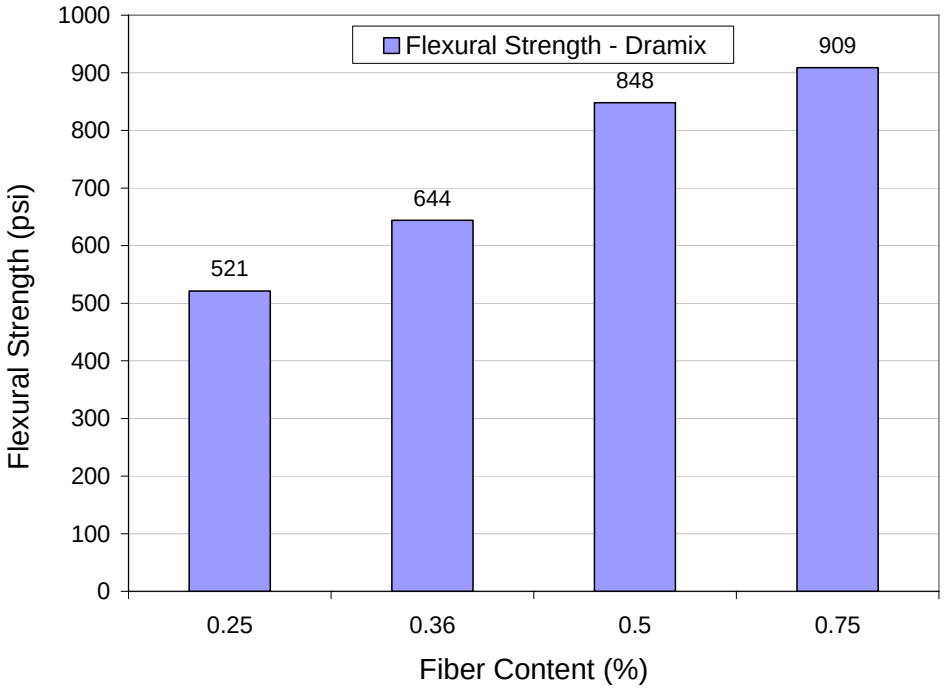

Figure 3-14: Flexural Strength of Dramix SFRC.

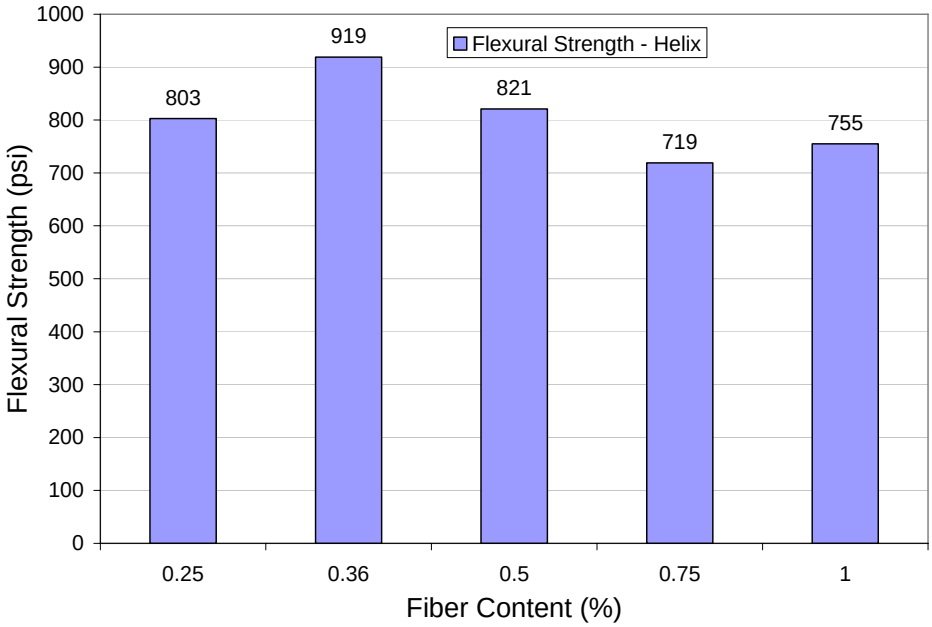

Figure 3-15: Flexural Strength of Helix SFRC.

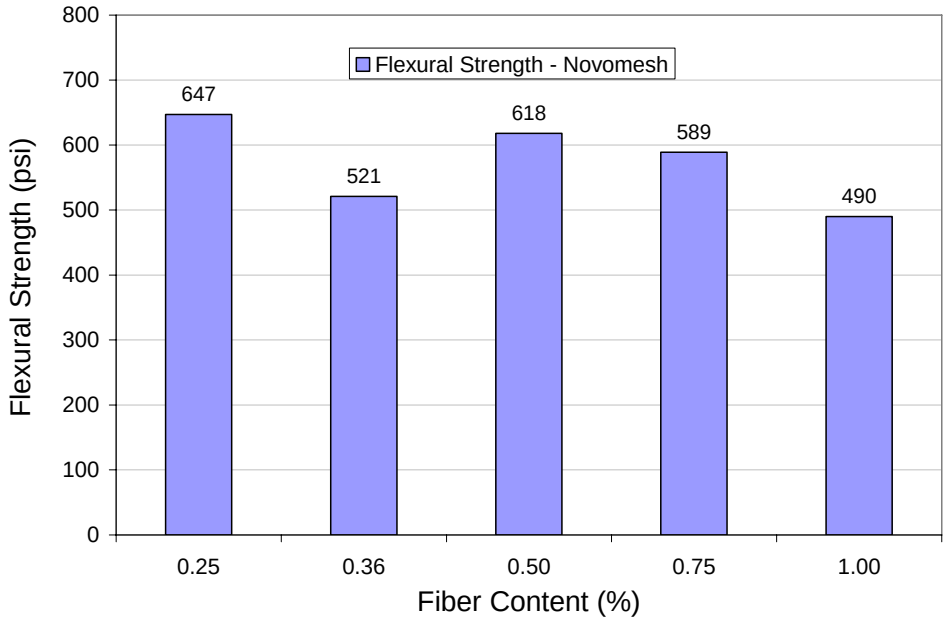

Figure 3-16: Flexural Strength of Novomesh SFRC.

Haroon (2003), produced almost similar results as of the current study (Tables 3-10 to 3-12). However, in his study, Harbourite H-330 fiber did not follow the trends of the other fibers. For this particular type of fiber, the increase in the percentage of fiber resulted in significant reductions in the compressive, split tensile and flexural strength values. Additionally, Haroon's design mix was different than the one used in this study.

Table 3-10: Compressive Strength of SFRC (Haroon 2003)

Type of Fiber	Fiber volume (%)	Compressive strength results	
		Test value psi	Difference with control(%)
Control Specimen	0	6350	-
XOREX	0.5	6600	+3.94
	0.75	6900	+8.66
	1.0	7350	+15.75
ZP305	0.5	7300	+14.9
	0.75	74001	+16.5
	1.0	7510	+18.2
Harbourite	0.5	5100	-19.6
H-330	0.75	3410	-46.3
	1.0	3800	-40.1

Table 3-11: Split Tensile Strength of SFRC (Haroon 2003)

Type of Fiber	Fiber volume (%)	Split Tensile strength results	
		Test value psi	Difference with control (%)
Control specimen with no fiber	0	630	-
XOREX	0.5	660	+4.7
	0.75	670	+6.6
	1.0	690	+9.5
ZP305	0.5	660	+5.5
	0.75	730	+15.8
	1.0	870	+37.3
Harbourite	0.5	580	-7.1
H-330	0.75	400	-36.5
	1.0	530	-16.7

Table 3-12: Flexural Strength of SFRC (Haroon 2003)

Type of Fiber	Fiber volume (%)	Flexural toughness results	
		First crack strength psi	Difference with control (%)
Control specimen with no fiber	0	1000	-
XOREX	0.5	990	-1.0
	0.75	1020	+2.0
	1.0	1085	+8.5
ZP305	0.5	1160	+6.0
	0.75	1190	+19.0
	1.0	1345	+34.5
Harbourite	0.5	990	-1.0
H-330	0.75	1090	+9.0
	1.0	1015	+1.5

A study by Nataraja et al (2005) showed a reduction in the compressive strength of concrete specimens when percentages of steel fiber increased from 0.5% to 1.5% (Tables 3-13 and 3-14). Cucchiara et al (2004), presented different trend for the addition of steel fiber in concrete. Increasing the percentage of fiber from 0 to 2 percent improved the compressive strength by only 2%. However, increasing the percentage of steel fiber resulted in a significant increase in the split tensile strength for the same concrete mixes (Table 3.15).

Table 3-13: Compressive Strength of SFRC FOR 30 MPa Mix (Nataraja et al., 2005)

Test results of reproportioned mix — 30 MPa (mix 1 : 2.67 : 1.9)

Volume fraction v_f, %	Average compressive strength in MPa	
	7 days	28 days
0.0	18.02 (1.34)*	33.15 (0.38)
0.5	24.44 (0.56)	30.65 (1.23)
1.0	17.59 (1.12)	27.98 (1.59)
1.5	23.36 (1.36)	28.04 (134)

* Value within the brackets represents standard deviation.

Table 3-14: : Compressive Strength of SFRC for 50 MPa Mix (Nataraja et al., 2005)

Test results of reproportioned mix — 50 MPa (mix 1 : 1.47 : 1.24)

Volume fraction v_f, %	Average compressive strength in MPa	
	7 days	28 days
0.0	37.41 (0.84) *	50.62 (0.68)
0.5	39.34 (0.56)	50.36 (1.01)
1.0	32.99 (0.98)	47.25 (1.33)
1.5	43.76 (1.02)	50.66 (1.56)

* Value within the brackets represents standard deviation.

Table 3-15: Compressive and Tensile Strength for SFRC (Cucchiara et al., 2004)

Properties of concrete mixtures

V_f (%)	f'_c (MPa)	$\varepsilon_0 \times 10^3$	E_c (MPa)	f'_t (MPa)
0	41.20	2.513	26094	2.02
1	40.85	2.780	26236	4.65
2	43.23	2.898	26373	5.49

CHAPTER 4

ANCHORAGE SPECIMENS SELECTION AND TESTING

4.1 Introduction to Specimen Selection

In this study the dimensions of the tested samples were selected based on preliminary analyses conducted using finite element modeling (Figure 4-1). Initially, a bridge segment was chosen, modeled and thoroughly analyzed under post tensioned loading conditions similar to what are encountered in the field. The purpose this analysis was to define the extent of the post-tensioning stresses around the anchorage zones in a full scale mode. Such a step was necessary to delineate the boundary conditions of the anchorage zone if smaller sections were to be considered. Constitutive properties for finite element modeling including compressive strength, tensile strength and percentage of fiber contents were selected from a similar study conducted by Haroon 2003 using the steel fiber proposed for this investigation.

After the full scale analyses of the bridge segment, a scaled block containing two posttensioning anchors was separated from the web area of the bridge segment. This block was then analyzed using three dimensional finite element modeling to determine the boundary conditions at which stress distributions were not affected by the length of the block. For this block, the final

dimensions were confirmed based on (1) the definition of the local and general posttensioning anchorage zone of AASHTO code, and (2) the joint manufacturer's recommendations concerning minimum edge distances and minimum anchor spacing.

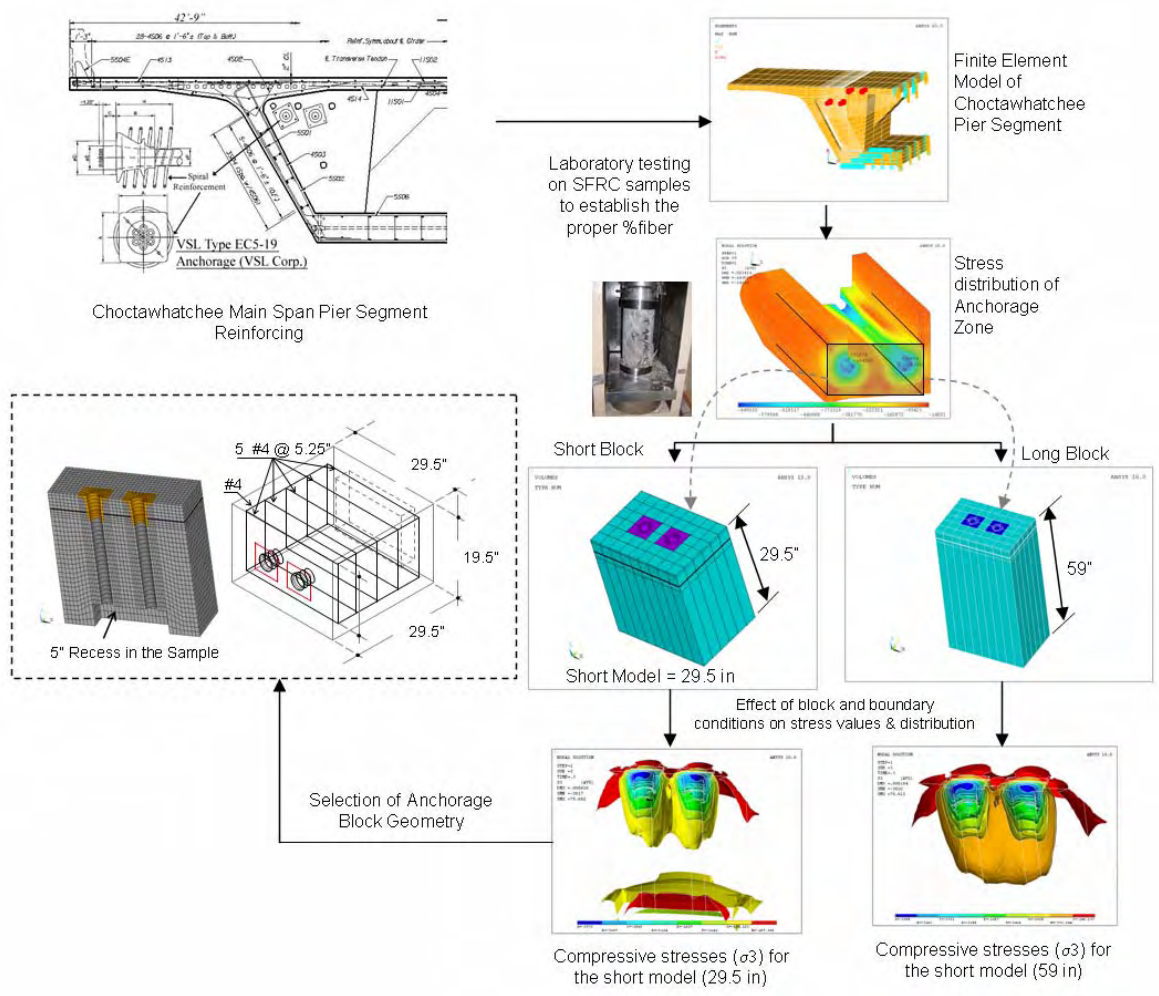

Figure 4-1: Steps followed in this study to select the geometry of the anchorage block specimen.

4.2 Selection of Full Scale Bridge Segment

Several existing bridge segments were first considered in order to determine a common bridge cross section for modeling. Among the bridges considered were the Santa Rosa Bay Bridge, and

the Choctawhatchee Bay Bridge (Mid-Bay). Both bridges were designed by FIGG Engineering Group. Further comparison between the two bridge segments revealed that the cross sections were also fairly similar (Table 4.1). Due to geometry and modeling complexity, the Choctawhatchee Bay Bridge was chosen to be a representative model and a simplified drawing can be seen in Figure 4.1.

Table 4-1: Comparison of Bridge Dimensions

Project	Width	Height	Length
Santa Rosa Bay Bridge	7’-10”	8’-0”	9’-5”
Choctawhatchee Bay Bridge	8’-1”	9’-0”	9’-5”

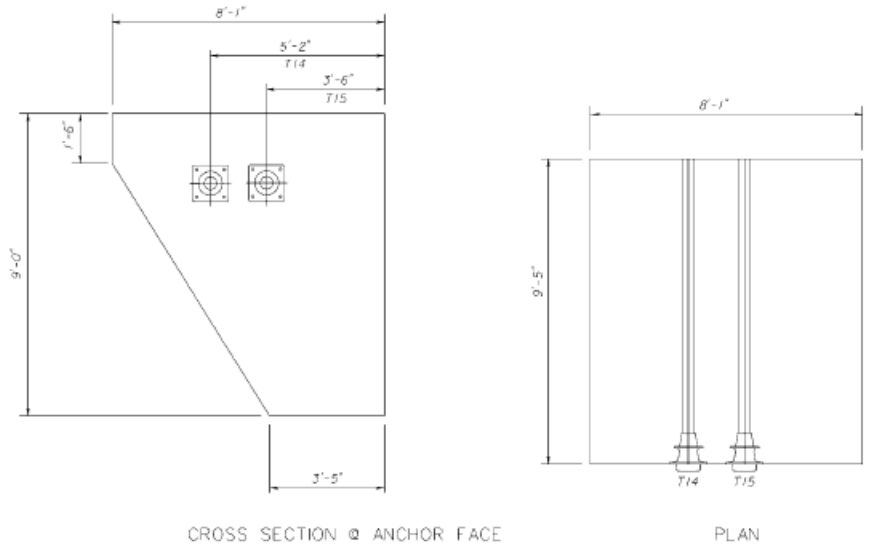

Figure 4-2: Choctawhatchee Bay Bridge Segment

The post-tensioning steel required for the bridge was provided in the contract plans of the Choctawhatchee Bay Bridge. The segment that was chosen detailed two 19-0.6” diameter longitudinal tendons (Figure 4-2) on each face. VSL type EC 5-19 anchorages were used in

this bridge and modeled in this study (Figure 4-3). The ultimate post-tensioning force (P_u) for this anchorage is determined by the following equation:

$$P_u = A_s * n * f_{pu} \quad (4\text{-}1)$$

$$P_u = 0.153 * 19 * 270 = 785 \text{ kips} \quad (4\text{-}2)$$

where A_s is the area of each strand, n is the number of strands, and f_{pu} is the ultimate strength of the tendon. An ultimate post-tensioning force of 785 kips was applied to the modeled specimen. The duct that is provided with the VSL type EC 5-19 anchorage is 3.75” in diameter and was modeled in the specimen. The local zone reinforcement is specified by VSL Corporation to accompany the chosen anchorage and includes a #5 spiral around the anchorage. The spiral has an outside diameter of 15” and 8 turns with a 2.25” pitch.

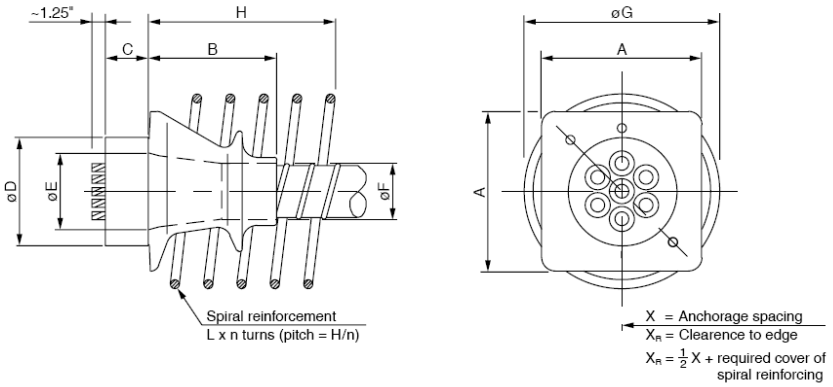

Figure 4-3: VSL Type EC5-19 Anchorage (VSL Corp.)

The mild reinforcing steel required in the general zone for the chosen segment was provided in the contract plans of the Choctawhatchee Bay Bridge and is rather complex. The detailed contract drawing can be seen in Figure 4-4.

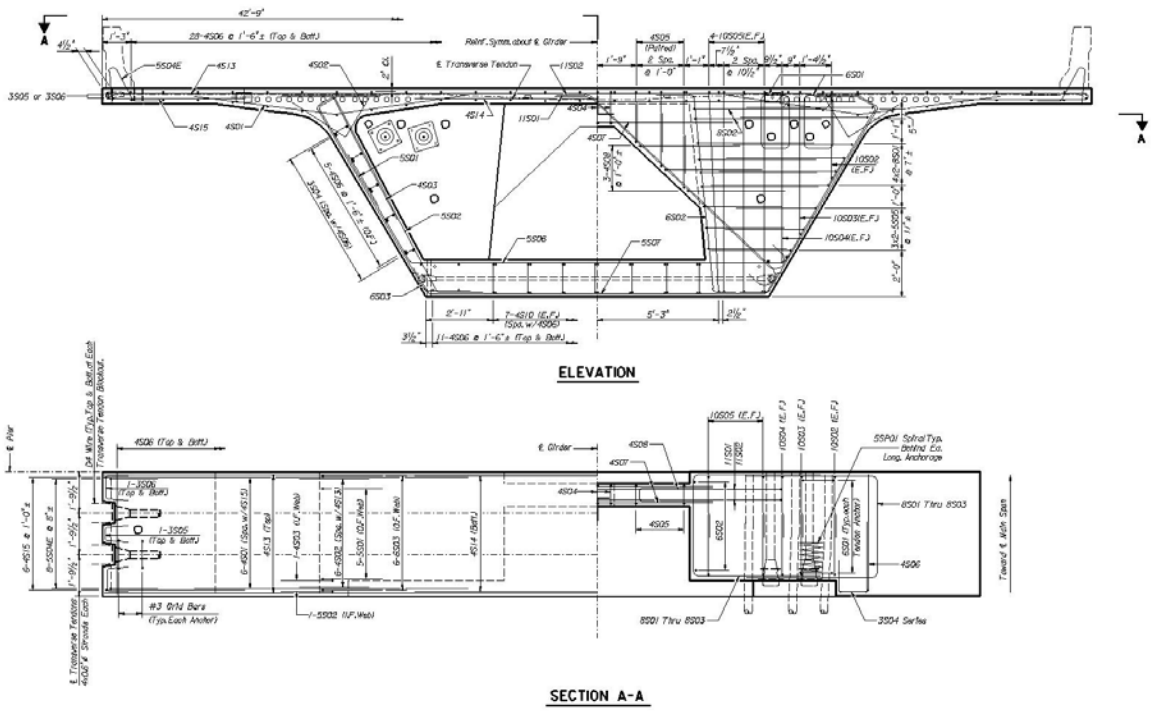

Figure 4-4: Choctawhatchee Main Span Pier Segment Reinforcing (FIGG)

4.3 Development of the Finite Element Model for Bridge Segment

The first step in developing the 3-D finite element model was to input the geometry of the segment, including the post-tensioning duct and anchorage, into ANSYS. First, the key points for the model were defined. Then the lines were drawn between key points to form the boundaries of the segment and also to break the segment into subunits for meshing purposes. Lastly, volumes were created based on the areas in the model. Several ways of breaking up the segment were explored and the optimal segment was taken as seen in Figure 4.5.

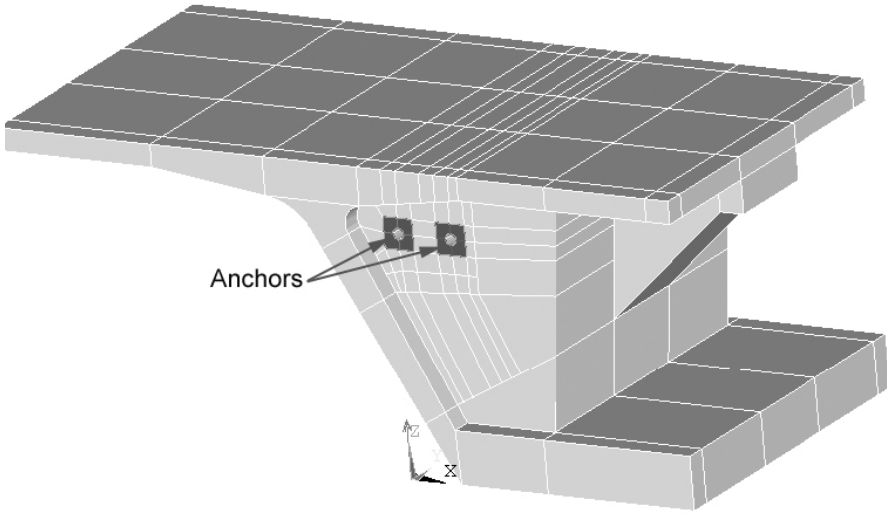

Figure 4-5: ANSYS Model of Volumes

The optimal designation has to do with the meshing capabilities of the program. A few rules to follow are given. The mesh should consist of quad (brick) elements; therefore all volumes must be either four or six sided. Due to the complex geometry of the segment, there were volumes that had to be five sided. In this situation two sides were chosen to act as one, which the program calls concatenation. This means that the mesh will flow from one side and disperse to the two concatenated sides. The mesh should also be fairly consistent. The density of the mesh should be similar throughout the segment to prevent clusters of nodes from forming in places with tight geometry. These clusters can cause stress concentrations in the analysis, raising questions on the validity of the results. The current model has the 463 key points, 1,155 lines, 914 areas, 230 volumes, and 6,082 solid and shell elements.

4.4 Elements & Material Properties

Once the geometry was input, the necessary properties of the segment had to be input in ANSYS. The necessary properties involved choosing the element that would be used to mesh the segment along with defining the material properties of the segment. The segment consists of concrete (with reinforcing steel), steel anchorages, and steel ducts. A complete list of the required material properties is provided in Table 4-2.

Table 4-2: Material Properties for ANSYS Finite Element Model

Concrete Properties	
Density	150 pcf
Modulus of Elasticity	4,792,817 psi
Poisson's Ratio	0.20
Steel Properties	
Density	490 pcf
Modulus of Elasticity	29,000,000 psi
Poisson's Ratio	0.30

The concrete portion of the segment was meshed using the SOLID65-3D reinforced concrete element from ANSYS. This element is used for the 3-D modeling of solids with or without reinforcing bars. It is capable of simulating tension cracks, compressive crushing, plastic deformation, and creep for the concrete. It also simulates tension and compression in the reinforcing (ANSYS 10.0, 2004). In concrete applications, for example, the solid capability of the element may be used to model the concrete while the rebar capability is available for modeling reinforcement behavior. Other cases for which the element is also applicable would be reinforced composites (such as fibers). The element is defined by eight nodes each having three degrees of freedom: translations in the nodal x, y, and z directions. Up to three different

rebar specifications may be defined. The meshed finite element model is shown in Figure 4-6.

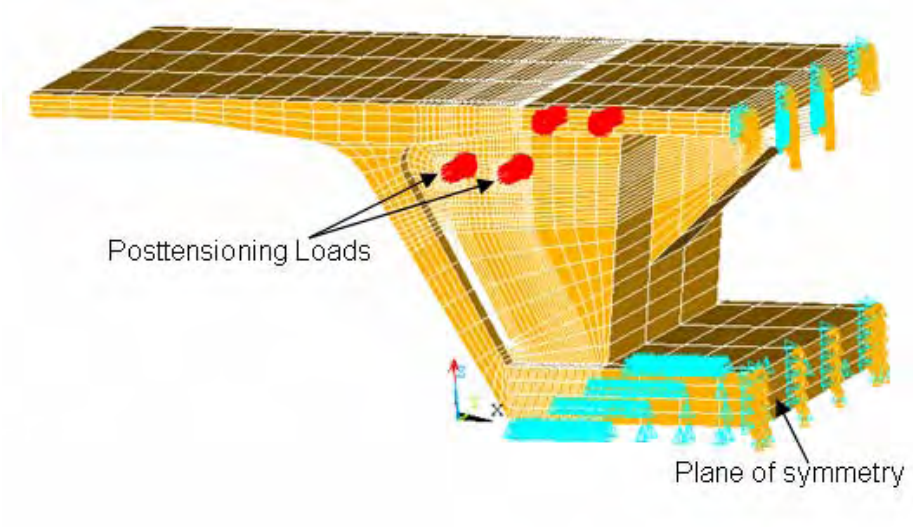

Figure 4-6: Segments Modeled for FEM Analysis

Table 4-3 details these segments. As previously mentioned, the compressive and tensile strengths increase with the addition of steel fiber. The segments had varying amounts of steel fibers and the design required mild steel reinforcement. The designation of 100% mild reinforcement is based on the design-required amount and indicates that 100% of what was required by design was modeled. The purposes of the differing amounts of fiber were to determine the optimal amount of fiber to add for increased strength. Additional segments were analyzed with the optimal amount of fiber and decreased mild reinforcement to prove that the addition of fiber allows a reduction in mild reinforcement.

Table 4-3: Segments Modeled Using ANSYS

Finite Element Model No.	Fiber Volume (% concrete vol.)	Mild Reinforcement (% required)	Compressive Strength (psi)	Tensile Strength (psi)
1	0	100	6,250	625
2	0.25	100	7,112	631
3	0.25	0	7,112	631
4	0.50	100	7,187	655
5	0.50	0	7,187	655
6	0.75	100	7,281	724
7	0.75	0	7,281	724
8	1.0	100	7,393	863
9	1.0	0	7,393	863

4.5 FEM Stress Results & Discussion

Stress results obtained from the FEM are presented and discussed in this section. A discussion of each analysis along with the reasoning behind the particular analysis follows. Individual analysis results are presented separately. Finally, a comparison of the analyses is presented. Segment 1 (Table 4.3) was the control analysis that contained the design required amount of mild steel reinforcement with no steel fiber reinforcement. This analysis was performed to provide predicted results to a solution in order to prove the validity of the model. It also gave a basis for which to compare results of segments with fiber. This segment was loaded with 1,256 kips of post-tensioning force on each face and the resulting stress contours at the general zone can be seen in Figures 4.7 through 4.14. Figures 4.7 through 4.9 show the X-, Y-, and Z-component stresses, respectively. Figures 4.10 through 4.12 show the 1^{st}, 2^{nd}, and 3^{rd} principal stresses, respectively and Figure 4.13 shows the Von Mises stress

contour. These are shown in order to emphasize that all stresses were studied to provide confidence in the finite element model and results. Out of all of the stresses considered in this study, the X-component stress is the most important since it reflects the tensile bursting force in the general anchorage zone. Figure 4-14 shows a plot of the X-component stresses versus distance across the ducts in the general zone. Table 4-4 details the maximum X-component stress results in the general zone for segment 1.

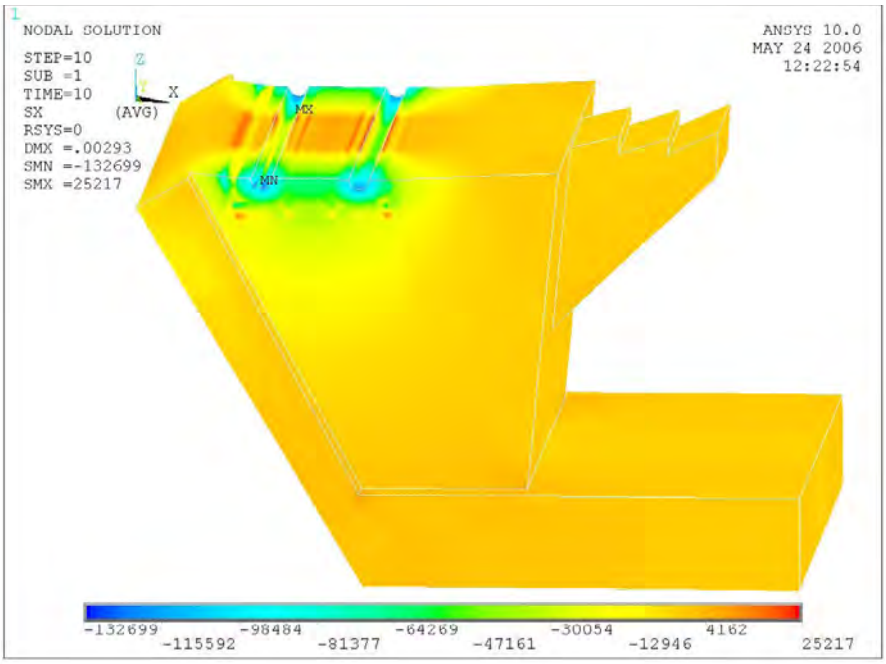

Figure 4-7: X-Component Stress (lb/ft^2) Contour in Segment 1

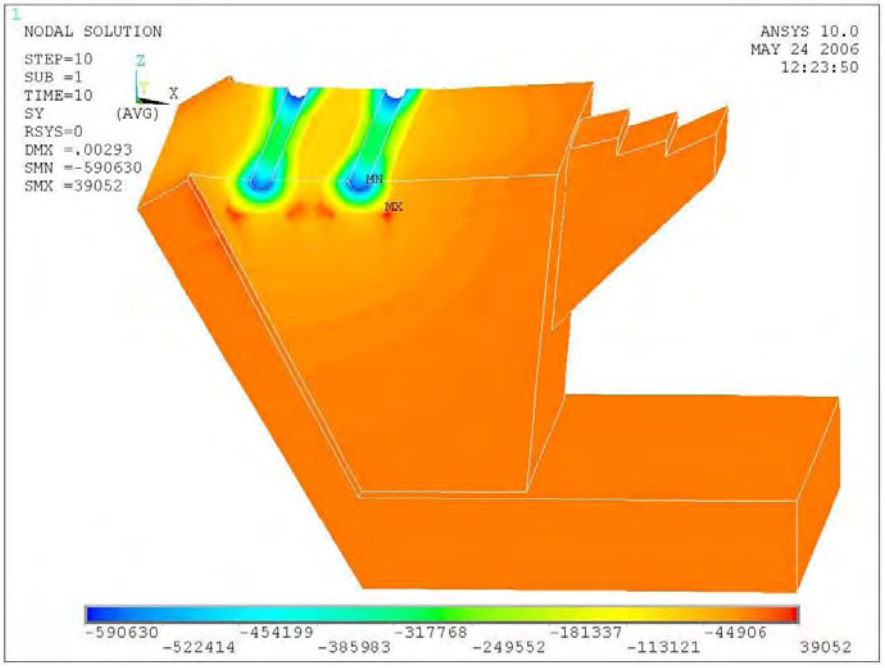

Figure 4-8: Y-Component Stress (lb/ft^2) Contour in Segment 1

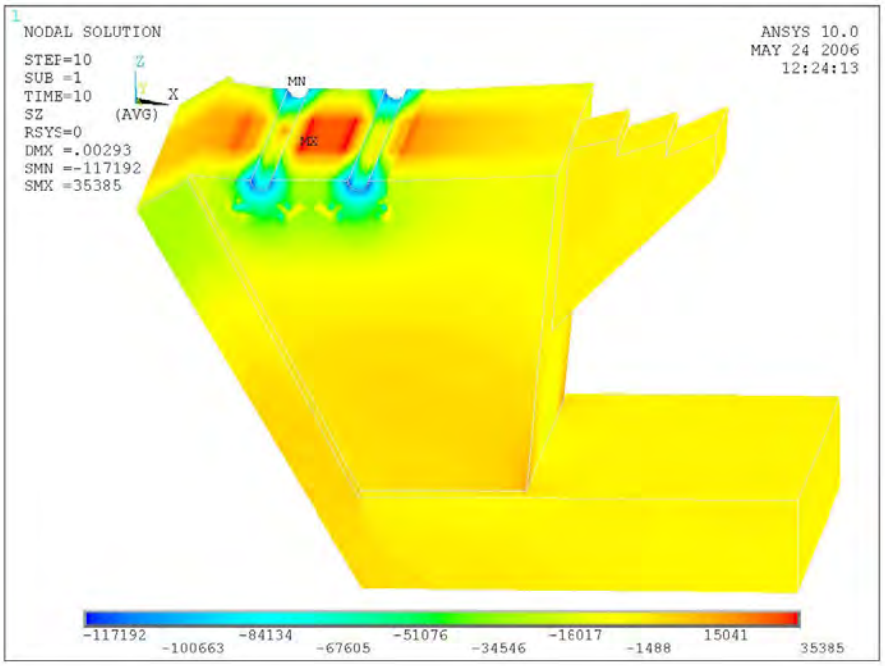

Figure 4-9: Z- Component Stress (lb/ft^2) Contour in Segment 1

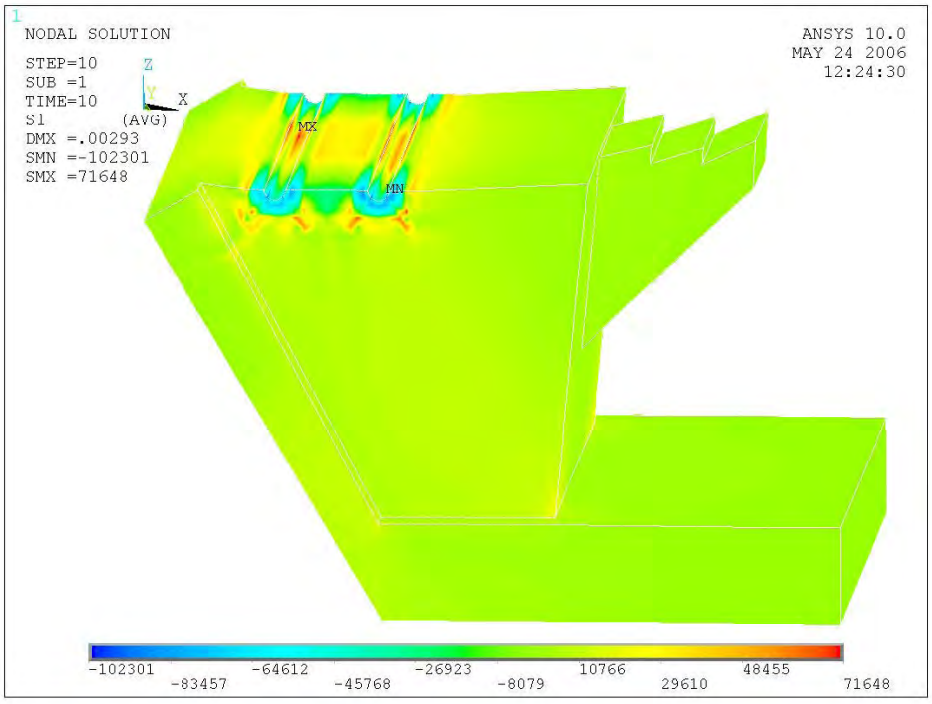

Figure 4-10: 1st Principal Stress (lb/ft^2) Contour in Segment 1

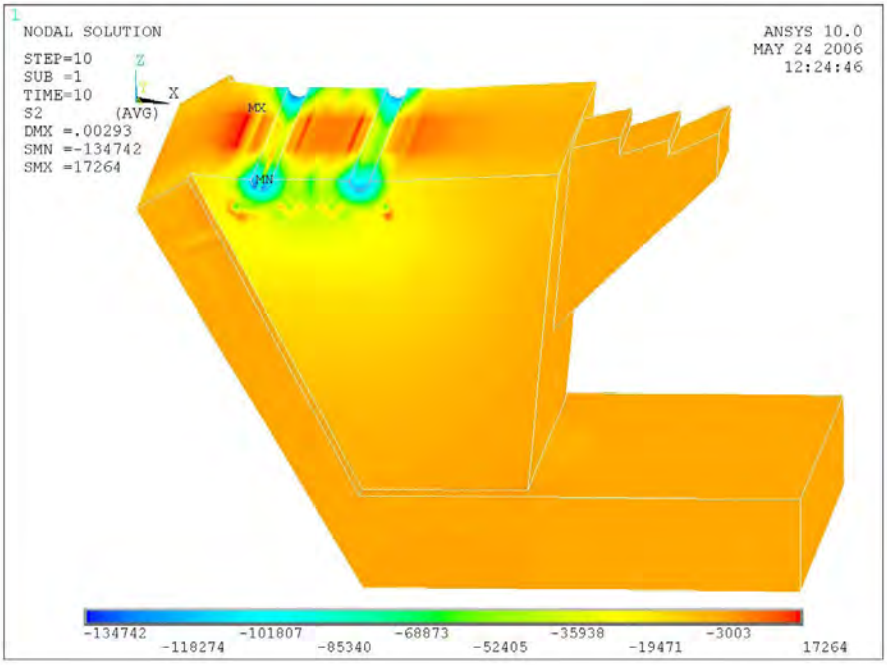

Figure 4-11: 2nd Principal Stress (lb/ft^2) Contour in Segment 1

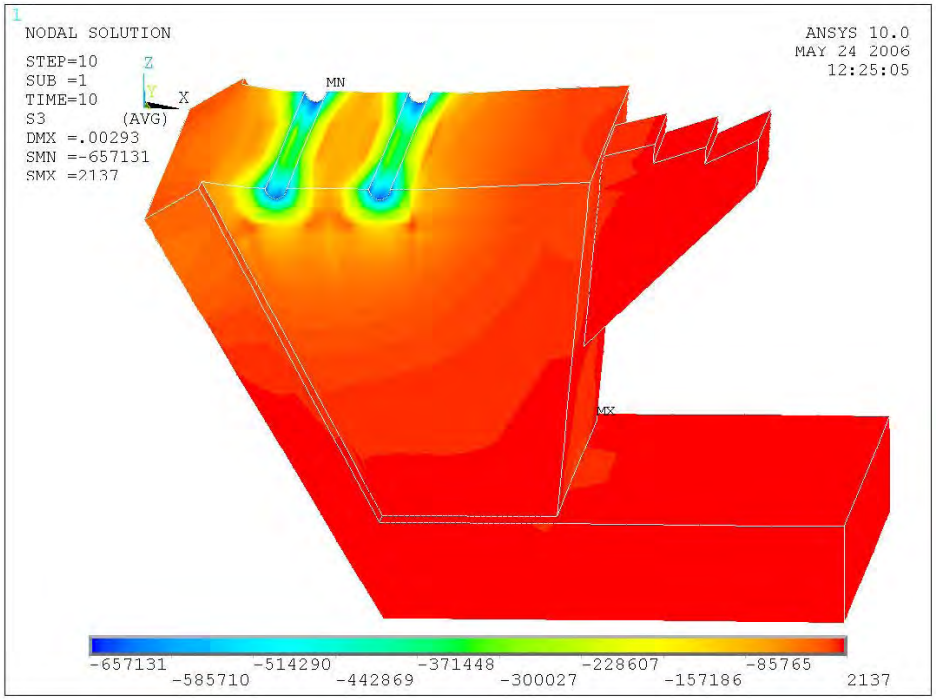

Figure 4-12: 3rd Principal Stress (lb/ft^2) Contour in Segment 1

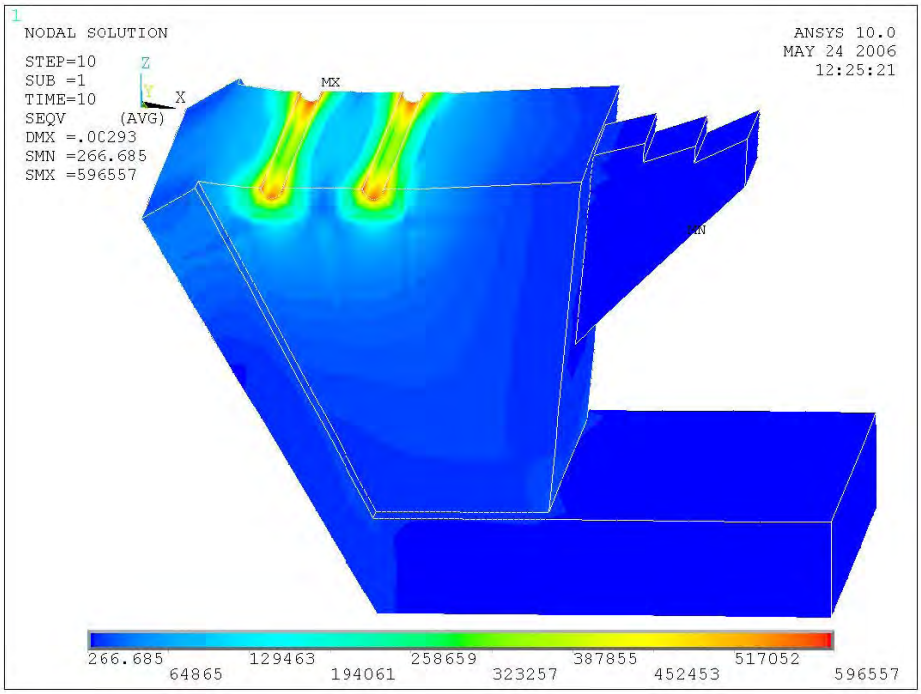

Figure 4-13: Von Mises Stress (lb/ft^2) Contour in Segment 1

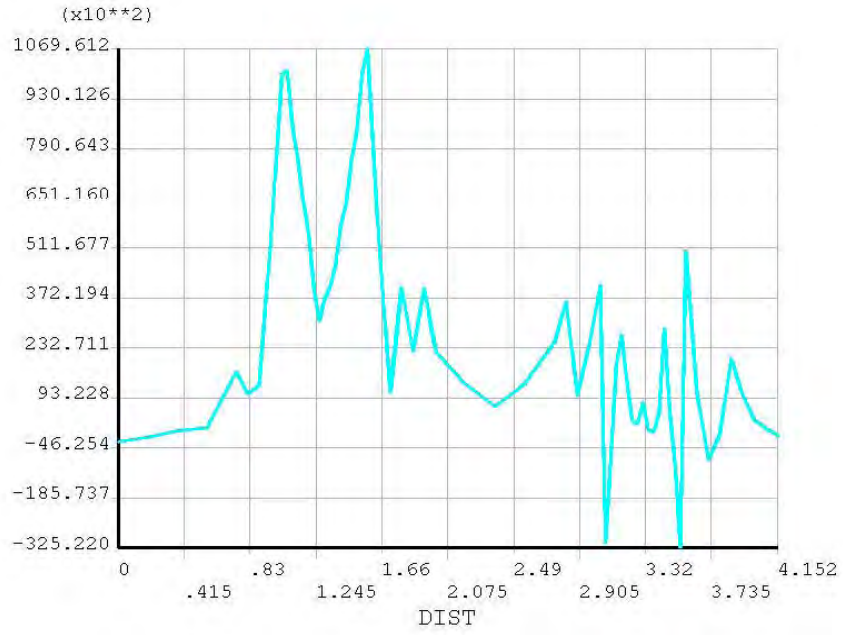

Figure 4-14: X-Component Stress (lb/ft^2) vs. Distance across Ducts in Segment 1

Segments 2, 4, 6, and 8 contained 100% of the design required amount of mild steel reinforcement and 0.25%, 0.50%, 0.75%, and 1.0% steel fiber reinforcement, respectively. A post-tensioning force of 1,256 kips was applied to these models on each face. These analyses were performed in order to determine the effect of the corresponding percentage of steel fibers on the modeled segments. Figures 4-15 through 4-17 show the X-, Y-, and Z-component stress contours, respectively. Figure 4.18 shows the Von Mises stress contour for Segment 2. Figure 4-19 shows a plot of the X-component stresses versus the distance across the ducts in Segment 2. Figures 4-20 through 4-22 show the X-, Y-, and Z-component stress contours, respectively. Figure 4-23 shows the Von Mises stress contour for Segment 4. Figure 4-24 shows a plot of the X-component stresses versus the distance across the ducts in Segment 4. Figures 4-25 through 4-27 show the X-, Y-, and Z-component stress contours, respectively. Figure 4.28 shows the Von

Mises stress contour for Segment 6. Figure 4-29 shows a plot of the X-component stresses versus the distance across the ducts in Segment 6. Figures 4-30 through 4-32 show the X-, Y-, and Z-component stress contours, respectively and Figure 4-33 shows the Von Mises stress contour for Segment 8. Figure 4-34 shows a plot of the X-component stresses versus the distance across the ducts in Segment 8. Table 4-4 also details the maximum X-component stresses in the general zones of segments 2, 4, 6, and 8.

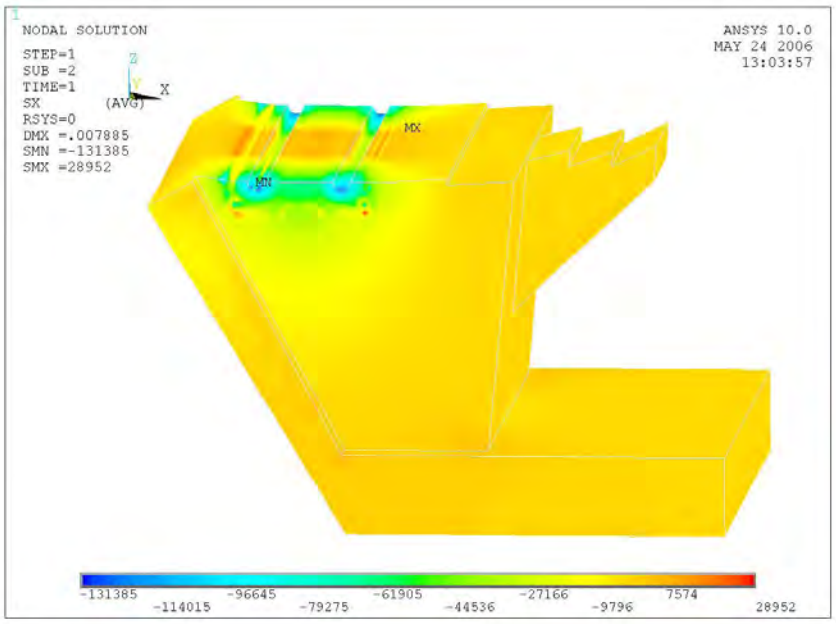

Figure 4-15: X-Component Stress (lb/ft^2) Contour in Segment 2

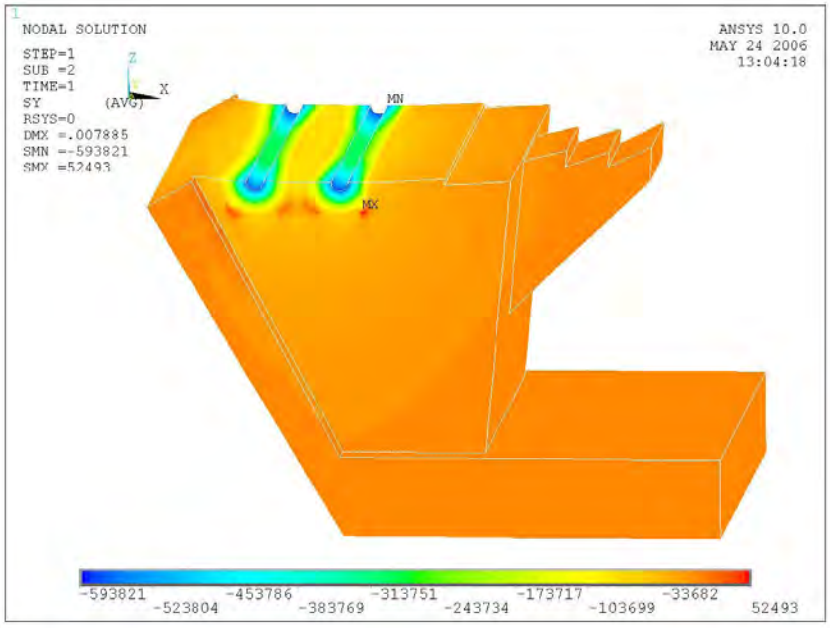

Figure 4-16: Y-Component Stress (lb/ft^2) Contour in Segment

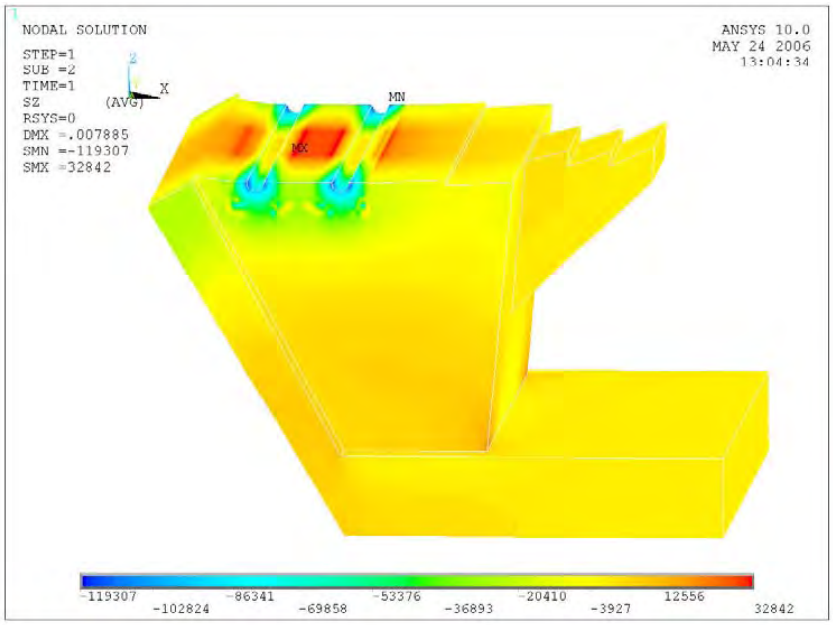

Figure 4-17: Z-Component Stress (lb/ft^2) Contour in Segment 2

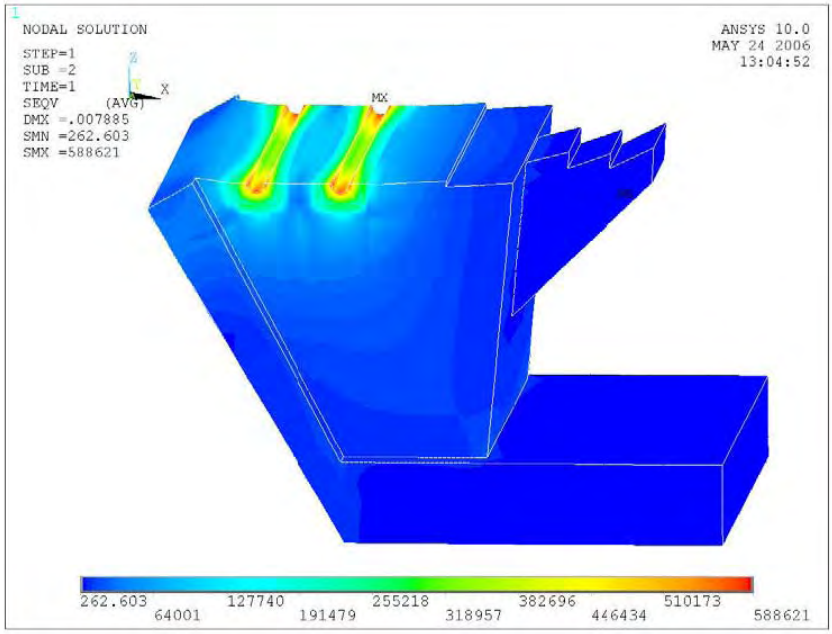

Figure 4-18: Von Mises Stress (lb/ft^2) Contour in Segment 2

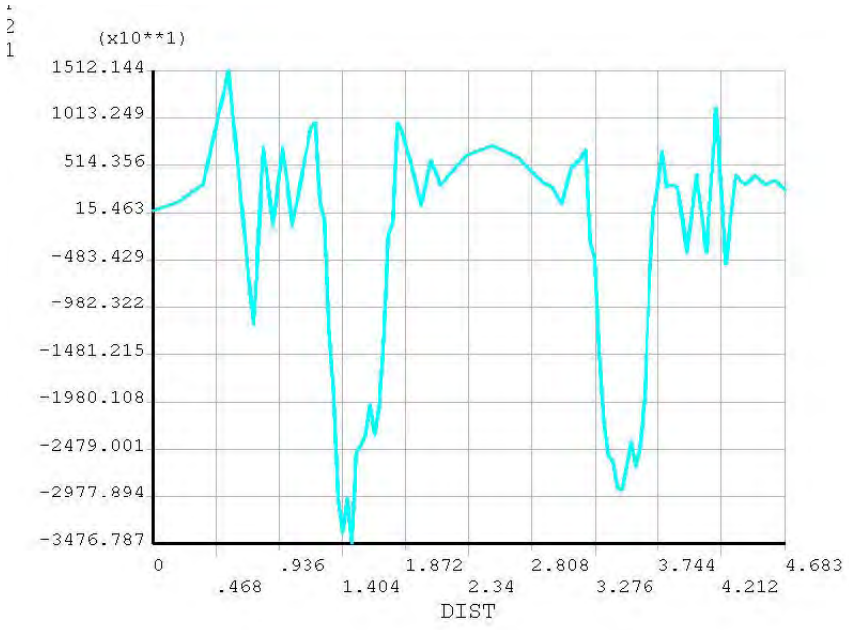

Figure 4-19: X-Component Stress (lb/ft^2) vs. Distance Across Ducts in Segment 2

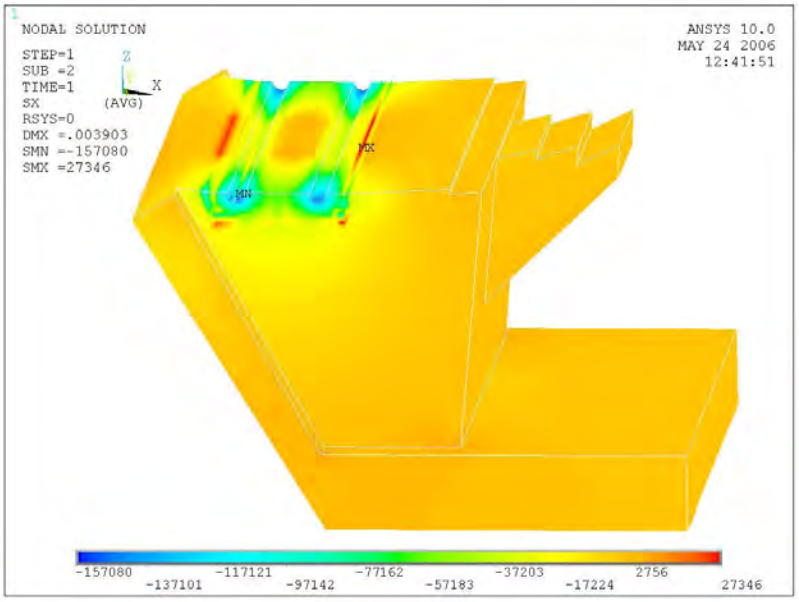

Figure 4-20: X-Component Stress (lb/ft^2) Contour in Segment 4

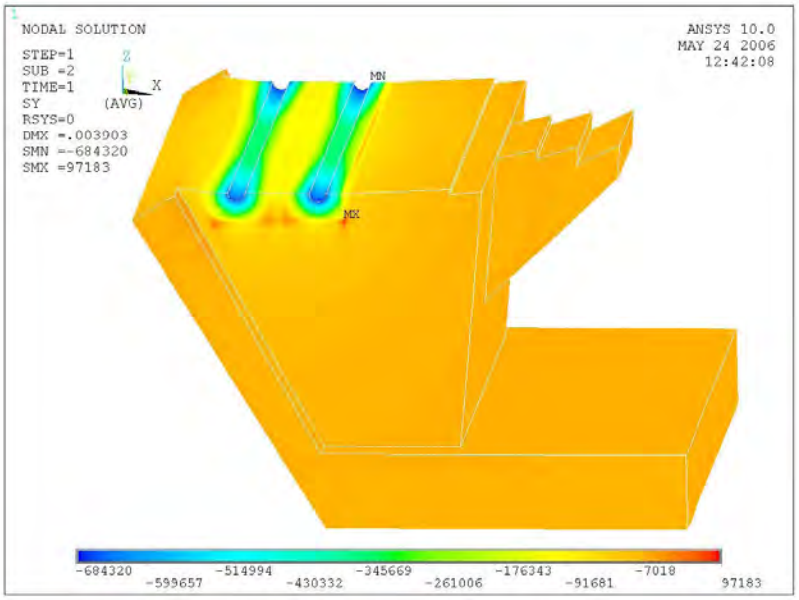

Figure 4-21: Y-Component Stress (lb/ft^2) Contour in Segment 4

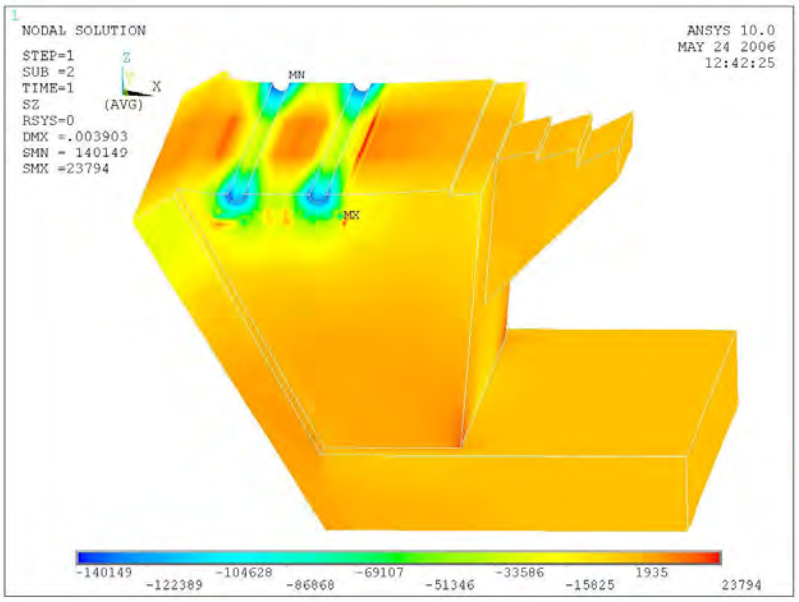

Figure 4-22: Z-Component Stress (lb/ft^2) Contour in Segment 4

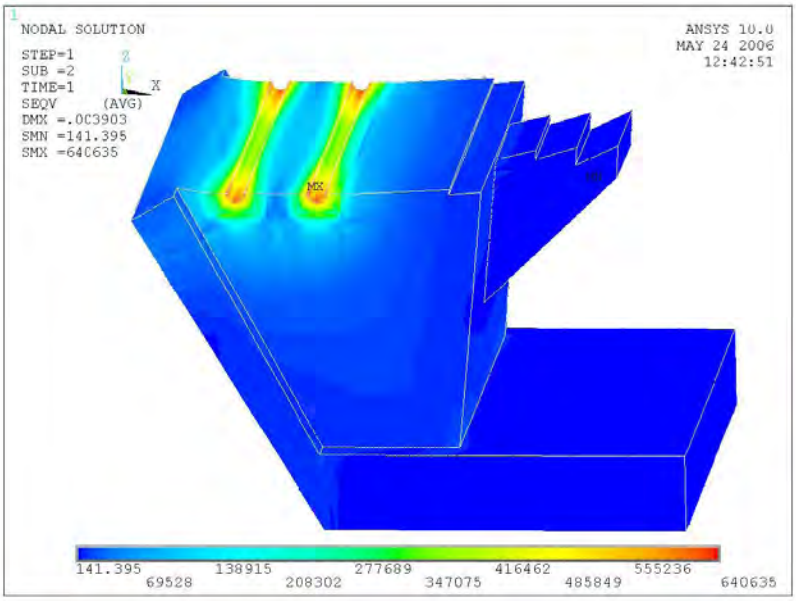

Figure 4-23: Von Mises Stress (lb/ft^2) Contour in Segment 4

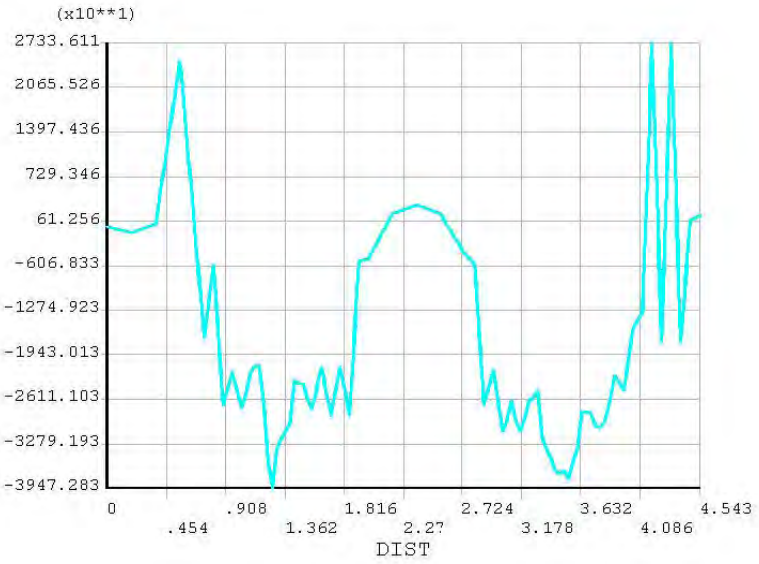

Figure 4-24: X-Component Stress(lb/ft^2) vs. Distance Across Ducts n Segment 4

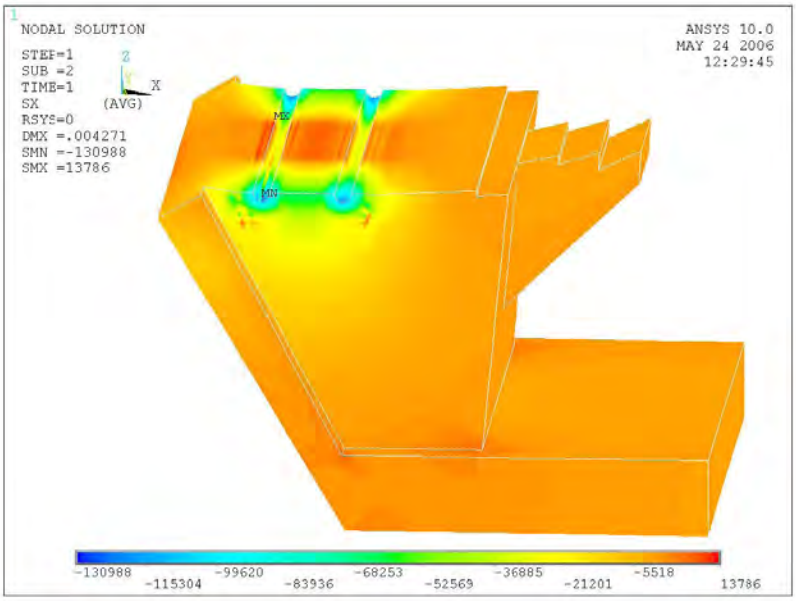

Figure 4-25: X-Component Stress (lb/ft^2) Contour in Segment 6

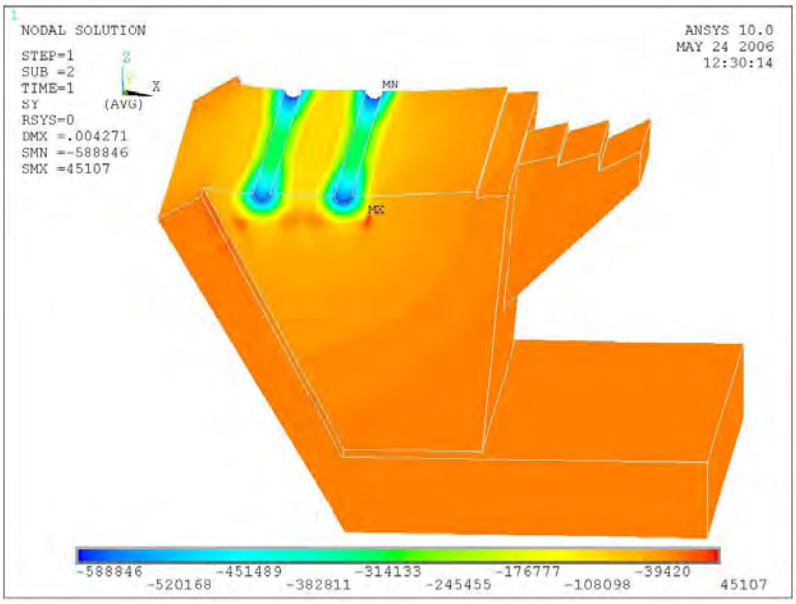

Figure 4-26: Y-Component Stress (lb/ft^2) Contour in Segment 6

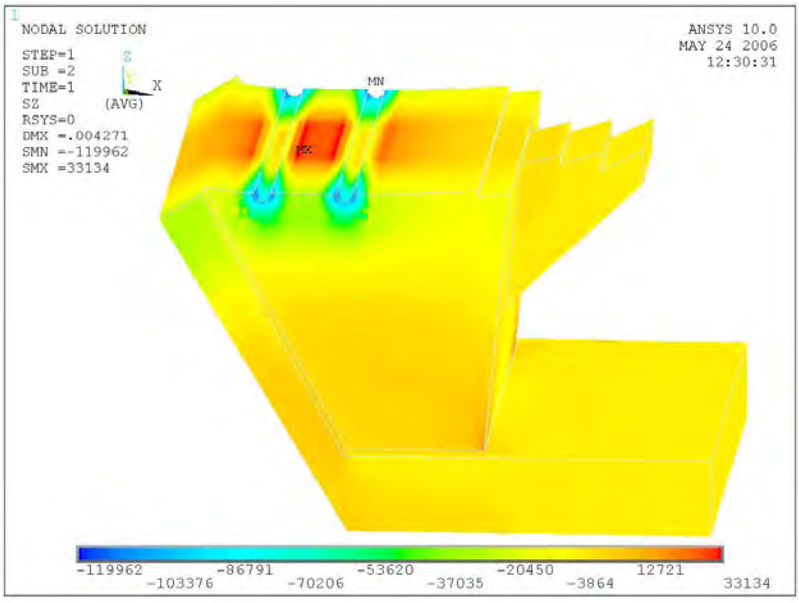

Figure 4-27: Z-Component Stress (lb/ft^2) Contour in Segment 6

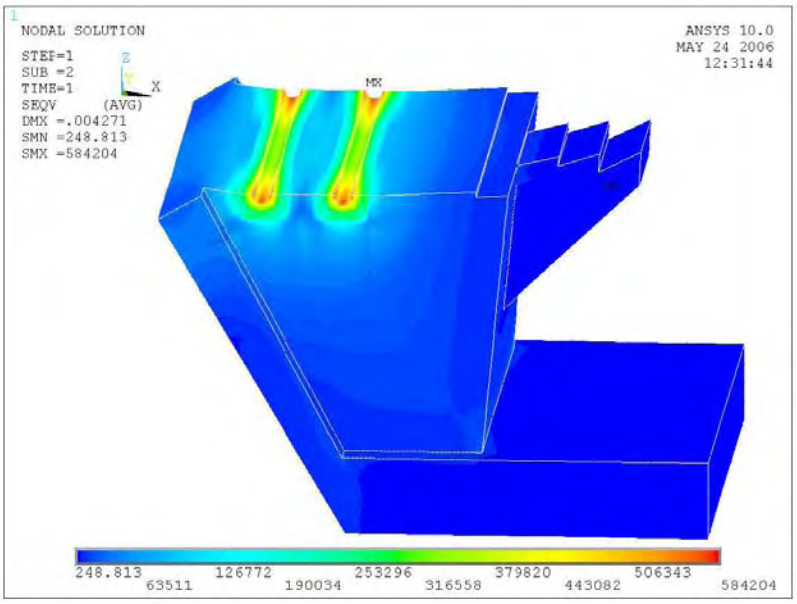

Figure 4-28: Von Mises Stress (lb/ft^2) Contour in Segment 6

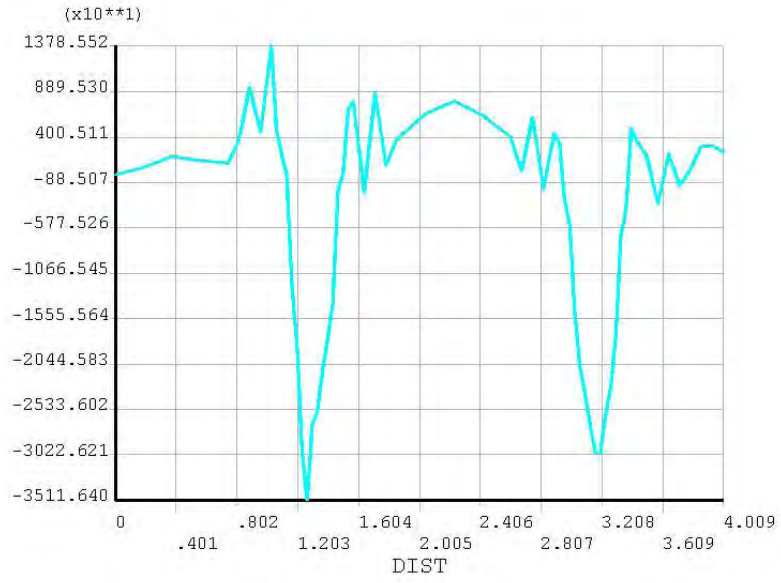

Figure 4-29: X-Component Stress (lb/ft^2) vs. Distance across Ducts in Segment 6

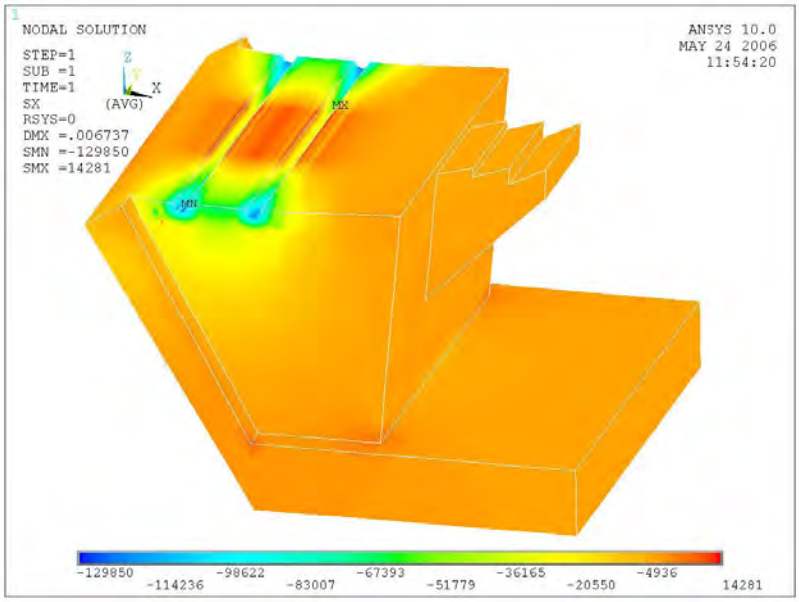

Figure 4-30: X-Component Stress (lb/ft^2) Contour in Segment 8

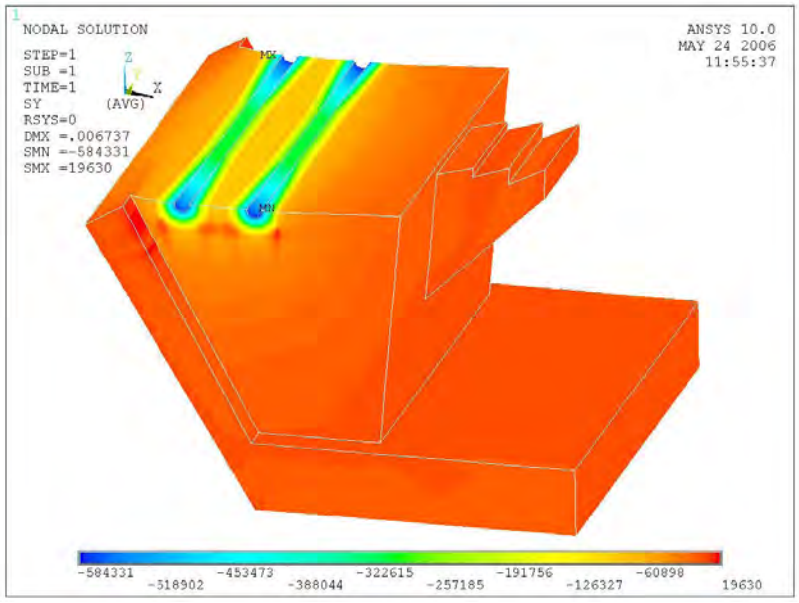

Figure 4-31: Y-Component Stress (lb/ft^2) Contour in Segment 8

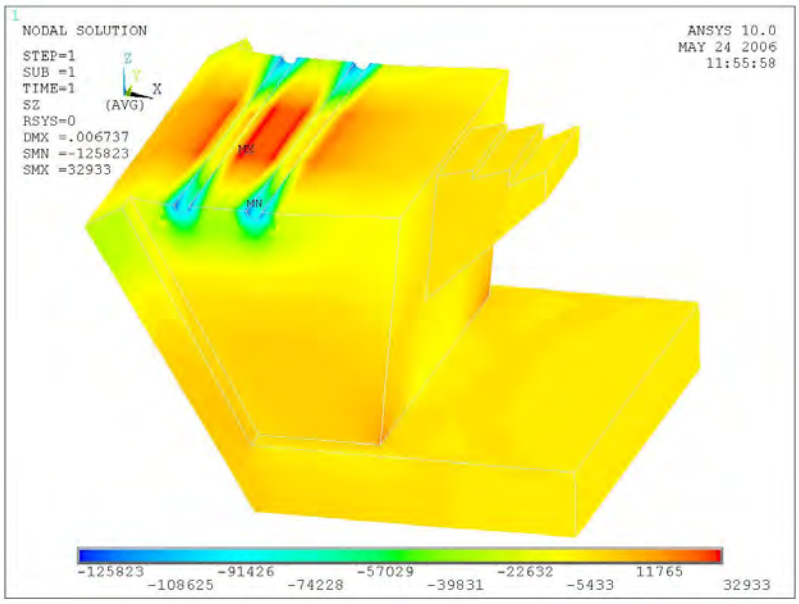

Figure 4-32: Z-Component Stress (lb/ft^2) Contour in Segment 8

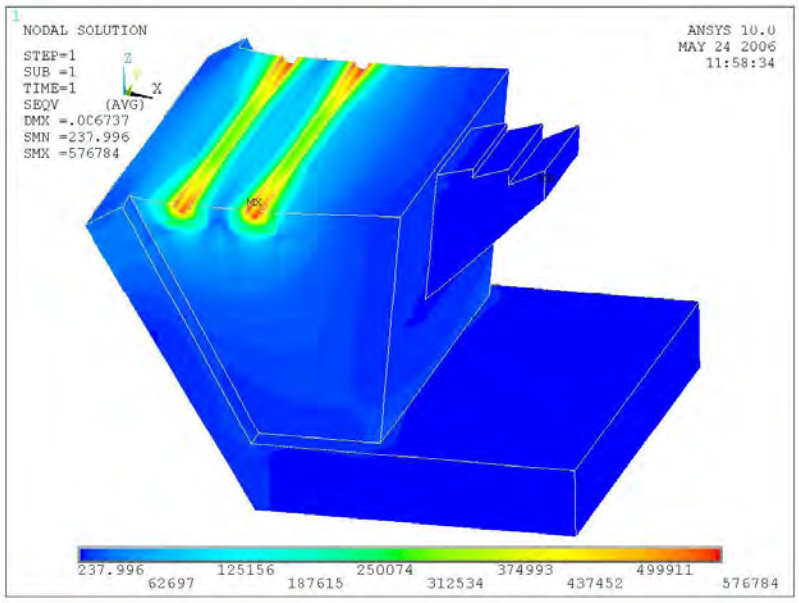

Figure 4-33: Von Mises Stress (lb/ft^2) Contour in Segment 8

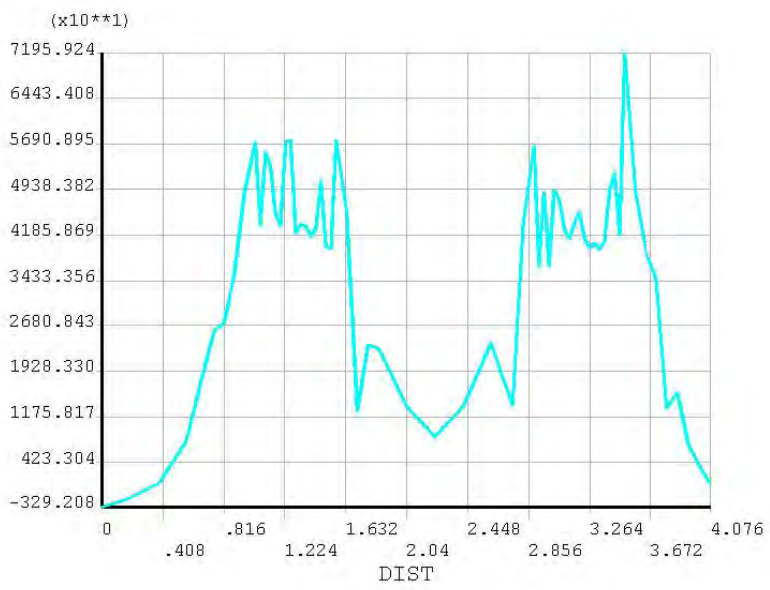

Figure 4-34: X-Component Stress (lb/ft^2) vs. Distance across Ducts in Segment 8

Table 4-4: Comparison of Maximum X-Component Stresses

Finite Element Model No.	Fiber Volume (% concrete volume)	Mild Reinforcement (% required)	Max. X-Component Stress (psi)
1	0	100	175.1
2	0.25	100	105.0
4	0.50	100	97.0
6	0.75	100	95.7
8	1.0	100	99.2

Segments 3, 5, 7, and 9 contained no mild steel reinforcement and 0.25%, 0.50%, 0.75%, and 1.0% steel fiber reinforcement, respectively. These analyses were performed in order to study the behavior of segments that contain only steel fiber reinforcement in the corresponding amounts. Segments 3 and 5 failed at approximately 40% of the load application in the

analyses. This was determined because the finite element model would not produce a converged solution past the 40% load step. Failure cracking occurred around the ducts and can be seen in Figures 4-35 and 4-36. Segments 7 and 9 sustained the entire load. However, severe cracks formed around the ducts similar to those in segments 3 and 5, and can be seen in Figures 4-37 and 4-38. It may be inferred that mild steel in the general zone cannot be completely replaced by steel fiber, at least in the amounts studied. Therefore, these cases were not further investigated herein. See Table 4-5 for failure load results of segments 3, 5, 7, & 9.

Table 4-5: Failure Load Results

Finite Element Model No.	Fiber Volume (% concrete volume)	Mild Reinforcement (% required)	Failure Load (kips)
3	0.25	0	502.4
5	0.50	0	502.4
7	0.75	0	1256
9	1.00	0	1256

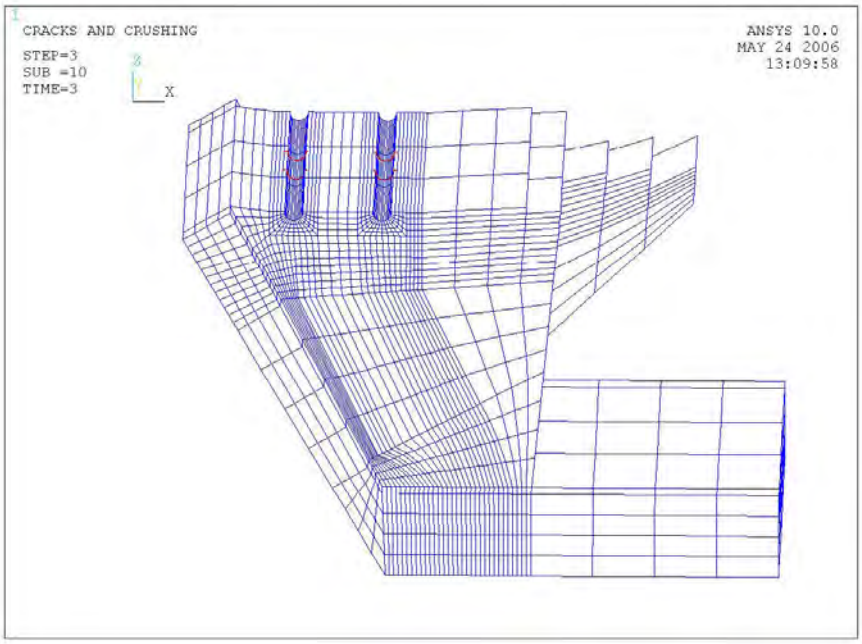

Figure 4-35: Cracks in Segment 3 at Failure

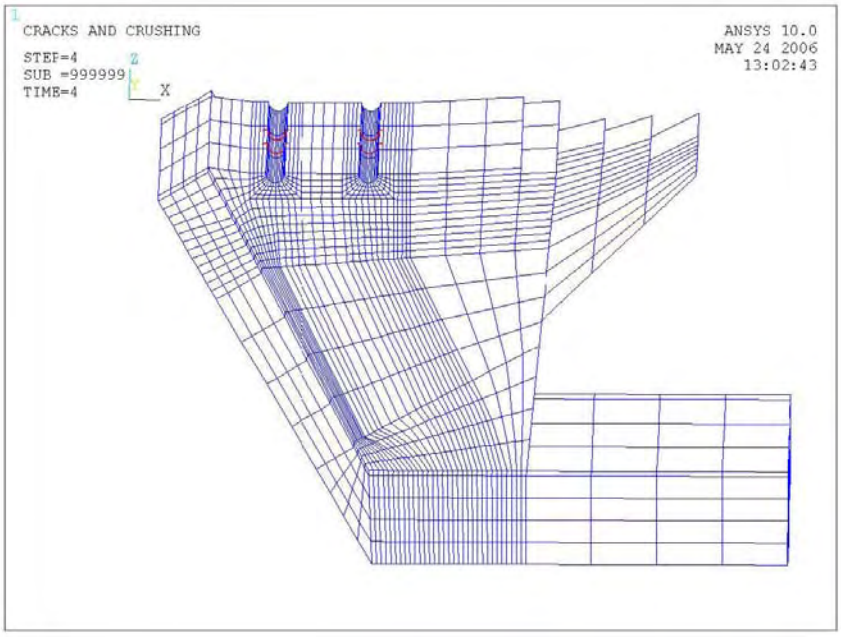

Figure 4-36: Cracks in Segment 5 at Failure

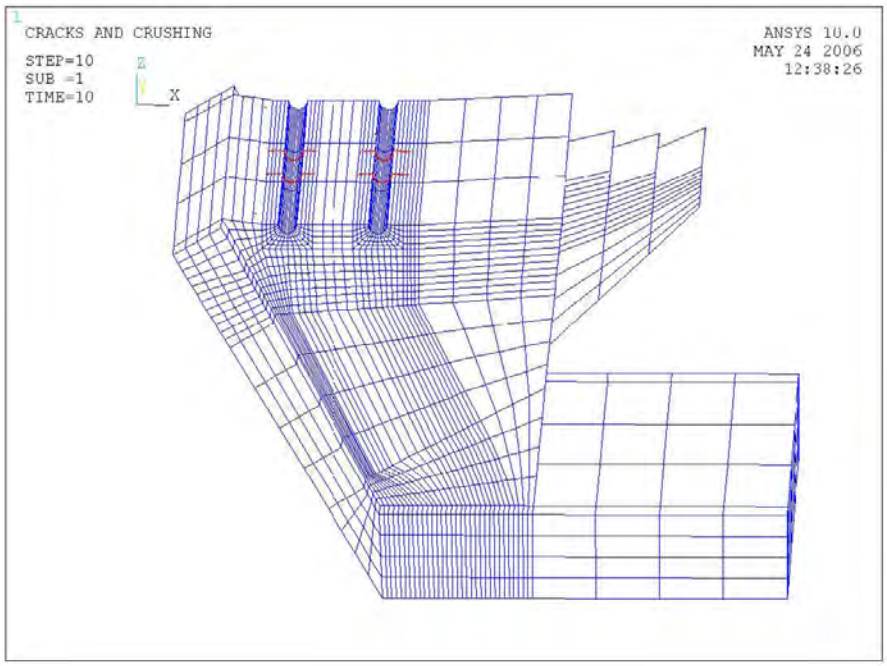

Figure 4-37: Cracks in Segment 7

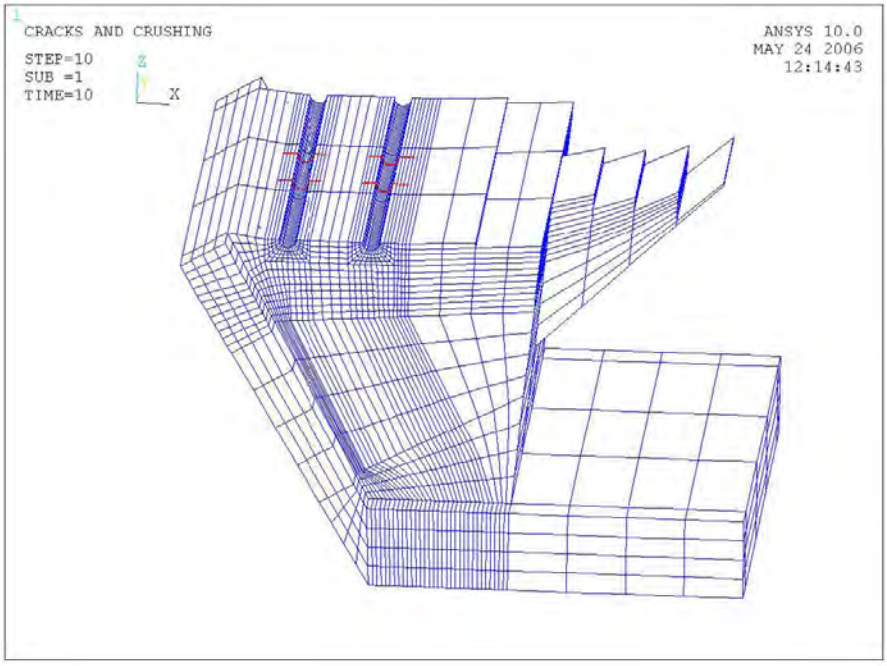

Figure 4-38: Cracks in Segment 9

Maximum stress versus amount of steel fiber results were plotted for segments 1, 2, 4, 6, and 8 and are shown in Figure 4-39. As expected, the curve shows that stresses decreased with the addition of steel fiber. From the curve, it can be seen that the greatest stress reduction occurred when 0.75% steel fibers were added to the concrete. It can also be seen that the addition of steel fiber in 1.0% amounts actually causes an increase in stresses in the general zone as compared to the 0.50% and 0.75%. Placement of steel fiber adds dead load to the segment. This increase in dead load causes an increase in stresses in all directions, since the steel fibers are placed in all directions. Table 4-6 shows the amount of load that was added to the general zone with each amount of steel studied. These loads are relatively small in comparison to the post-tensioning load and the increase in stress is relatively small in comparison to the lower fiber percentages.

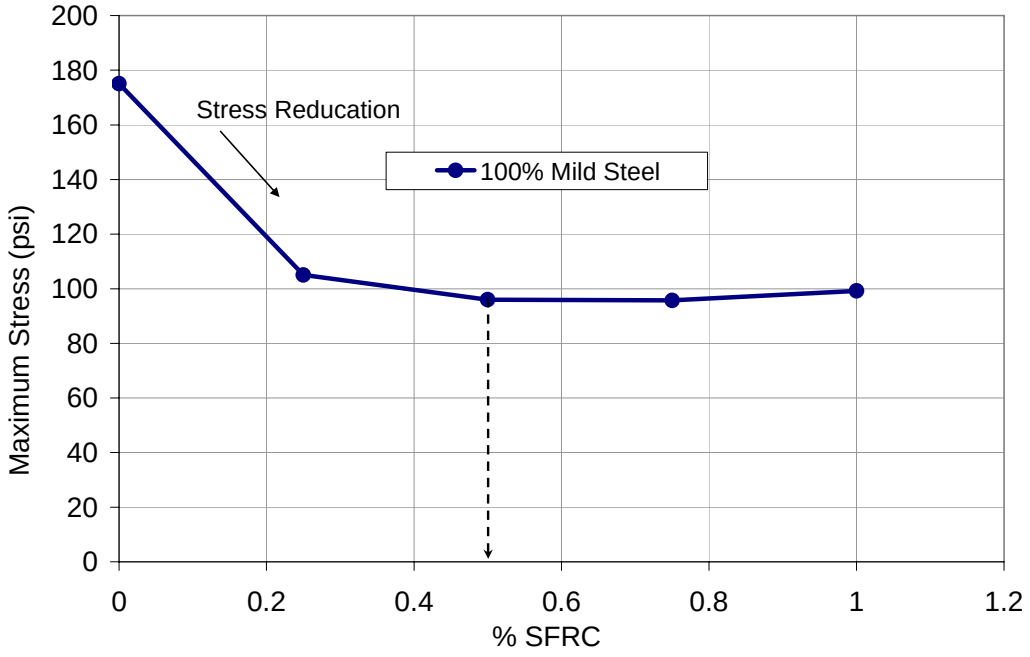

Figure 4-39: Maximum X-Component Stress vs. % Fiber

Table 4-6: Load Addition due to Steel Fiber

Segment	% Steel Fiber	Load Addition (lbs.)
2	0.25	68
4	0.50	135
6	0.75	203
8	1.0	270

Based on the comparison in Figure 4-39, it was reasoned that by adding 0.50% steel fiber the mild steel reinforcement could be decreased. The selection of 0.50% was made due to the fact that steel fiber in this amount will be more workable in construction situations than higher amounts, as previously discussed in Chapter 2. So, the next task involved finding the maximum amount by which the mild steel reinforcement could be reduced with 0.50% fiber application. Several FEM analyses were performed in order to complete this task. Three

additional segments were loaded with 1256 kips and studied. Table 4-7 shows results for steel amounts and X-component stress values in comparison to the control analysis.

Table 4-7: Comparison of Additional Segments

Segment	Fiber Volume (% concrete volume)	Mild Reinforcement (% required)	Max. X-Component Stress (psi)
1	0	100	175.1
10	0.50	50	129.3
11	0.50	45	143.1
12	0.50	44	Failure

Segment 10 contained 0.50% steel fiber and 50% design required mild steel reinforcement. Figure 4-40 shows the X-component stress contour of segment 10 at the general zone. Figure 4-41 shows a plot of X-component stresses versus distance across the ducts. The resulting maximum X-component stress was lower than the control analysis; so further reduction of the mild steel reinforcement was possible. Segment 11 contained 0.50% steel fiber and 45% design required mild steel. Figure 4-42 shows the X-component stress contour of segment 11 at the general zone. Figure 4-43 shows a plot of X-component stresses versus distance across the ducts. The maximum stress was still lower than the control analysis. In a final attempt to determine the maximum reduction, segment 12 was analyzed with 0.50% steel fiber and 44% mild steel reinforcement. The segment failed at 70% load application, or at approximately 879 kips. The cracking around the ducts was similar to segments 7 and 9 and is presented in Figure 4-44. The geometry of the block that contains the general stress zone in the segment is shown in Figure 4-45.

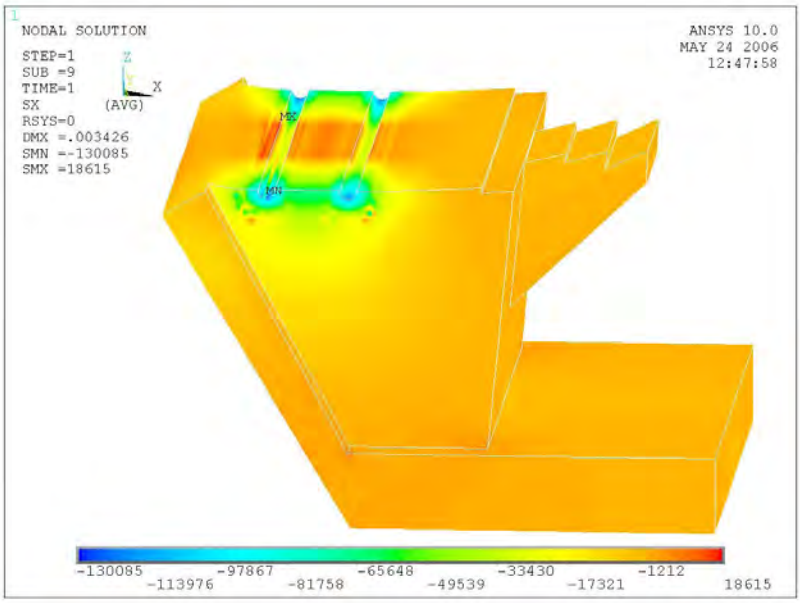

Figure 4-40: X-Component Stress (lb/ft^2) Contour in Segment 10

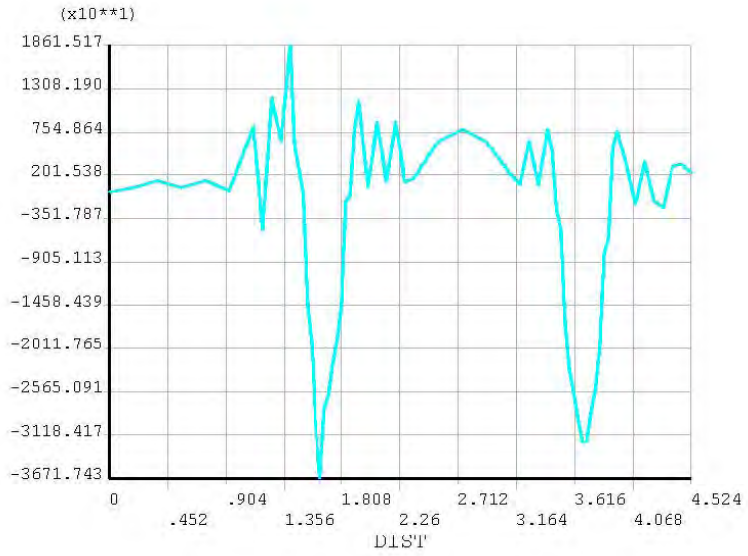

Figure 4-41: X-Component Stress (lb/ft^2) vs. Distance Across Ducts in Segment 10

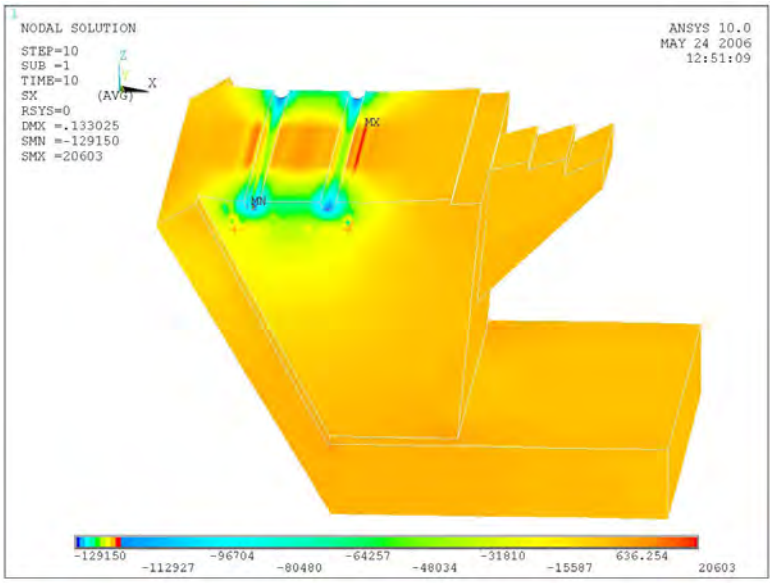

Figure 4-42: X-Component Stress (lb/ft^2) Contour in Segment 11

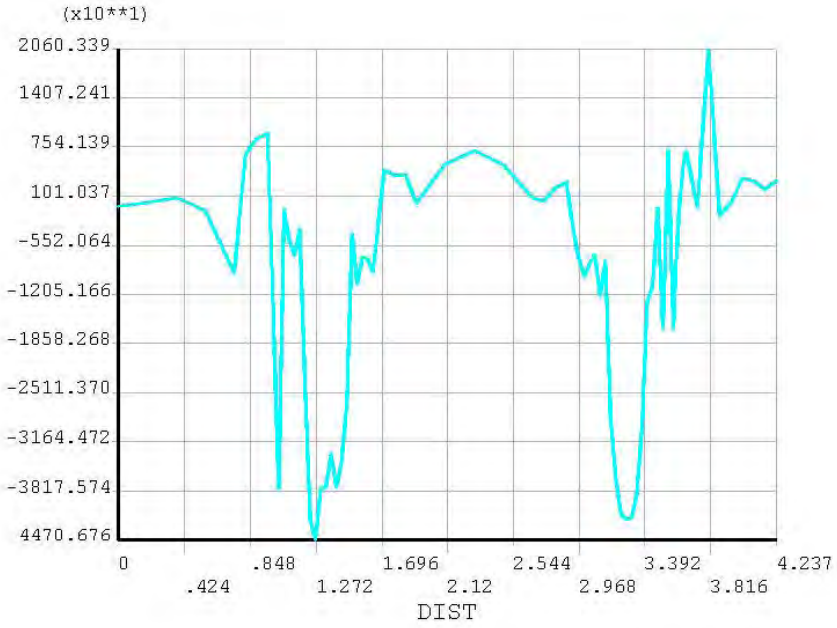

Figure 4-43: X-Component Stresses (lb/ft^2) vs. Distance across Ducts in Segment 11

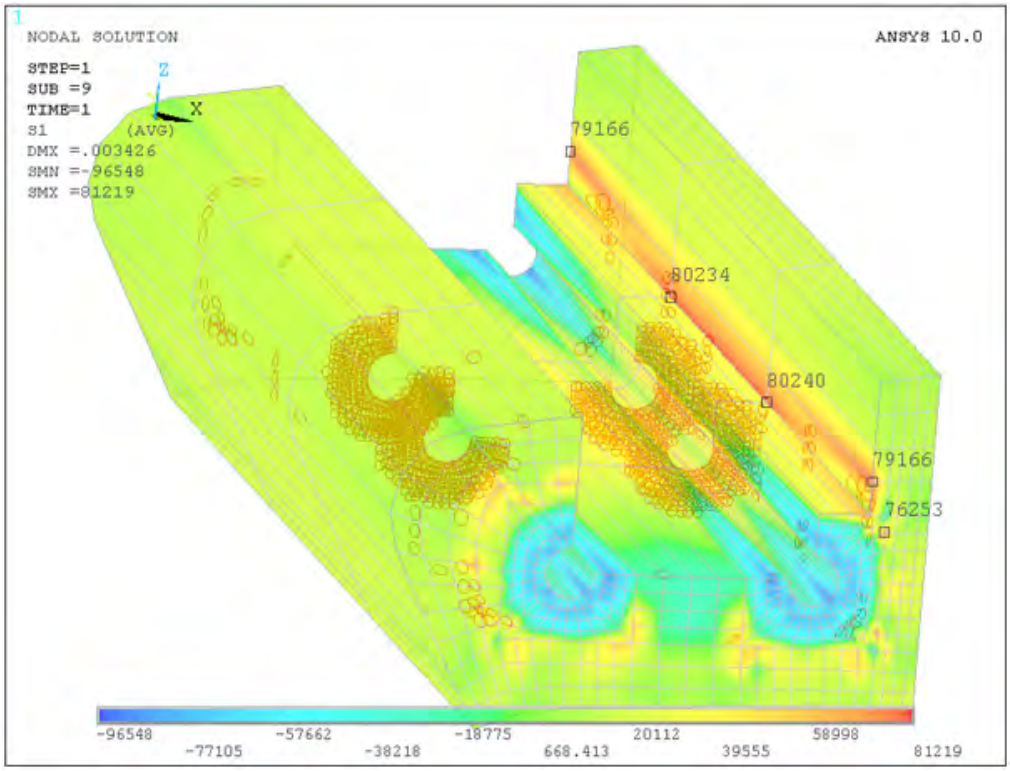

Figure 4-44: Crack distribution at Failure (red circles) in Segment 12

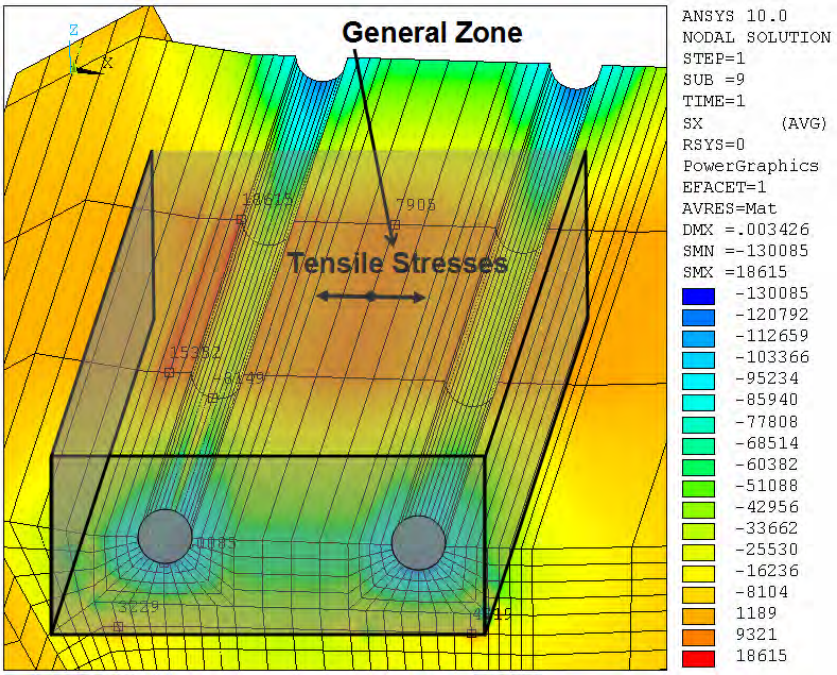

Figure 4-45: Stresses in General Zone

The maximum permissible reduction of mild steel reinforcement with the addition of 0.50% steel fiber was 55% in the general zone. However, the segment failed with a 56% reduction. Therefore, reducing the mild steel reinforcement in the general zone by 55% is not recommended. The optimal reduction would occur at 50% in order to be conservative and safe.

As previously mentioned, the addition of the steel fiber added self weight of the segment. It is reasonable to consider that the increased self weight would also impact other areas of the segment. Figure 4-46 shows the overall stress contour of segment 8, which contained 1.0% steel fiber and 100% mild steel reinforcement. Some stress concentrations could be seen at the top slab of the segment near the web-flange connection and at the unsupported portion of the top slab of the segment near the diaphragm (where the plates are located).

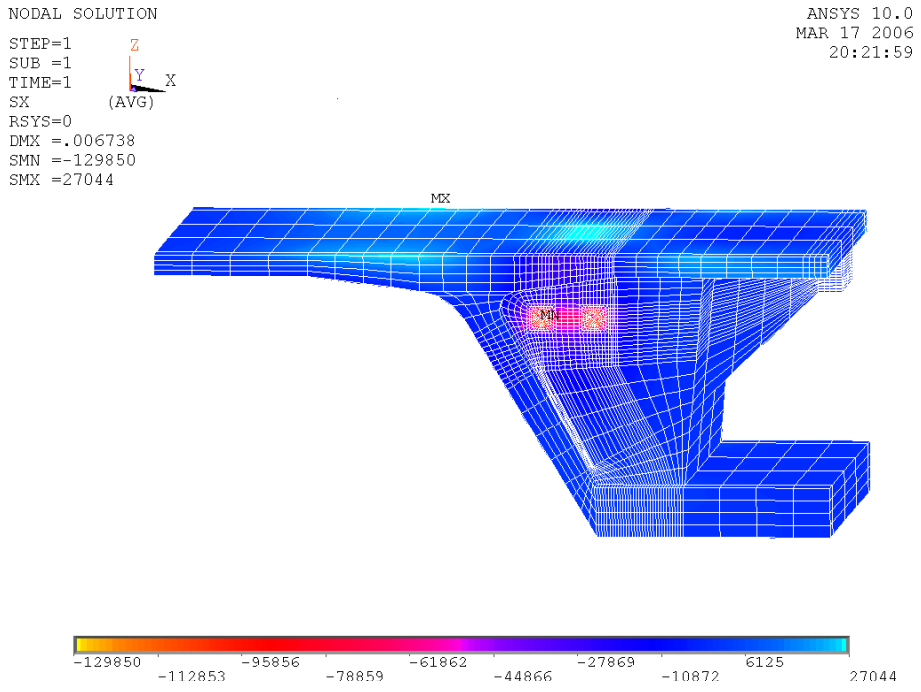

Figure 4-46: Overall Stress (lb/ft^2) Contour for Segment 8

4.6 AASHTO Requirements for General Zone Size

Section 5.10.9.6.1 of the AASHTO code lists conditions that must be true for stresses and forces to be estimated using the approximate stress analyses and design equations. One of the conditions stated in AASHTO Section 5.10.9.6.1 is that "the minimum edge distance of the anchorage in the main plane of the member is not less than 1.5 times the corresponding lateral dimension, a, of the anchorage device." Since the research team believed consideration should be given to the stresses that will develop between the two anchorage devices, the size of the anchorage test specimen was based upon the use of two (2) VSL EC 5-7 anchorage devices embedded in each specimen.

By considering the conditions necessary for use of the approximate analysis method, calculations were made to help determine the anchorage test specimen size needed to meet the conditions. The calculated values are shown Table 4-8 to Table 4-14. An examination of these tables will show that several different parameters were considered in determining the size of the anchorage test specimen. These parameters included number, of PT anchorages, size of PT anchorages, and concrete cover. From Table 4-8 to Table 4-9, it can be seen that for using two (2) VSL anchors, the minimum specimen dimensions are X = 29.03", Y = 19.5" and Z = 29.03". Therefore, the anchorage test specimen was chosen to be 29.5" x 19.5" x 29.5" (or 19.5" x 29.5" x 29.5" depending upon the orientation of the specimen). The bearing surface for the anchorages was selected to be 19.5" x 29.5". The length of the specimen (parallel to the tendon path) was selected to be 29.5". As shown in the other tables, values were computed for the approximate bursting force, bursting steel, etc. However, these values were based upon using the design force

for the tendons, a total tendon force of 520.2 Kips (1.2 x the tendon jacking force) for the two tendons. For this load, T_{burst} and d_{burst} were computed as 64.86 Kips and 14.52", respectively.

Maximum load values from the load tests were used to compute T_{burst} and d_{burst} based upon the approximate stress analysis method and the equations given in Section 5.10.9.6.3 of the AASHTO code. These computed values are shown in Table 4-15 for the block specimens which will be used in the laboratory testing program. The geometric dimensions of the PT test specimens and a photograph of one test specimen are shown in Figure 4-47 and Figure 4-48. The laboratory testing program is presented in Chapter 5.

Table 4-8: Stress Analysis Used To Size Anchorage Test Specimen, Part 1

Post-Tensioning Anchorage Zone Design for Various Proposed Test Specimens

Specimen #	Specimen Description	Specimen Dimensions WxHxL (bxhxl) Maximum L =1.5W For Approximate Stress Analysis (AASHTO 5.10.9.6)	Vol (CY)		VSL Anchorage Device	GUTS Equivalent (Kips)	1.2Pj= .2(0.75)GUTS 0.9GUTS Design for PT Anchorage Zones AASHTO 3.4.3.2	0.8GUTS Equivalen (Kips)	VSL Anchorage Device	VSL A Anchor Plate (Lateral Dimensio a=a_{eff}=b_{eff}	VSL Minimum Anchor Spacing X
1	Minimum Size Specimen General Zone Defined by AASHTO Min. Edge Distance	W=	19.5	ONE TENDON	EC 5-7	289	260.1	231.2	EC 5-7	6.50	9.53
		H=	19.5		EC 5-12	496	446.4	396.8	EC 5-12	8.88	12.48
		L=	19.5		ECI 5-12	496	446.4	396.8	ECI 5-12	8.50	12.5
		Volume=	0.16		ECI 6-7	410.2	369.18	328.16	ECI 6-7	8.50	12.5
		W=	29.25	TWO TENDONS							
		H=	19.5		EC 5-7	578	520.2	462.4	EC 5-7	6.50	9.53
		L=	29.25		EC 5-12	992	892.8	793.6	EC 5-12	8.88	12.48
		Volume=	0.36		ECI 5-12	992	892.8	793.6	ECI 5-12	8.50	12.5
					ECI 6-7	820.4	738.36	656.32	ECI 6-7	8.50	12.5

Table 4-9: Stress Analysis Used To Size Anchorage Test Specimen, Part 2

Post-Tensioning Anchorage Zone Design

VSL Anchorage Device	AASHTO Concrete Cover 5.12.3 1 "to 1.5" c	VSL Edge Clearance Xr (c= 1.5")	Minimum Edge Distance for use AASHTO 5.10.9.6 (=1.5A)	Min General Transverse Zone Dim. w/ AASHTO Edge Distance 5.10.9.6 (b= width) 2(1.5A) X1	Min General Transverse Zone Dim. w/ AASHTO Edge Distance 5.10.9.6 (h= height) 2(1.5A) Y1	Min General Longitudinal Zone Dim. w/ AASHTO Edge Distance (l= Length) greater of b & w Z1	Max General Longitudinal Zone Dim. w/ AASHTO Edge Distance (l= Length) 1.5(Z1) Z1M	Minimum Section Area Cross Section (in2xin2) X1 x Y1	USE Area=WxH (in2xin2)	GUTS (Kips)
For Approximate Stress Analysis (AASHTO 5.10.9.6)										
EC 5-7	1 "to 1.5"	6.27	9.75	19.5	19.5	19.5	29.25	380.25	380.25	289
EC 5-12	1 "to 1.5"	7.74	13.32	26.64	26.64	26.64	39.96	709.69	380.25	496
ECI 5-12	1 "to 1.5"	7.75	12.75	25.5	25.5	25.5	38.25	650.25	380.25	496
ECI 6-7	1 "to 1.5"	7.75	12.75	25.5	25.5	25.5	38.25	650.25	380.25	410.2
				X2 2(1.5A)+X	Y2	Z2	ZLM	X2 x Y2		
EC 5-7	1 "to 1.5"	6.27	9.75	29.03	19.5	29.03	43.55	566.09	570.38	578
EC 5-12	1 "to 1.5"	7.74	13.32	39.12	26.64	39.12	58.68	1042.16	570.38	992
ECI 5-12	1 "to 1.5"	7.75	12.75	38	25.5	38	57.00	969.00	570.38	992
ECI 6-7	1 "to 1.5"	7.75	12.75	38	25.5	38	57.00	969.00	570.38	820.4

Table 4-10: Stress Analysis Used To Size Anchorage Test Specimen, Part 3

Post-Tensioning Anchorage Zone Design

VSL Anchorage Device	Confinement Steel VSL Anchor Spiral #xturns@pitch	Legnth of Anchorage Zone Confining Rebar VSL H (in.)	Diameter of Spiral Confinement Rebar VSL G(in) D	pitch of the spiral s	AASHTO LOCAL ZONE DEFINITION Transverse Dimension 5.10.9.7.1 (c=1.0") NOT VERIFIED	AASHTO LOCAL ZONE DEFINITION Transverse Dimension 5.10.9.7.1 (c=1.0") VERIFIED	AASHTO LOCAL ZONE DEFINITION longitudinal Dimension 5.10.9.7.1 MIN	AASHTO LOCAL ZONE DEFINITION longitudinal Dimension 5.10.9.7.1 MAX NOT VERIFIED	F=(1.2Pj)/(A)(A) (ksi)
EC 5-7	#4x6 @2"	12.0	9.00	2.00	11.00	9.53	12.00	16.50	6.16
EC 5-12	#4, 8 turns @	16.0	11.75	2.00	13.75	12.48	16.00	20.63	5.66
ECI 5-12	#4x6.5 @3"	11.5	11.00	3.00	13.00	12.50	13.00	19.50	6.18
ECI 6-7	#4x6.5 @3"	11.5	11.00	3.00	13.00	12.50	13.00	19.50	5.11
					One anchor	One anchor	One anchor	One anchor	
EC 5-7	#4x6 @2"	12.0	9.00	2.00	11.00	9.53	12.00	16.50	6.16
EC 5-12	#4, 8 turns @	16.0	11.75	2.00	13.75	12.48	16.00	20.63	5.66
ECI 5-12	#4x6.5 @3"	11.5	11.00	3.00	13.00	12.50	13.00	19.50	6.18
ECI 6-7	#4x6.5 @3"	11.5	11.00	3.00	13.00	12.50	13.00	19.50	5.11

Table 4-11: Stress Analysis Used To Size Anchorage Test Specimen, Part 4

Note: AASHTO Eq 5.10.9.7.2-1 is applicable if general zone rebar satisfies AASHTO 5.10.9.3.2 and the concrete along the tendon ahead of the ancohr is at least twice the length of the local zone of 5.10.9.7.1.

Post-Tensioning Anchorage Zone Design

VSL Anchorage Device	AASHTO LOCAL ZONE Bearing Resistance Pr=ΦfnAb 5.10.9.7.2 (of anchorages) Φ=0.7	fn = 2.25fci or … (5.10.9.7.2-2) IF L = 2x local zone One Anchor	Check Pr=ΦfnAb > Bearing load Check Pr >0.9GUTS IF L = 2x local zone One Anchor	Needeed fci (KSI) IF L = 2x local zone One Anchor	AASHTO Design Force 1.2Pj 1.2(.75)GUTS 0.9GUTS (3.4.3.2)	AASHTO General Zone Factored Compressive Stress Limit 0.7Φf'ci (5.10.9.3.1) For Test, f'c=f'ci) (ksi)	Check Pr=ΦfnAg> Bearing load Check
	K	Ksi					
EC 5-7	**192.12**	**7.35**	**NO**	**4.21**	260.1	1.96	**217.38**
EC 5-12	**366.12**	**7.35**	**NO**	**3.79**	446.4	1.96	**405.71**
ECI 5-12	**314.90**	**7.35**	**NO**	**4.41**	446.4	1.96	**371.73**
ECI 6-7	**307.07**	**7.35**	**NO**	**3.74**	369.18	1.96	**371.73**
	Two Anchors	Two Anchors	Two Anchors				
EC 5-7	**192.12**	**7.35**	**NO**	**8.42**	520.2	1.96	**217.38**
EC 5-12	**391.51**	**7.35**	**NO**	**7.09**	892.8	1.96	**405.71**
ECI 5-12	**349.27**	**7.35**	**NO**	**7.95**	892.8	1.96	**371.73**
ECI 6-7	**307.07**	**7.35**	**NO**	**7.48**	738.36	1.96	**371.73**

Table 4-12: Stress Analysis Used To Size Anchorage Test Specimen, Part 5

Post-Tensioning Anchorage Zone Design

Resistance Factors:

Bearingon concrete,	Φ_b	0.7
Comp. Strut & Tie	Φ_s	0.7
Comp. Anchorage zone	Φ_{ca}	0.8
Steel tension in Anchorage zon	Φ_{ta}	1

Bursting Force Steel Ast Ast=T/fy fy=60ksi in^2	Bursting Force Steel N, #5 Bars Ab=0.31 in2 db=0.625 in Smax = 12	Bursting Force Steel N, #4 Bars Ab=0.2 in2 db=0.5 in Smax = 12	VSL Anchorage Device	width of plate a	h	Approximate Bursting Force Tburst 5.10.9.6.3 Tburst =0.25P(1-a/h) T Kips	d burst AASHTO 5.10.9.6.3 0.5h (e=0) (angle=0) in	Bursting Rebar Distribution Distance 2.5dburst <= 1.5h	Bursting Rebar Distribution Distance 1.5h	Bursting Rebar Distribution Distance 2.5dburst	Minimum f'ci (psi) per VSL
0.80	**3**	5	EC 5-7	6.50	19.50	48.17	9.75	24.38	29.25	24.38	3500
1.38	**5**	7	EC 5-12	8.88	26.64	82.67	13.32	33.30	39.96	33.30	3500
1.38	**5**	7	ECI 5-12	8.50	25.50	82.67	12.75	31.88	38.25	31.88	3500
1.14	**4**	6	ECI 6-7	8.50	25.50	68.37	12.75	31.88	38.25	31.88	3500
1.08	**4**	6	EC 5-7	16.00	29.03	64.86	14.52	36.29	43.55	36.29	3500
1.88	**7**	10	EC 5-12	21.38	39.25	112.91	19.63	49.06	58.68	49.06	3500
1.22	**4**	7	ECI 5-12	26.75	38.00	73.42	19.00	47.50	57.00	47.50	3500
2.65	**9**	14	ECI 6-7	8.50	38.00	159.22	19.00	47.50	57.00	47.50	3500

Table 4-13: Stress Analysis Used To Size Anchorage Test Specimen, Part 6

Post-Tensioning Anchorage Zone Design

VSL Anchorage Device	Minimum f'ci (psi) per VSL	Specimen Description	Compresive Stress Limit 0.7(0.8)f'ci ksi	Compresive Stress Limit 0.6(0.8)f'ci ksi (large Rotations)	Compresive Stress 5.10.9.6.2 ksi fca	s	aeff	beff	Pu =1.2Pj 0.75(1.2)GUTS 0.9GUTS	n	K	t	lc
		Size Specimen	AASHTO	AASHTO	AASHTO		CHECK VALUES						
		General Zone	5.5.4.2.1	5.5.4.2.1	3.4.3.2								
		Defined by AASHTO	Φ=0.8	Φ=0.8	CHECK VALUES								
		Min. Edge Distance	5.10.9.3	5.10.9.3	Pu=1.2Pj								
EC 5-7	3500		1.96	1.68	2.631	9.53	6.50	6.50	260.10	1	1	19.5	7.48
EC 5-12	3500		1.96	1.68	2.264	12.48	8.88	8.88	446.40	1	1	26.64	10.21
ECI 5-12	3500		1.96	1.68	3.865	12.50	8.50	8.50	446.40	1	1	25.5	9.78
ECI 6-7	3500	**ONE TENDON**	1.96	1.68	3.326	12.50	8.50	8.50	369.18	1	1	25.5	9.78
EC 5-7	3500	**TWO TENDONS**	1.96	1.68	6.048	9.53	6.50	6.50	520.20	2	1.23	29.03	7.48
EC 5-12	3500		1.96	1.68	4.960	12.48	8.88	8.88	892.80	2	1.26	39.12	10.21
ECI 5-12	3500		1.96	1.68	7.580	12.50	8.50	8.50	892.80	2	1.23	38	9.78
ECI 6-7	3500		1.96	1.68	7.633	12.50	8.50	8.50	738.36	2	1.23	38	9.78

Table 4-14: Stress Analysis Used To Size Anchorage Test Specimen, Part 7

Post-Tensioning Anchorage Zone Design

VSL Anchorage Device	1.15aeff 1.15beff	Ab Ause-Aduct	Ause	Aplate Ag (5.10.9.7.2)	Aconf	Ab = Aplate-Aduct	2Aplate	Dduct	VSL Anchorage Device	Plate Diameter	Tendon Area At	Aduct AASHTO 5.4.6.2 >=2.0 At or >= 2.5At	
	CHECK VALUES												
EC 5-7	7.48	33.58	38.48	42.25	38.48	37.34	84.5	2.5	EC 5-7		1.07	4.91	
EC 5-12	10.21	66.97	74.66	78.85	74.66	71.16	157.709	3.13	EC 5-12		1.84	7.69	
ECI 5-12	9.78	39.22	50.27	72.25	50.27	61.21	144.5	3.75	EC 5-19		2.91	11.04	
ECI 6-7	9.78	37.70	50.27	72.25	50.27	59.68	144.5	4	E 6-19		4.12	12.57	**Assumed =4" dia.**
EC 5-7	7.48	33.58	38.48	42.25	38.48	37.34	84.5	2.5	EC 5-7		1.07	4.91	
EC 5-12	10.21	71.90	74.66	78.85	74.66	76.09	157.709	3.13	EC 5-12		1.84	2.76	
ECI 5-12	9.78	45.90	50.27	72.25	50.27	67.89	144.5	3.75	EC 5-19		2.91	4.37	
ECI 6-7	9.78	37.70	50.27	72.25	50.27	59.68	144.5	4	E 6-19		4.12	12.57	**Assumed =4" dia.**

Table 4-15: Approximate Stress Analysis For S1 and S2 Specimens

Specimen #	Fiber/Spiral/Ties	Load (K) P	0.5P	0.25P	a/h1	a/h2	a/h2	h1/2	h2/2	AASHTO	AASHTO	Tie Total	Tie Total
				a=length of the anchor				dburst1	dburst2	Tburst1 (kips)	Tburst2 (kips)	(Kips)	(Kips)
		Load (K)			a=6.5	a=6.5		h1=19.5	h2=29.5	Short	Long	Long	Short
S1-1	None/Y/Y	627.92	313.96	156.98	0.33	0.22	0.22	9.75	14.75	104.7	122.4	86.8	67.3
S1-2	Dramix/N/N	794.00	397.00	198.50	0.33	0.22	0.22	9.75	14.75	132.3	154.8	108.8	85.1
S1-3	Dramix/Y/N	865.65	432.82	216.41	0.33	0.22	0.22	9.75	14.75	144.3	168.7	119.1	92.7
S1-4	Dramix/N/Y	999.23	499.62	249.81	0.33	0.22	0.22	9.75	14.75	166.5	194.8	138.1	107.1
S1-5	Dramix/0.5/0.6	1000.36	500.18	250.09	0.33	0.22	0.22	9.75	14.75	166.7	195.0	138.4	107.2
S1-6	Helix/N/N	600.00	300.00	150.00	0.33	0.22	0.22	9.75	14.75	100.0	116.9	82.2	64.3
S1-7	Helix/Y/N	677.21	338.60	169.30	0.33	0.22	0.22	9.75	14.75	112.9	132.0	93.5	72.6
S1-8	Helix/N/Y	916.70	458.35	229.17	0.33	0.22	0.22	9.75	14.75	152.8	178.7	126.8	98.2
S1-9	Helix/0.5/0.6	869.23	434.61	217.31	0.33	0.22	0.22	9.75	14.75	144.9	169.4	120.2	93.1
S1-10	Novomesh/N/N	838.53	419.27	209.63	0.33	0.22	0.22	9.75	14.75	139.8	163.4	115.5	89.8
S1-11	Novomesh/Y/N	706.32	353.16	176.58	0.33	0.22	0.22	9.75	14.75	117.7	137.7	97.4	75.7
S1-13	None/0.5/0.6	732.53	366.26	183.13	0.33	0.22	0.22	9.75	14.75	122.1	142.8	101.1	78.5
S1-14	Novomesh/0.5/0.6	995.59	497.80	248.90	0.33	0.22	0.22	9.75	14.75	165.9	194.1	137.3	106.7
					a=7	a=7							
S2-1	None/Y/Y	723.25	361.62	180.81	0.36	0.24	0.24	9.75	14.75	115.9	137.9	100.4	77.5
S2-2	Dramix/N/N	557.22	278.61	139.31	0.36	0.24	0.24	9.75	14.75	89.3	106.3	76.9	59.7
S2-3	Dramix/Y/N	628.33	314.17	157.08	0.36	0.24	0.24	9.75	14.75	100.7	119.8	87.3	67.3
S2-4	Dramix/N/Y	673.97	336.99	168.49	0.36	0.24	0.24	9.75	14.75	108.0	128.5	92.6	72.2
S2-5	Dramix/0.5/0.6	665.57	332.78	166.39	0.36	0.24	0.24	9.75	14.75	106.7	126.9	90.8	71.3
S2-6	Helix/N/N	567.68	283.84	141.92	0.36	0.24	0.24	9.75	14.75	91.0	108.2	78.8	60.8
S2-7	Helix/Y/N	691.14	345.57	172.79	0.36	0.24	0.24	9.75	14.75	110.8	131.8	95.6	74.1
S2-8	Helix/N/Y	747.71	373.86	186.93	0.36	0.24	0.24	9.75	14.75	119.8	142.6	103.0	80.1
S2-9	Helix/0.5/0.6	752.59	376.30	188.15	0.36	0.24	0.24	9.75	14.75	120.6	143.5	103.2	80.6
S2-10	Novomesh/N/N	653.64	326.82	163.41	0.36	0.24	0.24	9.75	14.75	104.7	124.6	90.3	70.0
S2-11	Novomesh/Y/N	569.72	284.86	142.43	0.36	0.24	0.24	9.75	14.75	91.3	108.6	78.7	61.0
S2-12	Novomesh/N/Y	750.05	375.03	187.51	0.36	0.24	0.24	9.75	14.75	120.2	143.0	103.5	80.4
S2-13	Novomesh/0.5/0.6	752.68	376.34	188.17	0.36	0.24	0.24	9.75	14.75	120.6	143.5	103.3	80.6
S2-14	None/0.5/0.6	645.77	322.89	161.44	0.36	0.24	0.24	9.75	14.75	103.5	123.1	89.6	69.2

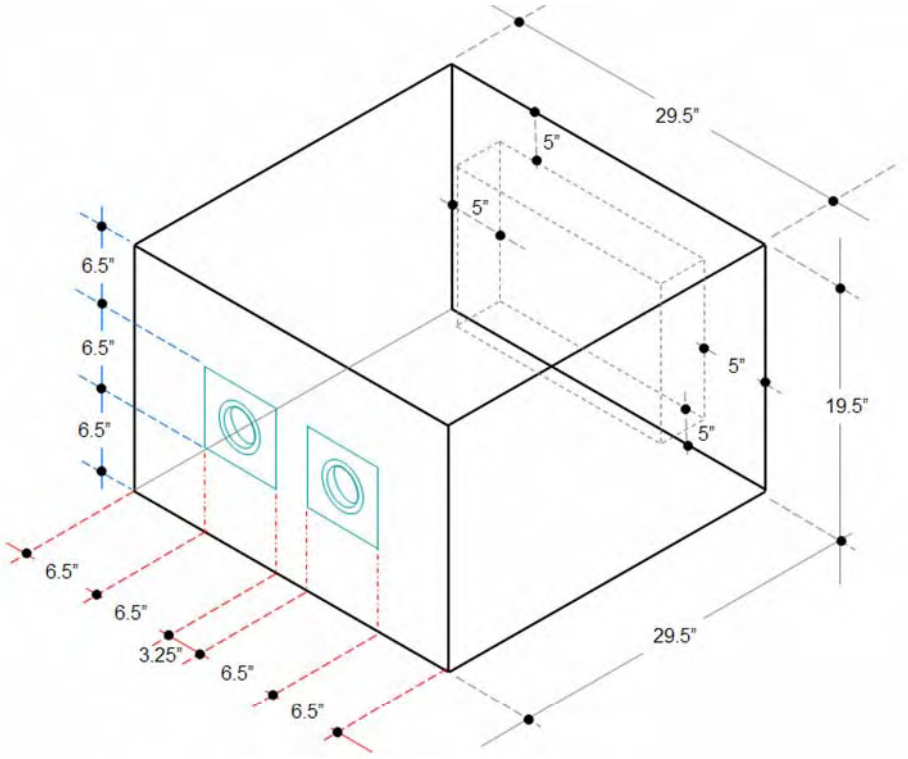

Figure 4-47: Dimensions of the PT Anchorage Specimen

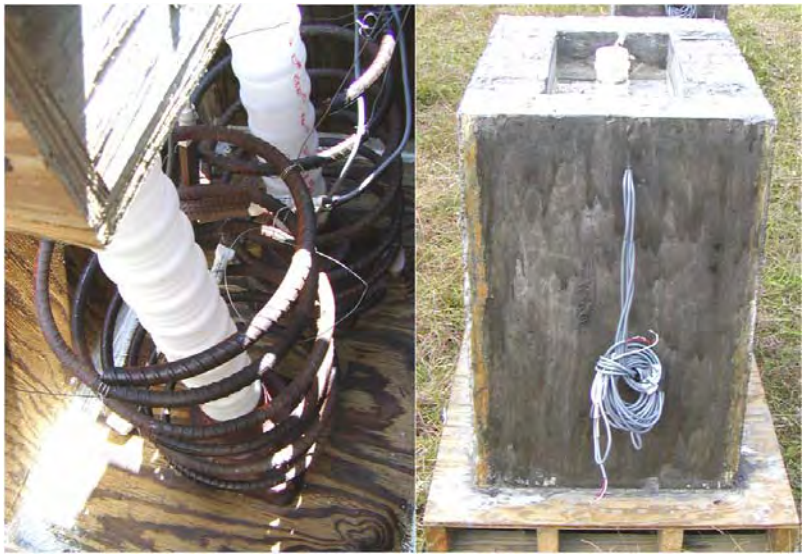

Figure 4-48: Block Specimens during Construction Showing Internal Instrumentation

CHAPTER 5

LABORATORY TESTING OF BLOCK SPECIMENS

5.1 Post-Tensioning Anchorages and Ducts

Two of the major post-tensioning anchorage system suppliers in the United States are VSL Corporation and Dywidag Systems International. Two (2) different post-tensioning anchorage systems (one supplied by each of the two manufacturers) were used in this test program. The size of the post-tensioning anchors was limited based upon consideration of the 1000K load capacity of the FDOT load testing frame. Thus, based upon the size of the test specimen and the use of two (2) anchors in each specimen, a relatively small anchor system (with design capacity of 289K) was used. The PT test specimen size was selected with the intent of ensuring that most of the specimens would fail under loading prior to reaching the load capacity of the FDOT 1,000 kips loading frame.

5.2 VSL EC 5-7 Post-Tensioning Anchorages and Ducts

The VSL anchor designation for the 289Kips capacity PT anchor is VSL Type EC 5-7. Figure 5-1 shows the geometry of the EC 5-7 anchor. In addition to PT anchors, post-tensioning ducts and spirals were embedded in the test specimens. The duct used is a plastic duct.

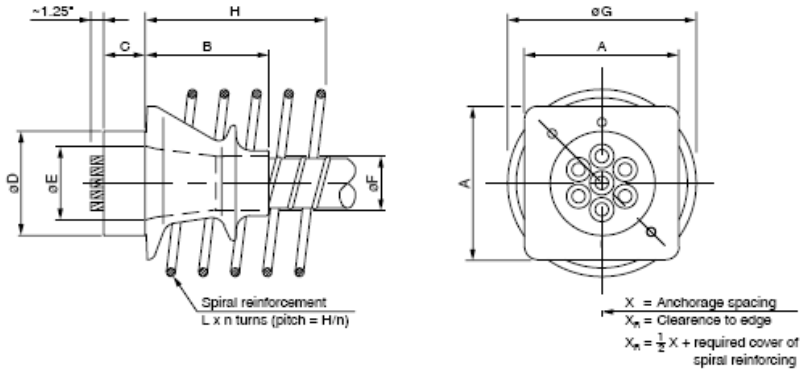

Tendon Unit		Dimensions Inches										
		A	B	C	øD	øE	øF	øG	H	L	n	X
Strand Type 0.5"	5-7	6.50	5.25	2.38	4.50	2.91	2.50	9.00	12.00	#4	6	9.50
	5-12	8.88	7.06	2.38	6.00	4.31	3.13	11.75	16.00	#4	8	12.50
	5-19	11.00	10.25	3.00	7.00	5.56	3.75	15.00	18.00	#5	8	15.75
	5-27	12.38	13.63	4.00	9.00	7.00	4.75	18.00	18.00	#6	8	18.75
	5-31	14.00	13.63	4.00	9.00	7.00	4.75	19.00	20.25	#6	9	20.00

Figure 5-1: VSL EC 5-7 Post-Tensioning Anchor

5.3 Dywidag MA 5-0.6 Post-Tensioning Anchorages and Ducts

The Dywidag anchor designation for the 289K capacity PT anchor is Dywidag MA 5-0.6. Figure 5-2 gives the dimensions for the anchor. In addition to PT anchors, the post-tensioning ducts were also used in the test specimens. The duct used is a 59 mm plastic duct.

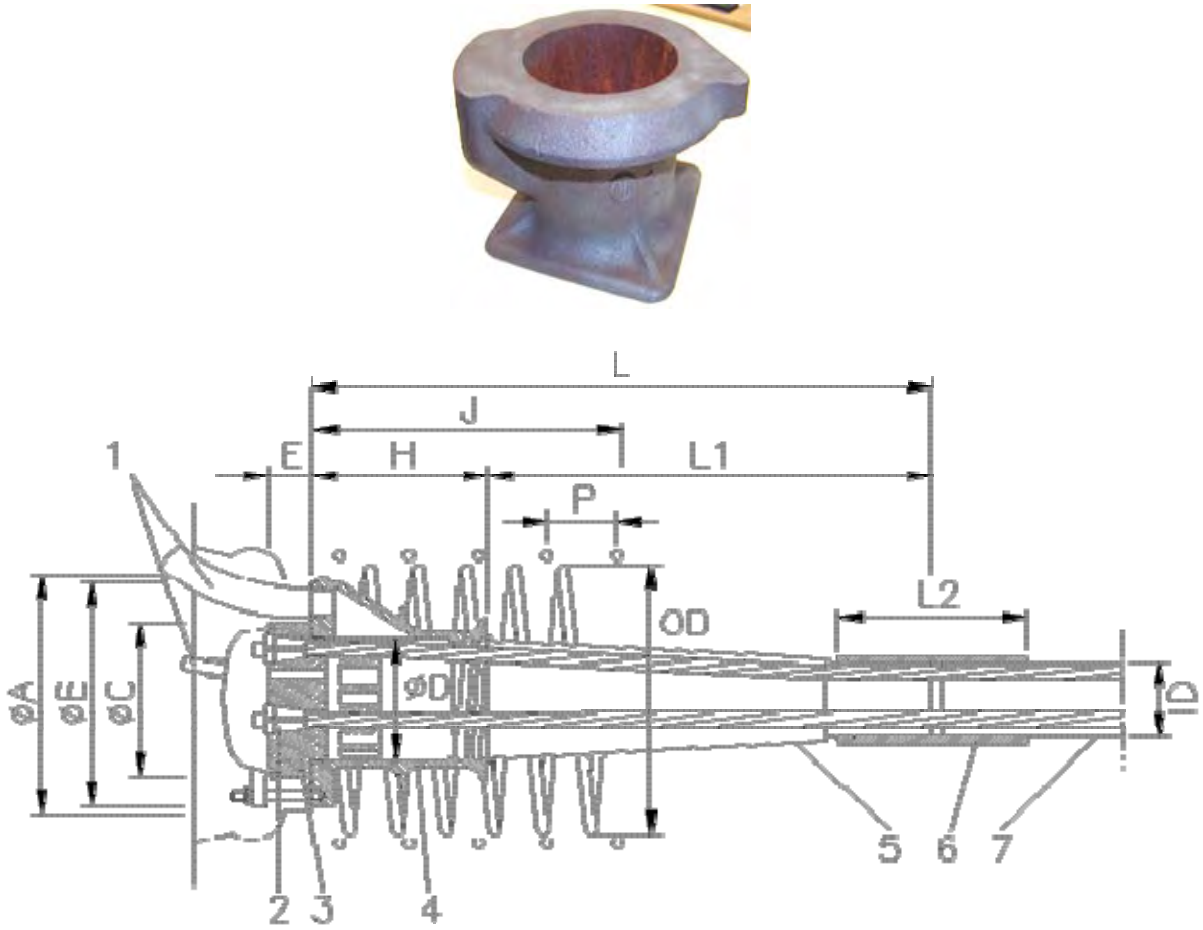

Figure 5-2: Dywidag MA 5-0.6 Post-Tensioning Anchor

5.4 Non-Prestressed Steel Reinforcement

The AASHTO code divides the post-tensioning (PT) anchorage zone into two sections, the local zone and the general zone. In accordance with the AASHTO code, the anchorage device supplier is responsible for providing anchorage devices and records of acceptance tests which comply with the AASHTO requirements. In addition, the anchorage device supplier "shall specify auxiliary and confining reinforcement, minimum edge distance, minimum anchor spacing, and minimum concrete strength at time of stressing required for proper performance of the local zone (AASHTO, 2007)". The local zone includes the anchor system and the surrounding concrete. To help prevent failure of the anchor system, for both the VSL and the

Dywidag anchors, the anchorage device design includes a steel spiral which is to be installed with the anchors. Thus, the spiral size and geometry are specified for each anchor. In the general zone, bursting steel is provided to prevent excessive cracking due to the bursting stresses that develop in the concrete. For PT test specimens, the bursting steel design is based upon the equations given in Sections 5.9 and 5.10 of the AASHTO LRFD Bridge Design Specifications (2007).

5.4.1 Spiral Reinforcement for VSL Anchors

As shown in the VSL Type E anchor table, Figure 5-1, the spiral to be used with the VSL EC 5-7 anchor was # 4 bar spiral with a diameter of 9.0 inches and 6 turns. Twelve inches (12”) is the distance that the spiral shall extend beyond the outer surface of the PT anchor into the PT anchor zone. Using this information, the computed pitch for the spiral is 2” (Figure 5-3).

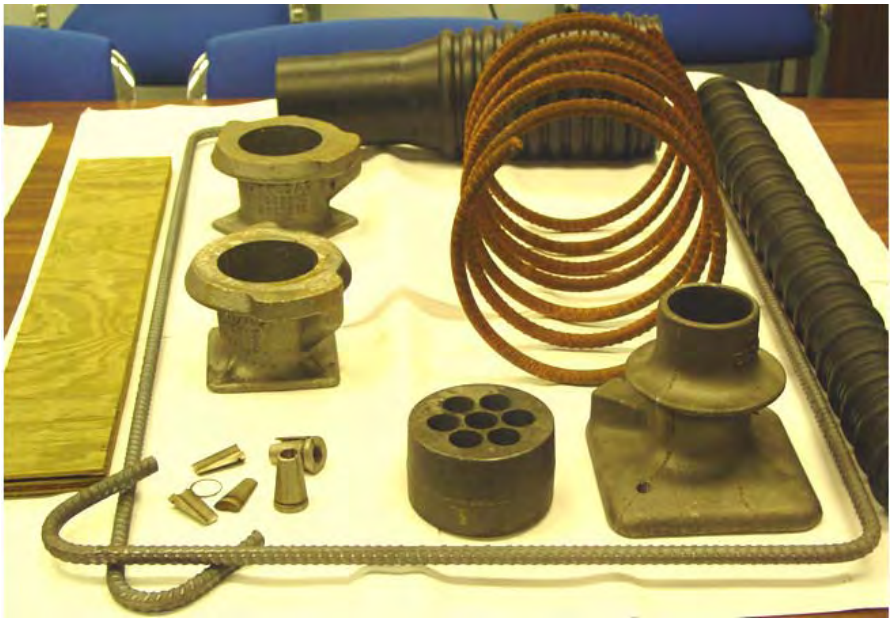

Figure 5-3: Anchors used in the Study

5.4.2 Spiral Reinforcement for Dywidag Anchors

As shown in the Dywidag Multi-plane Anchorage MA table, Figure 5-2, the spiral used with the MA 5-0.6 anchor was # 4 bar with a diameter of 7.75 inches. Ten inches (10”) is the distance that the spiral shall extend beyond the outer surface of the PT anchor into the anchor zone. The pitch for the spiral is 1.875”.

5.4.3 Tie Reinforcement for VSL and Dywidag Anchors

The tie reinforcement used for the anchor test specimens was determined by considering the 2004 AASHTO code, Section 5.10.9.6.3 and Section 5.10.10.1 for post-tensioned anchorage zone design using “Approximate Stress Analysis”. For the VSL EC 5-7 anchor with a Guaranteed Ultimate Tensile Strength (GUTS) of 289 K, the approximate bursting force, T_{burst} was computed to be 48.2 K. The distance used to determine the distribution distance for the bursting steel, d_{burst}, was computed to be 9.75”. In accordance with AASHTO Section 5.10.9.6.3 the bursting rebar should be distributed for a distance of $2.5(d_{burst})$ but less than or equal to a distance of 1.5h, where h equals 19.5” for the anchorage specimen using two (2) EC5-7 anchors. Tie reinforcement was provided to satisfy the AASHTO recommendation by using five (5) # 4 bars spaced at 5.25” (Figure 5-4). However, in the test specimen matrix, in order to consider the effect of reducing the amount of bursting steel in favor of adding steel fiber, some specimens were cast with only three (3), # 4 bars spaced at 10.5 inches.

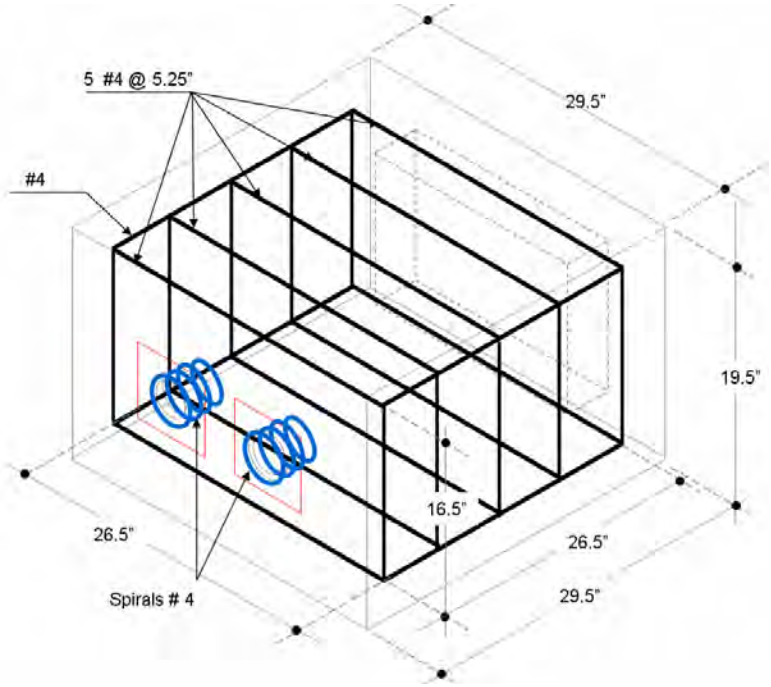

Figure 5-4: Anchorage Test Specimen Steel Tie Reinforcement.

5.5 Fibers and Fiber Percentages Used In Anchorage Test Specimens

The three (3) fibers used in the research project are Dramix ZP305, Helix, and Novomesh 850. Dramix ZP305 (a steel fiber) was used in earlier tests conducted for the Florida Department of Transportation (FDOT) by Yazdani, et al (2002) and Haroon (2003). The Dramix, Helix and Novomesh fibers are shown in Figure 3-1. PT anchorages test specimens were cast using each of the three fibers.

5.6 Anchorage Specimens

In an effort to consider the effects of several variables (type of steel fiber, confinement steel, bursting steel and anchorage device), twenty-seven (27) test specimens were cast with embedded post-tensioning anchors and ducts. Twenty-three (23) of the specimens were cast with steel fibers and four (4) were cast with plain concrete.

5.7 Concrete Used for Anchorage Test Specimens

As presented in Chapter 3, the concrete mix design selected for use in this project is a 4000 psi mix recommended by the FDOT Materials Lab. A mix with a relatively high slump was used since the addition of steel fibers was expected to reduce the concrete slump. Table 3-1 shows the concrete mix design for the 4000 psi which is the minimum concrete strength recommended for post-tensioned anchorage.

A total of 8 batches of concrete were cast to make the twenty-seven (27) test specimens: Thirteen (13) specimens (S1 Specimens) were cast with VSL PT anchors. Fourteen (14) specimens (S2 Specimens) were cast with Dywidag PT anchors. Table 3-3 and Table 3-9 show the mix proportions of the four concrete batches used to cast S1 Specimens. The four concrete batches used to cast the S2 Specimens are shown in Table 3-9. Based upon the preliminary material test results (which were presented in Chapter 3) and the finite element modeling (Chapter 4), the fiber percentage used for the test specimens was 0.5% for each of the three fibers.

From each concrete batch, concrete cylinders were cast and tested to obtain material properties for the anchorage test specimens. From these cylinders, compressive strength tests and split tensile strength tests were performed. The test results were presented earlier (Figure 3-2 to Figure 3.7). For S1 Specimens, The average 28 day compressive strengths for Plain, Dramix, Helix and Novomesh cylinders were 4846 psi, 4767 psi , 2848 psi, and 4305 psi, respectively.

For S1 Specimens, the average 28 day split tensile strengths for Plain, Dramix, Helix and Novomesh cylinders were 362 psi, 427 psi, 389 psi and 408 psi, respectively.

5.8 Instrumentation and Data Acquisition Equipment

This section provides information about the instrumentation and data acquisition system used in the test program. Internal instrumentation, strain gages were purchased from Vishay Micromeasurements. All external gages and the data acquisition system were supplied by the Florida Department of Transportation's Structures Research Center.

5.8.1 Instrumentation of Anchorage Test Specimens

During the test, both strains and displacements were measured and recorded. Internal and external strain gages were used. The internal gages were mainly 5" gages by Vishay Micromeasurements (models EPG-5-350W and EPG-5-120W). The external (surface) gages were TML Model PL-60-11, 60 mm, 120 ohm, foil strain gages. Displacements of the test specimens were measured using a TML Model SDP-2000, full bridge, displacement transducers and Balluf Model BOD 66M Class II Laser distance measurement sensors. Instrument locations for internal gages are as indicated in Figure 5-5 and Figure 5-6. Installation of internal gages is shown in Figure 5-7.

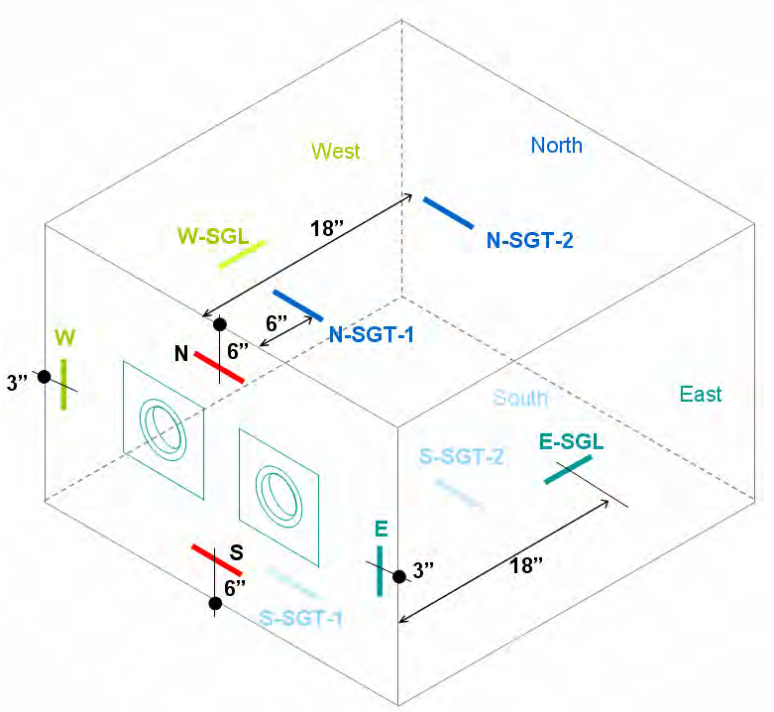

Figure 5-5: Instrumentation of Block Specimen

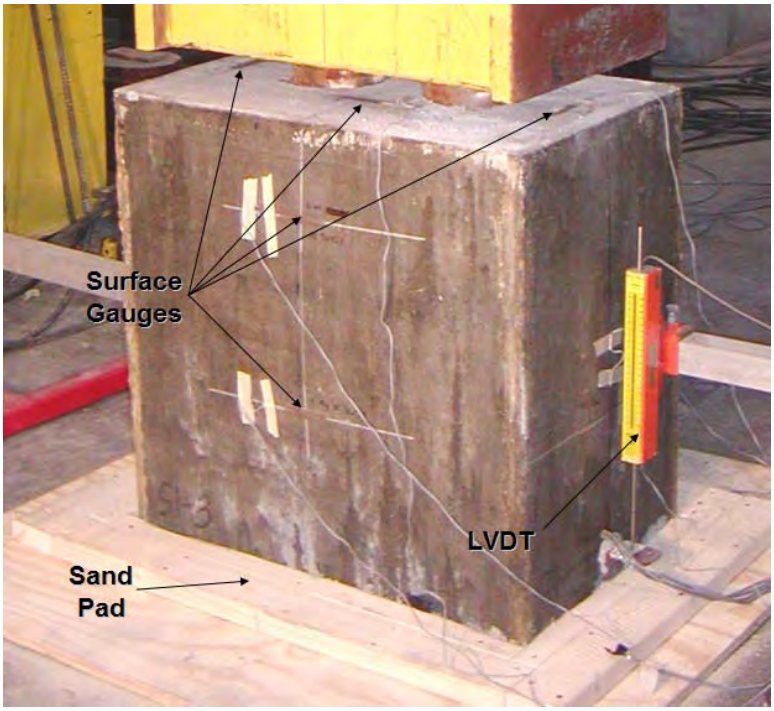

Figure 5-6: Block Specimen Instrumentation

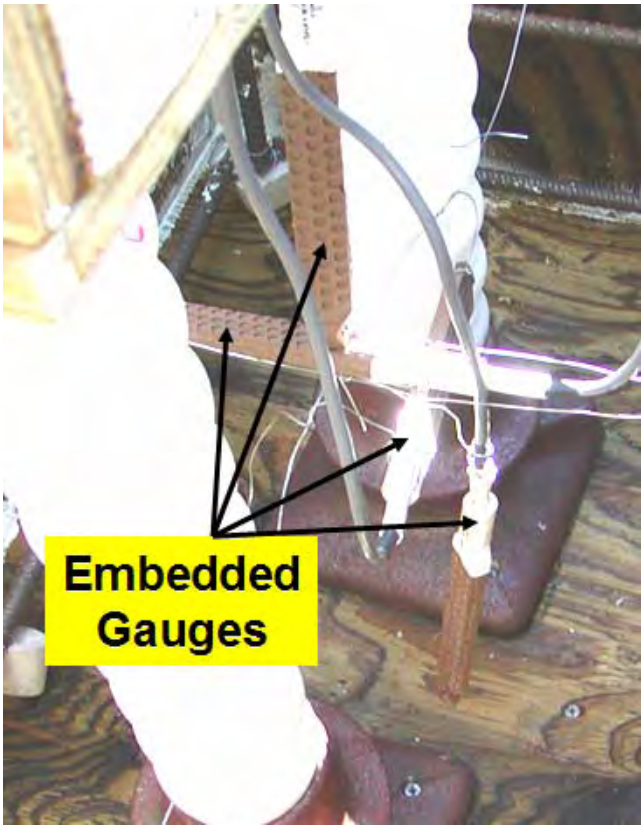

Figure 5-7: Installation of Embedded Gauges

5.8.2 Data Acquisition System

The test data was sampled and recorded using a data acquisition system manufactured by National Instruments: Chassis Model PXI-1011 combo PXI/SCXI, Controller Model PXI-8176 embedded controller running Windows XP/LabView, DAC (ADC) Card Model PXI-6251, Signal Conditioning Model SCXI-1530 strain gage module. With this data acquisition system, the data was sampled at 1 kHz, averaging every 100 samples for a recording rate of 10 Hz. During testing the target strain rate was three (3) microstrains per second.

5.9 Testing Setup

The PT anchor test specimens were load tested at the Florida Department of Transportation's Structures Research Center in Tallahassee, Florida. Photographs of the test setup is shown in Figure 5-8. As shown in the figure, the 1000 Kip load frame (RSFrame) provided resistance for two (2) 800 Kips Enerpac actuators (Model #RR-40018). The load of each actuator was measured by an Interface 600 Kips load cell (Model #1260CHG-600K). The loads were applied to a heavy steel box which transferred the load to two (2) round steel tendon wedge anchor plates which loaded the anchors of the test specimen. For the first specimen tested, S1-1, the concrete test specimen rested on a neoprene bearing pad. For all other tests, the specimens rested in a box of sand.

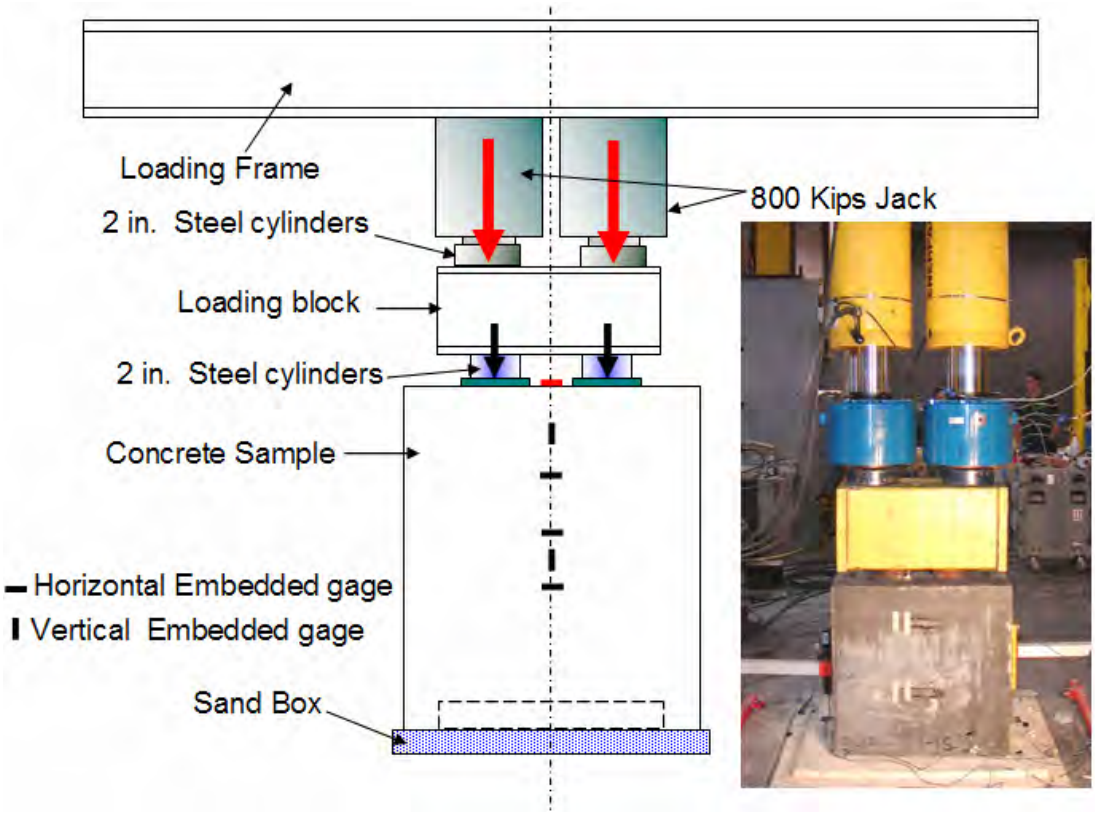

Figure 5-8: Test Set up used in the Study

5.10 Testing Procedure

Once a test specimen was properly positioned, instrumented and connected to the data acquisition system, the load was applied to the specimen. Using manual controls, the equipment operator controlled the load rate and relative magnitude of the load being applied by each Enerpac actuator. The target load range was three (3) microstrains per second. In general, the load was applied continuously to a test specimen until the specimen either failed or the capacity of the load frame was reached. In a few instances, based upon the behavior of the specimen (i.e. cracking) the load was held steady for a brief period. However, due to the high capacity of the applied loads, the specimens were observed from a distance until the load cycles were completed. After the end of a load test, the tested specimen was examined closely. Cracks were noted and the specimen was photographed. During and after testing, any notable information was recorded (i.e. load at first cracking, failure mechanism). In the following sections the load test results for the twenty-seven (27) anchorage test specimens are presented and discussed.

5.11 Anchorage Test Specimens with VSL Anchors (S1)

The bearing surface (bottom surface) of the first test specimen, Specimen S1-1, rested on a neoprene bearing pad. This pad was larger on all sides than the specimen and was approximately 5" thick. The pad was not new. It was a salvaged bridge bearing pad which was being stored at the FDOT lab. During testing, Specimen S1-1 experienced differential settlement at the bottom. This contributed to spalling originating on the east side (one of the narrow sides) of the specimen. To improve bearing conditions for the next tested specimen, S1-2, the bearing end rested in a wooden sandbox. Based upon the performance of Specimen S1-2 during the load test, using the sandbox was considered an improvement. Therefore, all other S1 and S2

specimens were tested with the sandbox at bearing surface. In the load testing program, each specimen was loaded until 1) it failed suddenly due to punching shear or bursting tension, 2) it failed to carry additional load, or 3) the capacity of the load frame was reached.

Each of the S1 Specimens was cast with two (2) EC5-7 VSL anchors, and each anchor was designed for a tendon with at Guaranteed Ultimate Tensile Strength (GUTS) of 289 kips. This is the minimum breaking load for a tendon made of seven (7), 0.5", 270 ksi low relaxation strands. Thus, for two anchors the GUTS is 578 kips. For design purposes, VSL literature allows a temporary overstressing to 80% of the GUTS for the anchor. This load, 80% of GUTS, is 231.2 kips for each anchor. For each test specimen, 80% of GUTS for two anchors is 462.4 kips.

The AASHTO code, Section 5.10.9.7.2 limits the factored bearing resistance of the anchorage to be $P_r = F\, f'_n\, A_b$ where f_n is the lesser of $fn = 0.7f'_{ci}\, S\, (A/Ag)$ and $fn = 2.25\, f'_{ci}$. In the equation for P_r, A_b is the effective area of the bearing plate. If f'_{ci}, the specified compressive strength of concrete at the time of initial loading or prestressing, is 3,500 psi (the minimum concrete compressive strength required for applying maximum prestress force to the anchor), and $f_n = 2.25f'_{ci}$, then for the VSL EC 5-7 anchor, P_r would be calculated as approximately 222 kips for each anchor. Thus for two anchors, the total bearing resistance would be approximately 444 kips.

By considering 80% of GUTS and the limiting bearing resistance computed above for each anchor, a total applied load in excess of 444 kips applied to a S1 test specimen would be a load that approximately exceeds the design capacity of the VSL anchors based on the assumed design

parameters. For load testing purposes, if a specimen successfully resists 462.4 kips, the specimen has fulfilled load capacity requirements for the VSL EC5-7 anchor system.

5.11.1 Anchorage Test Specimen S1-1

Specimen S1-1 was the first one load tested at the FDOT Structures Lab. This specimen contained plain concrete, two (2) VSL EC5-7 anchors & ducts, a steel spiral and steel ties. Specimen S1-1 was tested at the age of 138 days. The 28 day compressive strength and the ninety-six (96) day compressive strength were 4846 psi and 6618 psi, respectively. The 28 day tensile strength and the ninety-five (95) day tensile strength were 362 psi and 457 psi, respectively. The first visible surface crack occurred at a load in excess of 400 K. The failure load of 627.92 Kips was approximately 9% greater than twice the GUTS for one VSL anchor (2x289K = 578 K).

During the load test it was evident that differential settlement was taking place. At the bottom of the test specimen on the east side the concrete started to spall before other signs of deterioration were evident. Failure was initiated by excessive crushing and cracking at the bottom of the specimen, particularly on the east side. At the highest applied load (627.9 Kips), the northeast corner of the specimen sheared off. Figure 5-9 shows a network of cracked developed on the top surface. The development of the cracks can be attributed to the presence of the bursting reinforcement (#4 bar ties spaced at 5.25”) and the spirals in the local zone. Figure 5-10 to Figure 1-1Figure 5-11 show deflection and strain data from the surface and embedded gages for Specimen S1-1.

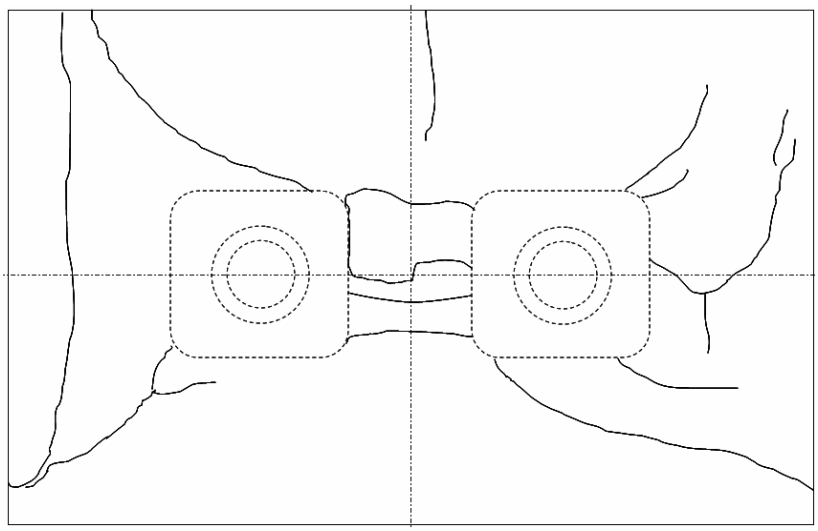

Figure 5-9: Crack Patterns for S1 Block (Spirals + Ties)

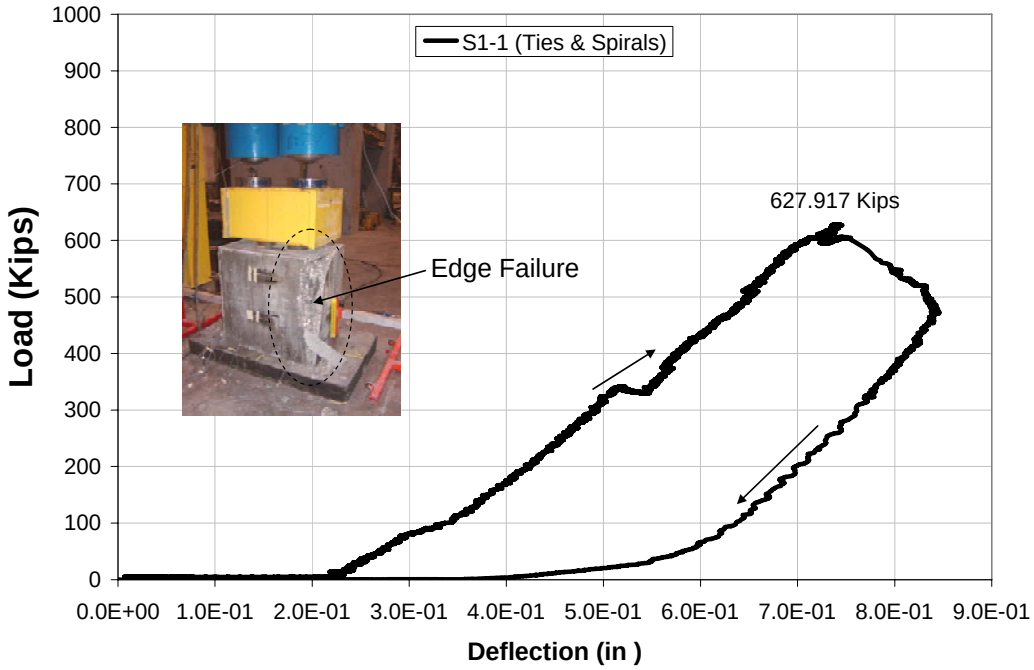

Figure 5-10: Applied Load vs. Deflection for S1 Block (Spirals + Ties).

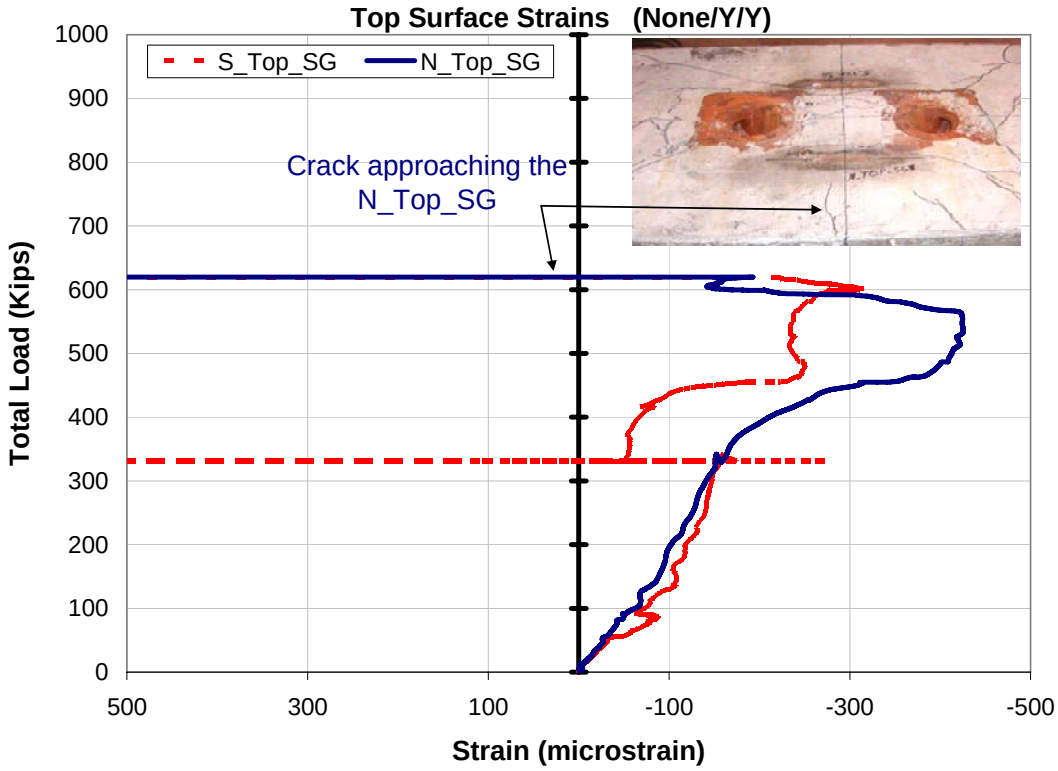

Figure 5-11: Range of Compressive and Tensile Stains at the Top Gauges

5.11.2 Anchorage Test Specimen S1-13

Specimen S1-13 contained plain concrete two (2) VSL EC5-7 anchors, two ducts, approximate 50% of the steel spiral recommended by VSL for the local zone and 60% of the steel ties used in Specimen S1-1. For this Specimen, the spacing of the steel ties was twice the tie spacing used in Specimens S1-1. At the bearing end of the specimen, the specimen rested in a wooden sandbox.

S1-13 was tested at an age of 155 days. Cracks developed on all surfaces of Specimen S1-13 during testing. These cracks are show in Figure 5-14 to 5-15. After the load was removed and the Specimen's bottom was exposed, it was noted that the bottom surface was greatly deteriorated with large concrete spalls and cracks. On a portion of the bottom of the specimen, the bottom layer of the tie reinforcement was exposed.

Specimen S1-13 was loaded until failure; a total load of 732.53 Kips was reached. From looking at the bottom surface of the Specimen it seems that structural integrity of the specimen was exceeded prior to the application of the final load. However, the specimen was loaded until it failed to carry additional load since the deteriorated condition of the bottom was not evident until after the load test was concluded. Similar to S1 block, punching shear did not occur at the anchors. With a 50% reduction in steel spirals and a 40% reduction in steel ties, Specimen S1-13 accepted 17% more load than Specimens S1-1. Figure 5-12 to Figure 5-13 show plots of load vs. deflection and load vs. stain measurements, respectively.

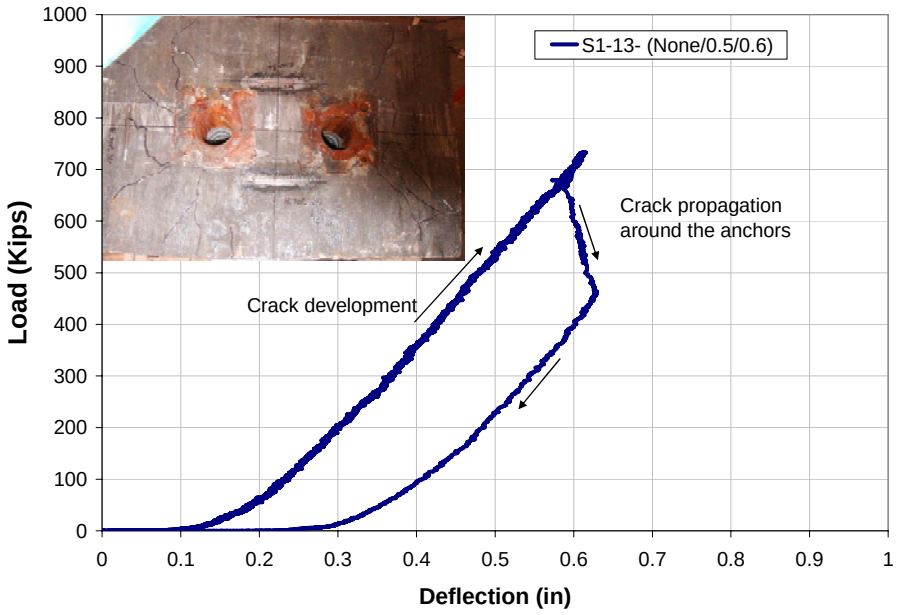

Figure 5-12: Load vs. Deflection of S1-13.

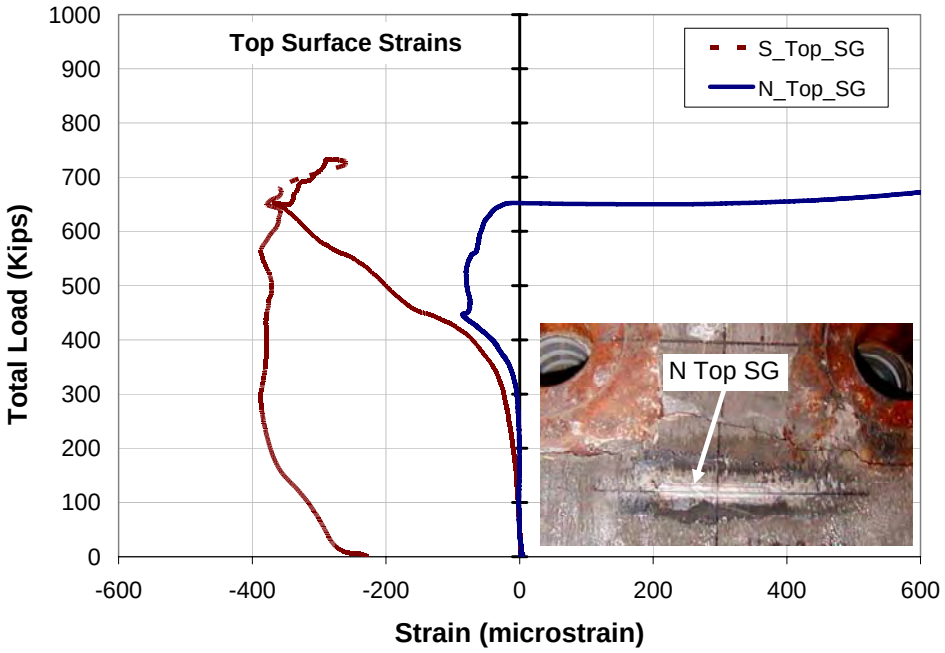

Figure 5-13: Load vs. Strain Relationship for Embedded Gauges in S1-13.

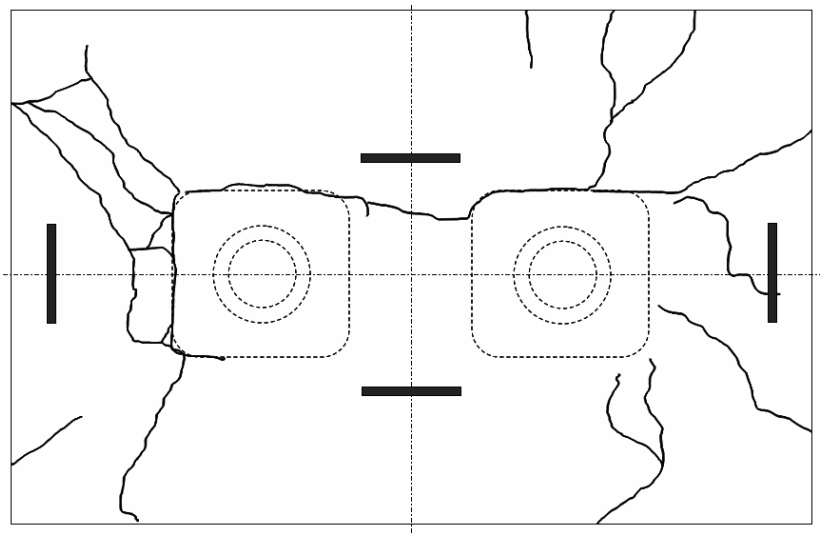

Figure 5-14: Crack Pattern at the Top Surface of S1-13.

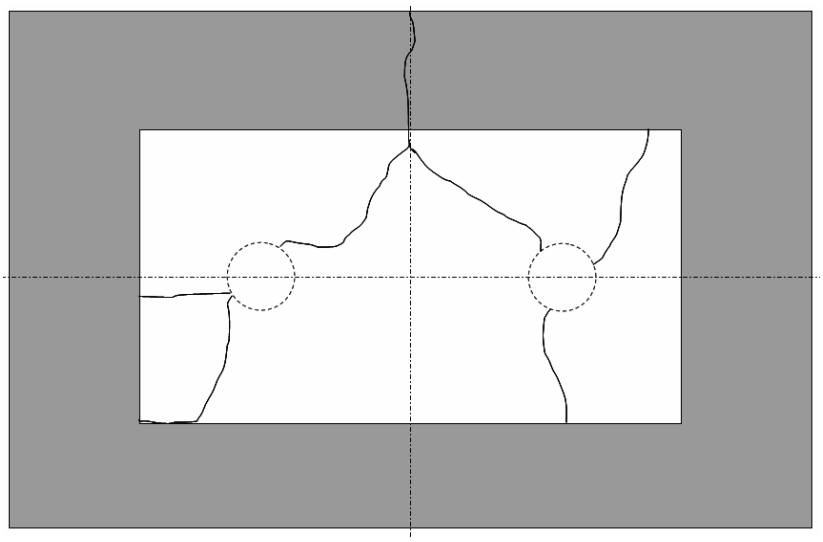

Figure 5-15: Crack Pattern at the Bottom Surface of S1-13.

5.11.3 Anchorage Test Specimen S1-2

Specimen S1-2 contained concrete with 0.5% Dramix ZP305 fibers by volume, two (2) VSL EC5-7 anchors and ducts. The specimen did not contain spirals and ties. At the bearing end of the specimen, the specimen rested in a wooden sandbox. This was considered an improvement over using the neoprene bearing pad. Therefore, all other specimens were tested with the sandbox at bearing surface.

Specimen S1-2 was tested at the age of 153 days. The 28 day compressive strength and the ninety-six (96) day compressive strength were 4767 psi and 5748 psi, respectively. The 28 day tensile strength and the ninety-six (96) day tensile strength were 408 psi and 359 psi, respectively. The failure load of 794 Kips was approximately 137% greater than twice the GUTS for each VSL anchor (2x289Kips = 578 Kips) (Figure 5-16). Although both the compressive strength and the tensile strength of the concrete in Specimen S1-2 was less than that for Specimen S1-1, the failure load of Specimen S1-2 was 26% greater than the failure load for

S1-1. The differential settlement of S1-1 may have been the reason for early failure of S1-1. Strain measurements from embedded gauges show the sudden punching failure for these types of block specimens Figure 5-17.

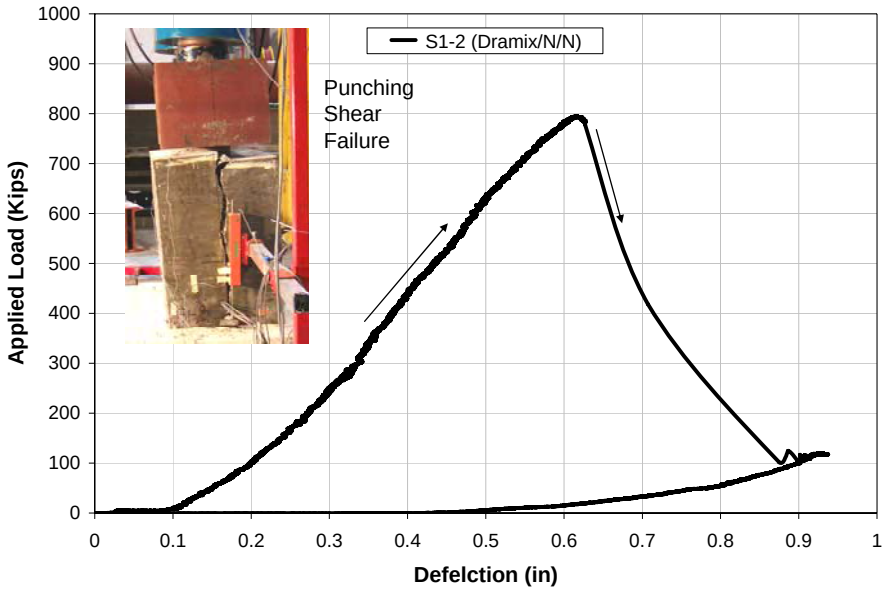

Figure 5-16: Load vs. Deflection of S1-2.

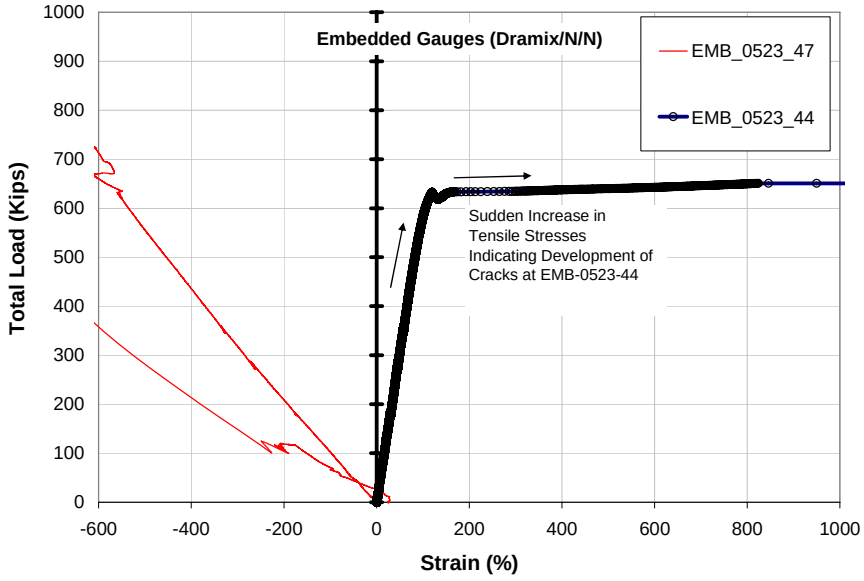

Figure 5-17: Load vs. Strain Relationship for Embedded Gauges in S1-2.

At failure, a major tension (bursting) crack developed on both the east and west faces (on the 19.5'' sides) of the specimen (Figure 5-19). Steel ties were not present to resist the tensile forces. Figure 5-19 to Figure 5-20 show the specimen split into two halves. The major break through the specimen was not accompanied by a network of many small cracks as was the case in Specimen S1-1. Few other cracks developed on the surfaces. This indicates that the steel fibers were effective in reducing tension cracks in the surface even though no steel spirals or tie reinforcement were present. The failure due to punching of the anchors and development of the large splitting crack on the short sides was sudden and accompanied with a loud explosive sound. Another major crack was noticed along the lower part of the block indicating bursting stresses due to the strut and tie action in the general stress zone.

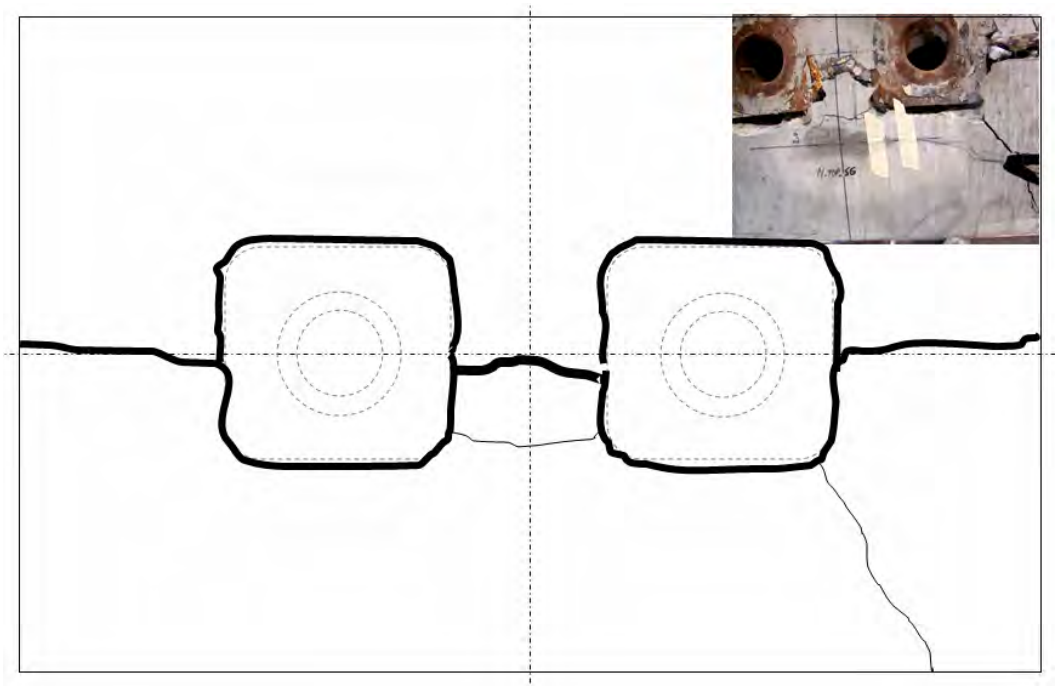

Figure 5-18: Crack Pattern on the Top of S1-2; Typical for all Specimens without Ties.

Figure 5-19: Punching Shear Failure of the Anchors in S1-2.

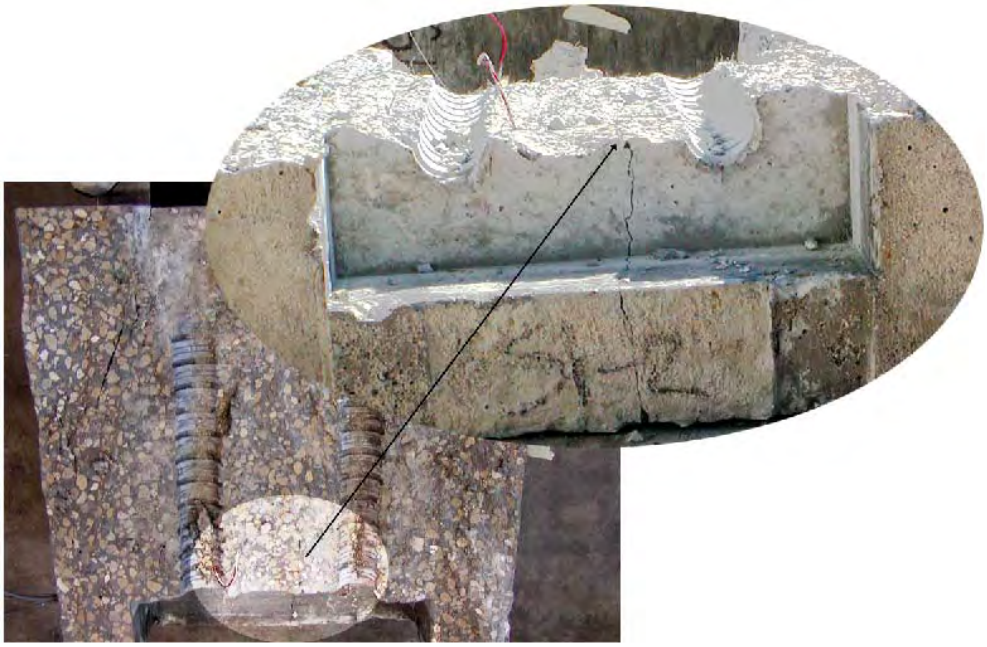

Figure 5-20: Zone of Bursting Cracks Between the two Ducts in S1-2.

5.11.4 Anchorage Test Specimen S1-3

Specimen S1-3 contained concrete with 0.5% Dramix ZP305 fibers by volume, two (2) VSL EC5-7 anchors, two ducts, and steel spirals. The specimen did not contain steel ties. Using the typical load set-up (the same as used for Specimen S1-2), Specimen S1-3 was loaded until it failed at a total load of 865.48K (Figure 5-21). Figure 5-22 shows the magnitudes of strain measurements of embedded gauges.

Specimen 1-3 was tested at the age of 154 days. Specimens S1-2 through S1-5 were all cast from the same batch of concrete. Thus, the 96 day compressive strength and the 96 day tensile strength were 5748 psi and 359 psi, respectively. The failure load of this specimen was 9% higher than the failure load of Specimen S1-2. Thus, test results indicated that the presence of spirals in the local zone contributed to a 9% increase in load capacity.

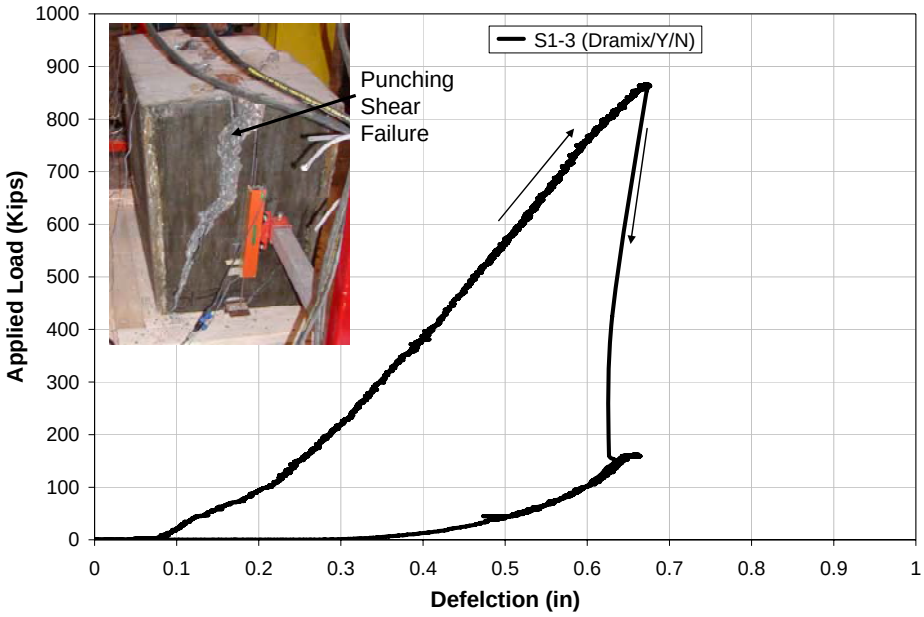

Figure 5-21: Load vs. Deflection of S1-3.

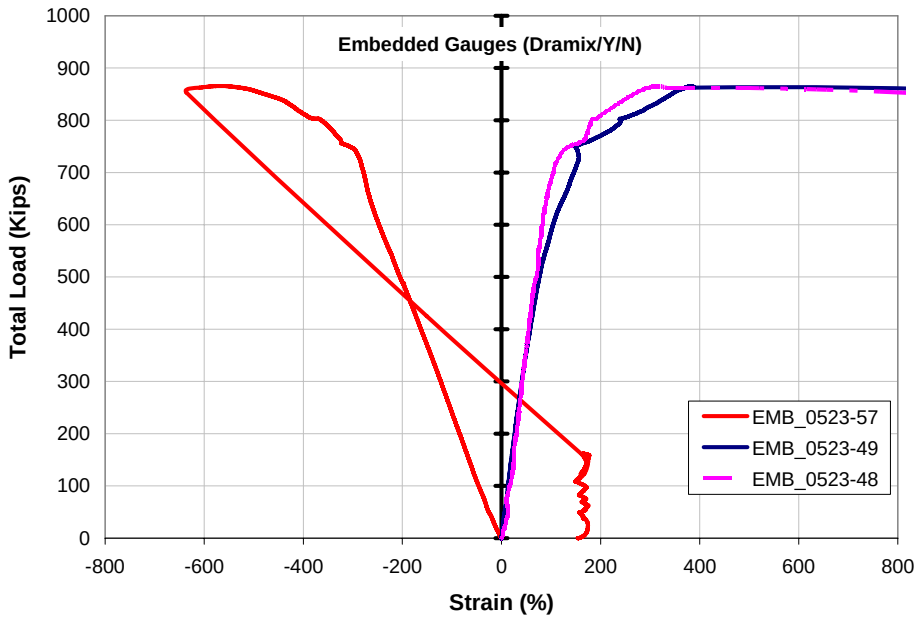

Figure 5-22: Load vs. Strain Relationship for Embedded Gauges in S1-3.

At failure, a major tension (bursting) crack developed on both the east and west faces (on the 19.5'' sides) of the specimen (Figure 5-23). The major break through the specimen was not accompanied by a networks of many small cracked as was the case in Specimen S1-1. Few other cracks developed on the surfaces (Figure 5-24). This indicates that the steel fibers were effective in reducing tension cracks in the surface even though no steel tie reinforcement was present. Although, the failure was relatively sudden without a good network of cracks developing, Unlike S1-2, the punching failure in S1-3 was for the block of steel anchors and the spirals. Two distinct blocks were resulted from the failure of this specimen as shown in Figure 5-24.

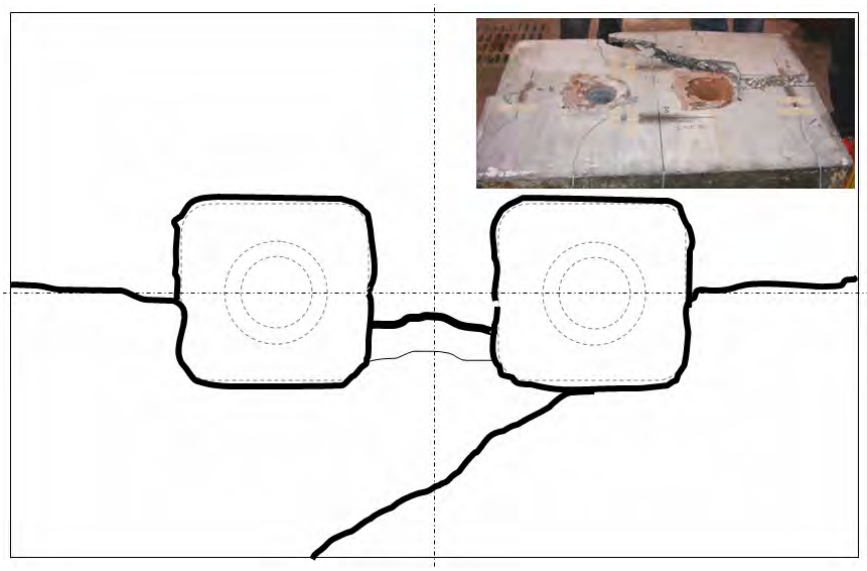

Figure 5-23: Crack Pattern on the Top of S1-3

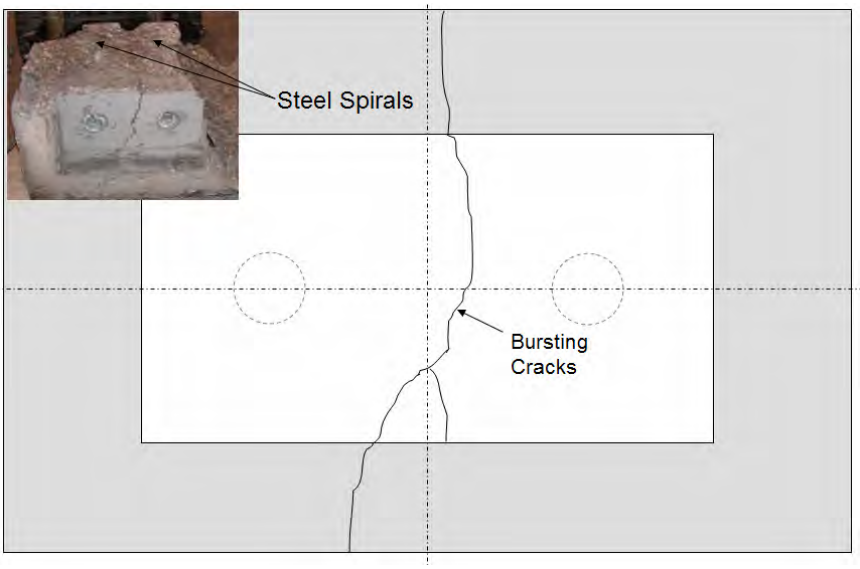

Figure 5-24: Cracks at the Base of S1-13

5.11.5 Anchorage Test Specimen S1-4

Specimen S1-4 contained concrete with 0.5% Dramix ZP305 fibers by volume, two (2) VSL EC5-7 anchors, two ducts, and steel ties. The specimen did not contain steel spirals. Specimen S1-4 was loaded until the total load of 999.23 kips was applied. The Specimen did not fail and

did not show any signs of distress during testing. Loading was stopped because the load capacity of the load test frame (1000 Kips) was reached.

A 1000 Kips load is 1.59 times greater than the load applied to Specimen S1-1 and 1.29 times greater than the load applied to Specimen 1-2. Thus, the presence of ties (even without spirals) results in more than a 26% increase in load capacity above the capacity of the specimen with 0.5% Dramix fibers by volume without ties and spirals, Specimen S1-2.

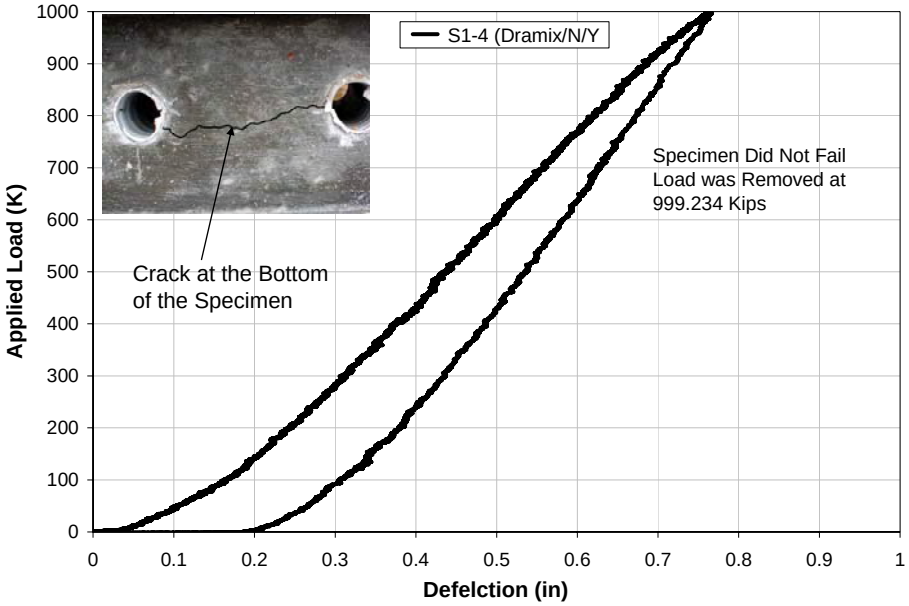

Figure 5-25: Load vs. Deflection of S1-4

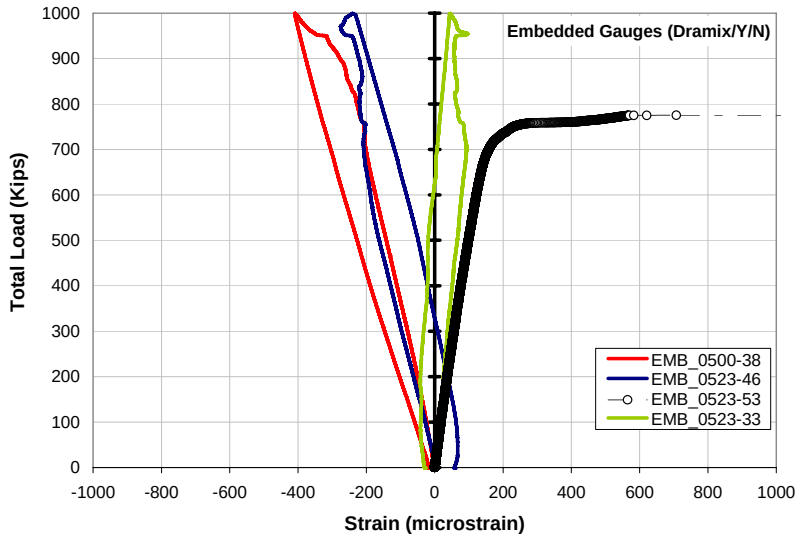

Figure 5-26: Load vs. Strain Relationship for Embedded Gauges of S1-4.

5.11.6 Anchorage Test Specimen S1-5

Specimen S1-5 contained concrete with 0.5% Dramix ZP305 fibers by volume, two (2) VSL EC5-7 anchors, two ducts, approximate 50% of the steel spiral recommended by VSL for the local zone and 60% of the steel ties used in Specimen S1-1. For this specimen, the spacing of the steel ties was twice the spacing used in Specimens S1-1 and S1-3. Specimen S1-5 was loaded until a total load of 1000.36 Kips was reached Figure 5-27. The load test was stopped because the capacity of the load frame was reached.

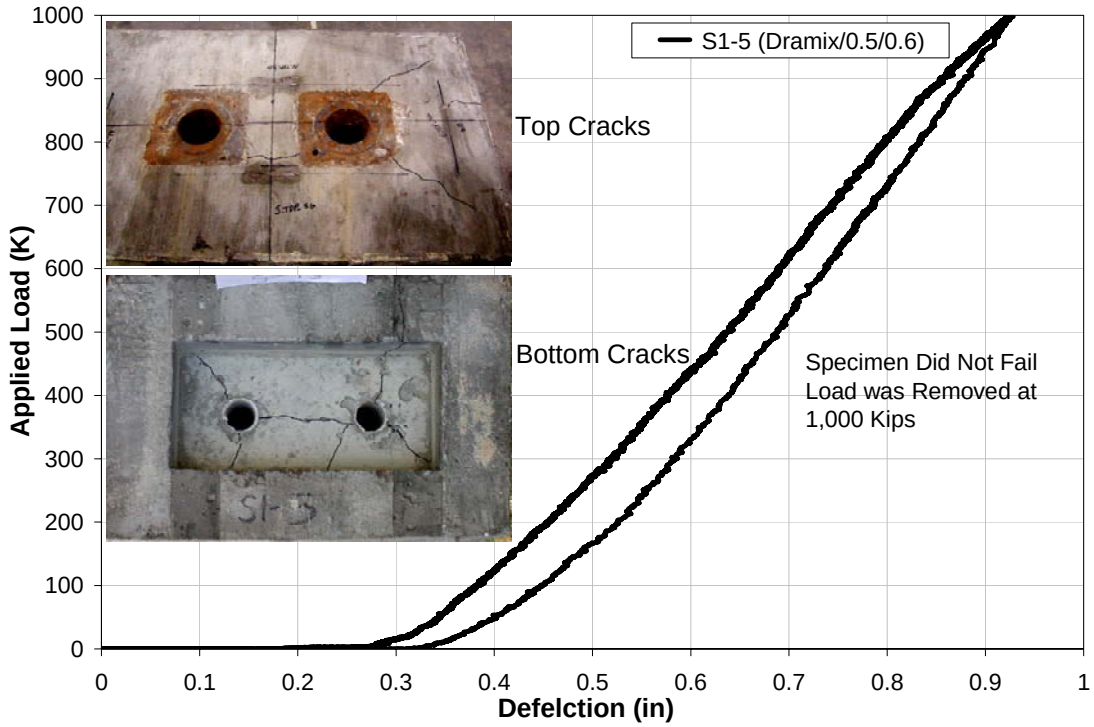

Figure 5-27: Load vs. Deflection of S1-5.

Cracks developed on the top surface, the east face and the bottom surface of Specimen S1-5 during testing. These cracks are shown in Figure 5-27 and Figure 5-28. The development of more cracks on the surface than developed for Specimen S1-4 can be attributed to the doubled tie spacing used in Specimen S1-5. Based upon the strain gage data it is estimated that the first cracks did not develop until after an applied load of approximately 850 Kips was reached (Figure 5-28).

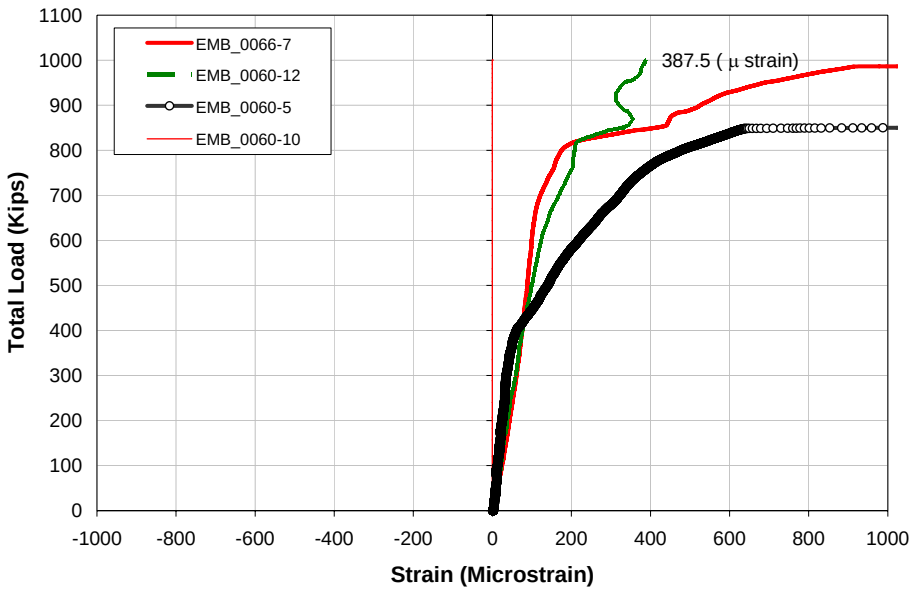

Figure 5-28: Load vs. Strain Relationship for Embedded Gauges of S1-5.

With 0.5% fiber by volume, a 50% reduction in steel spirals and a 40% reduction in steel ties, Specimen S1-5 had greater than 59% more load capacity than Specimen S1-1. Specimens S1-2 through S1-5 were cast from the same batch of concrete with 0.5% Dramix fibers by volume. Specimen S1-2 had no spiral or ties. Specimens S1-3 had spirals but not ties. Specimen S1-4 had ties but no spirals. The load capacity of Specimen S1-5 was over 26% and 16% greater than that of Specimens S1-2 and S1-3, respectively. Since load application was stopped at 1000 K for both Specimens S1-4 and S1-5, a strength comparison of the two is not feasible. From comparing Specimen S1-5 with Specimen S1-13, it is evident that the steel fibers contribute a 37% increase in load capacity. This is case even though both the concrete compressive strength and the tensile strength for Specimen S1-13 (plain concrete specimen) are greater than those for the S1-5 (Dramix specimen).

5.11.7 Anchorage Test Specimen S1-6

Specimen S1-6 contained concrete with 0.5% Helix fibers by volume, two (2) VSL EC5-7 anchors and ducts. The specimen did not contain steel spirals and steel ties. Specimen S1-6 was tested at the age of 145 days. The 28 day compressive strength and the 136 day compressive strength were 2848 psi and 3770 psi, respectively. The 28 day tensile strength and the 135 day tensile strength were 389 psi and 350 psi, respectively. The failure load of 600 Kips was approximately 3.8% greater than twice the GUTS for each of the two VSL anchors (2x289Kips = 578 Kips).

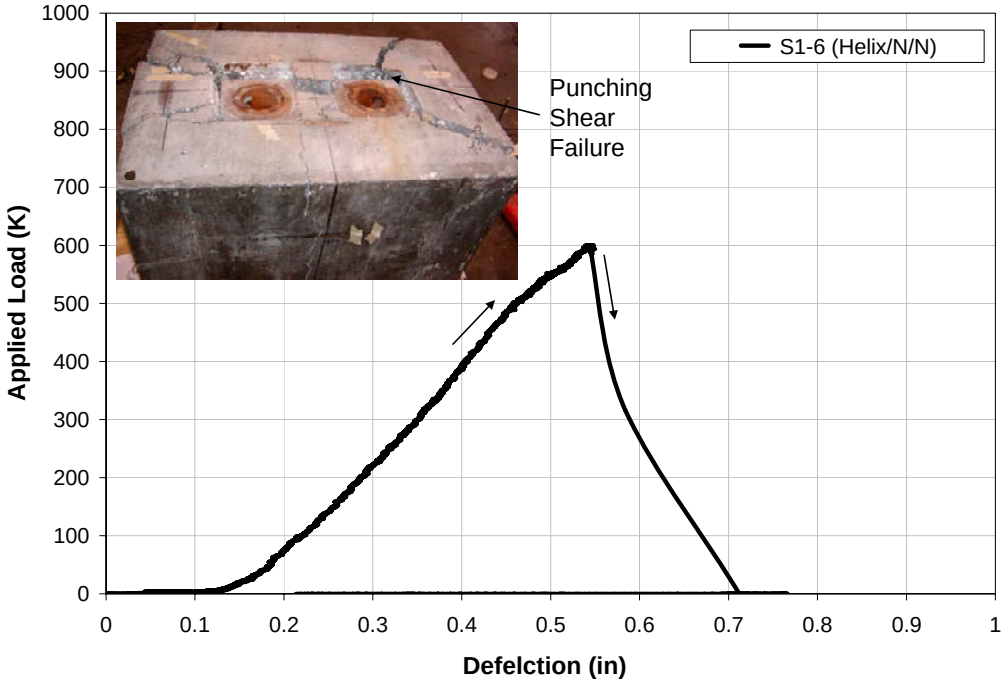

Figure 5-29: Load vs. Deflection of S1-5.

Both the compressive strength and the tensile strength of the concrete in Specimen S1-6 was less than that for Specimen S1-1. The 28 day strength (2848 psi) of the concrete used in the Helix Specimens, S1-6 to S1-9, was less than the 4000 psi mix design strength. The ratios of the 28 day compressive strengths and the tensile strengths of the Helix Specimens to that of plain

concrete specimens were 0.59 and 1.07, respectively. Thus, although the compressive strength of the concrete with Helix fibers was approximately 41% less, the tensile strength was approximately 7% greater than that of the plain concrete specimens. For the highest ages recorded, the ratio of compressive strength of Helix specimens to that of the plain concrete specimens was 0.57 and the ratio of tensile strength of the Helix specimens to that of plain concrete specimens was 0.77. Even with these strength differences, the failure load of Specimen S1-6 (with Helix) was only 4% less than the failure load for S1-1. Thus, the presence of Helix fibers in the concrete mix, even with low strength concrete, improves the tensile strength of the specimen. Perhaps, the use of the neoprene bearing pad for Specimen S1-1 contributed to a lower load capacity for Specimen S1-1. Although this may be the case, it still must be noted that Specimen S1-6 carried a maximum load (600 K) that was 1.04 times greater than the GUTS load (578Kips) for the two (2) VSL anchors. In the final stage of loading, failure was initiated by punching shear at the anchors. This was accompanied by the development of bursting tension cracks on the side surfaces. Figure 5.30 shows the specimen broke into pieces and the development of bursting stresses at the lower part of the sample. At maximum applied load the tensile strains ranged between 147 to 180 microstrain (Figure 5-30).

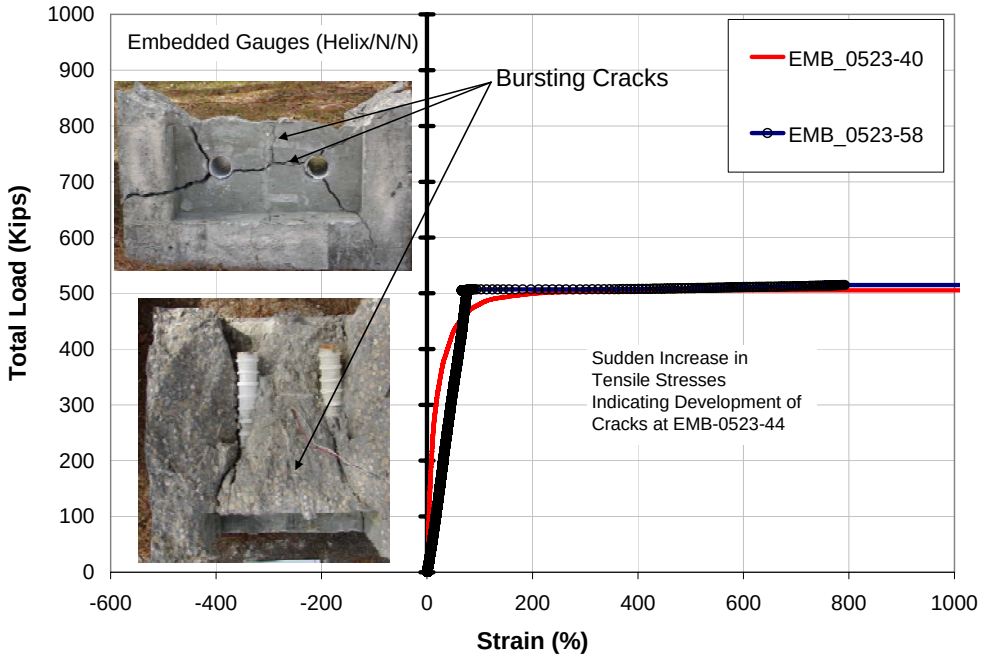

Figure 5-30: Load vs. Strain Relationship for Embedded Gauges of S1-6.

5.11.8 Anchorage Test Specimen S1-7

Specimen S1-7 contained concrete with 0.5% Helix fibers by volume, two (2) VSL EC5-7 anchors, two ducts, and steel spirals. The specimen did not contain steel ties. Using the typical load set-up (the same as used for Specimen S1-2), Specimen S1-7 was loaded until it failed at a total load of 677.21 Kips (Figure 5-31).

Specimen 1-7 was tested at the age of 148 days. Specimens S1-6 through S1-9 were all cast from the same batch of concrete. The failure load for S1-7 was 17% greater the GUTS for the two anchors. With lower strength concrete, the strength capacity of S1-7 was 1.08 times greater than that of S1-1. Comparing the ultimate load applied to S1-7 and S1-6, reveals that the inclusion of spirals in the local zone contributes to a 13% increase in load capacity. Figure 5-32 presents relationship of load vs. strain measurements from embedded gauges.

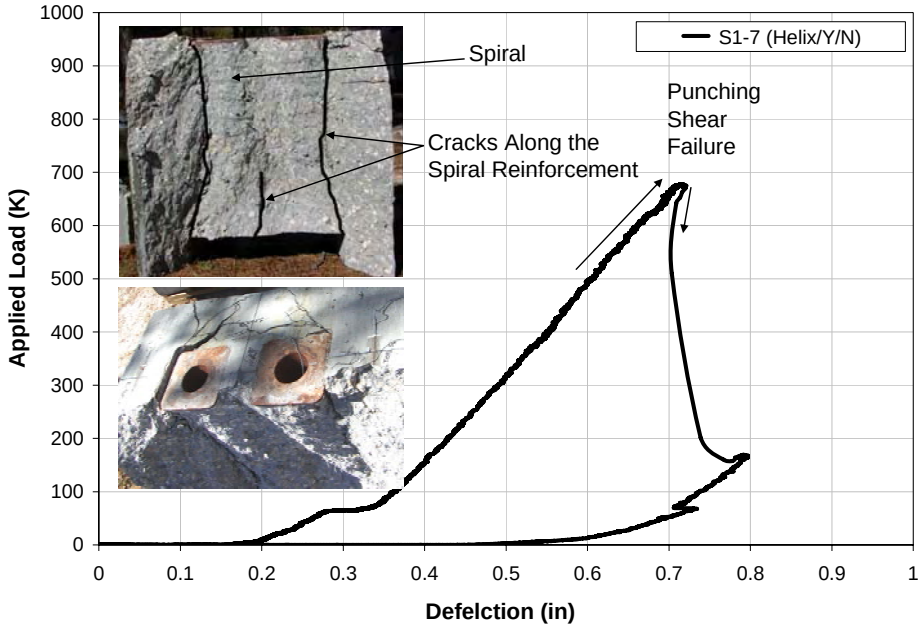

Figure 5-31: Load vs. Deflection of S1-7.

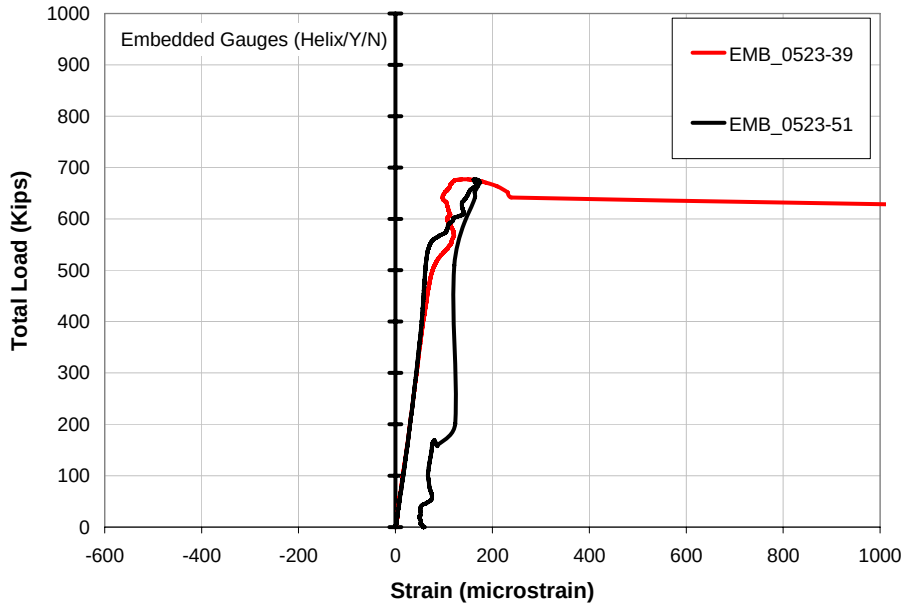

Figure 5-32: Load vs. Strain Relationship for Embedded Gauges of S1-7.

5.11.9 Anchorage Test Specimen S1-8

Specimen S1-8 contained concrete with 0.5% Helix fibers by volume, two (2) VSL EC5-7 anchors, two ducts, and steel ties. The specimen did not contain steel spirals. Specimen S1-8

was loaded until the total load of 919.7 kips was applied (Figure 5-33). Figure 5-34 shows the relationship between applied load and strain measurements for embedded gauges. A 919.7 Kips load is 1.38 times greater than the load applied to Specimen S1-1 and 1.59 times greater than the load GUTS for the VSL anchors. Comparing the ultimate load applied to S1-8 and the ultimate load applied to S1-6 (which has 0.5% fiber but not spirals and ties), the test results showed that the presence of steel ties results in a 53% increase in load capacity. Even with low strength concrete, the addition of Helix fibers to the section results in a significant increase in load carrying capacity. The increase in strength attributable to ties in the specimen with Helix fibers is even greater than the 26% increase attributable to ties in the specimens with Dramix fibers.

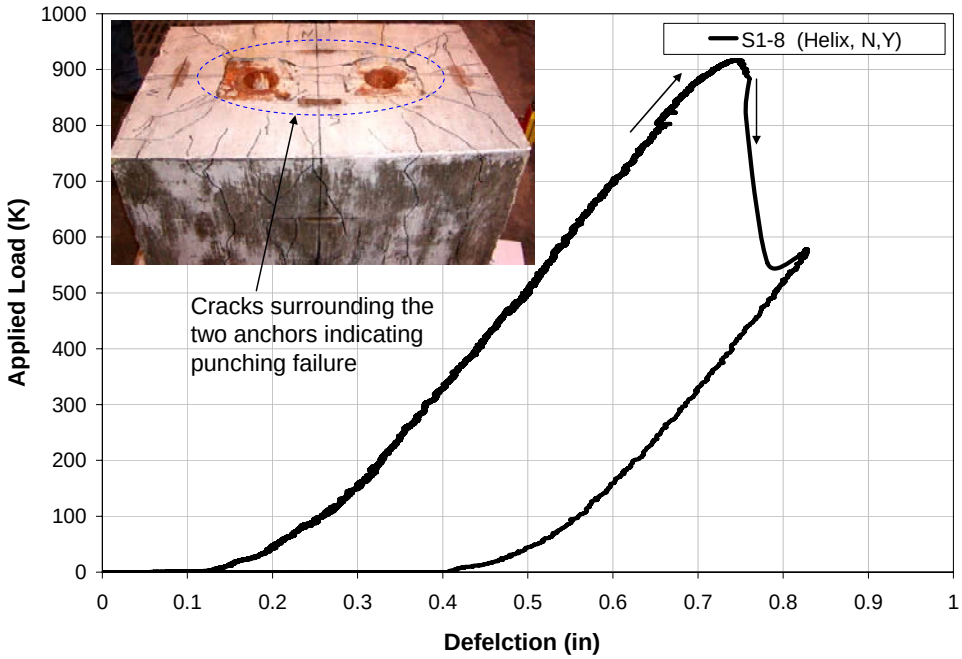

Figure 5-33: Load vs. Deflection of S1-8.

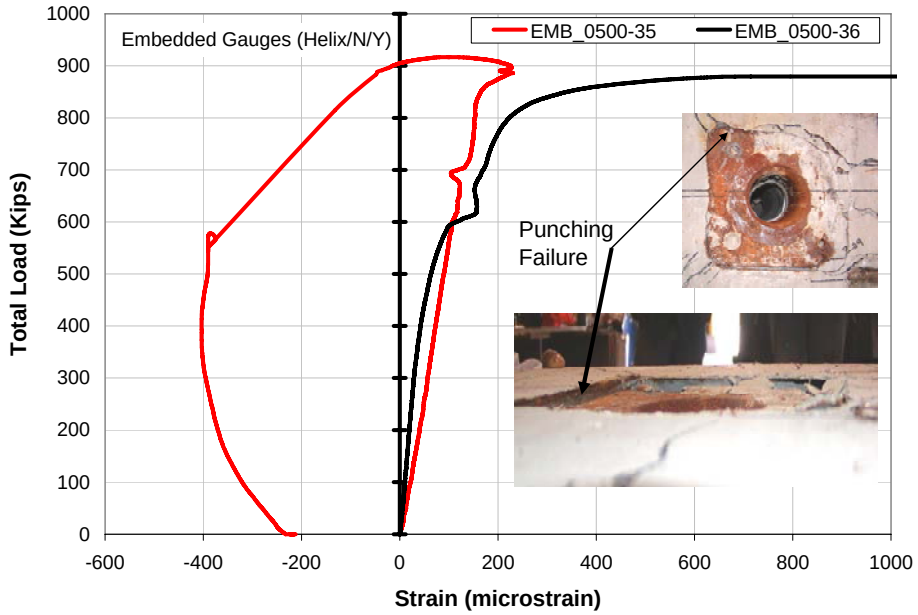

Figure 5-34: Load vs. Strain Relationship for Embedded Gauges of S1-8.

5.11.10 Anchorage Test Specimen S1-9

Specimen S1-9 contained concrete with 0.5% Helix fibers by volume, two (2) VSL EC5-7 anchors, two ducts, approximate 50% of the steel spiral recommended by VSL for the local zone and 60% of the steel ties used in Specimen S1-1. For this Specimen, the spacing of the steel ties was twice the tie spacing used in Specimens S1-1 and S1-8. Specimen S1-9 was loaded until a total load of 869.2 Kips was reached (Figure 5-35). While cracks developed on all visible surfaces during load testing, failure was not dramatic. The specimen simply ceased to resist any load greater than the final applied load. Figure 5-36 shows strain values from embedded gauges and pattern of cracks at the top and the bottom of the block.

With 0.5% fiber by volume, a 50% reduction in steel spirals and a 40% reduction in steel ties, Specimen S1-9 had 38% more load capacity than Specimens S1-1. Specimens S1-6 through S1-

9 were all cast from the same batch of concrete with 0.5% Helix fibers by volume. Specimen S1-6 had no spiral or ties. Specimens S1-7 had spirals but not ties. Specimen S1-8 had ties but no spirals. The load capacity of Specimen S1-9 was 45% and 28% greater than that of Specimen S1-6 and Specimen S1-7, respectively. The load capacity for Specimen S1-9 was 5% less than the load capacity of Specimen S1-8. Based upon these load tests, the presence of steel ties in the general zone contributes more to load capacity than does the presence of spirals in the local zone. Comparing Specimen S1-9 with Specimen S1-13 shows that the steel fibers contributed to a 19% increase in load capacity.

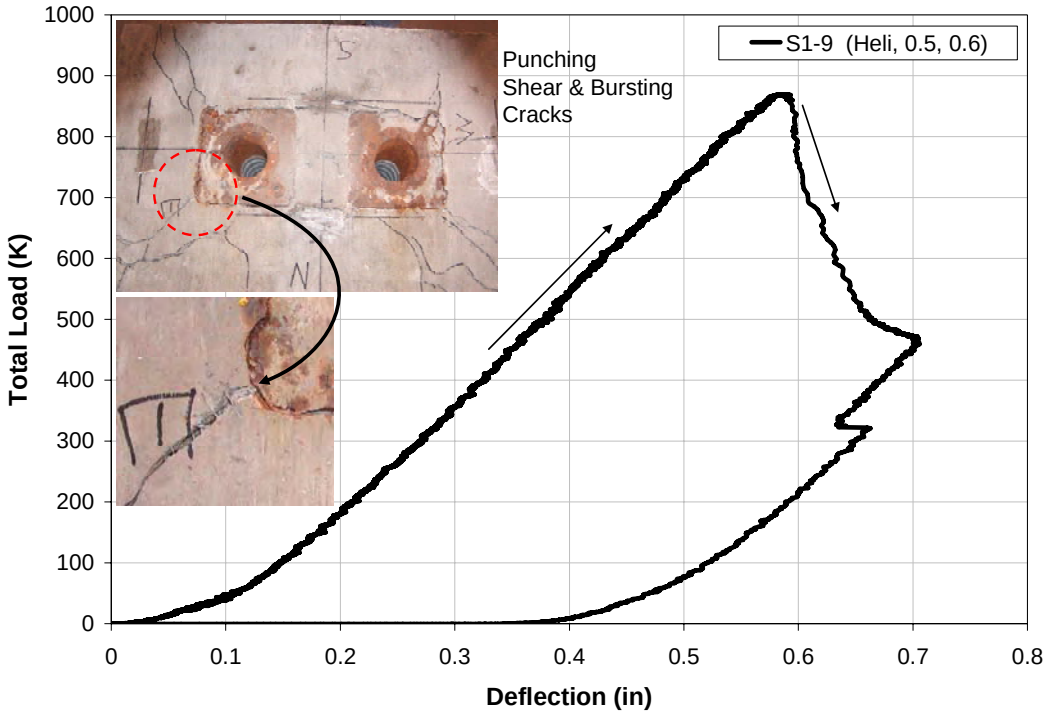

Figure 5-35: Load vs. Deflection of S1-9.

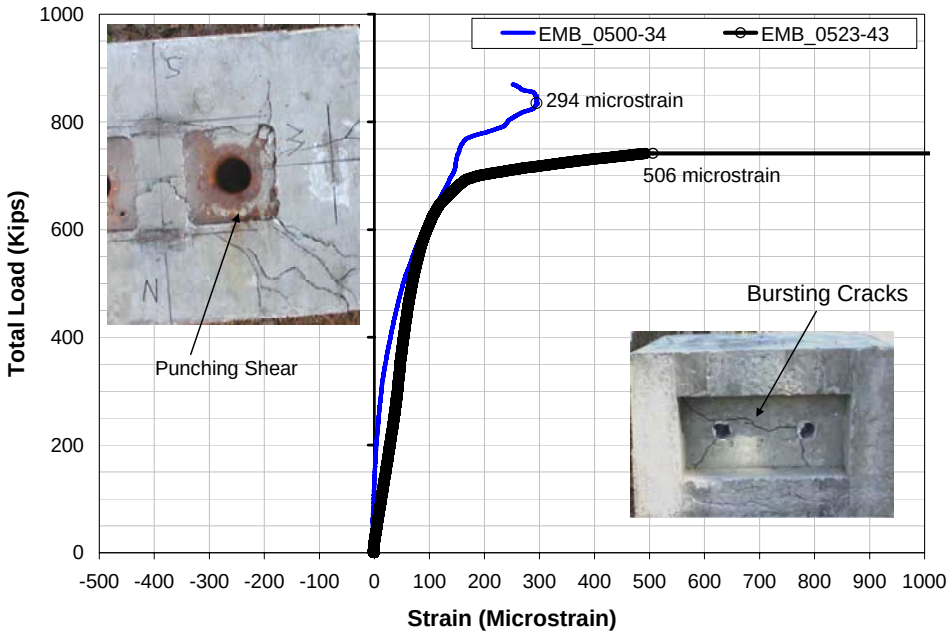

Figure 5-36: Load vs. Strain Relationship for Embedded Gauges of S1-9

5.11.11 Anchorage Test Specimen S1-10

Specimens S1-10, S1-11 and S1-14 were all cast from the same batch of concrete with 0.5% Novomesh fibers by volume. In addition to the Novomesh fibers, Specimen S1-10 contained two (2) VSL EC5-7 anchors and ducts. The specimen did not contain steel spirals and steel ties. Specimen S1-10 was tested at the age of 149 days. The 28 day compressive strength and the 154 day compressive strength were 4305 psi and 5752 psi, respectively. The 28 day tensile strength and the 154 day tensile strength were 410 psi and 295 psi, respectively. The failure load of 838.5 Kips was approximately 45% greater than twice the GUTS for each VSL anchor (2x289Kips = 578 Kips) and 34% greater than the maximum load applied to Specimen S1-1. The failure of Specimen S1-10 was a sudden, explosive failure (Figure 5-37). The first visible surface crack did not develop until a load of approximately 750 Kips was applied to the specimen (Figure 5-38). Steel ties were not present to resist the bursting tensile stresses.

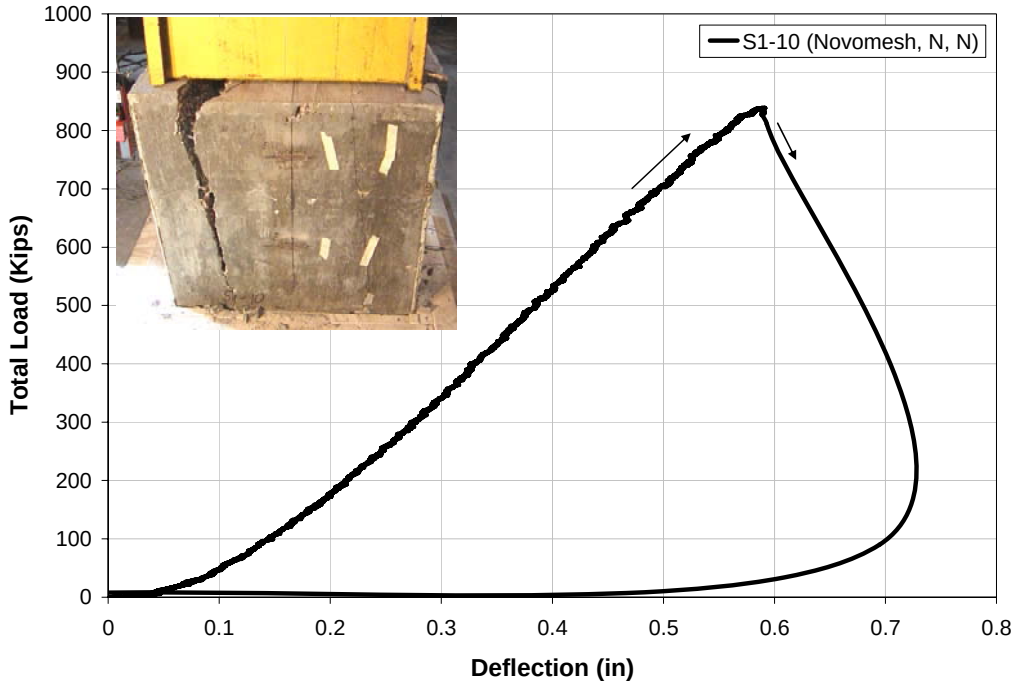

Figure 5-37: Load vs. Deflection of S1-10

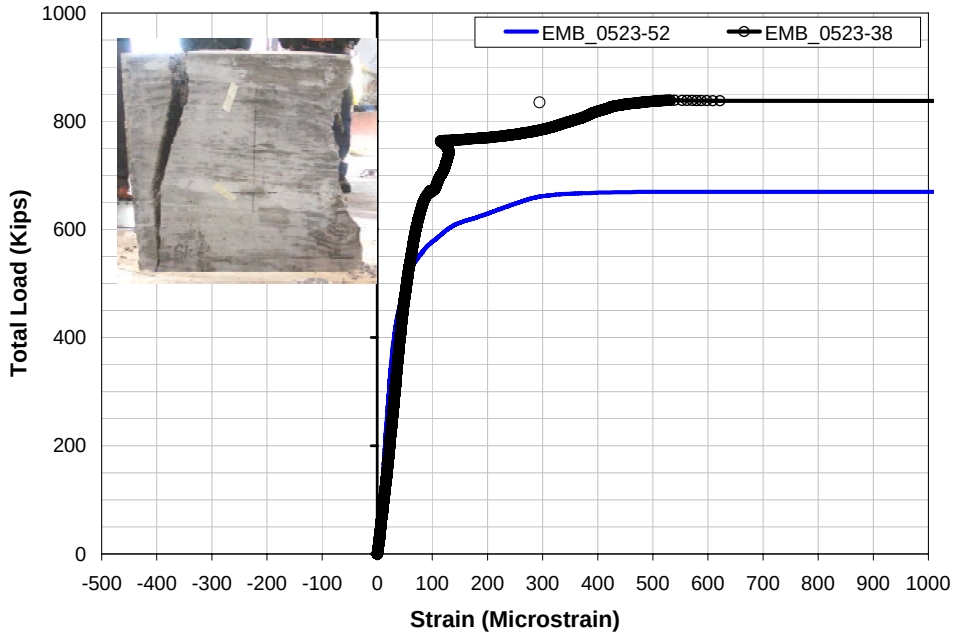

Figure 5-38: Load vs. Strain Relationship for Embedded Gauges of S1-10

5.11.12 Anchorage Test Specimen S1-11

Specimen S1-11 contained concrete with 0.5% Novomesh fibers by volume, two (2) VSL EC5-7 anchors, two ducts, and steel spirals. The specimen did not contain steel ties. Using the typical load setup, Specimen S1-11 was loaded until it failed at a total load of 706.32 Kips (Figure 5-39). Specimen S1-11 was tested at the age of 149 days. The failure load for S1-11 was 22% greater the GUTS for the two anchors and 12% greater than the load applied to Specimen S1-1. However, the total load applied to Specimen S1-11 was 16% less than the load applied to Specimen S1-10. Based upon the shape of Specimen S1-11, form racking occurred during the casting of the specimen. The top and side surfaces of the specimen were slightly angled. This may have contributed to the reduced load capacity. For both Dramix and Helix specimens, the addition of spirals in the local zone resulted in an increase in load capacity not a decrease.

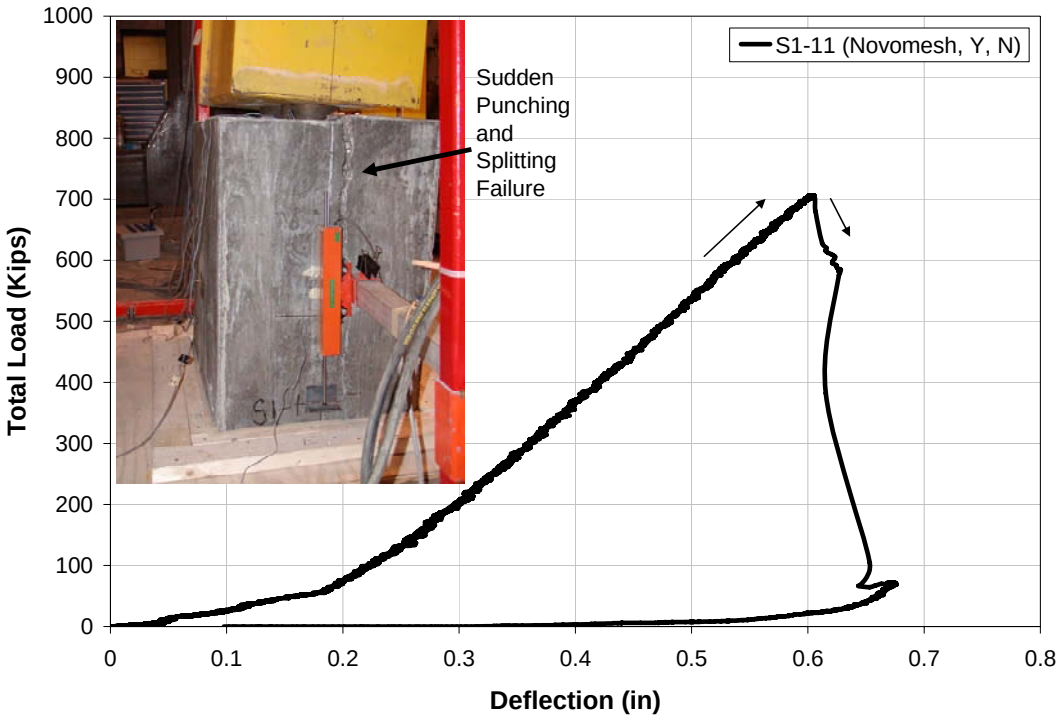

Figure 5-39: Load vs. Deflection of S1-11

During loading, the first cracks occurred at approximately 450 Kips. The cracks grew in size and number until the specimen completely failed at 706.3 Kips (Figure 5-40). As noted for other load tests, in specimens without steel ties the number of cracks were much less but were much larger than cracks that develop in specimens with steel ties.

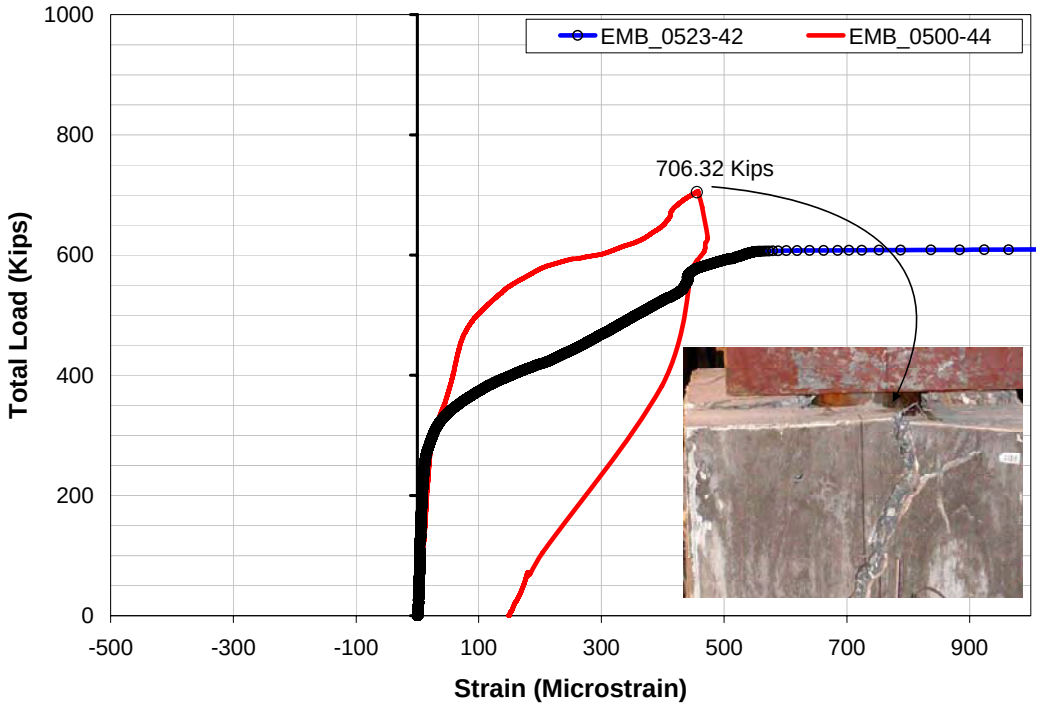

Figure 5-40: Load vs. Strain Relationship for Embedded Gauges of S1-11

5.11.13 Anchorage Test Specimen S1-14

Specimen S1-14 contained concrete with 0.5% Novomesh fibers by volume, two (2) VSL EC5-7 anchors, two ducts, approximate 50% of the steel spiral recommended by VSL for the local zone and 60% of the steel ties used in Specimen S1-1. For this Specimen, the spacing of the steel ties was twice the tie spacing used in Specimen S1-1.

Specimen S1-14 was loaded until a total load of 995.59 Kips was reached. The Specimen did not fail. The load application was stopped because the load limit for the load testing frame (1000 Kips) was reached, essentially. At the conclusion of the load test, there were no visible cracks on the surface of Specimen S1-14. When the load was removed the specimen looked as if no load had been applied. Figure 5-41 shows load vs. deflection relationship for S1-14.

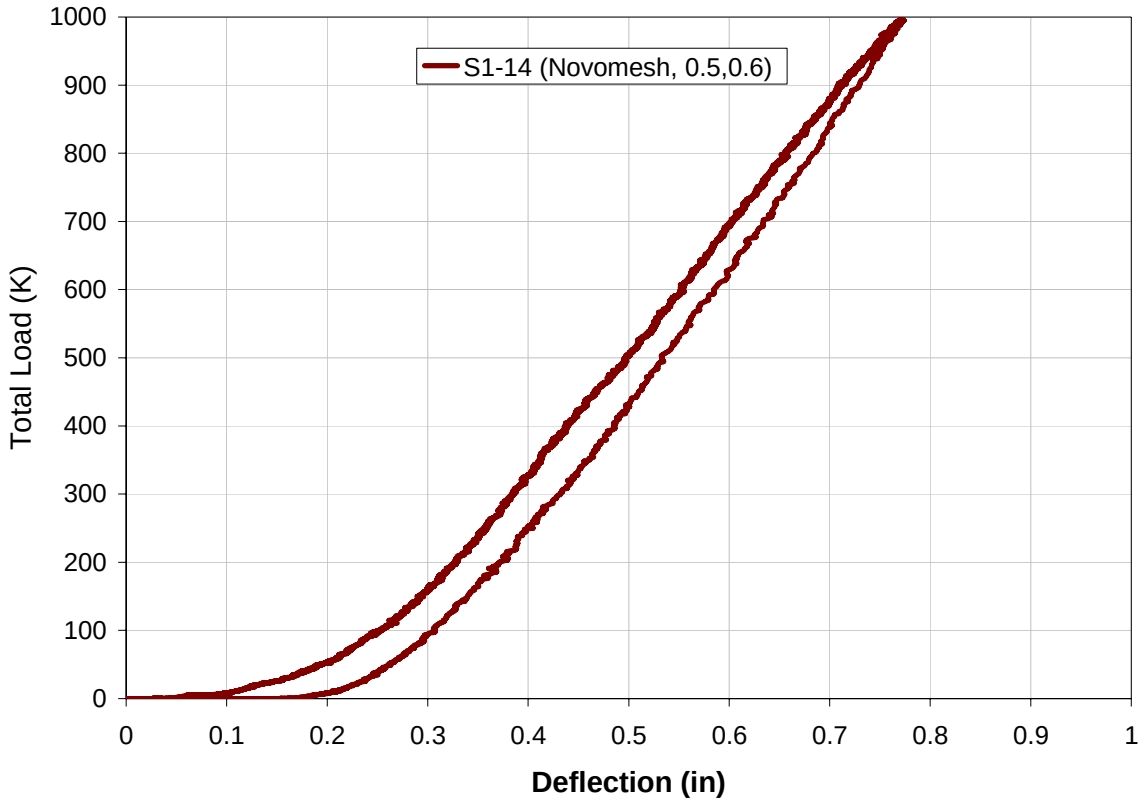

Figure 5-41: Load vs. Deflection of S1-12

Considering a final load capacity in excess of 1000 Kips, Specimen S1-14 was greater than 59% stronger than Specimen S1-1 and greater than 19% stronger than Specimen S1-10. Since Specimen S1-14 had a load capacity that was over 1.36 times greater than that of Specimen S1-13, the steel fibers contributed at least a 36% increase in load capacity.

The load capacity for the specimen was over 1.73 times greater than the GUTS for the VSL anchors. The facts that no cracks developed at 1000 Kips indicates that the polypropylene fibers helped to prevent the development of cracks on the surface of the specimen. Figure 5-42 shows load vs. strain data for S1-14.

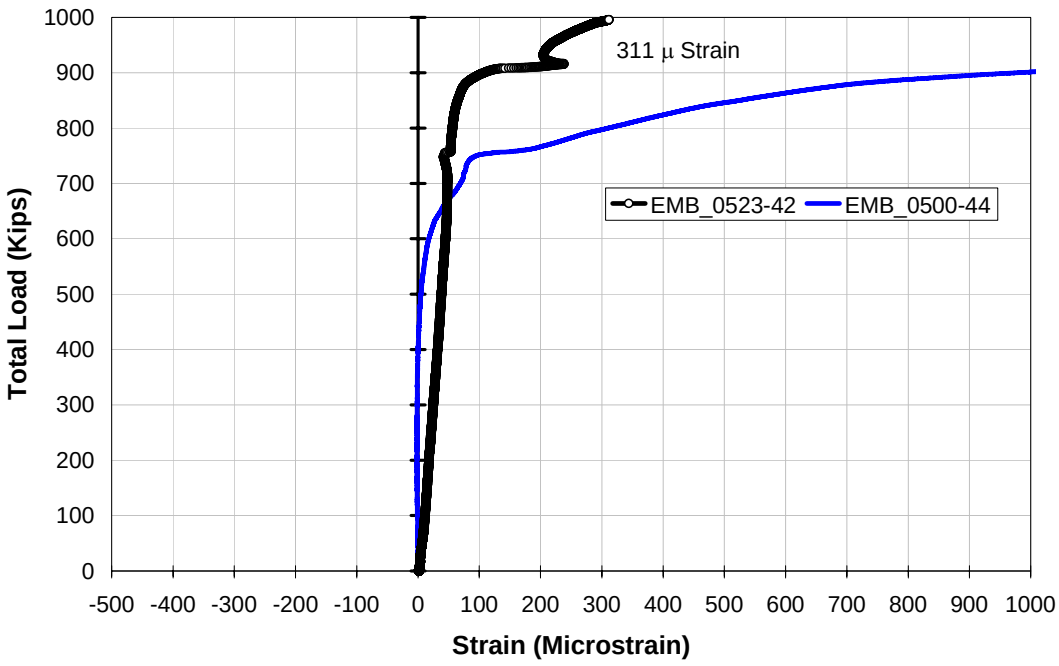

Figure 5-42: Load vs. Strain Relationship for Embedded Gauges of S1-14

5.12 Anchorage Test Specimens with Dywidag Anchors (S2)

Each of the S2 Specimens was cast with two (2) Dywidag Multiple Plane Anchorages, MA 5-0.6", and two ducts. The guaranteed ultimate tensile strength (GUTS) for each anchor is 289 Kips. With two anchors in each specimen, the total GUTS is 589 Kips; the same as was used for the specimens with the VSL anchors. The trumpets needed to connect the Dywidag anchors to the ducts, were not available. Thus, duct material was used to create a connection between the anchors and the ducts. This was not the Dywidag anchor system as designed. Thus, the

strengths obtained in the test program may have been affected by the absence of the trumpets. However, since all of the S2 specimens were fabricated in the same way, strength comparisons can still be made for the various fiber and steel combinations considered in the S2 specimens. The bearing surface for all S2 specimens was a wooden sandbox.

5.12.1 Anchorage Test Specimen S2-1

Specimen S2-1 contained plain concrete, two Dywidag MA 5-0.6 anchors with ducts, two steel spirals and steel ties. Specimens 2-1 was tested at the age of 55 days. The 28 day compressive strength and the fifty-five (55) day compressive strength were 4406 psi and 5598 psi, respectively. The 28 day tensile strength and the fifty-six (56) day tensile strength were 265 psi and 275 psi, respectively.

The maximum load applied to the specimen was 723.25 Kips. This load was 1.25 times greater than the GUTS for the two anchors. Figure 5-44 shows some punching did occur at the anchors. However, this occurred near the upper limit of the load applied to the specimen. Failure occurred due to the application of an excessive load; significant cracking and/or breaking of the specimen occurred on all surfaces during the load test.

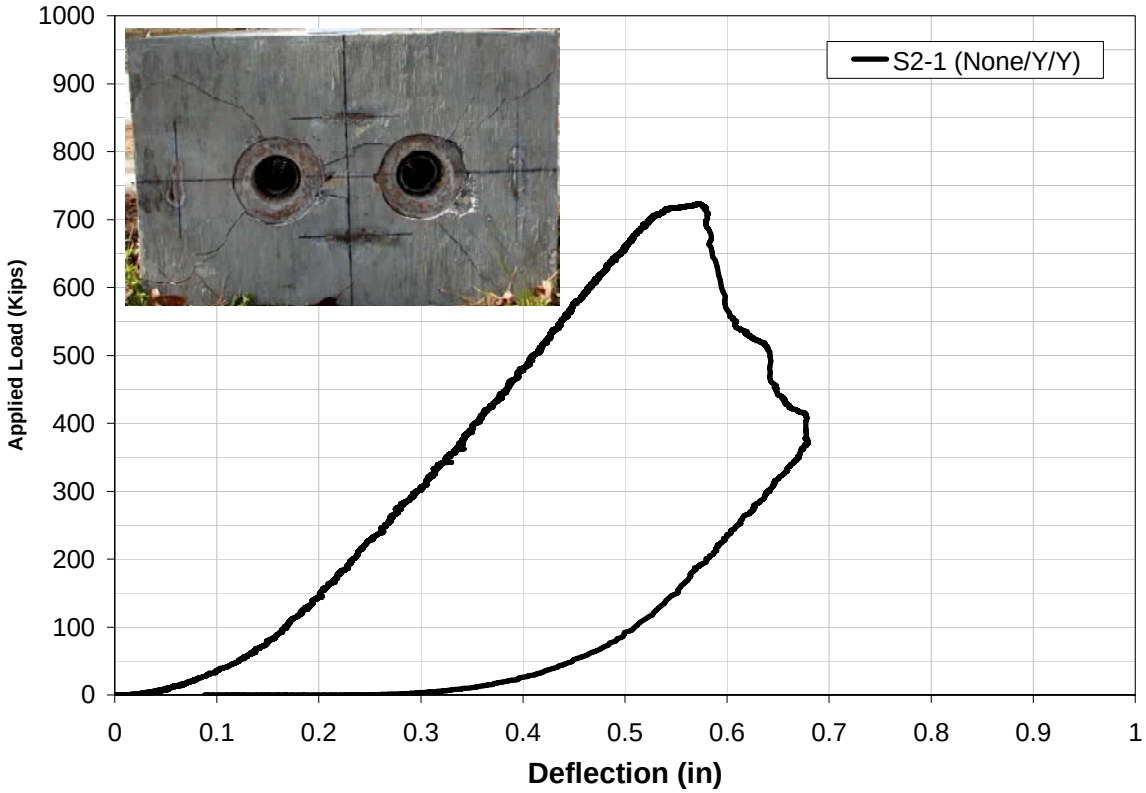

Figure 5-43: Load vs. Deflection of S2-1

A major difference between Specimens S2-1 and Specimen S1-1 are the anchors that were embedded in each; S2-1 had Dywidag anchors and S1-1 had VSL anchors. Another difference was in the testing setup for the two specimens. At the bearing surface, for Specimen S1-1 a neoprene bearing pad was used instead of the sandbox that was used for Specimen S2-1. The maximum load applied to Specimen S2-1 was approximately 15% greater than the maximum load applied to S1-1. However, the concrete compressive strength of the S2-1 was approximately 15% less than the concrete strength of Specimen S1-1. The relationship between load vs. strain measurements is shown in Figure 5-44.

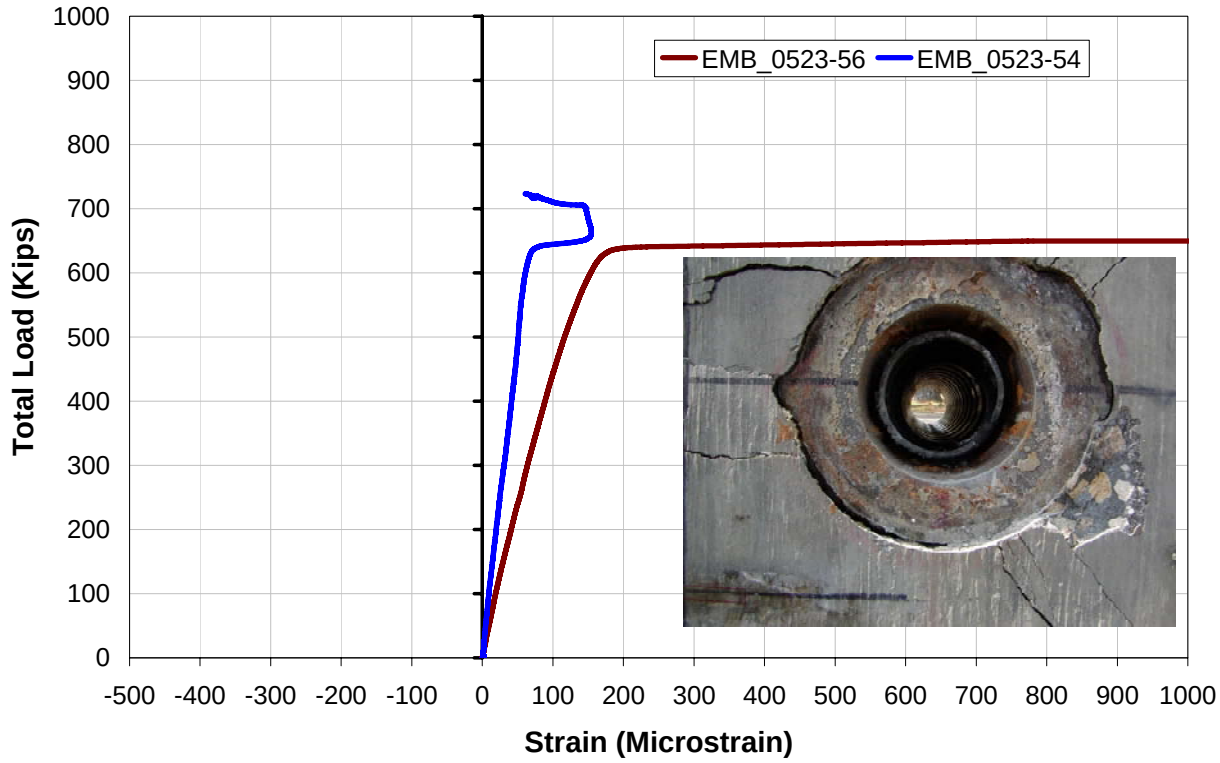

Figure 5-44: Load vs. Strain Relationship for Embedded Gauges of S2-1

5.12.2 Anchorage Test Specimen S2-14

Specimen S2-14 contained plain concrete two (2) Dywidag MA5-0.6" anchors, two ducts, approximate 50% of the steel spiral recommended by Dywidag for the local zone and 60% of the steel ties used in Specimen S2-1. For this specimen, the spacing of the steel ties was twice the tie spacing used in Specimens S2-1 (and the same as that used in S1-2). At the bearing end of the specimen, the specimen rested in a wooden sandbox.

Specimen S2-14 was tested at an age of 56 days. The first visible cracks on the surface of the specimen did not develop until a load in excess of 600 kips was reached. Medium cracks exist on all surfaces of the specimen. Bursting tension cracks are on the east and west faces of the walls. Failure was initiated in the general zone of the anchorage specimen. The failure load

was 645.8 Kips (1.117 times greater than GUTS). Figure 5-45 load vs. deflection relationship, and Figure 5-46 shows strain measurements of embedded gauges in S1-14.

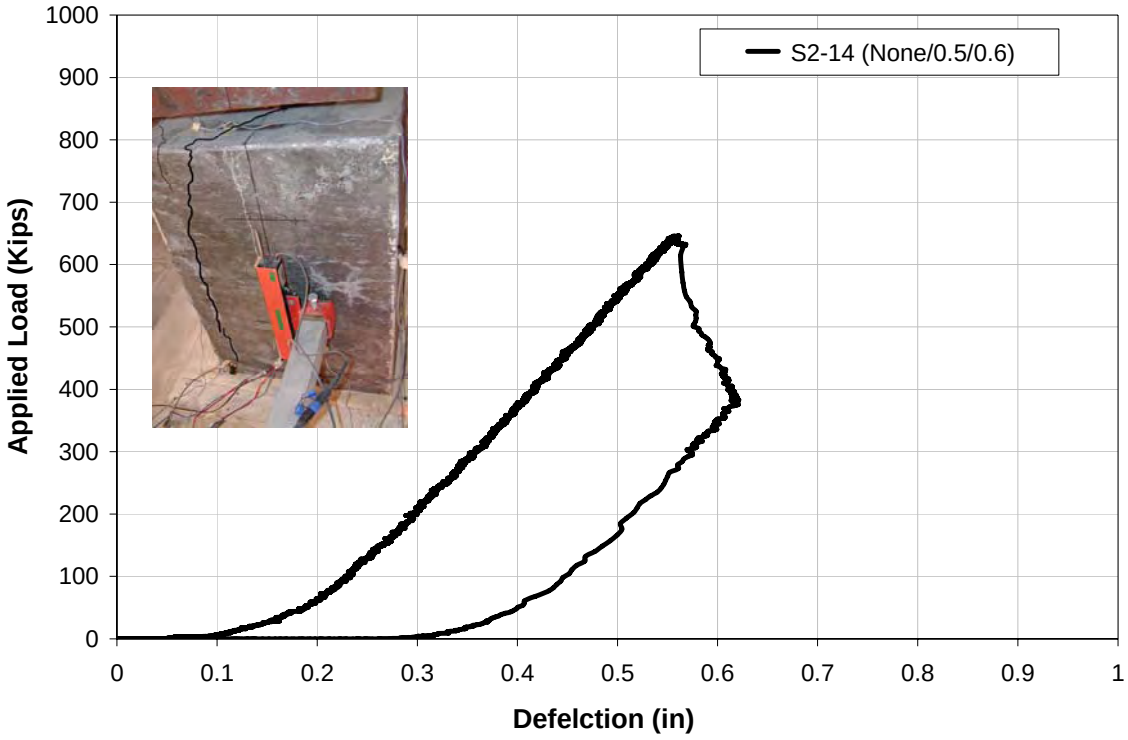

Figure 5-45: Load vs. Deflection of S2-14

With approximately 50% of the spiral steel and 60% of the tie steel used in Specimen S2-1, Specimen S2-14 had over 89% of the strength of Specimen S2-1. Except for the different anchors and the different concrete strengths, Specimens S2-14 and S1-13 were similar. The total load applied to S2-14 (646 Kips) was 12% less than the load applied to S1-13. As stated previously, the concrete strength of Specimen S2-14 was over 15% less than that of Specimen S1-13.

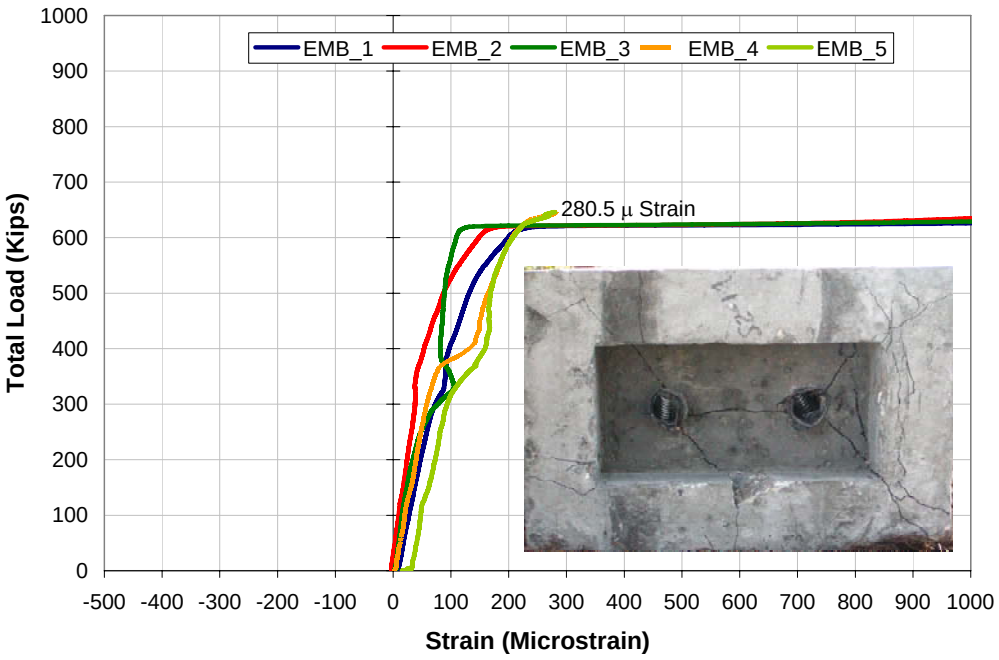

Figure 5-46: Load vs. Strain Relationship for Embedded Gauges of S2-14

5.12.3 Anchorage Test Specimen S2-2

Specimen S2-2 contained concrete with 0.5% Dramix ZP305 fibers by volume, two (2) Dywidag MA5-0.6" anchors and ducts. The specimen did not contain steel spirals and steel ties. Specimens S2-2 through Specimen S2-5 were all cast from the same batch of concrete with 0.5% Dramix ZP305 fibers by volume. Specimen S2-2 was tested at the age of 55 days. The 28 day compressive strength and the 55 day compressive strength were 3463 psi and 4200 psi, respectively. The 28 day split tensile strength and the 56 day split tensile strength were 323 psi and 365 psi, respectively. The compressive strength of 4200 psi was slightly above the concrete mix design strength of 4000 psi.

The failure load of 557.2 Kips (Figure 5-47) was approximately 4% less than twice the GUTS for the anchors (578 Kips). The failure was sudden and without warning. The two factors which

most contributed to this reduced load capacity are absence of steel spirals and the absence of steel ties. Even without the reinforcing steel, the load capacity of Specimen S2-2 was approximately 77% of the load capacity of Specimen S2-1, which contained plain concrete, the full Dywidag recommended spirals, and steel ties.

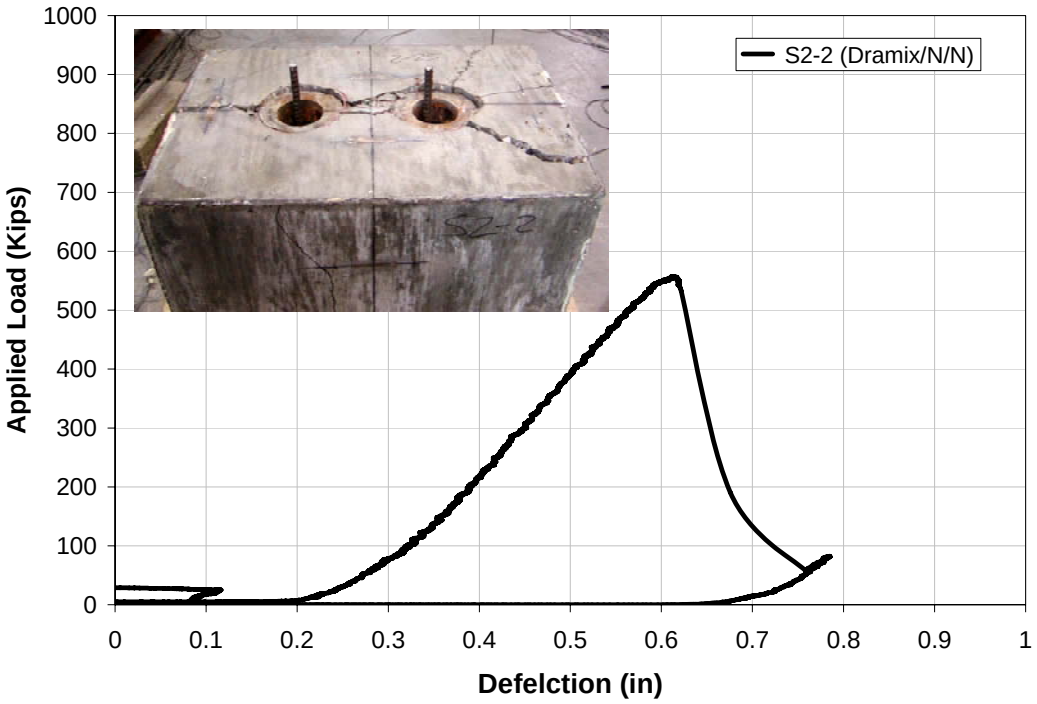

Figure 5-47: Load vs. Deflection of S2-2

Figure 5-48 shows strain values from embedded gauges along with an image of the anchors punching through the concrete. Large cracks developed on the east and west faces (short sides) of the specimen. These cracks were very wide because steel tie reinforcement was not present to distribute the tensile forces. Much smaller cracks developed on the north and south faces of the specimen.

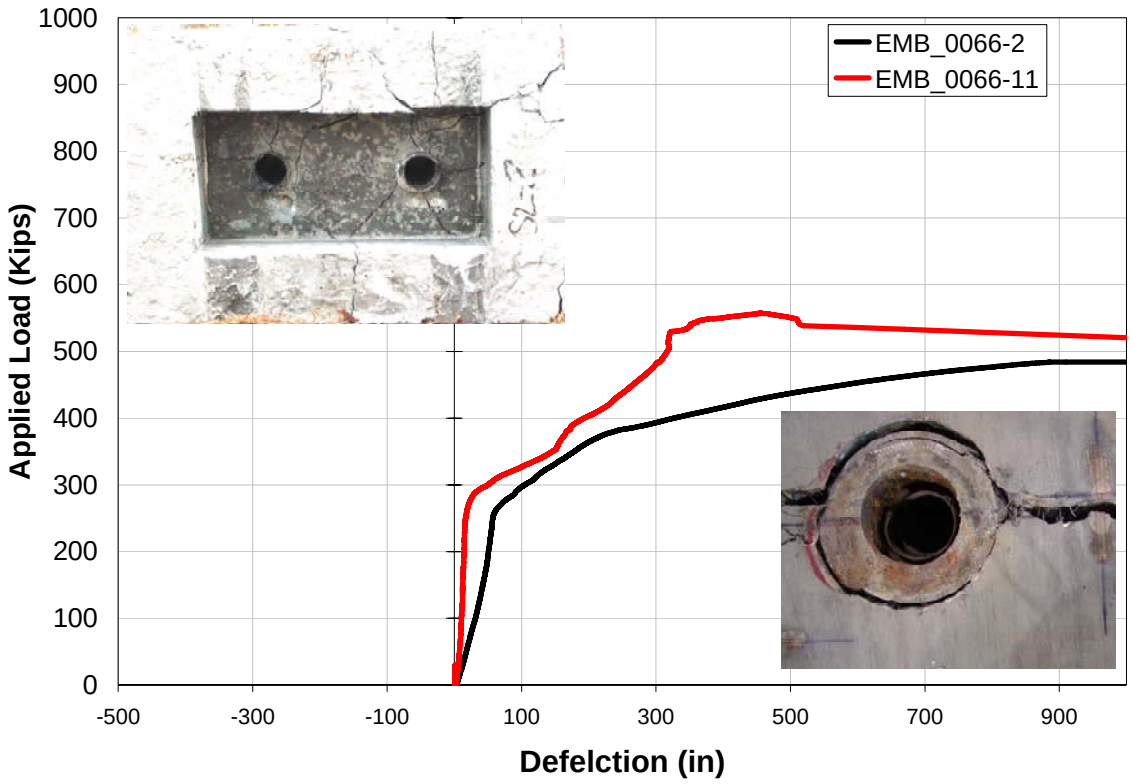

Figure 5-48: Load vs. Strain Relationship for Embedded Gauges of S2-2

5.12.4 Anchorage Test Specimen S2-3

Specimen S2-3 contained concrete with 0.5% Dramix ZP305 fibers by volume, two (2) Dywidag MA5-0.6" anchors, two ducts, and steel spirals. The specimen did not contain steel ties. Specimen S2-3 was tested at the age of 55 days. Using the typical load set-up, Specimen S2-3 was loaded until it failed at a total load of 628.3 Kips (Figure 5-49).

The first visible crack developed at approximately 600 Kips. This crack developed on the north face of the specimen. At the failure load, a large tension (bursting) crack developed on west face (on a 19.5'' side) of the specimen. Figure 5-50 shows strain measurements from embedded gauges. As shown from the figure a very large crack developed on the west face of the specimen

at the failure load. At the final load magnitude, some punching did occur at the anchors. The failure load of this specimen was approximately 13% higher than the failure load of Specimen S2-2. Thus, test results indicate that the presence of spirals in the local zone contributes to a 13% increase in load capacity.

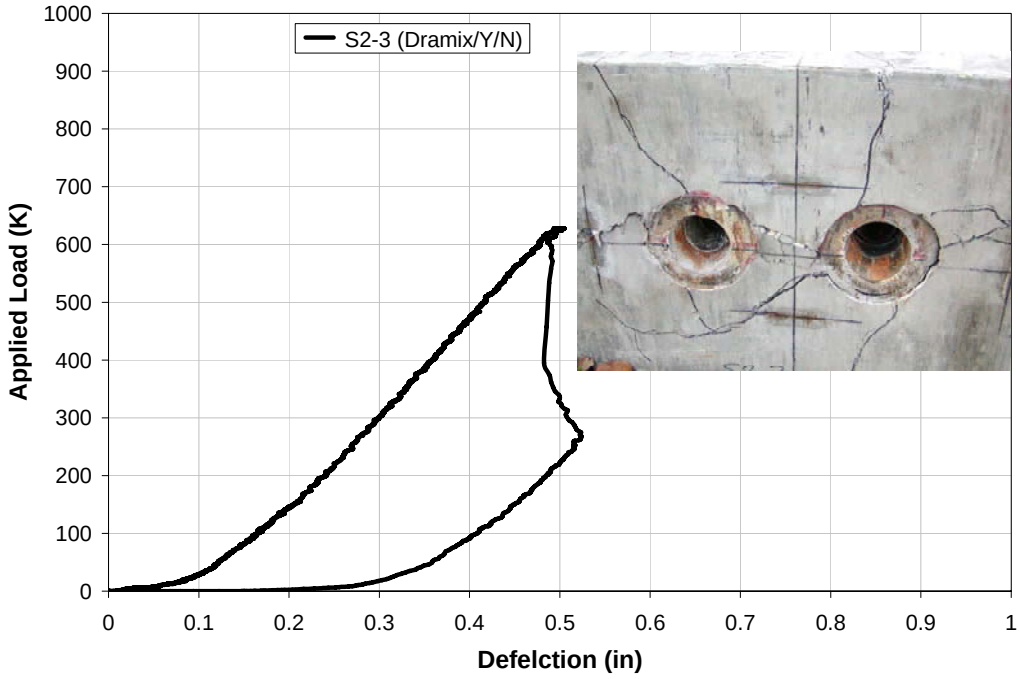

Figure 5-49: Load vs. Deflection of S2-3

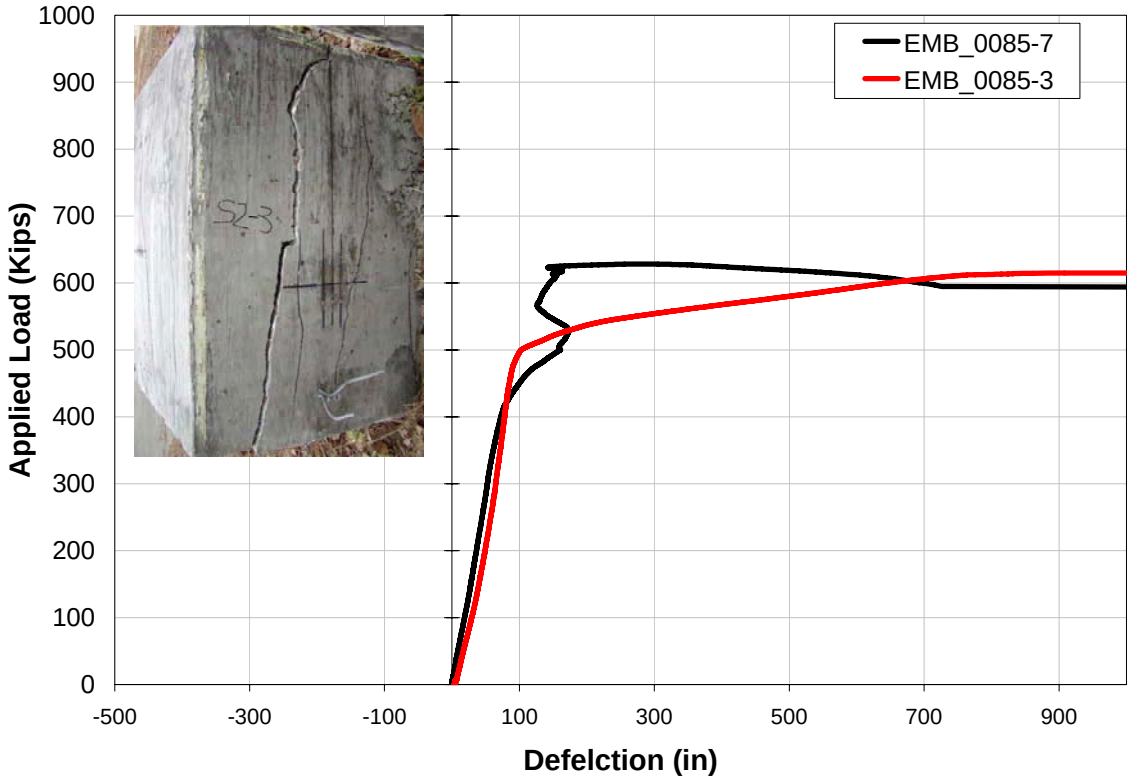

Figure 5-50: Load vs. Strain Relationship for Embedded Gauges of S2-3

5.12.5 Anchorage Test Specimen S2-4

Specimen S2-4 contained concrete with 0.5% Dramix ZP305 fibers by volume, two (2) Dywidag MA5-0.6" anchors, two ducts, and steel ties. The specimen did not contain steel spirals. Specimen S2-4 was loaded until the total load of 673.97 kips was applied (Figure 5-51). During testing, the first visible crack developed on the north face at a load of approximately 560 kips. At the failure load, the specimen could not maintain the applied load. Therefore, the load test was stopped. Figure 5-52 shows the load vs. strain relationship of embedded gauges in the specimen.

The failure load was approximately 17% greater than GUTS for the anchors, 7% less than the load applied to Specimen S2-1, 21% greater than the load applied to S2-2 and 7% greater than the load applied to S2-3. Thus, the presence of ties without spirals results in more than a 21% increase in load capacity above the capacity of the specimen with 0.5% Dramix fibers by volume without ties and spirals, Specimen S2-2.

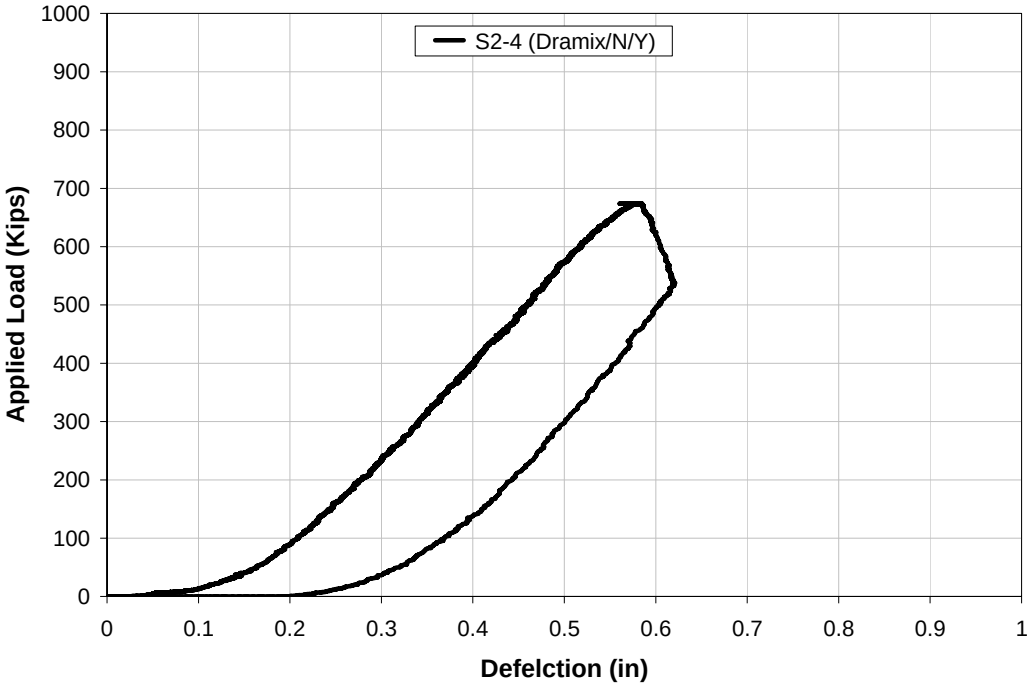

Figure 5-51: Load vs. Deflection of S2-4

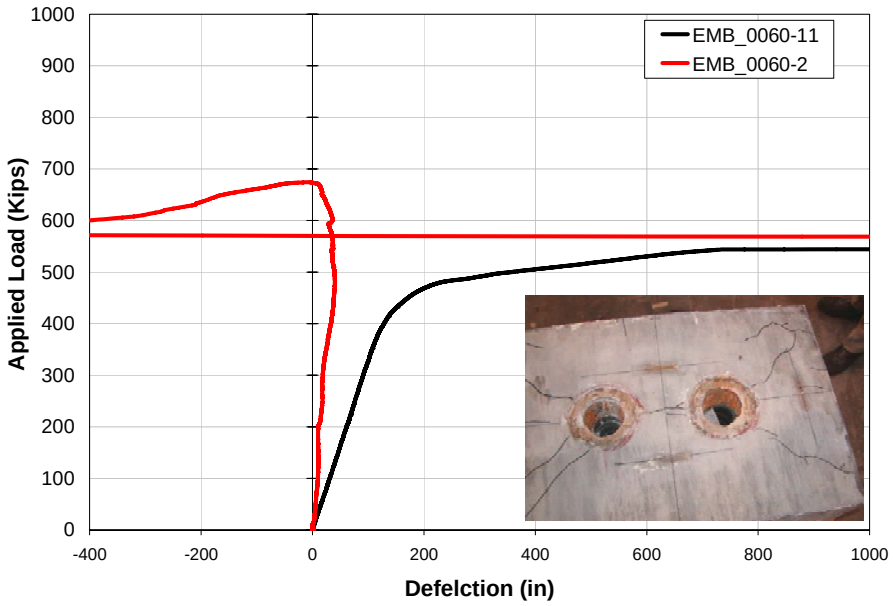

Figure 5-52: Load vs. Strain Relationship for Embedded Gauges of S2-4

5.12.6 Anchorage Test Specimen S2-5

Specimen S2-5 contained concrete with 0.5% Dramix ZP305 fibers by volume, two (2) Dywidag MA5-0.6" anchors, two ducts, approximate 50% of the steel spiral recommended by Dywidag for the local zone and 60% of the steel ties used in Specimen S2-1. For this Specimen, the spacing of the steel ties was twice the tie spacing used in Specimens S2-1 and S2-3. Specimen S2-5 was loaded until a total load of 665.56 Kips was reached.

The first cracks developed a total load in excess of 500 Kips. At the failure load, approximately 666 Kips, the specimen ceased to maintain the applied load (Figure 5-53). Thus, the load test was stopped. Some punching of the anchors did occur. Based upon the crack pattern, it appears that the failure of the specimen was due to both local and general zone failure. Figure 5-54 shows load vs. strain relationship for the two embedded gauges in the block.

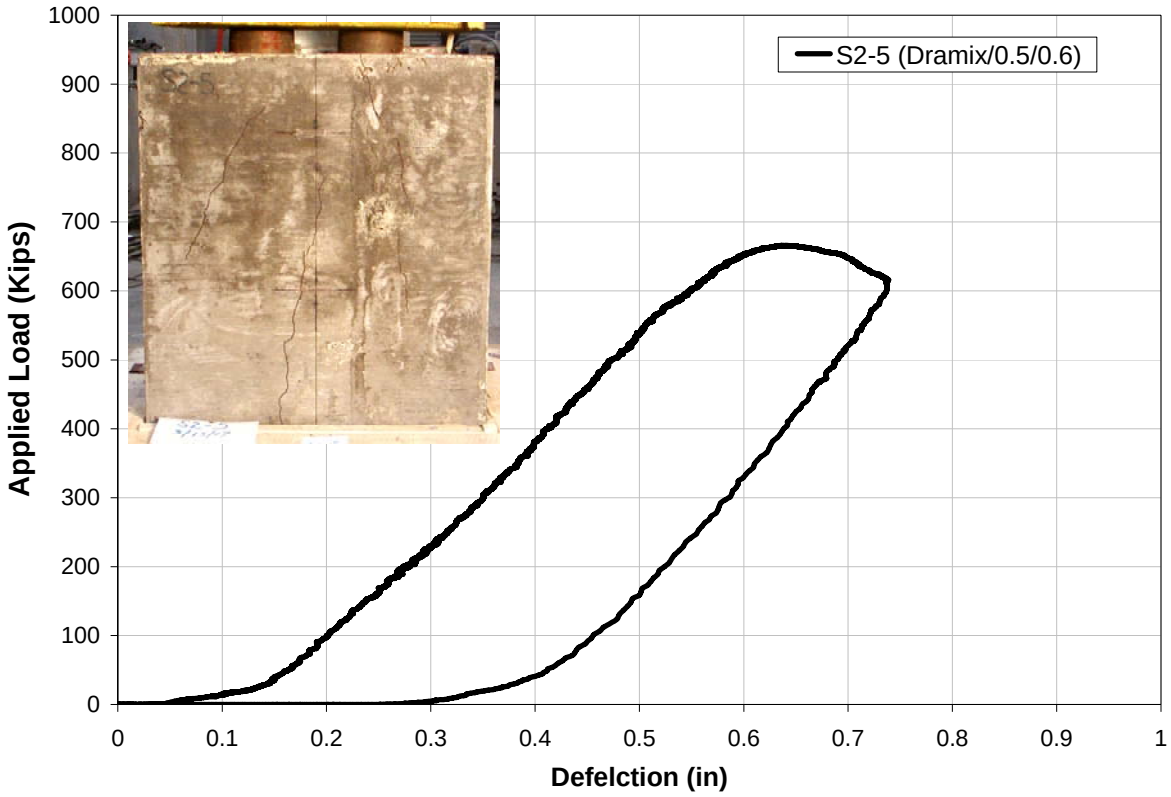

Figure 5-53: Load vs. Deflection of S2-5

With 0.5% fiber by volume, a 50% reduction in steel spirals and a 40% reduction in steel ties, Specimen S2-5 had 8% less load capacity than Specimen S2-1. Specimens S2-2 through S2-5 were cast from the same batch of concrete with 0.5% Dramix fibers by volume. Specimen S2-2 had no spiral or ties. Specimens S2-3 had spirals but not ties. Specimen S1-4 had ties but no spirals. The load capacity of Specimen S2-5 was 8% less, 19% greater, 6% greater and 1% less than the strengths of Specimens S2-1, S2-2, S2-3, and S2-4, respectively. Although the strength of S2-5 was less than that of Specimen S2-1, load capacity of S2-5 was 15% greater than the GUTS for the anchors. Figure 5-54 shows load vs. strain data for Specimen S2-5.

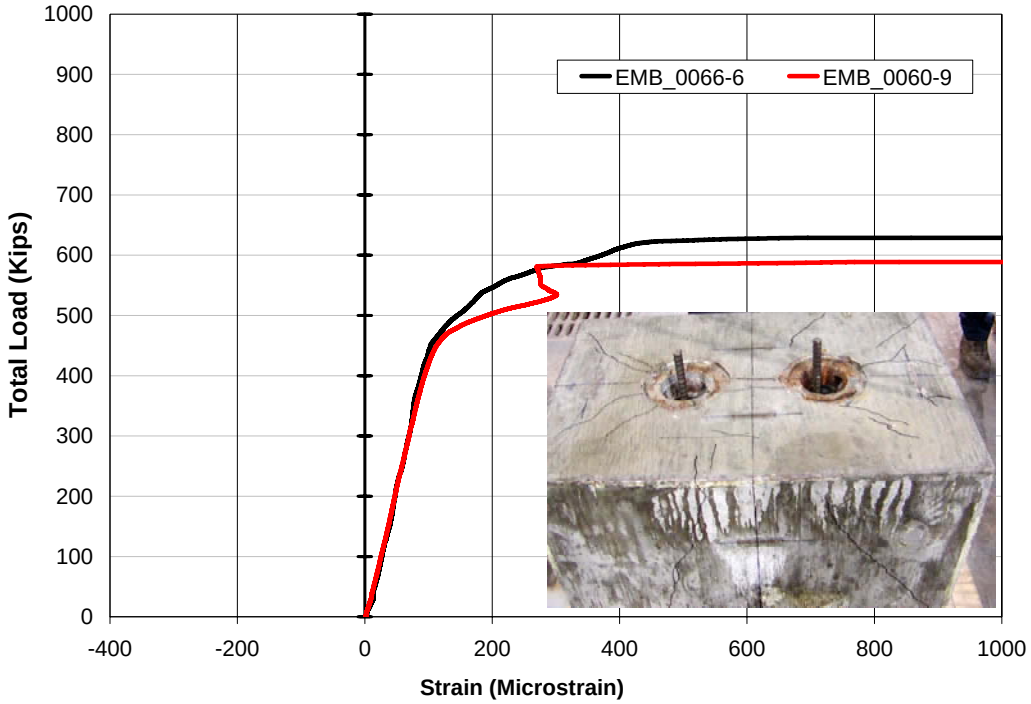

Figure 5-54: Load vs. Strain Relationship for Embedded Gauges of S2-5

5.12.7 Anchorage Test Specimen S2-6

Specimens S2-6, S2-7, S2-8 and S2-9 were all cast from the same batch of concrete, which contained 0.5% Helix fiber by volume. Specimen S2-6 contained concrete with 0.5% Helix fibers by volume, two (2) Dywidag MA5-0.6" anchors and ducts. The specimen did not contain steel spirals and did not contain steel ties. Specimen S2-6 was tested at the age of 56 days. The 28 day compressive strength and the 56 day compressive strength were 4550 psi and 5757 psi, respectively. The 28 day split tensile strength and the 56 day split tensile strength were 361 psi and 388 psi, respectively. The failure load of 567.7 Kips was approximately 2% less than the GUTS for the two anchors (578 Kips).

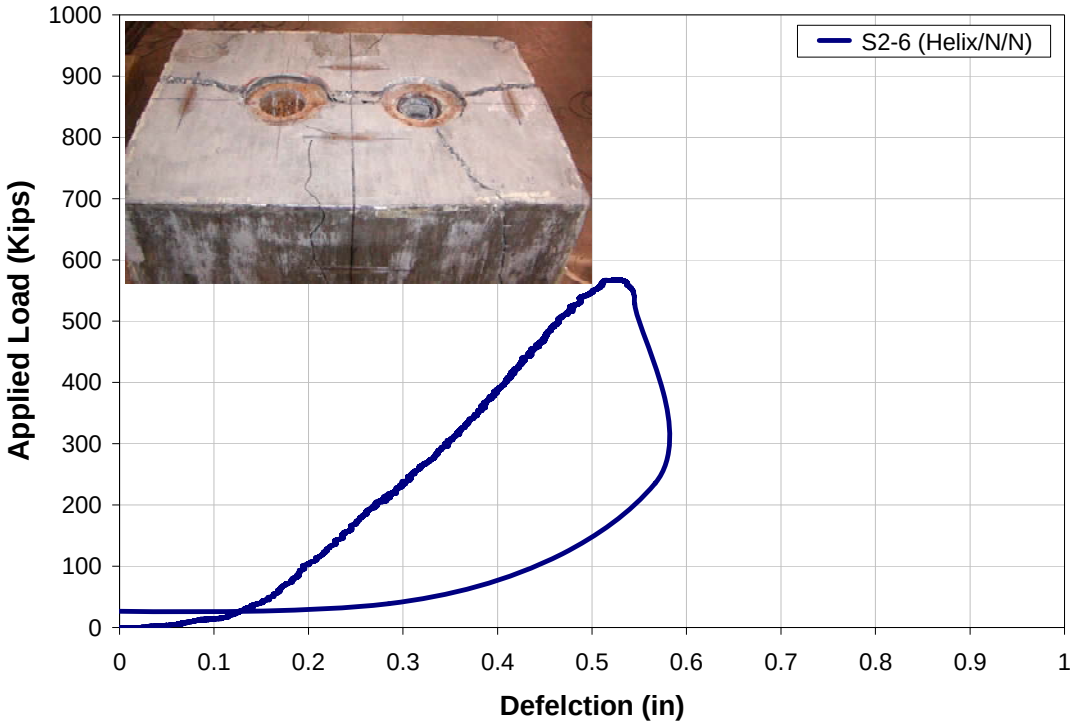

Figure 5-55: Load vs. Deflection of S2-6

The first visible surface crack occurred at approximately 450 Kips. During the load test, cracks developed on all visible surfaces of the Specimen (Figure 5-55 and Figure 5-56). For this specimen, failure resulted from punching shear at the anchors. The absence of steel spirals contributed to this result. The compressive strength and the tensile strength of the concrete in Specimen S2-6 was greater than the strengths of the concrete in the S2-1 Specimen. However, the failure load of Specimen S2-6 was 22% less than the failure load for S2-1. Comparing S2-6 with S2-2, reveals that the two Specimens broke at approximately the same strength (an average of about 97% of the GUTS load for the two anchors); the failure load for Specimen S2-6 was approximately 2% greater than the failure load of Specimen S2-2. Both of these specimens had steel fibers but did not have any other steel reinforcement.

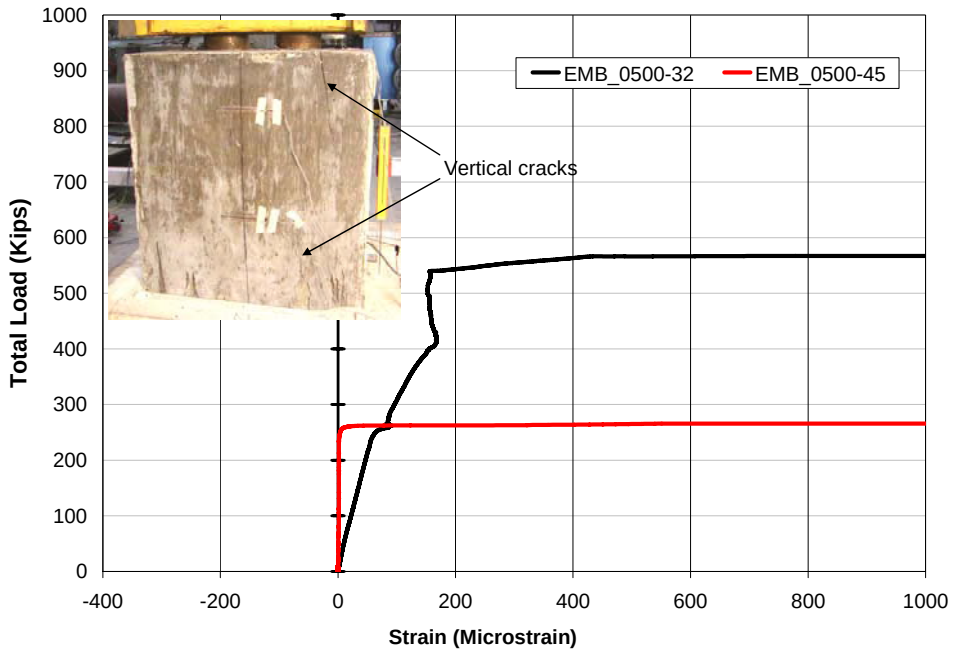

Figure 5-56: Load vs. Strain Relationship for Embedded Gauges of S2-6

5.12.8 Anchorage Test Specimen S2-7

Specimen S2-7 contained concrete with 0.5% Helix fibers by volume, two (2) Dywidag MA5-0.6" anchors, two ducts, and two steel spirals. The specimen did not contain steel ties. Specimen S2-7 was tested at the age of 56 days. Using the typical load set-up (the same as used for all specimens except S2-1), Specimen S2-7 was loaded until it failed at a total load of 691.14 Kips (Figure 5-57).

The first visible cracks developed on the north and west sides of the specimen at an approximate applied load of 400 Kips. Failure was noted when the specimen ceased to withstand additional applied load; an increase in load resulted in an increase in deflection which prevented resistance of the load. The failure load for Specimen S2-7 was approximately 20% greater than the GUTS

for the two anchors. The strength capacity of Specimen S2-7 was 4% less than that of Specimen S2-1.

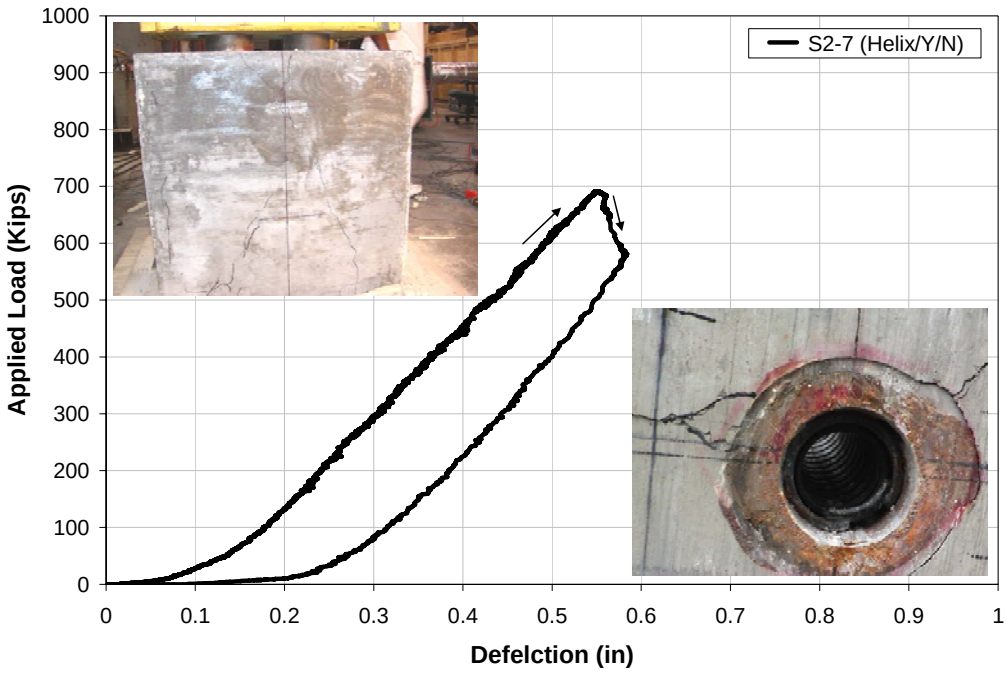

Figure 5-57: Load vs. Deflection of S2-7

Comparing the ultimate load applied to Specimens S2-7 and S2-6, revealed that the inclusion of spirals in the local zone contributed to a 22% increase in load capacity. A relatively small displacement of the anchors (punching) did occur in Specimen S2-7. Cracks developed on all surfaces of the specimen. The crack widths were small to medium. The cracks appear larger in the photographs because (to increase visibility) the cracks were traced with a marker. Figure 5-58 presents the load-strain relationship for the two embedded gauges inside the specimen.

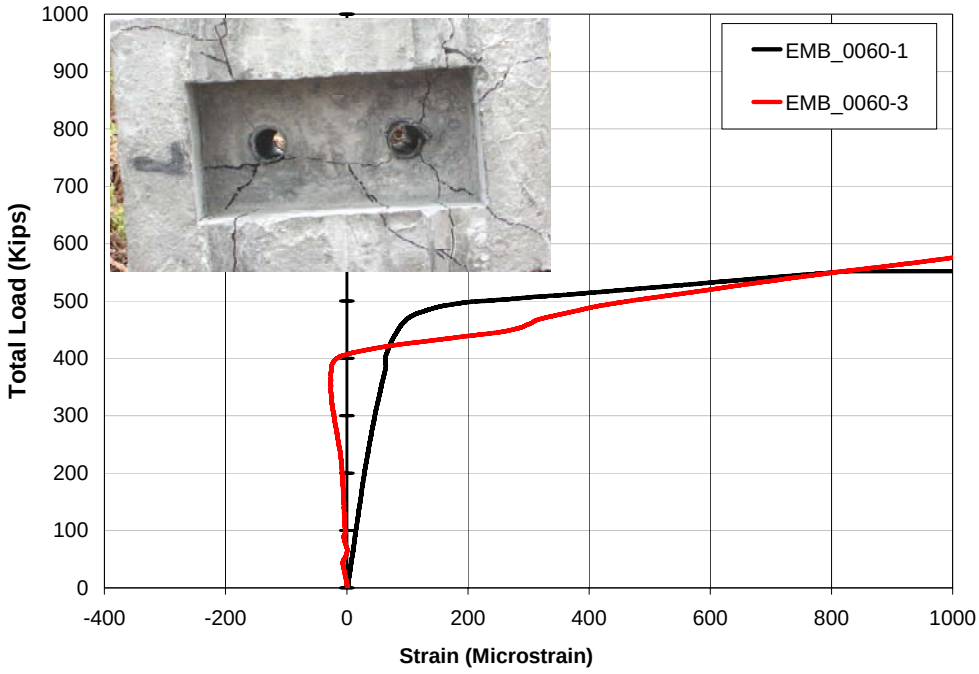

Figure 5-58: Load vs. Strain Relationship for Embedded Gauges of S2-7

5.12.9 Anchorage Test Specimen S2-8

Specimen S2-8 contained concrete with 0.5% Helix fibers by volume, two (2) Dywidag MA5-0.6" anchors, two ducts, and steel ties. The specimen did not contain steel spirals. Specimen S2-8 was loaded until the total load of 747.7 kips was applied (Figure 5-59). Figure 5-60 presents load vs. strain measurements. Also, it can be seen that some displacement of the anchors did occur during testing. The first cracks on the specimen developed at an applied load of approximately 675 Kips. Cracks developed on all surfaces of the specimen. Some cracks initiated on the bearing surface and some cracks initiated on the load surface at or near the anchors. Both local and general zone failure occurred in this specimen.

At the maximum applied load, the specimen would not adequately resist additional loads; the system load would not stabilize. A 747.7 K final load was 1.03 times greater than the load

applied to Specimen S2-1 and 1.29 times greater than the GUTS load for the Dywidag anchors. Comparing the ultimate load applied to S2-8 and the ultimate load applied to S2-6 (which has 0.5% fiber but no spirals and no ties) showed that the presence of steel ties results in a 32% increase in load capacity. This increase in strength attributable to ties in the specimen with Helix fibers was greater than the 21% increase attributable to ties in the specimen with Dramix fibers.

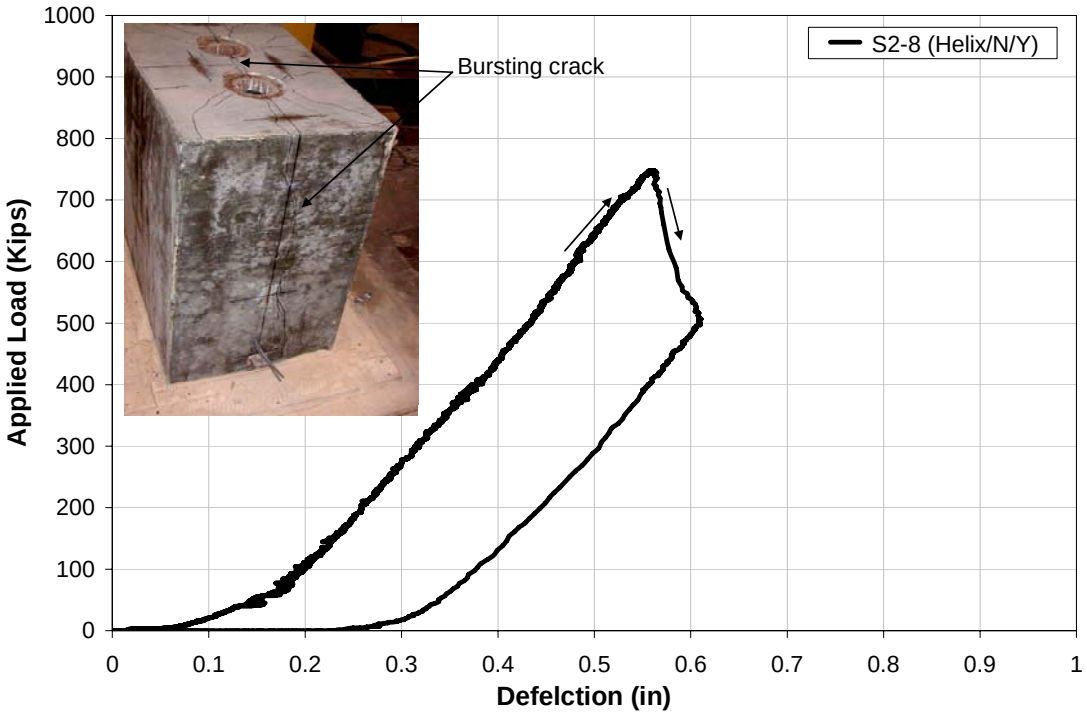

Figure 5-59: Load vs. Deflection of S2-8

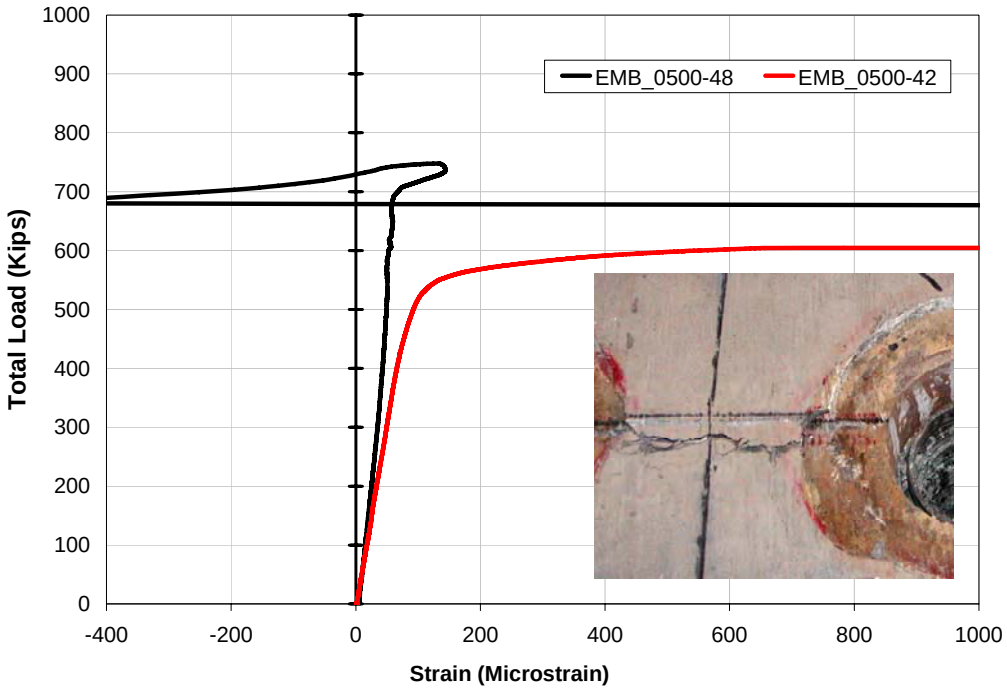

Figure 5-60: Load vs. Strain Relationship for Embedded Gauges of S2-8

5.12.10 Anchorage Test Specimen S2-9

Specimen S2-9 contained concrete with 0.5% Helix fibers by volume, two (2) Dywidag MA5-0.6" anchors, two ducts, approximate 50% of the steel spirals recommended by Dywidag for the local zone and 60% of the steel ties used in Specimen S2-1. For this specimen, the spacing of the steel ties was twice the tie spacing used in Specimens S2-1, S2-4 and S2-8. Specimen S2-9 was loaded until a total load of 752.594 Kips was reached (Figure 5-61). This load was 30% greater than the GUTS for the two anchors.

The first crack (a crack on the north face) occurred at the bottom of the specimen at approximately 550 Kips. The second crack (also on the north face starting at the bottom) occurred at approximately 740 Kips. At the maximum applied load, the specimen would not adequately resist additional loads; the magnitude of the applied load would not stabilize due to

deflection of the specimen at the load application points. At the end of the load cycle, only small width cracks existed on the surfaces of the specimen. However, it appears that the failure was due to both local and general zone failure; failure of the local anchorage zone was apparent. Figure 5-61 shows the surfaces of Specimen S2-9 after the load after the load test was complete.

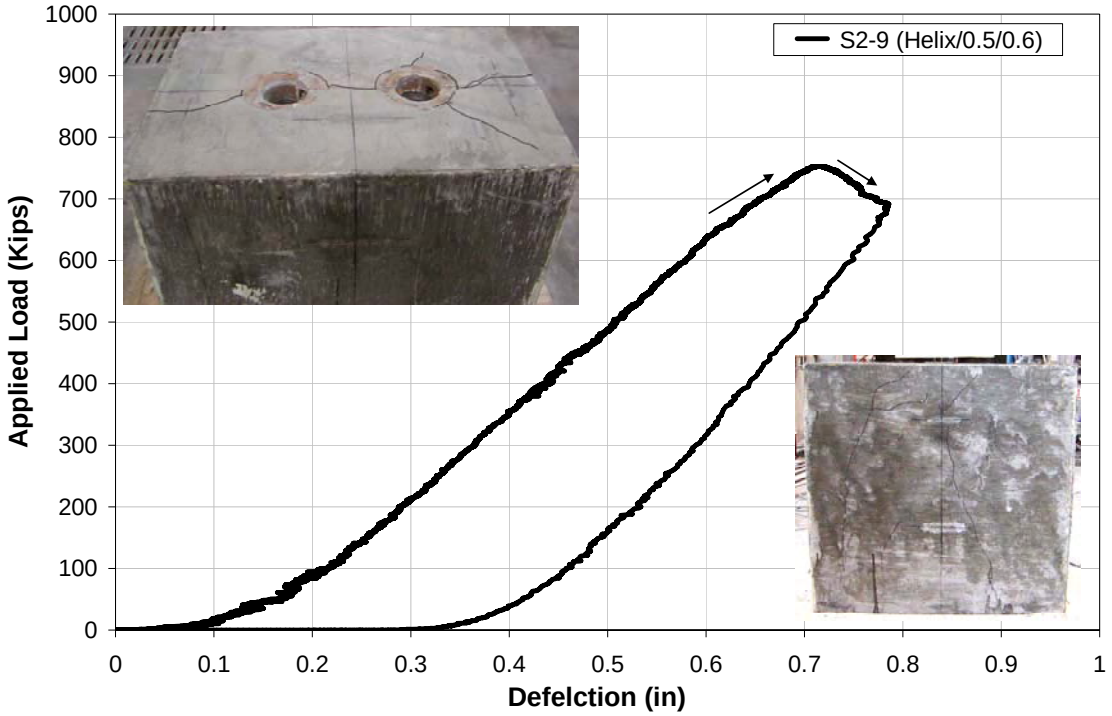

Figure 5-61: Load vs. Deflection of S2-9

With 0.5% fiber by volume, a 50% reduction in steel spirals and a 40% reduction in steel ties, Specimen S2-9 had 4% more load capacity than Specimen S2-1. Specimens S2-6 through S2-9 were all cast from the same batch of concrete with 0.5% Helix fibers by volume. Specimen S2-6 had no spiral or ties. Specimen S2-7 had spirals but no ties. Specimen S2-8 had ties but no spirals. Specimen S2-9 had 33%, 9% and 1% greater load capacity of than did specimen S2-6, Specimen S2-7 and Specimen S2-8, respectively. Figure 5-62 shows load-strain data for Specimen S2-9.

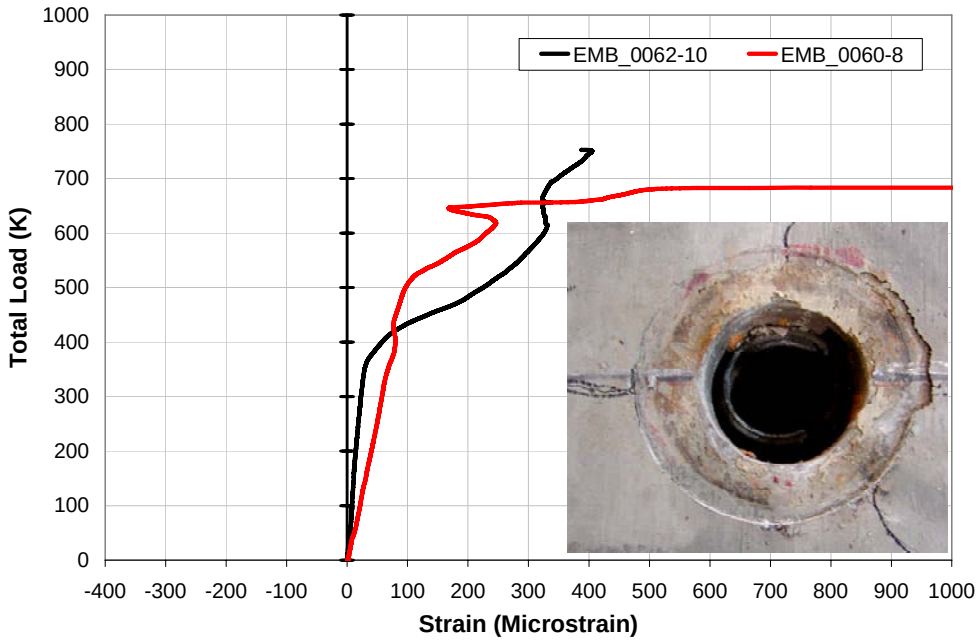

Figure 5-62: Load vs. Strain Relationship for Embedded Gauges of S2-9

5.12.11 Anchorage Test Specimen S2-10

Specimens S2-10, S2-11, S2-12 and S1-13 were all cast from the same batch of concrete with 0.5% Novomesh fibers by volume. In addition to the Novomesh fibers, Specimen S2-10 contained two (2) Dywidag MA5-0.6" anchors and two ducts. The specimen did not contain steel spirals and steel ties. Specimen S2-10 was tested at the age of 57 days. The 28 day compressive strength and the 61 day compressive strength were 4127 psi and 5179 psi, respectively. The 28 day tensile strength and the 61 day tensile strength were 410 psi and 295 psi, respectively.

The first crack developed on the east side of the specimen at an applied load of approximately 600 Kips. The failure of Specimen S2-10 was sudden and due to punching shear. As a result of the punching shear failure, major tension cracks developed on the east and west faces (short

sides) of the specimen. Since tie reinforcement was not present in the specimen, the specimen broke into sections. Figure 5-61 shows the surface cracks on the specimen after failure. Figure 5-64 presents load-strain relationship of the two embedded gauges in the specimen.

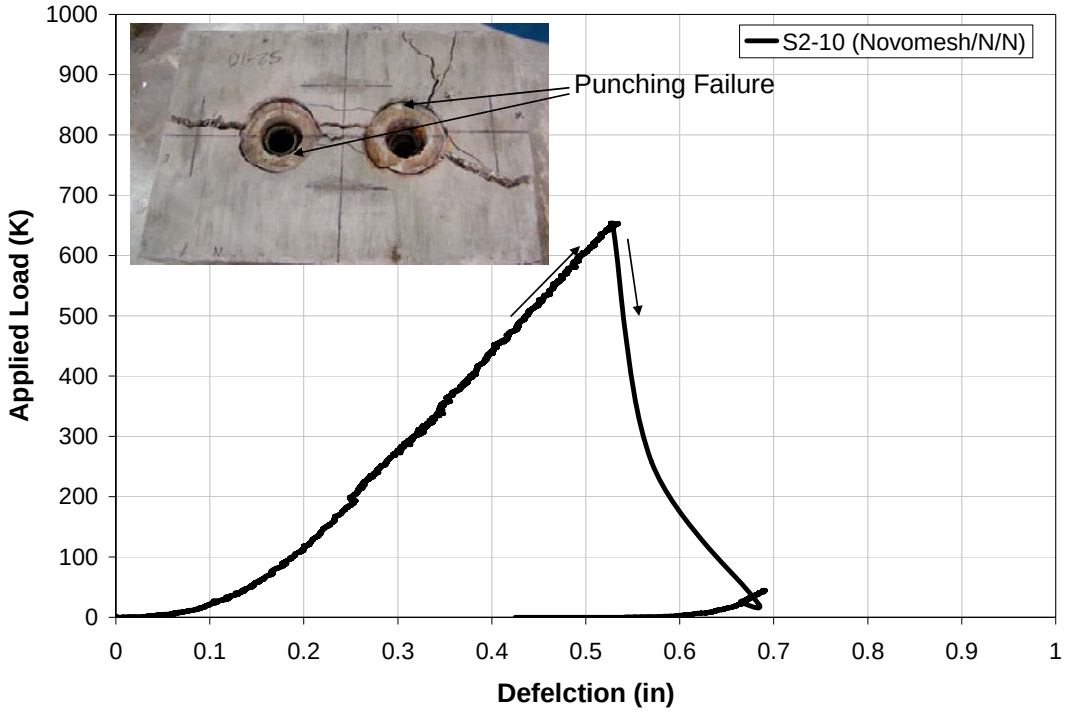

Figure 5-63: Load vs. Deflection of S2-10

The failure load of 653.64 Kips was approximately 13% greater than twice the GUTS for Dywidag anchors. This failure load was 10% less than the maximum load applied to Specimen S2-1, 15% greater than the load applied to Specimen S2-6 (the specimen with Helix fibers), and 17% greater than S2-2 (the specimen with Dramix fibers).

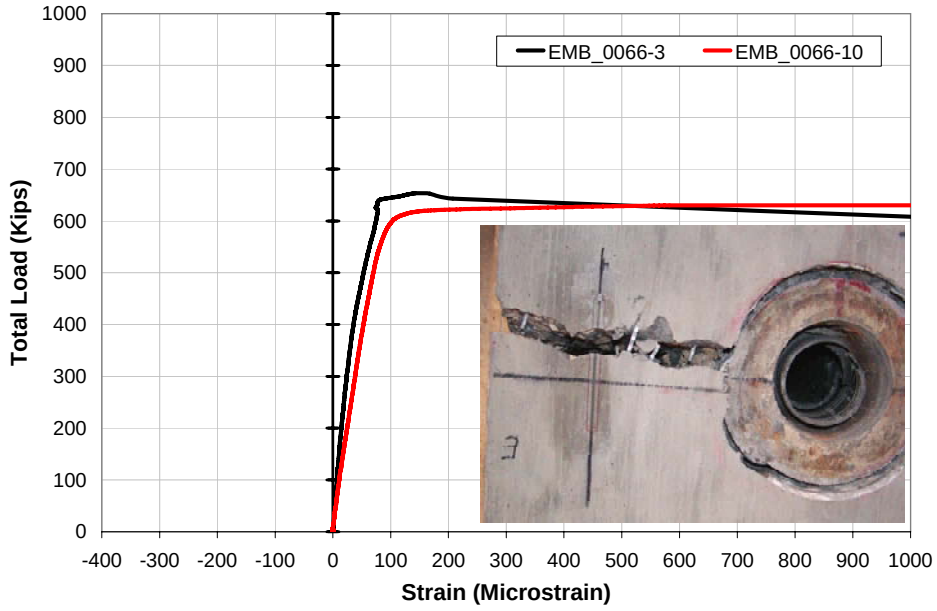

Figure 5-64: Load vs. Strain Relationship for Embedded Gauges of S2-10

5.12.12 Anchorage Test Specimen S2-11

Specimen S2-11 contained concrete with 0.5% Novomesh fibers by volume, two (2) Dywidag MA5-0.6" anchors, two ducts, and steel spirals. The specimen did not contain steel ties. Specimen S2-11 was tested at the age of 57 days. Using the typical load setup, Specimen S2-11 was loaded until it failed at a total load of 569.723 Kips (Figure 5-65).

The first cracks occurred on the north and south faces of the specimen at approximately 450 Kips. The failure at approximately 570 Kips was accompanied by a small "thud". Figure 5-65 shows the failed Specimen S2-11, and Figure 5-66 presents load-strain relationship. The failure load for S2-11 was approximately 99% of the GUTS for the two anchors and 21% less than the load applied to Specimen S2-1. The maximum load applied to Specimen S2-11 was only 91% and 82% of the total load applied to Specimens S2-3 and S2-7, respectively.

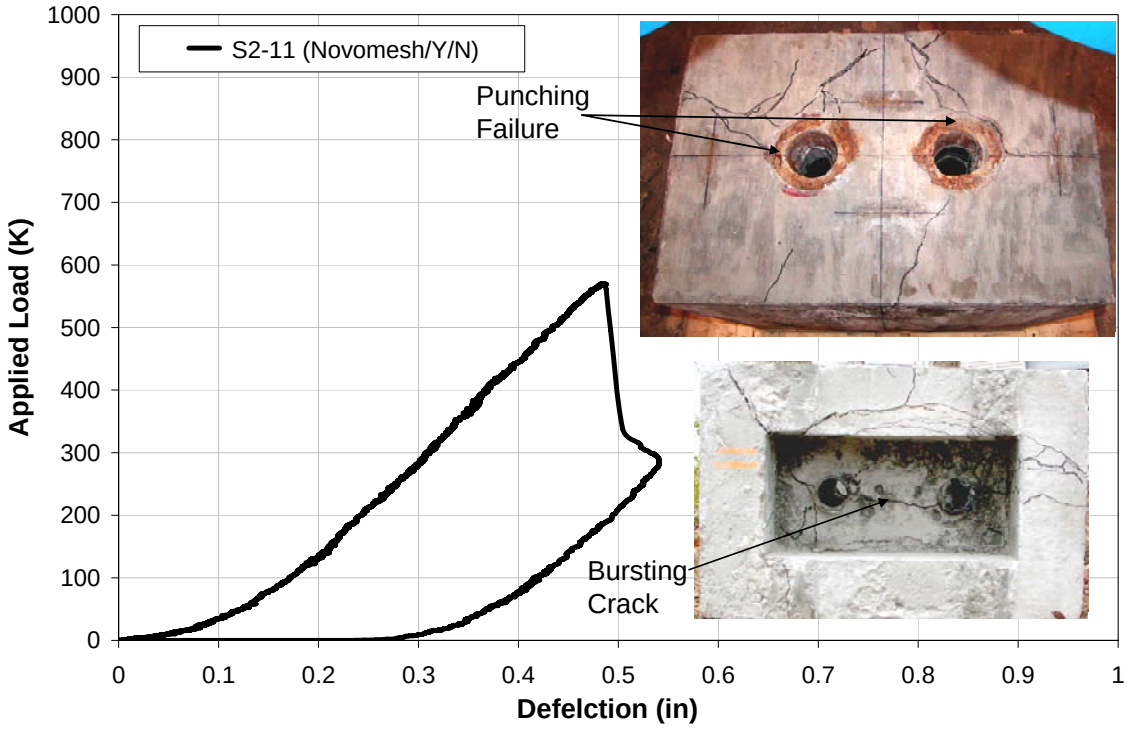

Figure 5-65: Load vs. Deflection of S2-11

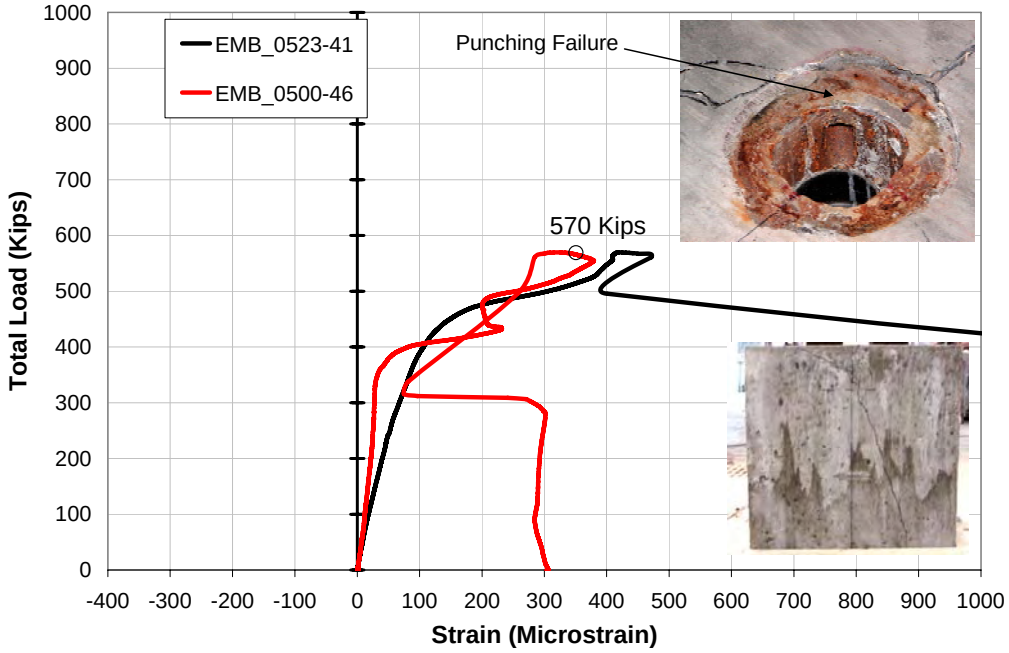

Figure 5-66: Load vs. Strain Relationship for Embedded Gauges of S2-11

5.12.13 Anchorage Test Specimen S2-12

Specimen S2-12 contained concrete with 0.5% Novomesh fibers by volume, two (2) Dywidag MA5-0.6" anchors, two ducts, and steel ties. The specimen did not contain steel spirals. Specimen S2-12 was loaded at an age of 61 days until a total load of 750 Kips was reached (Figure 5-67). The first crack on the surface of the specimen was not visible until approximately 750 Kips, just prior to the final load application. At higher loads, visible displacement of the anchors occurred such that additional load was not resisted by the specimen. Figure 5-68 presents load-strain relationship. The final load of 750 Kips was 4% greater than the load capacity of Specimen S2-1 and approximately 30% greater than the GUTS for the anchors in the specimen. The strength of S2-12 was 15% greater than S2-10 and 32% greater than Specimen S2-11.

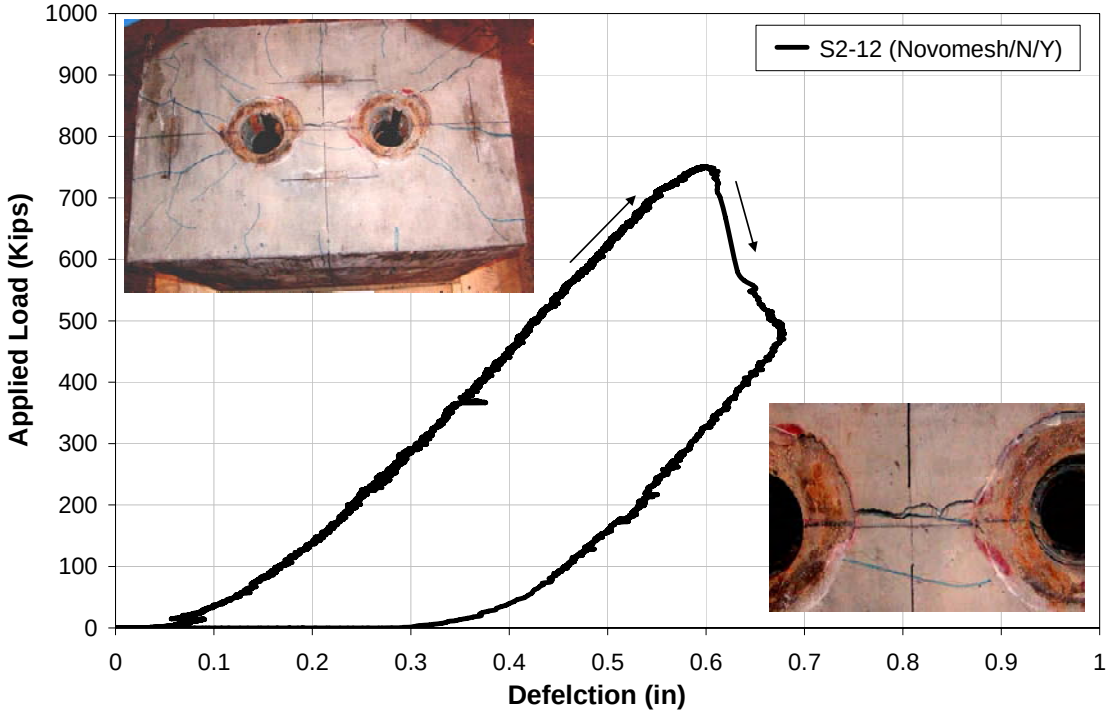

Figure 5-67: Load vs. Deflection of S2-12

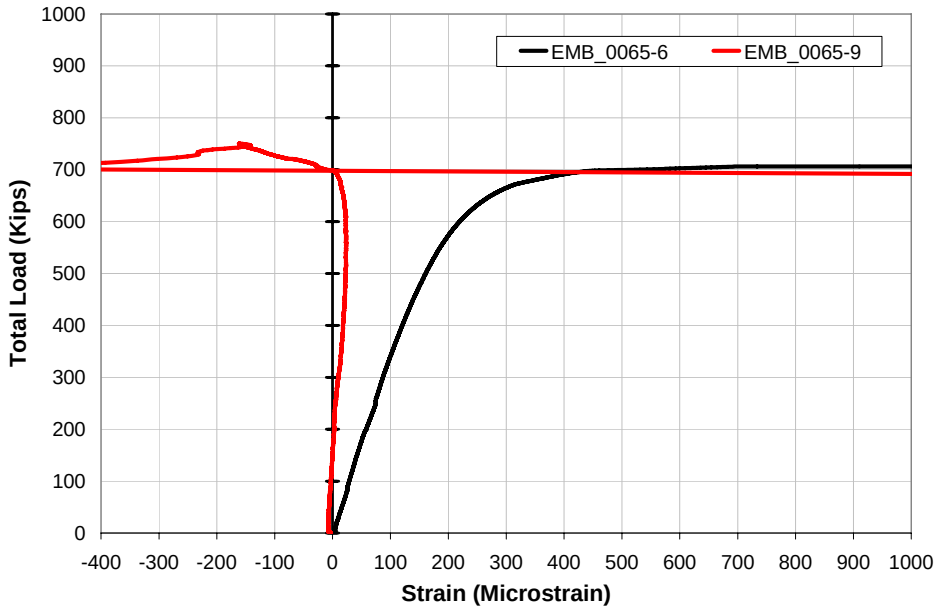

Figure 5-68: Load vs. Strain Relationship for Embedded Gauges of S2-12

5.12.14 Anchorage Test Specimen S2-13

Specimen S2-13 contained concrete with 0.5% Novomesh fibers by volume, two (2) Dywidag MA5-0.6" anchors, two ducts, approximate 50% of the steel spiral recommended by Dywidag for the local zone and 60% of the steel ties used in Specimen S2-1. For this Specimen, the spacing of the steel ties was twice the tie spacing used in Specimens S2-1, S2-4, S2-8 and S2-12.

At an age of 61 days, Specimen S2-13 was loaded until a total load of 752.68 Kips was reached (Figure 5-69). At this load, only hairline cracks were on the surface of the specimen. The failure was a local zone failure of the anchor system. Load-strain relationships of embedded gauges are presented in Figure 5-70.

The final load applied to Specimen S2-13 was 4% greater than the load applied to S2-1. The load was 30% greater than the GUTS for the Specimen. The load capacity for Specimen S2-13 was approximately the same as the capacity for S2-12. This further indicates that the failure was due to local zone failure in the vicinity of the anchorage system. Essentially, Specimens S2-8, S2-9, S2-12 and S2-13 all failed at approximately 752 Kips and the failure appeared to be due to failure in the local anchorage zone.

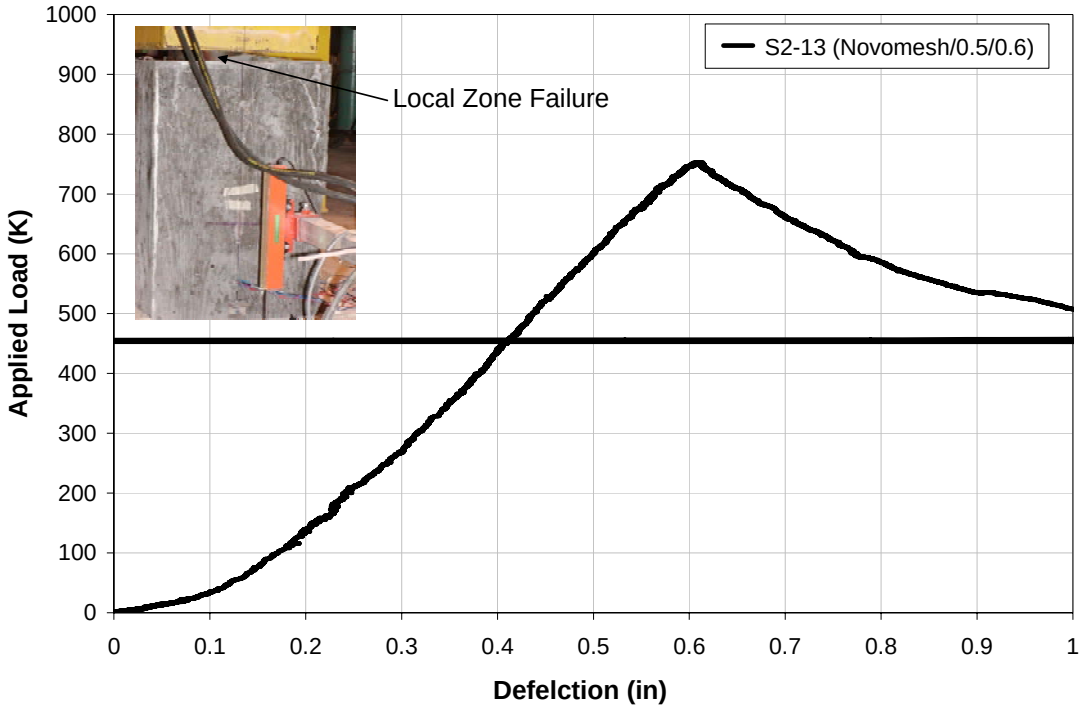

Figure 5-69: Load vs. Deflection of S2-13

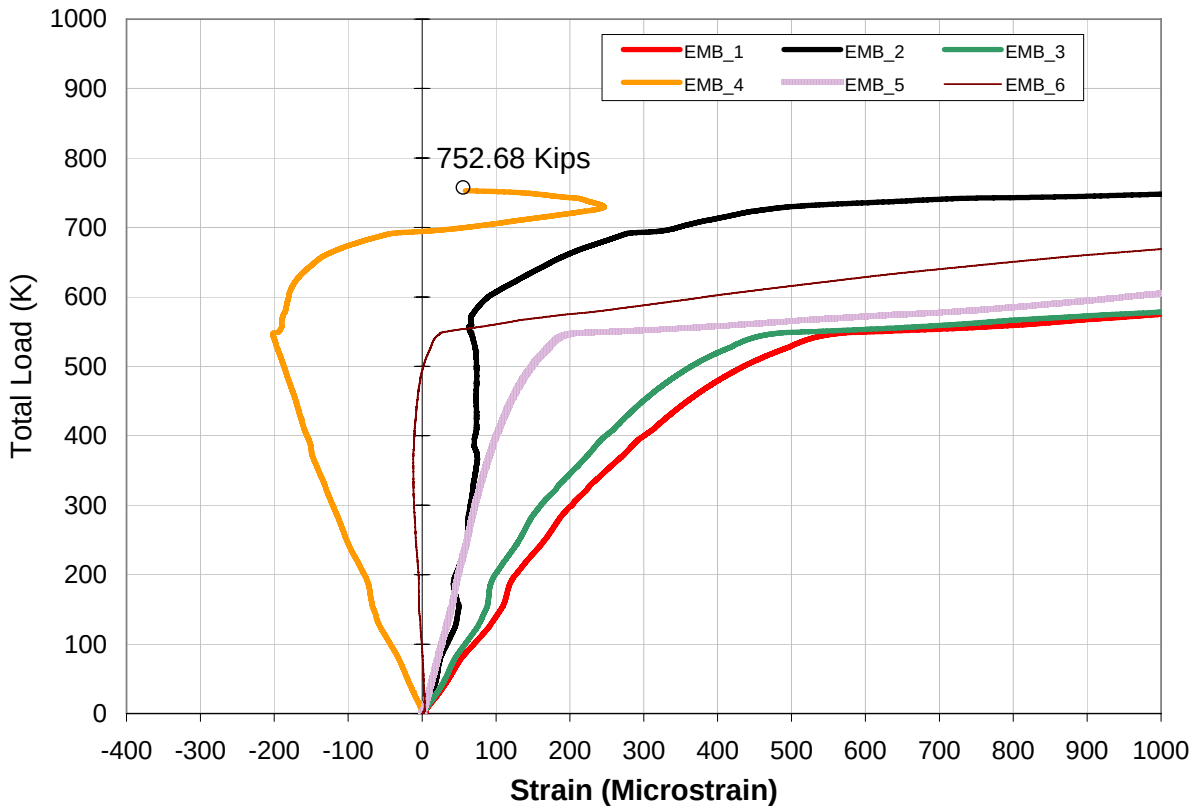

Figure 5-70: Load vs. Strain Relationship for Embedded Gauges of S2-13

5.13 Discussion of Anchorage Specimens Test Results

In this section the load test results for the various test specimens are summarized. An attempt is made to discuss in brief the relevant findings from the two sets of test specimens. The discussion includes a comparison of the performance of the S1 and S2 specimens. Table 5-1, Figure 5-71 Figure 5-72 show comparison of the two sets of specimens based on the maximum applied load (kips) and development of first crack.

Table 5-1: Comparison of the Two Sets S1 and S2

Specimen	Fiber/Spiral/Ties	Failure Load (Kips)	First Crack (Kips)	Observations
S1-1	None/Y/Y	627.9	400+	
S1-2	Dramix/N/N	794.0	287	Major Bursting Tension Crack on E and W Faces
S1-3	Dramix/Y/N	865.6	830+	
S1-4	Dramix/N/Y	999.2	1000	Stopped at 1000K, No visible cracks on the surfaces
S1-5	Dramix/0.5/0.6	1000.4	1000	Stopped At 1000K, Few small cracks E sides. Cracks on bottom.
S1-6	Helix/N/N	600.0	535+	Punching Shear. Loud boom At failure.
S1-7	Helix/Y/N	677.2		
S1-8	Helix/N/Y	916.7	800	
S1-9	Helix/0.5/0.6	869.2		Specimen Began to Loose Load; Ceased to accept additional load.
S1-10	Novomesh/N/N	838.5	750	Sudden, explosive failure.
S1-11	Novomesh/Y/N	706.3	450	
S1-13	None/0.5/0.6	732.5	500	
S1-14	Novomesh/0.5/0.6	995.6	NA	Load Stopped At 995K, No visible cracks at 980K.
S2-1	None/Y/Y	723.2		Punching Shear (Test Not Observed by FAM/FSU)
S2-2	Dramix/N/N	557.2	550	Sudden Failure
S2-3	Dramix/Y/N	628.3	600	Large Crack on West face.
S2-4	Dramix/N/Y	674.0	560	Specimen Began to Loose Load; Ceased to accept additional load.
S2-5	Dramix/0.5/0.6	665.6	500+	Specimen Began to Loose Load; Ceased to accept additional load.
S2-6	Helix/N/N	567.7	450	Bursting Tension, Punching Shear
S2-7	Helix/Y/N	691.1	400	Specimen Began to Loose Load; Ceased to accept additional load.
S2-8	Helix/N/Y	747.7	675	Only minor cracks at 725K
S2-9	Helix/0.5/0.6	752.6	550	Specimen Began to Loose Load; Failure of Anchor System.
S2-10	Novomesh/N/N	653.6	600	Punching/Bursting Tension
S2-11	Novomesh/Y/N	569.7	450	Sudden/ Small Thud/ Bursting Tension
S2-12	Novomesh/N/Y	750.1	720+	Sudden, Soft Punching (displacement) of anchors.
S2-13	Novomesh/0.5/0.6	752.7	550	Specimen Began to Loose Load; Ceased to accept additional load.
S2-14	None/0.5/0.6	645.8	600+	Bursting Tension Crack on E and W Faces

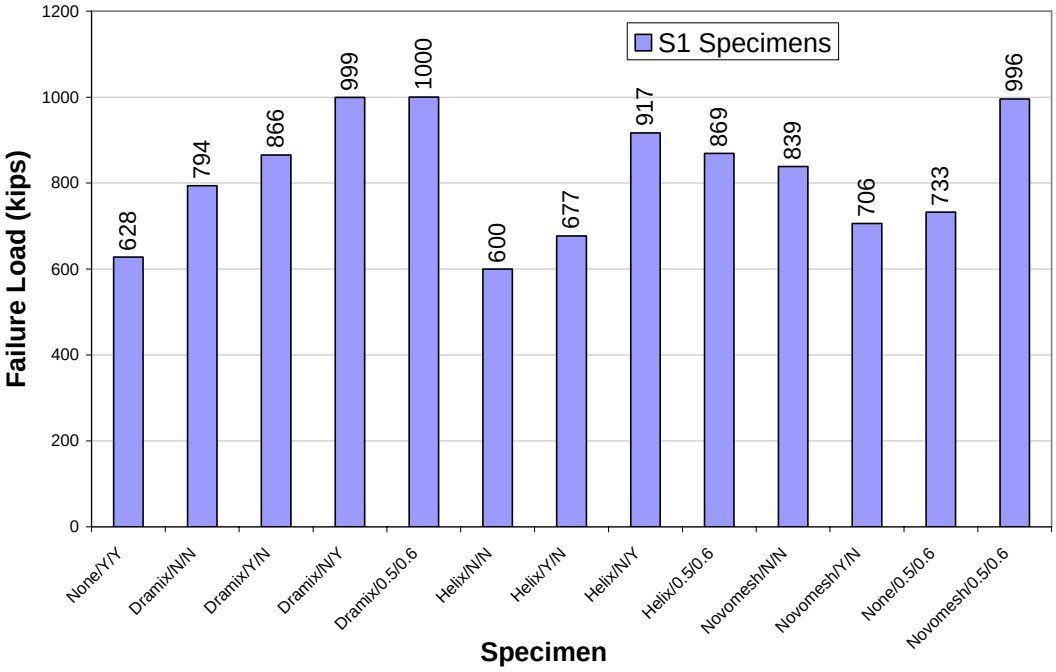

Figure 5-71: Load Capacity for S1 Specimens

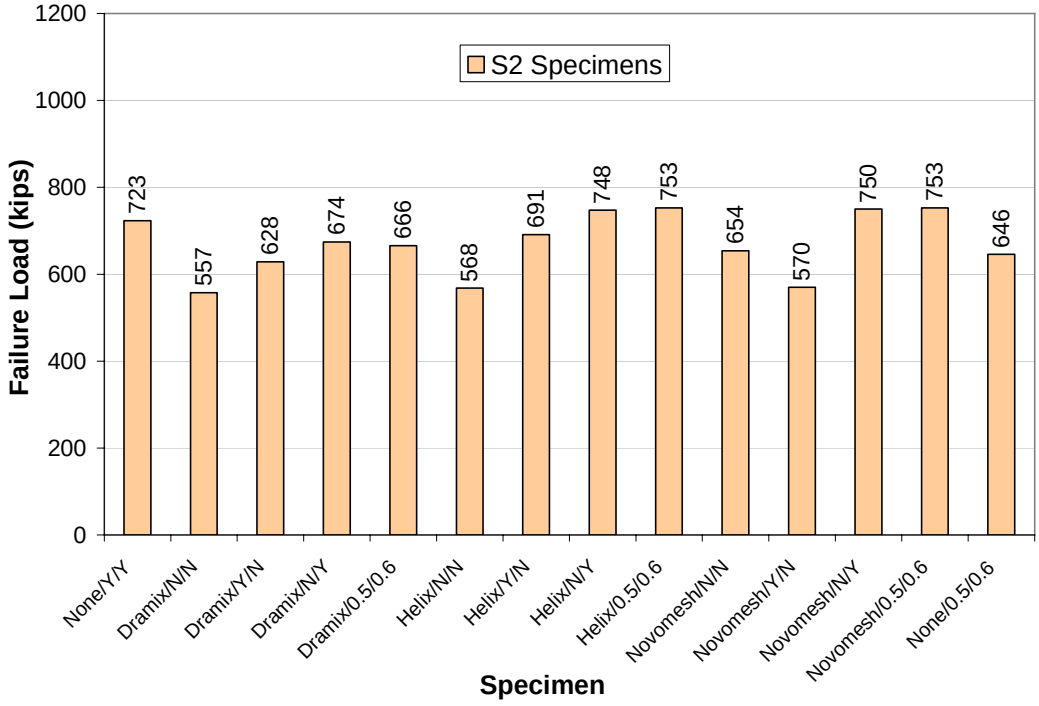

Figure 5-72: Load Capacity for S2 Specimens

5.13.1 Discussion of VSL Anchor Test Specimens Results

A review of the results for the S1 test specimens, specimens cast with VSL anchors, showed that adding steel fibers to the concrete mix did improve the performance of concrete in post-tensioned anchorage zones. This was true for all three of the fiber types.

Comparing specimens cast with Dramix ZP305 fibers with plain concrete specimens showed that steel fibers provide enough tensile strength such that it was possible to totally eliminate both steel spirals and ties without reducing the load capacity of the specimen. In fact, for Specimen S1-2, the load capacity was 26% greater than that of Specimen S1-1. The Dramix Specimen S1-3 indicated that adding steel spiral with the steel fibers in the local anchorage zone resulted in a 9% increase in strength. While the Dramix Specimen S1-4 showed that adding steel ties with the steel fibers resulted in a 26% increase in strength. However, the test results showed that spiral reinforcement was necessary to prevent sudden failure due to punching shear and tie reinforcement was necessary to prevent sudden failure due to excessive bursting tension. Thus, it was not feasible to totally eliminate non-prestressed reinforcement. Yet, consideration of Dramix Specimen S1-5 clearly showed that it was possible to greatly reduce the amount of non-prestressed reinforcement when steel fiber reinforcement was added to the concrete. The load capacity of Specimen S1-5 was over 1.59 times greater than the capacity of Specimen S1-1 with plain concrete and full spiral and tie reinforcement. Comparing Specimen S1-5 and Specimen S1-13 clearly showed that adding steel fibers greatly improved the load capacity of the anchorage zone. While both specimens had 50% less spirals and 40 % less ties than S1-1, the difference in the two specimens is that S1-5 had 0.5% steel fiber by volume and S1-13 had plain concrete (no steel fibers). The use of the steel fibers resulted in a 37% increase in load capacity.

In addition to improving load capacity, the presence of steel fibers resulted in less surface crack development. This can be a significant factor relating to durability of structural elements.

The beneficial effects of adding steel fibers to the anchorage zone was also evident by comparing the different specimens cast with Helix fibers. Although, the specimen that was cast with 0.5% Helix fiber and without any non-prestressed reinforcement (Specimen S1-6) did not have as great a load capacity as Specimen S1-1; the load capacity of Specimen S1-6 was 96% as great as the load capacity of Specimen S1-1. This was so even though the concrete compressive and tensile strengths for Specimen S1-6 were significantly less than the concrete strengths of Specimen S1-1. This showed that the addition of steel fibers did contribute to increased strength in the anchorage zone. The Helix Specimen S1-7 indicated that adding steel spiral in the local anchorage zone resulted in a 13% increase in strength. The Helix Specimen S1-8 showed that adding steel ties resulted in a 53% increase in strength. Thus, the Helix fibers coupled with steel ties resulted in a very large increase in load capacity. As was stated for the Dramix Specimen, the load test results showed that adding Helix steel fibers resulted in increased strength and an improved failure mechanism when steel spirals and ties were present. Helix Specimen S1-9, which had 0.5% fiber, 50% steel spiral and 40% steel ties, was loaded to a 19% higher load capacity than Specimen S1-13, which had plain concrete, 50% steel spiral and 40% steel ties. The load capacity of Specimen S1-9 was over 1.38 times greater than the capacity of Specimen S1-1 with plain concrete and full spiral and tie reinforcement. Thus, steel fibers did increase the strength and improve the behavior of local and general post-tensioned anchorage zones.

Using Novomesh steel and polypropylene fibers resulted in improved strengths in the anchorage zone also. Specimen S1-10 was cast with steel fibers but without other steel reinforcement in the local and general anchorage zones. The load test results showed that the load capacity of S1-10 was 34% greater than that of S1-1 which had plain concrete and 100% steel spirals and 100% steel ties. While Specimen S1-11, which had 0.5% fiber and spirals, had less load capacity that S1-10, the capacity of S1-11 was 12% greater than that of S1-1. The reduced load capacity of S1-11 may have been due to a small degree of raking of the forms during pouring. In spite of this, the Novomesh fibers contributed to an increase of load capacity. The load capacity of Specimen S1-14 was greater than 1000 K, the capacity of the load frame. The load application was stopped prematurely due to the close proximity of the applied load to the load frame capacity. Novomesh Specimen S1-14, which had 0.5% fiber, 50% steel spiral and 40% steel ties, was loaded to a 36% higher load capacity than Specimen S1-13, which had plain concrete, 50% steel spiral and 40% steel ties. This Novomesh Specimen S1-14 performed similarly to the Dramix Specimen S1-5. Possibly, the Helix Specimen S1-9 would have achieved a higher strength, similar to the strengths of S1-5 and S1-14, if the concrete strength for the Helix specimen was not reduced. In summary, the load test results for the S1 Specimens showed that adding 0.5% steel fibers by volume to the concrete mix improved the load capacity of the anchorage zones to the degree that the spiral and tie reinforcement could be greatly reduced by 50% and 40%, respectively. The spiral and tie reinforcement should not be totally eliminated.

5.13.2 Discussion of Dywidag Anchor Test Specimens Results

For the greatest failure loads applied to the S2 Specimens which contained Dywidag anchors, the loads caused failure in the local and the general zones. In several specimens, deflection at the

anchors prevented the specimen from resisting additional loads. Thus, the failure loads were closer to the limiting loads, Guaranteed Ultimate Strength, of the anchor systems. Yet, the S2 Specimen test results do indicate that steel fibers improve the tensile strength of the anchorage zones. As was the case for the S1 Specimens, with 0.5% steel fibers in the concrete mix, the addition of steel spirals resulted in an increase in load capacity. The addition of steel ties resulted in a greater strength increase than was found for the spirals.

For S2 Specimens with 0.5% Dramix fibers, Specimen S2-2, which had no spirals or ties, had 77% of the load capacity of the S2-1 Specimen which had plain concrete and 100% of steel spirals and 100% of steel ties based upon design recommendations. Similarly, the specimens with 0.5% Helix fiber (Specimen S2-6) and 0.5% Novomesh fibers (Specimen S2-10) had 78% and 90% the load capacity of Specimen S2-1. Thus, fibers in concrete contributes to a the specimens having a load capacity of 77% to 90% of the strength of the sections with steel spirals and ties with plain concrete. The Dramix Specimens S2-3 and S2-4 showed that adding steel spirals and steel ties added 13% and 21%, respectively, to the strength of the sections. Although Specimen S2-5 had less capacity than S2-1, the measured load capacity for S2-5 showed that the strength achieved by using 0.5% steel fibers by volume, 50% steel spirals and 40% steel ties was 92% of the load capacity of Specimen S2-1 and 15% greater than the GUTS strength of the two PT anchors. Thus, it was feasible to achieve more than adequate strength in the anchorage zone using 0.5% steel fiber and significant reductions in non-prestressed reinforcement.

Considering the Helix Specimens S2-7 and S2-8 showed that adding steel spirals and steel ties with the 0.5% fiber resulted in a 22% and a 32%, increase in load capacity. The presence of steel

ties contributed greater strength than the presence of steel spirals. The measured load capacity for S2-9 showed that the strength achieved by using 0.5% steel fibers, 50% steel spirals and 40% steel ties was 104% of that of Specimen S2-1. Thus, adding Helix steel fibers and reducing the non-prestressed reinforcement yielded a specimen 4% stronger than the plain concrete specimen with full spirals and ties. The presence of steel fibers did improve the load carrying ability of the anchorage zone.

Novomesh S2-11 did not show an increase in load capacity due to the addition of spirals; it showed a 13% decrease in load capacity. However, the maximum applied load was 99% of the GUTS load for the specimen. Since the maximum anticipated post-tensioning force is 80% of the GUTS load, the strength of the specimen was more than adequate. In addition, it is not recommended that an anchorage zone be constructed without steel ties. The load capacity of S2-12 showed a 15% increase in capacity over S2-10 due to the addition of steel ties. Specimen S2-13 with 0.5% fibers, 50% steel spirals and 40% steel ties had 4% greater load capacity than did Specimen S2-1. Since Specimens S2-8, S2-9, S2-12 and S2-13 all failed at approximately the same load, approximately 750 K, this seems to be the upper limit of the specimens ability to resist the general zone bursting tensile forces and the compression forces in the local zone. The upper limit on strength capacity for these four specimens was 4% greater than the strength capacity of specimen S2-1 and 30% greater than the GUTS for the two anchors. Comparing Specimens S2-5, S2-9 and S2-13, to Specimen S2-14 which was cast with the same reinforcing configuration but plain concrete instead of fibers, showed that the addition of steel fibers resulted in strength increase of 3% to 17%. From these tests, it is evident that adding fibers to the anchorage zones resulted in increased load capacities which were more than adequate for the

strength of the PT anchors even when the non-prestressed reinforcement was significantly reduced.

5.13.3 PT Anchor Test Specimens Results Summary

In summary, consideration of both S1 Specimens test results and S2 Specimens test results showed the following:

1. Adding 0.5% steel fibers to the concrete mix without adding non-prestressed reinforcement in the local and general anchorage zones resulted in test specimens having load capacities that ranged from 77% to 134% of the load capacity of test specimens with plain concrete and 100% of the local zone reinforcement recommended by the anchorage manufacturer and 100% of the general zone reinforcement recommended by the approximate design method of the AASHTO code.

2. Adding steel spirals along with the 0.5% steel fibers resulted in strength increases of up to 22%. However, for two specimens cast with Novomesh fibers (S1-11 and S2-11) the addition of spiral did not result in increases in strength instead a 13% to 17% decrease in strength resulted.

3. Adding steel ties along with the 0.5% steel fibers resulted in strength increases of up to 32%.

4. Even though the addition of 0.5% steel fibers did add up to 37% increase in strength to test specimens, steel spirals and steel ties are needed to prevent sudden failure due to punching shear at the anchors (in the local zone) and to prevent sudden failure due to bursting tension in the general zones.

5. With 0.5% fibers by volume, 50% of steel spirals (recommended by PT anchor manufacturers) and 40% of steel ties (based upon AASHTO design guidelines) , the load capacities of the anchorage zone test specimens were from 92% to 159% the load capacity of the plain specimens with the recommend local and general zone reinforcement. Thus, the addition of steel fibers did increase the strength of the anchorage zone even with reductions in non-prestressed reinforcing steel.

6. In addition, to improving the strength of the specimens, the addition of fibers (steel and steel and polypropylene fibers) resulted in smaller and few cracks developing on the surface of the test specimens. Thus, the use of fibers in PT anchorage zones may contribute to improvements in the durability of structural elements.

CHAPTER 6

COMPARISON OF NUMERICAL ANALYSIS AND EXPERIMENTAL RESULTS

6.1 Numerical Modeling of Laboratory Specimens

As stated in Chapter 4, the geometry of the block specimens used in laboratory testing was based on prior finite element analysis on a typical bridge segment to determine the magnitudes and distribution of the stresses in the anchor zone and on the AASHTO requirements for the general zone size. After the completion of laboratory tests on anchor specimens, another round of finite element analysis was conducted to compare results from both methods.

The finite element models used in the analysis comprise of blocks as shown in Figure 6-1 with reinforcements similar those used in the actual laboratory specimens. Steel as well as concrete with fiber reinforcement were modeled using different real constants for elements SOLID 45 and SOLID65, respectively. The smeared method was used to distribute the fiber inside the concrete elements. A more detailed description of the modeling process was presented in Chapter 4.

The load application on all Finite element block was set to maximum as 800 kips. The loading steps started with a gradual increase in the load by dividing the maximum load to 20 load steps.

This would allow the analysis to continue until non-convergence solution was reached. The same loading conditions and solution controls were followed for all the 27 models that simulate the tested specimen. After the second round of the finite element analysis was completed, the models were sliced and strain, stress and deflections measurements were recorded. Comparisons between the laboratory testing results and the finite element analysis are shown in Figure 6-1 to Figure 6-3 and Tables 6-1 and 6-2.

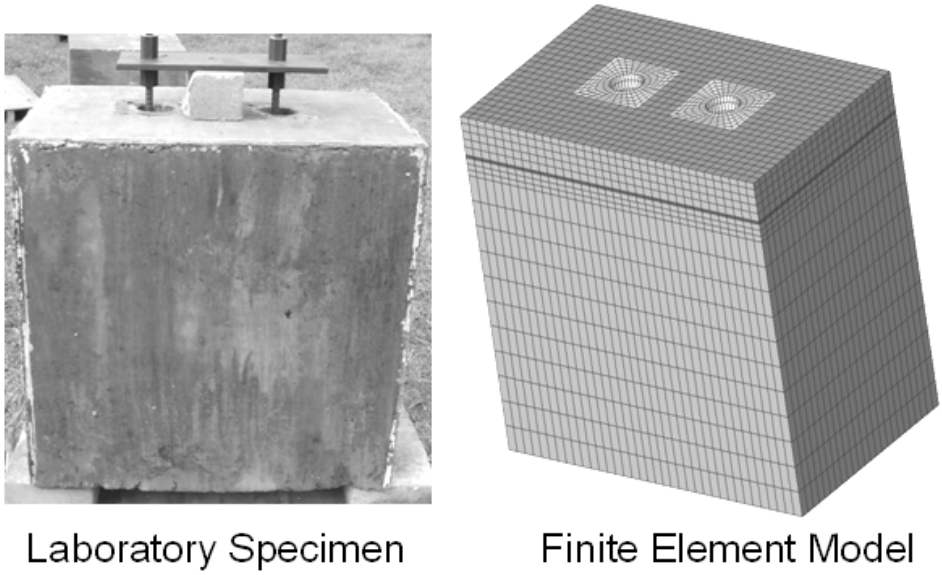

Figure 6-1: Anchor Specimen and Finite Element Model

Table 6-1: Comparison between Test and FEA results for S1 Specimens

Specimen	Strain Type	Failure Load (kips)	Deflection (in)	Embedded Strain Gauges (at 80% of the max load)			
				Emb 1 (strain)	Emb 2 (strain)	Emb 3 (strain)	Emb 4 (strain)
S1-1-None/Y/Y	Test	628	0.509	-205	112	158	96.4
	FEM	600	0.485	-170	120	146	110
S1-2- Dramix/N/N	Test	795	0.530	-	121	-	740
	FEM	600	0.505	-	120	-	270
S1-3-Dramix/Y/N	Test	866	0.594	-	313	385	-635
	FEM	600	0.500	-	210	255	-400
S1-4-Dramix/N/Y	Test	999	0.721	-407	-	262	-229
	FEM	600	0.495	-380	-	240	-186
S1-5-Dramix/0.5/0.6	Test	1000	0.651	-	224	208	-
	FEM	600	0.485	-	190	180	-
S1-6-Helix/N/N	Test	600	0.406	-	82	124	-
	FEM	600	0.505	-	120	170	-
S1-7-Helix/Y/N	Test	677	0.524	-	82	91	-
	FEM	600	0.500	-	126	136	-
S1-8-Helix/N/Y	Test	917	0.619	-	112	108	-
	FEM	600	0.495	-	120	160	-
S1-9-Helix/0.5/0.6	Test	869	0.556	-	140	174	-
	FEM	600	0.485	-	120	160	-
S1-10-Novomesh/N/N	Test	841	0.549	-	85	283	-
	FEM	600	0.505	-	120	160	-
S1-11-Novomesh/Y/N	Test	720	0.566	-	458	38	-
	FEM	600	0.500	-	120	160	-
S1-13- Novomesh/0.5/0.6	Test	734	0.501	-	-193	96	-
	FEM	600	0.485	-	120	160	-
S1-14- None/0.5/0.6	Test	996	0.684	-	38	83	-
	FEM	600	0.485	-	80	120	-

Table 6-2: Comparison between Test and FEA results for S2 Specimens

Specimen	Strain Type	Failure Load (kips)	Deflection (in)	Embedded Strain Gauges (at 80% of the max load)			
				Emb 1 (strain)	Emb 2 (strain)	Emb 3 (strain)	Emb 4 (strain)
S2-1-None/Y/Y	Test	723	0.550	62	-	158	-
	FEM	600	0.485	80	-	160	-
S2-2- Dramix/N/N	Test	557	0.434	58	-	100	-
	FEM	600	0.505	86	-	170	-
S2-3-Dramix/Y/N	Test	628	0.475	100	-	159	
	FEM	600	0.500	120	-	160	-
S2-4-Dramix/N/Y	Test	674	0.539	34	-	200	-
	FEM	600	0.495	60	-	170	-
S2-5-Dramix/0.5/0.6	Test	666	0.594	109	-	124	-
	FEM	600	0.485	120	-	140	-
S2-6-Helix/N/N	Test	568	0.480	17	-	165	-
	FEM	600	0.505	60	-	140	-
S2-7-Helix/Y/N	Test	691	0.503	-15	-	98	-
	FEM	600	0.500	60	-	120	-
S2-8-Helix/N/Y	Test	748	0.504	62	-	120	-
	FEM	600	0.495	80	-	120	-
S2-9-Helix/0.5/0.6	Test	753	0.650	39	-	200	-
	FEM	600	0.485	60	-	160	-
S2-10-Novomesh/N/N	Test	654	0.475	78	-	124	-
	FEM	600	0.505	60	-	120	-
S2-11-Novomesh/Y/N	Test	570	0.458	53	-	160	-
	FEM	600	0.500	60	-	120	-
S2-12-Novomesh/N/Y	Test	750	0.538	16	-	264	-
	FEM	600	0.495	60	-	180	-
S2-13-Novomesh/0.5/0.6	Test	753	0.595	71	-	194	-
	FEM	600	0.485	80	-	140-	-
S2-14-None/0.5/0.6	Test	646	0.570	239	186	143	280
	FEM	600	0.485	180	160	120	220

Tables 6-1 and 6-2 show that the finite element models sustained loads less that those encountered in the laboratory tests on anchor specimens. The maximum load in the lab was 1000 kips for S1-5 with Dramix steel fiber and 50% of the spiral reinforcement and 60% of the ties. The loading capacity for the equivalent FE model was 640 kips. In the second set of laboratory specimen, the loading capacity of S2-4 was 674 kips. On the other hand, the loading capacity of S1-1 with full reinforcement and no fibers was 628 kips and the equivalent FE model was 600 kips. For S2-1, the loading capacity was 723 kips. It was noticed that the cracking pattern of the S1-1 and S2-1 specimens were similar to those obtained from finite element model (Figure 6-2).

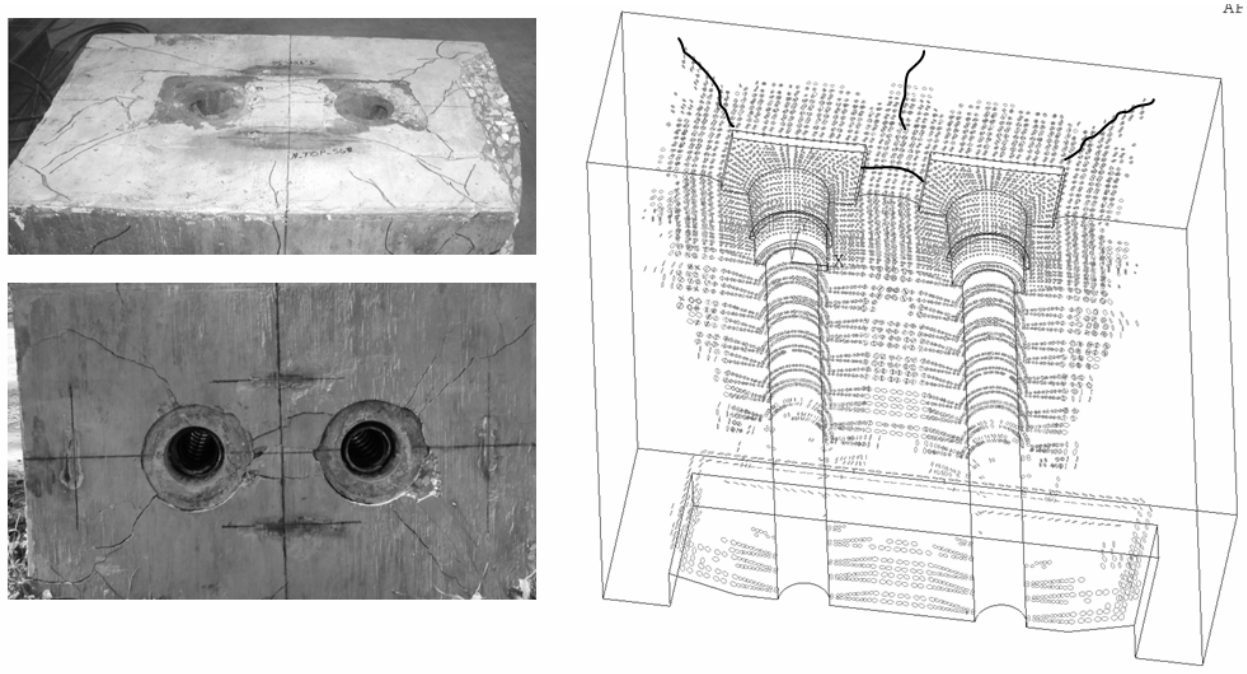

Figure 6-2: Cracking From Lab Testing and Finite Element Analysis

Strain measurements from laboratory testing were also compared with those obtained from the FEA (Figure 6-3). Tables 6-1 and 6-2 presented strain measurements from embedded gauges in all the specimens. Since compressive and tensile strains are very high at failure especially when cracking or crushing occurred at the gauges locations, it was decided to present measurements at loading levels less than the failure loads. This was also true for the finite element models. Therefore, it was decided to record strain values for the load steps preceding the failure loads. Figure 6-3 shows the strain value of the top gauge in S1-1. The Test measurements showed a value of 237 microstrain (compression) and the FE model resulted in 274 microstrain (compression).

In general, stress and strain results obtained from the first round of finite element analysis on a typical bridge segment and from the laboratory testing program on block specimens with two anchors were comparable. Further validation from the second round of finite element analysis after laboratory testing confirmed this conclusion. Strain measurements from lab testing were comparable to those obtained from the finite element models. Deflections from laboratory tests were mostly higher than those obtained from finite element analysis (Figure 6-4). The reasons for higher deflections in test specimens were the type of bearing pad underneath the specimens. At on test a rubber pad was used and then it was replaced by a sand box. Additionally, the initial applied load on the anchors caused some deflections before the two actuators' loads were fully transferred to a specimen. To pass the setting deflections, measurements were taken at the first inflection point of the load-deformations curve. In most of the cases the setting deflections ranged between 0.15 to 0.2 in and were subtracted from the total deflection of the specimens.

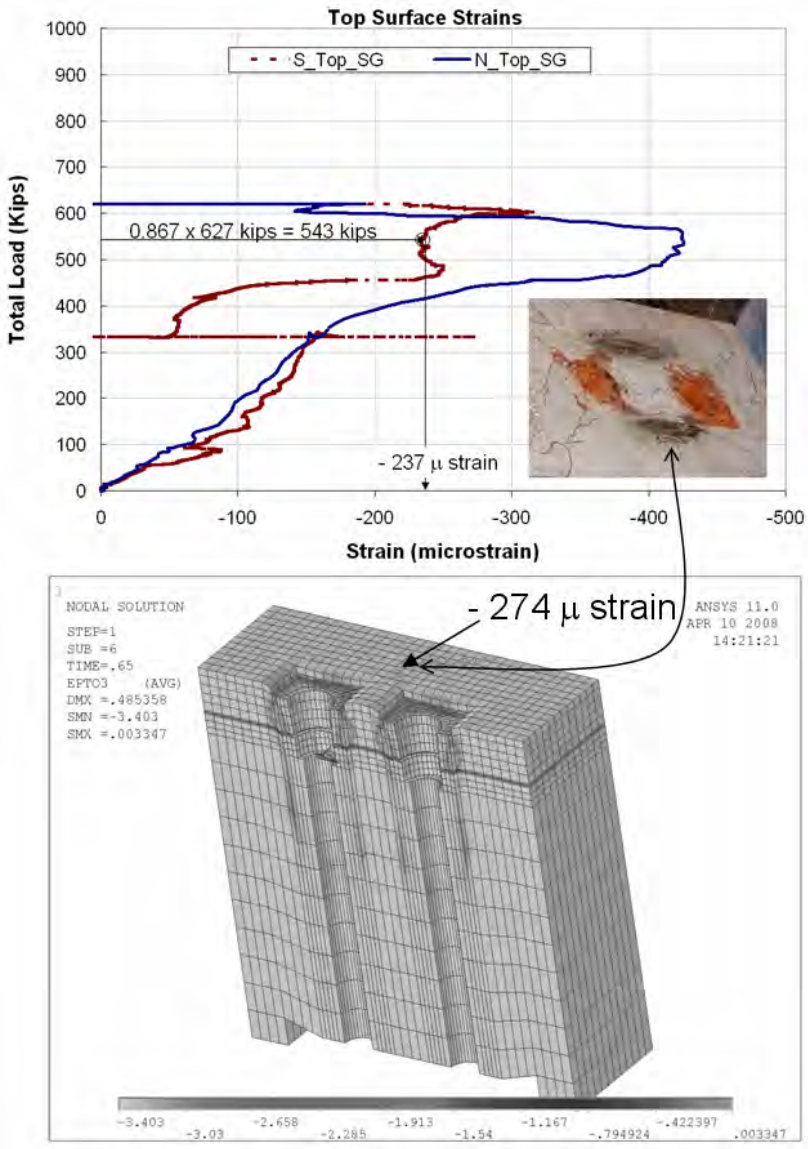

Figure 6-3: Strain Values From Laboratory Testing and Finite Element Analysis

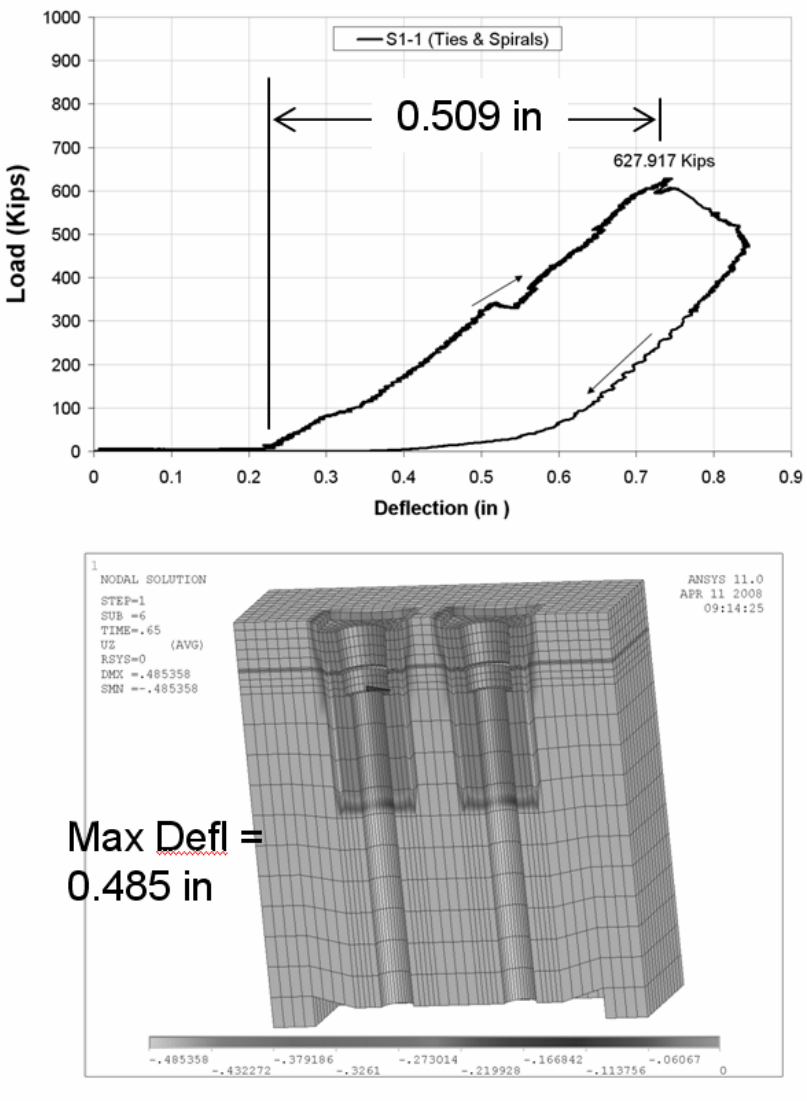

Figure 6-4: Deflection from Lab Testing for S1-1 and Finite Element Analysis

6.2 Post-Tensioned Anchorage Zone

In post-tensioning anchorage zones high stresses develop due to the transfer of prestressing force through bearing plates and anchors. To prevent these stresses from causing splitting, bursting and cracking of the concrete in the anchorage zone, adequate detailing is required. This detailing includes provision of sufficient concrete volume and reinforcing steel in the high stress

region. Design specifications, anchorage devices and systems, and design experience are important elements for successfully designing and detailing anchorage zones.

The 2007 AASHTO LRFD Bridge Design Specifications provides recommendations and guidelines for post-tensioned anchorage zones in Section 5.10.9. In 1994, researchers at the University of Texas proposed anchorage design specifications for AASHTO as requested through the National Cooperative Highway Research Program (Breen et al, 1994). The current AASHTO specification for post-tensioning anchorage zones is based upon the work of Breen et al. AASHTO states that "for anchorage zones at the end of a segment, the transverse dimensions may be taken as the depth and width of the section but not larger than the longitudinal dimension of the component or segment." The longitudinal dimension of the anchorage zone shall be greater than or equal to the larger of the transverse dimensions but not greater than 1.5 times this dimension. In section 5.10.9.2, AASHTO identifies two sections in the anchorage zone, the general zone and the local zone. The local zone is the region of high compressive stresses immediately ahead of the anchorage device. The general zone is the remainder of the anchorage zone and contains the region where the tensile stresses develop as a result of the tendon force spreading across the section. The Engineer of Record is responsible for the design of the anchorage zone. Section 5.9.10.9.3 of the AASHTO code lists three methods that may be used to design the general zone: 1. strut-and-tie models, 2. refined elastic analyses, or 3. other approximate methods.

6.3 Strut-And-Tie Method

Using the AASHTO Guidelines of Section 5.10.9.4 of the code, a strut-and-tie model was made for the anchorage specimen. The model assumes approximately a 45 degree angle for the compression struts. By assuming that the maximum bursting force occurs approximately in the middle of the anchorage zone (for the distance measured along the length of the tendon) and considering two dimensional approximations, the bursting forces (total tie forces) are computed for the cross-sectional dimensions of the anchorage block. As shown in the Table 6-3, the maximum tensile bursting force occurs along the widest cross-sectional dimension (width = 29.5”). The maximum tensile force varies with the magnitude of the applied load (which simulates the post-tensioning force). Based upon the anchor block geometry and the maximum applied load of 1000.36 kips, Specimen S1-5 has a maximum computed tie force, bursting force, of 138.44 kips.

Table 6-4 presents strut-and-tie calculations for Specimen S1-1 for various strut angles relative to the load surface. As shown in the table, as the angle of the strut with respect to the bearing surface increases, the magnitude of the bursting force decreases and the distance of the force away for the load surface increases. Table 6-5, Table 6-6, and Table 6-7 show strut-and-tie calculations for different strut angles for anchorage test specimens S1-5, S2-1, and S2-13, respectively. Similar calculations were done for all of the other anchorage test specimens.

Table 6-3: Strut And Tie Two Dimensional Approximation For Bursting Force

Strut & Tie (Truss Calculations) : Two - 2D Approximations Added Together																							
Specimen	Specimen ID	Total Load (K)	West Actuator P1 (K)	East Actuator P2 (K)	9+11 Tie Total (Kips)	10+12 Tie Total (Kips)	Members 1	2	3	4	5	6	7	8	9 Tie	10 Tie	11 Tie	12 Tie	13	14	15	16
	S1 Specimens				LONG	SHORT									LONG	SHORT	LONG	SHORT				
1	S1-1	627.92	314.93	312.99	86.82	67.28	43.41	33.53	43.41	33.74	175.44	174.52	174.52	175.44	43.41	33.53	43.41	33.74	157.32	156.84	156.84	157.32
2	S1-2	794.00	389.24	404.75	108.77	85.07	54.39	43.37	54.39	41.70	218.35	225.69	225.69	218.35	54.39	43.37	54.39	41.70	195.77	199.65	199.65	195.77
3	S1-3	865.33	428.84	436.49	119.07	92.71	59.53	46.77	59.53	45.95	239.77	243.39	243.39	239.77	59.53	46.77	59.53	45.95	214.99	216.90	216.90	214.99
4	S1-4	999.23	500.18	499.05	138.05	107.06	69.03	53.47	69.03	53.59	278.80	278.27	278.27	278.80	69.03	53.47	69.03	53.59	250.01	249.73	249.73	250.01
5	S1-5	1000.36	502.79	497.56	138.44	107.18	69.22	53.31	69.22	53.87	279.92	277.44	277.44	279.92	69.22	53.31	69.22	53.87	251.01	249.70	249.70	251.01
6	S1-6	599.94	293.80	306.15	82.15	64.28	41.08	32.80	41.08	31.48	164.86	170.71	170.71	164.86	41.08	32.80	41.08	31.48	147.81	150.90	150.90	147.81
7	S1-7	676.74	337.42	339.32	93.35	72.51	46.67	36.36	46.67	36.15	188.31	189.20	189.20	188.31	46.67	36.36	46.67	36.15	168.85	169.32	169.32	168.85
8	S1-8	916.70	460.24	456.45	126.81	98.22	63.40	48.91	63.40	49.31	256.31	254.52	254.52	256.31	63.40	48.91	63.40	49.31	229.84	228.89	228.89	229.84
9	S1-9	869.23	436.39	432.84	120.24	93.13	60.12	46.38	60.12	46.76	243.03	241.35	241.35	243.03	60.12	46.38	60.12	46.76	217.93	217.04	217.04	217.93
10	S1-10	827.22	403.18	424.04	113.06	88.63	56.53	45.43	56.53	43.20	226.58	236.44	236.44	226.58	56.53	45.43	56.53	43.20	203.13	208.35	208.35	203.13
11	S1-11	704.80	349.84	354.96	97.04	75.51	48.52	38.03	48.52	37.48	195.50	197.93	197.93	195.50	48.52	38.03	48.52	37.48	175.30	176.58	176.58	175.30
12	S1-13	732.53	365.46	367.07	101.07	78.49	50.53	39.33	50.53	39.16	203.92	204.68	204.68	203.92	50.53	39.33	50.53	39.16	182.85	183.25	183.25	182.85
13	S1-14	995.59	496.17	499.43	137.30	106.67	68.65	53.51	68.65	53.16	276.94	278.48	278.48	276.94	68.65	53.51	68.65	53.16	248.32	249.14	249.14	248.32
	S2 Specimens																					
14	S2-1	723.25	365.94	357.31	100.36	77.49	50.18	38.28	50.18	39.21	203.32	199.24	199.24	203.32	50.18	38.28	50.18	39.21	182.33	180.17	180.17	182.33
15	S2-2	552.87	273.10	279.77	75.97	59.24	37.99	29.97	37.99	29.26	152.85	156.00	156.00	152.85	37.99	29.97	37.99	29.26	137.04	138.71	138.71	137.04
16	S2-3	626.89	316.41	310.48	86.90	67.17	43.45	33.27	43.45	33.90	175.93	173.12	173.12	175.93	43.45	33.27	43.45	33.90	157.76	156.28	156.28	157.76
17	S2-4	673.86	332.58	341.29	92.57	72.20	46.28	36.57	46.28	35.63	186.18	190.30	190.30	186.18	46.28	36.57	46.28	35.63	166.93	169.11	169.11	166.93
18	S2-5	665.56	323.08	342.47	90.82	71.31	45.41	36.69	45.41	34.62	181.79	190.96	190.96	181.79	45.41	36.69	45.41	34.62	162.98	167.82	167.82	162.98
19	S2-6	566.51	280.34	286.17	77.90	60.70	38.95	30.66	38.95	30.04	156.81	159.57	159.57	156.81	38.95	30.66	38.95	30.04	140.60	142.06	142.06	140.60
20	S2-7	691.14	347.09	344.05	95.61	74.05	47.81	36.86	47.81	37.19	193.28	191.84	191.84	193.28	47.81	36.86	47.81	37.19	173.32	172.56	172.56	173.32
21	S2-8	747.70	371.67	376.03	103.01	80.11	51.50	40.29	51.50	39.82	207.61	209.68	209.68	207.61	51.50	40.29	51.50	39.82	186.16	187.25	187.25	186.16
22	S2-9	752.57	370.22	382.36	103.24	80.63	51.62	40.97	51.62	39.67	207.46	213.20	213.20	207.46	51.62	40.97	51.62	39.67	186.01	189.04	189.04	186.01
23	S2-10	653.63	327.53	326.10	90.34	70.03	45.17	34.94	45.17	35.09	182.51	181.83	181.83	182.51	45.17	34.94	45.17	35.09	163.66	163.30	163.30	163.66
24	S2-11	569.55	285.02	284.53	78.68	61.02	39.34	30.49	39.34	30.54	158.89	158.65	158.65	158.89	39.34	30.49	39.34	30.54	142.48	142.35	142.35	142.48
25	S2-12	749.99	374.45	375.53	103.51	80.36	51.75	40.24	51.75	40.12	208.89	209.40	209.40	208.89	51.75	40.24	51.75	40.12	187.31	187.58	187.58	187.31
26	S2-13	752.68	370.37	382.32	103.27	80.64	51.63	40.96	51.63	39.68	207.53	213.18	213.18	207.53	51.63	40.96	51.63	39.68	186.07	189.05	189.05	186.07
27	S2-14	645.77	326.27	319.50	89.56	69.19	44.78	34.23	44.78	34.96	181.36	178.15	178.15	181.36	44.78	34.23	44.78	34.96	162.64	160.94	160.94	162.64

Table 6-4: Strut And Tie Bursting Forces For Specimen S1-1

Strut & Tie (Truss Calculations) : Two - 2D Approximations Added Together																	
Specimen	Specimen ID	Total Load (K)	West Actuator P1 (K)	East Actuator P2 (K)	9+11 Tie Total (Kips)	10+12 Tie Total (Kips)		19.5 SHORT					29.5 LONG				
							X	H1	X/H1	Degrees Theta1	Radians Theta1	X	H2	X/H2	Degrees Theta2	Radians Theta2
1	S1-1	627.92	314.93	312.99	1571.77	1217.94	0.725	19.5	0.04	7.34	0.13	0.725	29.5	0.02	5.71	0.10
1	S1-1	627.92	314.93	312.99	930.23	720.82	1.225	19.5	0.06	12.29	0.21	1.225	29.5	0.04	9.59	0.17
1	S1-1	627.92	314.93	312.99	785.88	608.97	1.450	19.5	0.07	14.45	0.25	1.450	29.5	0.05	11.31	0.20
1	S1-1	627.92	314.93	312.99	523.92	405.98	2.175	19.5	0.11	21.14	0.37	2.175	29.5	0.07	16.70	0.29
1	S1-1	627.92	314.93	312.99	465.12	360.41	2.450	19.5	0.13	23.54	0.41	2.450	29.5	0.08	18.67	0.33
1	S1-1	627.92	314.93	312.99	392.94	304.49	2.900	19.5	0.15	27.27	0.48	2.900	29.5	0.10	21.80	0.38
1	S1-1	627.92	314.93	312.99	314.35	243.59	3.625	19.5	0.19	32.80	0.57	3.625	29.5	0.12	26.57	0.46
1	S1-1	627.92	314.93	312.99	310.08	240.27	3.675	19.5	0.19	33.16	0.58	3.675	29.5	0.12	26.88	0.47
1	S1-1	627.92	314.93	312.99	261.96	202.99	4.350	19.5	0.22	37.72	0.66	4.350	29.5	0.15	30.96	0.54
1	S1-1	627.92	314.93	312.99	232.56	180.21	4.900	19.5	0.25	41.06	0.72	4.900	29.5	0.17	34.05	0.59
1	S1-1	627.92	314.93	312.99	224.54	173.99	5.075	19.5	0.26	42.06	0.73	5.075	29.5	0.17	34.99	0.61
1	S1-1	627.92	314.93	312.99	196.47	152.24	5.800	19.5	0.30	45.88	0.80	5.800	29.5	0.20	38.66	0.67
1	S1-1	627.92	314.93	312.99	186.05	144.16	6.125	19.5	0.31	47.44	0.83	6.125	29.5	0.21	40.19	0.70
1	S1-1	627.92	314.93	312.99	174.64	135.33	6.525	19.5	0.33	49.24	0.86	6.525	29.5	0.22	41.99	0.73
1	S1-1	627.92	314.93	312.99	166.91	129.33	6.827	19.5	0.35	50.52	0.88	6.827	29.5	0.23	43.28	0.76
1	S1-1	627.92	314.93	312.99	157.18	121.79	7.250	19.5	0.37	52.19	0.91	7.250	29.5	0.25	45.00	0.79
1	S1-1	627.92	314.93	312.99	155.04	120.14	7.350	19.5	0.38	52.57	0.92	7.350	29.5	0.25	45.39	0.79
1	S1-1	627.92	314.93	312.99	146.70	113.68	7.768	19.5	0.40	54.09	0.94	7.768	29.5	0.26	46.97	0.82
1	S1-1	627.92	314.93	312.99	132.89	102.97	8.575	19.5	0.44	56.74	0.99	8.575	29.5	0.29	49.79	0.87
1	S1-1	627.92	314.93	312.99	116.88	90.57	9.750	19.5	0.50	60.02	1.05	9.750	29.5	0.33	53.37	0.93
1	S1-1	627.92	314.93	312.99	116.28	90.10	9.800	19.5	0.50	60.15	1.05	9.800	29.5	0.33	53.51	0.93
1	S1-1	627.92	314.93	312.99	103.36	80.09	11.025	19.5	0.57	62.97	1.10	11.025	29.5	0.37	56.67	0.99
1	S1-1	627.92	314.93	312.99	98.78	76.54	11.536	19.5	0.59	64.01	1.12	11.536	29.5	0.39	57.85	1.01
1	S1-1	627.92	314.93	312.99	93.02	72.08	12.250	19.5	0.63	65.34	1.14	12.250	29.5	0.42	59.38	1.04
1	S1-1	627.92	314.93	312.99	86.82	67.28	13.125	19.5	0.67	66.80	1.17	13.125	29.5	0.44	61.08	1.07
1	S1-1	627.92	314.93	312.99	77.26	59.87	14.750	19.5	0.76	69.13	1.21	14.750	29.5	0.50	63.82	1.11

Table 6-5: Strut And Tie Bursting Forces For Specimen S1-5

Strut & Tie (Truss Calculations) : Two - 2D Approximations Added Together

Specimen #	Specimen ID	Total Load (K)	West Actuator P1 (K)	East Actuator P2 (K)	9+11 Tie Total (Kips)	10+12 Tie Total (Kips)	19.5 SHORT X	19.5 SHORT H1	19.5 SHORT X/H1	19.5 SHORT Degrees Theta1	19.5 SHORT Radians Theta1	29.5 LONG X	29.5 LONG H2	29.5 LONG X/H2	29.5 LONG Degrees Theta2	29.5 LONG Radians Theta2
5	S1-5	1000.36	502.79	497.56	2506.23	1940.35	0.725	19.5	0.04	7.34	0.13	0.725	29.5	0.02	5.71	0.10
5	S1-5	1000.36	502.79	497.56	1483.28	1148.37	1.225	19.5	0.06	12.29	0.21	1.225	29.5	0.04	9.59	0.17
5	S1-5	1000.36	502.79	497.56	1253.12	970.17	1.450	19.5	0.07	14.45	0.25	1.450	29.5	0.05	11.31	0.20
5	S1-5	1000.36	502.79	497.56	835.41	646.78	2.175	19.5	0.11	21.14	0.37	2.175	29.5	0.07	16.70	0.29
5	S1-5	1000.36	502.79	497.56	741.64	574.18	2.450	19.5	0.13	23.54	0.41	2.450	29.5	0.08	18.67	0.33
5	S1-5	1000.36	502.79	497.56	626.56	485.09	2.900	19.5	0.15	27.27	0.48	2.900	29.5	0.10	21.80	0.38
5	S1-5	1000.36	502.79	497.56	501.25	388.07	3.625	19.5	0.19	32.80	0.57	3.625	29.5	0.12	26.57	0.46
5	S1-5	1000.36	502.79	497.56	494.43	382.79	3.675	19.5	0.19	33.16	0.58	3.675	29.5	0.12	26.88	0.47
5	S1-5	1000.36	502.79	497.56	417.71	323.39	4.350	19.5	0.22	37.72	0.66	4.350	29.5	0.15	30.96	0.54
5	S1-5	1000.36	502.79	497.56	370.82	287.09	4.900	19.5	0.25	41.06	0.72	4.900	29.5	0.17	34.05	0.59
5	S1-5	1000.36	502.79	497.56	358.03	277.19	5.075	19.5	0.26	42.06	0.73	5.075	29.5	0.17	34.99	0.61
5	S1-5	1000.36	502.79	497.56	313.28	242.54	5.800	19.5	0.30	45.88	0.80	5.800	29.5	0.20	38.66	0.67
5	S1-5	1000.36	502.79	497.56	296.66	229.67	6.125	19.5	0.31	47.44	0.83	6.125	29.5	0.21	40.19	0.70
5	S1-5	1000.36	502.79	497.56	278.47	215.59	6.525	19.5	0.33	49.24	0.86	6.525	29.5	0.22	41.99	0.73
5	S1-5	1000.36	502.79	497.56	266.14	206.05	6.827	19.5	0.35	50.52	0.88	6.827	29.5	0.23	43.28	0.76
5	S1-5	1000.36	502.79	497.56	250.62	194.03	7.250	19.5	0.37	52.19	0.91	7.250	29.5	0.25	45.00	0.79
5	S1-5	1000.36	502.79	497.56	247.21	191.39	7.350	19.5	0.38	52.57	0.92	7.350	29.5	0.25	45.39	0.79
5	S1-5	1000.36	502.79	497.56	233.92	181.10	7.768	19.5	0.40	54.09	0.94	7.768	29.5	0.26	46.97	0.82
5	S1-5	1000.36	502.79	497.56	211.90	164.05	8.575	19.5	0.44	56.74	0.99	8.575	29.5	0.29	49.79	0.87
5	S1-5	1000.36	502.79	497.56	186.36	144.28	9.750	19.5	0.50	60.02	1.05	9.750	29.5	0.33	53.37	0.93
5	S1-5	1000.36	502.79	497.56	185.41	143.55	9.800	19.5	0.50	60.15	1.05	9.800	29.5	0.33	53.51	0.93
5	S1-5	1000.36	502.79	497.56	164.81	127.60	11.025	19.5	0.57	62.97	1.10	11.025	29.5	0.37	56.67	0.99
5	S1-5	1000.36	502.79	497.56	157.51	121.95	11.536	19.5	0.59	64.01	1.12	11.536	29.5	0.39	57.85	1.01
5	S1-5	1000.36	502.79	497.56	148.33	114.84	12.250	19.5	0.63	65.34	1.14	12.250	29.5	0.42	59.38	1.04
5	S1-5	1000.36	502.79	497.56	138.44	107.18	13.125	19.5	0.67	66.80	1.17	13.125	29.5	0.44	61.08	1.07
5	S1-5	1000.36	502.79	497.56	123.19	95.37	14.750	19.5	0.76	69.13	1.21	14.750	29.5	0.50	63.82	1.11

Table 6-6: Strut And Tie Bursting Forces For Specimen S2-1

Strut & Tie (Truss Calculations) : Two - 2D Approximations Added Together

Specimen #	Specimen ID	Total Load (K)	West Actuator P1 (K)	East Actuator P2 (K)	9+11 Tie Total (Kips)	10+12 Tie Total (Kips)	19.5 SHORT X	19.5 SHORT H1	19.5 SHORT X/H1	19.5 SHORT Degrees Theta1	19.5 SHORT Radians Theta1	29.5 LONG X	29.5 LONG H2	29.5 LONG X/H2	29.5 LONG Degrees Theta2	29.5 LONG Radians Theta2
14	S2-1	723.25	365.94	357.31	1816.93	1402.85	0.725	19.5	0.04	7.34	0.13	0.725	29.5	0.02	5.71	0.10
14	S2-1	723.25	365.94	357.31	1075.32	830.26	1.225	19.5	0.06	12.29	0.21	1.225	29.5	0.04	9.59	0.17
14	S2-1	723.25	365.94	357.31	908.46	701.43	1.450	19.5	0.07	14.45	0.25	1.450	29.5	0.05	11.31	0.20
14	S2-1	723.25	365.94	357.31	605.64	467.62	2.175	19.5	0.11	21.14	0.37	2.175	29.5	0.07	16.70	0.29
14	S2-1	723.25	365.94	357.31	537.66	415.13	2.450	19.5	0.13	23.54	0.41	2.450	29.5	0.08	18.67	0.33
14	S2-1	723.25	365.94	357.31	454.23	350.71	2.900	19.5	0.15	27.27	0.48	2.900	29.5	0.10	21.80	0.38
14	S2-1	723.25	365.94	357.31	363.39	280.57	3.625	19.5	0.19	32.80	0.57	3.625	29.5	0.12	26.57	0.46
14	S2-1	723.25	365.94	357.31	358.44	276.75	3.675	19.5	0.19	33.16	0.58	3.675	29.5	0.12	26.88	0.47
14	S2-1	723.25	365.94	357.31	302.82	233.81	4.350	19.5	0.22	37.72	0.66	4.350	29.5	0.15	30.96	0.54
14	S2-1	723.25	365.94	357.31	268.83	207.57	4.900	19.5	0.25	41.06	0.72	4.900	29.5	0.17	34.05	0.59
14	S2-1	723.25	365.94	357.31	259.56	200.41	5.075	19.5	0.26	42.06	0.73	5.075	29.5	0.17	34.99	0.61
14	S2-1	723.25	365.94	357.31	227.12	175.36	5.800	19.5	0.30	45.88	0.80	5.800	29.5	0.20	38.66	0.67
14	S2-1	723.25	365.94	357.31	215.06	166.05	6.125	19.5	0.31	47.44	0.83	6.125	29.5	0.21	40.19	0.70
14	S2-1	723.25	365.94	357.31	201.88	155.87	6.525	19.5	0.33	49.24	0.86	6.525	29.5	0.22	41.99	0.73
14	S2-1	723.25	365.94	357.31	192.94	148.97	6.827	19.5	0.35	50.52	0.88	6.827	29.5	0.23	43.28	0.76
14	S2-1	723.25	365.94	357.31	181.69	140.29	7.250	19.5	0.37	52.19	0.91	7.250	29.5	0.25	45.00	0.79
14	S2-1	723.25	365.94	357.31	179.22	138.38	7.350	19.5	0.38	52.57	0.92	7.350	29.5	0.25	45.39	0.79
14	S2-1	723.25	365.94	357.31	169.58	130.93	7.768	19.5	0.40	54.09	0.94	7.768	29.5	0.26	46.97	0.82
14	S2-1	723.25	365.94	357.31	153.62	118.61	8.575	19.5	0.44	56.74	0.99	8.575	29.5	0.29	49.79	0.87
14	S2-1	723.25	365.94	357.31	135.10	104.31	9.750	19.5	0.50	60.02	1.05	9.750	29.5	0.33	53.37	0.93
14	S2-1	723.25	365.94	357.31	134.42	103.78	9.800	19.5	0.50	60.15	1.05	9.800	29.5	0.33	53.51	0.93
14	S2-1	723.25	365.94	357.31	119.48	92.25	11.025	19.5	0.57	62.97	1.10	11.025	29.5	0.37	56.67	0.99
14	S2-1	723.25	365.94	357.31	114.19	88.17	11.536	19.5	0.59	64.01	1.12	11.536	29.5	0.39	57.85	1.01
14	S2-1	723.25	365.94	357.31	107.53	83.03	12.250	19.5	0.63	65.34	1.14	12.250	29.5	0.42	59.38	1.04
14	S2-1	723.25	365.94	357.31	100.36	77.49	13.125	19.5	0.67	66.80	1.17	13.125	29.5	0.44	61.08	1.07
14	S2-1	723.25	365.94	357.31	89.31	68.95	14.750	19.5	0.76	69.13	1.21	14.750	29.5	0.50	63.82	1.11

Table 6-7: Strut And Tie Bursting Forces For Specimen S2-13

Strut & Tie (Truss Calculations) : Two - 2D Approximations Added Together																	
Specimen #	Specimen ID	Total Load (K)	West Actuator P1 (K)	East Actuator P2 (K)	9+11 Tie Total (Kips)	10+12 Tie Total (Kips)		19.5 SHORT		Degrees	Radians		29.5 LONG		Degrees	Radians
							X	H1	X/H1	Theta1	Theta1	X	H2	X/H2	Theta2	Theta2
26	S2-13	752.68	370.37	382.32	1869.51	1459.95	0.725	19.5	0.04	7.34	0.13	0.725	29.5	0.02	5.71	0.10
26	S2-13	752.68	370.37	382.32	1106.45	864.05	1.225	19.5	0.06	12.29	0.21	1.225	29.5	0.04	9.59	0.17
26	S2-13	752.68	370.37	382.32	934.76	729.97	1.450	19.5	0.07	14.45	0.25	1.450	29.5	0.05	11.31	0.20
26	S2-13	752.68	370.37	382.32	623.17	486.65	2.175	19.5	0.11	21.14	0.37	2.175	29.5	0.07	16.70	0.29
26	S2-13	752.68	370.37	382.32	553.22	432.02	2.450	19.5	0.13	23.54	0.41	2.450	29.5	0.08	18.67	0.33
26	S2-13	752.68	370.37	382.32	467.38	364.99	2.900	19.5	0.15	27.27	0.48	2.900	29.5	0.10	21.80	0.38
26	S2-13	752.68	370.37	382.32	373.90	291.99	3.625	19.5	0.19	32.80	0.57	3.625	29.5	0.12	26.57	0.46
26	S2-13	752.68	370.37	382.32	368.82	288.02	3.675	19.5	0.19	33.16	0.58	3.675	29.5	0.12	26.88	0.47
26	S2-13	752.68	370.37	382.32	311.59	243.32	4.350	19.5	0.22	37.72	0.66	4.350	29.5	0.15	30.96	0.54
26	S2-13	752.68	370.37	382.32	276.61	216.01	4.900	19.5	0.25	41.06	0.72	4.900	29.5	0.17	34.05	0.59
26	S2-13	752.68	370.37	382.32	267.07	208.56	5.075	19.5	0.26	42.06	0.73	5.075	29.5	0.17	34.99	0.61
26	S2-13	752.68	370.37	382.32	233.69	182.49	5.800	19.5	0.30	45.88	0.80	5.800	29.5	0.20	38.66	0.67
26	S2-13	752.68	370.37	382.32	221.29	172.81	6.125	19.5	0.31	47.44	0.83	6.125	29.5	0.21	40.19	0.70
26	S2-13	752.68	370.37	382.32	207.72	162.22	6.525	19.5	0.33	49.24	0.86	6.525	29.5	0.22	41.99	0.73
26	S2-13	752.68	370.37	382.32	198.53	155.03	6.827	19.5	0.35	50.52	0.88	6.827	29.5	0.23	43.28	0.76
26	S2-13	752.68	370.37	382.32	186.95	145.99	7.250	19.5	0.37	52.19	0.91	7.250	29.5	0.25	45.00	0.79
26	S2-13	752.68	370.37	382.32	184.41	144.01	7.350	19.5	0.38	52.57	0.92	7.350	29.5	0.25	45.39	0.79
26	S2-13	752.68	370.37	382.32	174.49	136.26	7.768	19.5	0.40	54.09	0.94	7.768	29.5	0.26	46.97	0.82
26	S2-13	752.68	370.37	382.32	158.06	123.44	8.575	19.5	0.44	56.74	0.99	8.575	29.5	0.29	49.79	0.87
26	S2-13	752.68	370.37	382.32	139.02	108.56	9.750	19.5	0.50	60.02	1.05	9.750	29.5	0.33	53.37	0.93
26	S2-13	752.68	370.37	382.32	138.31	108.01	9.800	19.5	0.50	60.15	1.05	9.800	29.5	0.33	53.51	0.93
26	S2-13	752.68	370.37	382.32	122.94	96.01	11.025	19.5	0.57	62.97	1.10	11.025	29.5	0.37	56.67	0.99
26	S2-13	752.68	370.37	382.32	117.49	91.75	11.536	19.5	0.59	64.01	1.12	11.536	29.5	0.39	57.85	1.01
26	S2-13	752.68	370.37	382.32	110.64	86.40	12.250	19.5	0.63	65.34	1.14	12.250	29.5	0.42	59.38	1.04
26	S2-13	752.68	370.37	382.32	103.27	80.65	13.125	19.5	0.67	66.80	1.17	13.125	29.5	0.44	61.08	1.07
26	S2-13	752.68	370.37	382.32	91.89	71.76	14.750	19.5	0.76	69.13	1.21	14.750	29.5	0.50	63.82	1.11

6.4 Elastic Stress Analysis

By considering the finite element results and the same procedure used to develop the AASHTO code equation for computing the maximum bursting force in the post-tensioned anchorage zone, an equation was developed to compute the bursting force when steel fibers are used in the concrete. To develop this equation, the bursting stress (maximum tensile stress, Sx) values resulting from the finite element analysis were used. The maximum tensile stress (Sx) versus x/h ratios for b/h=0.22 for steel fiber percentages of 0.0% to 3.0% are shown in Figure 6-5. The procedure used to develop the equation for the bursting force is summarized in this section.

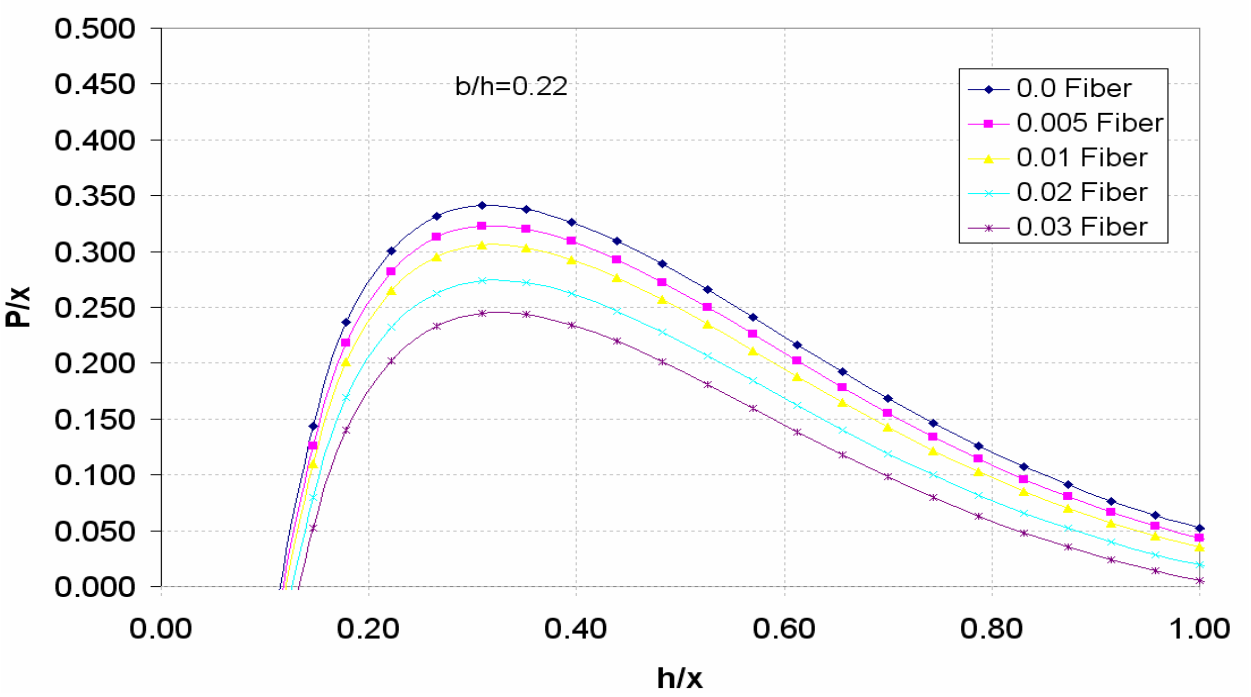

Figure 6-5: Maximum Tensile Stress, Sx, versus h/x for 0.0% To 3.0% Fiber

Using the finite element results, for different fiber percentages (0% to 3.0%), plots were made of the maximum tensile stress versus distances along the anchorage zone. The maximum tensile stress (Sx) versus x/h ratios plots for 0.0% to 3.0% steel fibers are shown in Figure 6-6 to Figure 6-10. The b/h ratios ranged from 0.0 to 1.0. The areas under the Sx versus x/h curves for each percentage of fiber were computed to obtain the bursting force, T_{max}. By plotting the bursting forces (areas under the stress curves) versus b/h for each percentage of fiber, an equation relating T_{max} to b/h was obtained by fitting a line through the plot. See Figure 6-11 to Figure 6-15. Each of these figures shows an equation for the best fit line to the curve for $T_{max.}$ These equations were used to compute the T_{max} values shown in Table 6-8. The bursting force (T_{max}) values computed in Table 6-8 to Table 6-11 are based on a one Kip (1 K) tendon force (unit value).

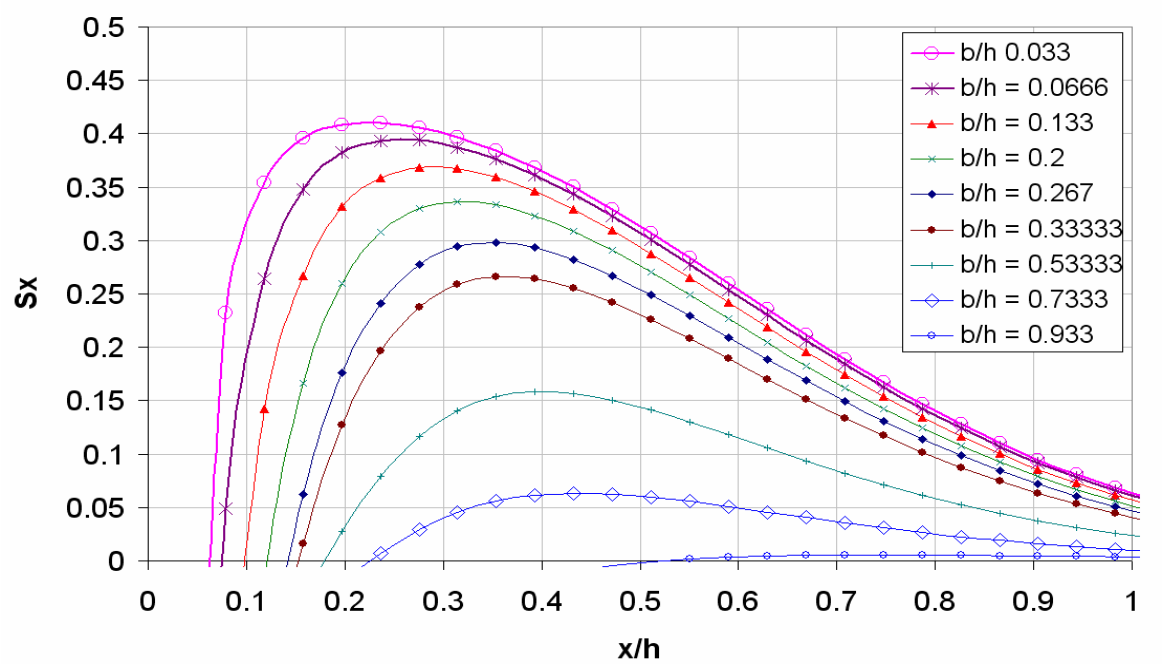

Figure 6-6: Maximum Tensile Stress, Sx, Versus x/h For 0.0% Fiber

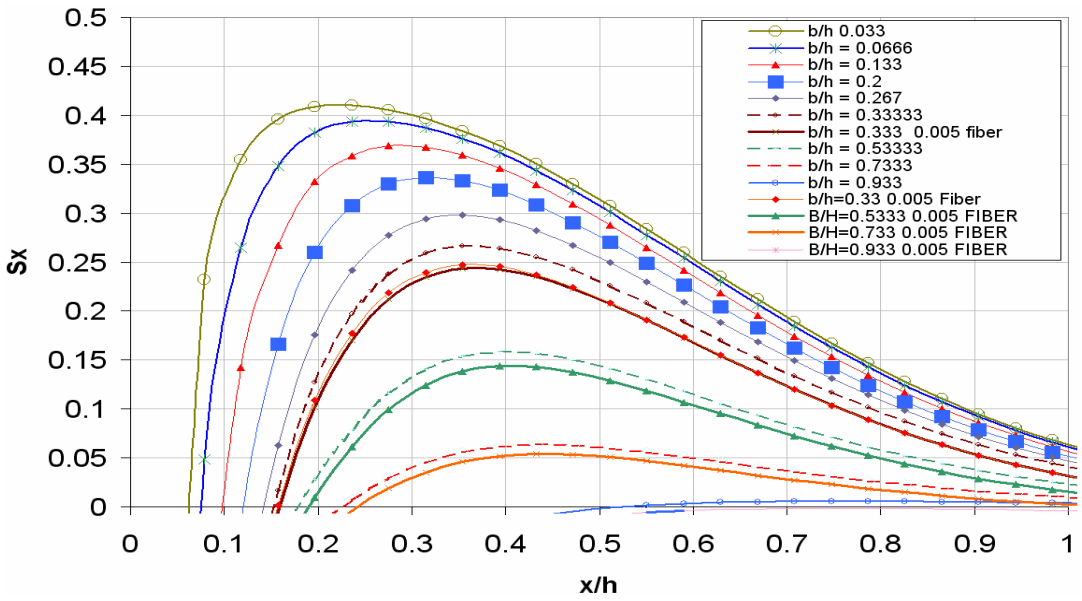

Figure 6-7 Maximum Tensile Stress, Sx Versus x/h For 0.5% Fiber

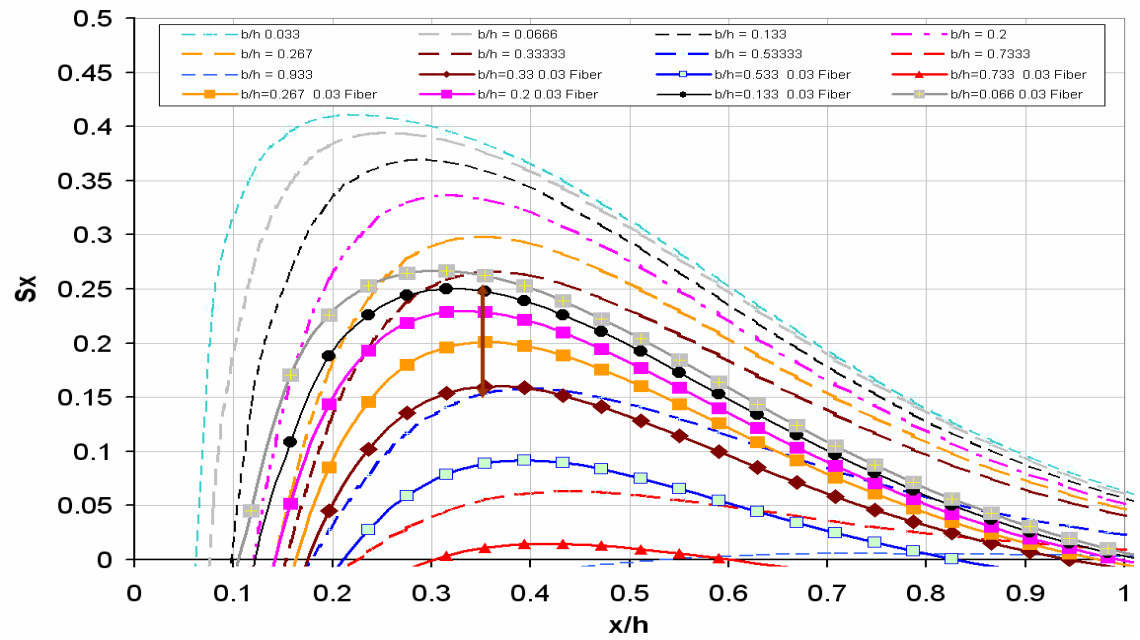

Figure 6-8: Maximum Tensile Stress, Sx, Versus x/h For 1.0% Fiber

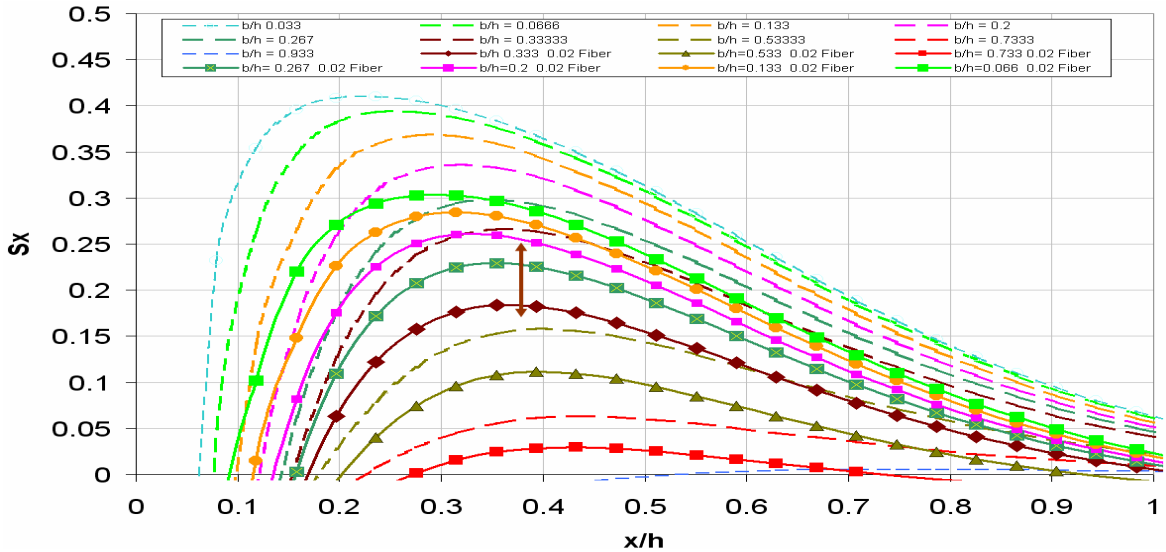

Figure 6-9: Maximum Tensile Stress, Sx, Versus x/h For 2.0% Fiber

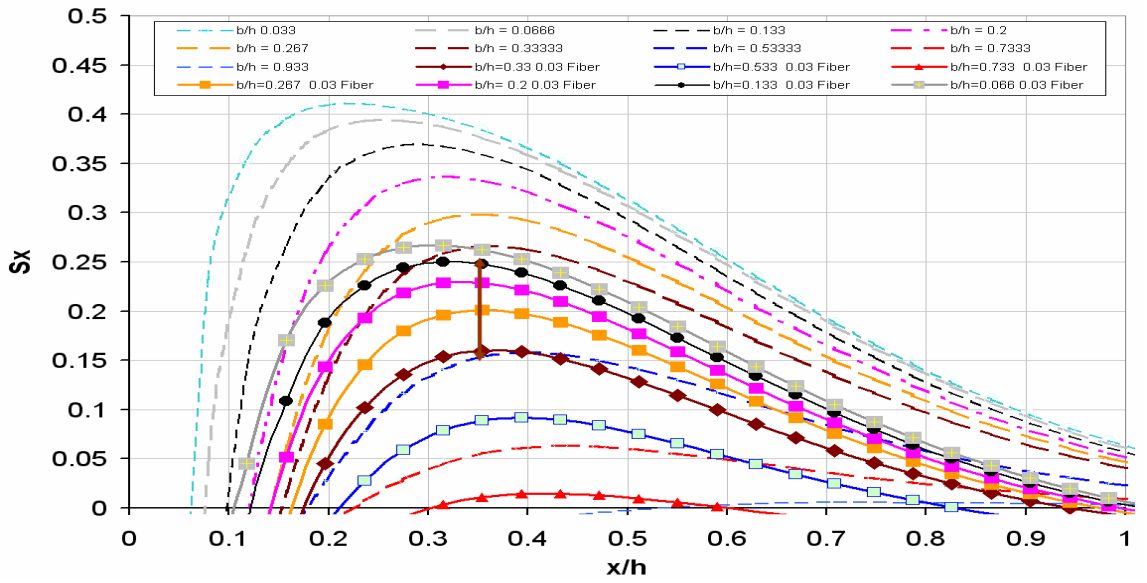

Figure 6-10: Maximum Tensile Stress, Sx, Versus x/h For 3.0% Fiber

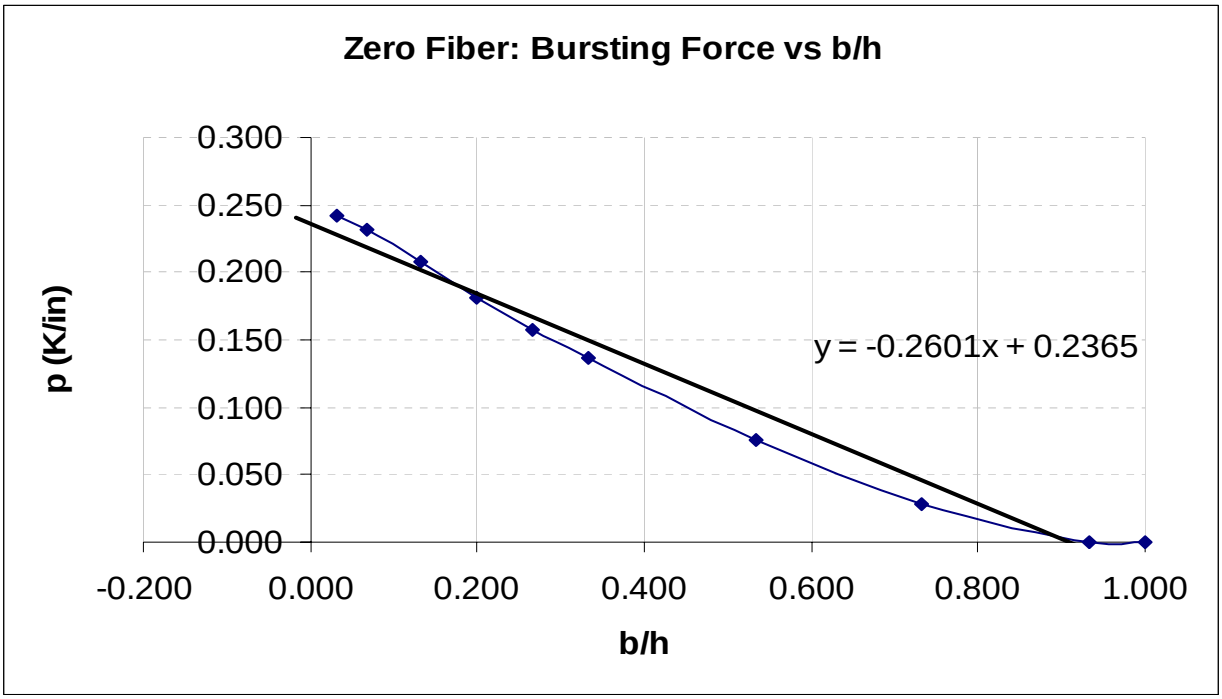

Figure 6-11: Zero Fiber Bursting Forces Versus b/h

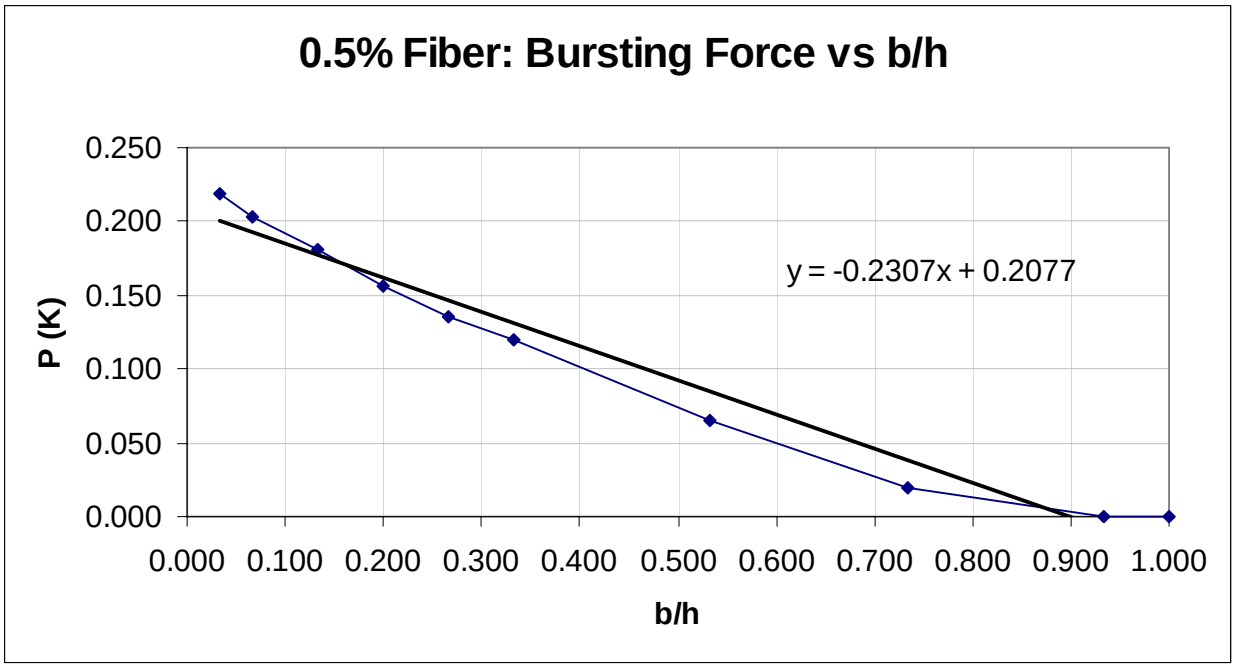

Figure 6-12: 0.5% Fiber Bursting Forces Versus b/h

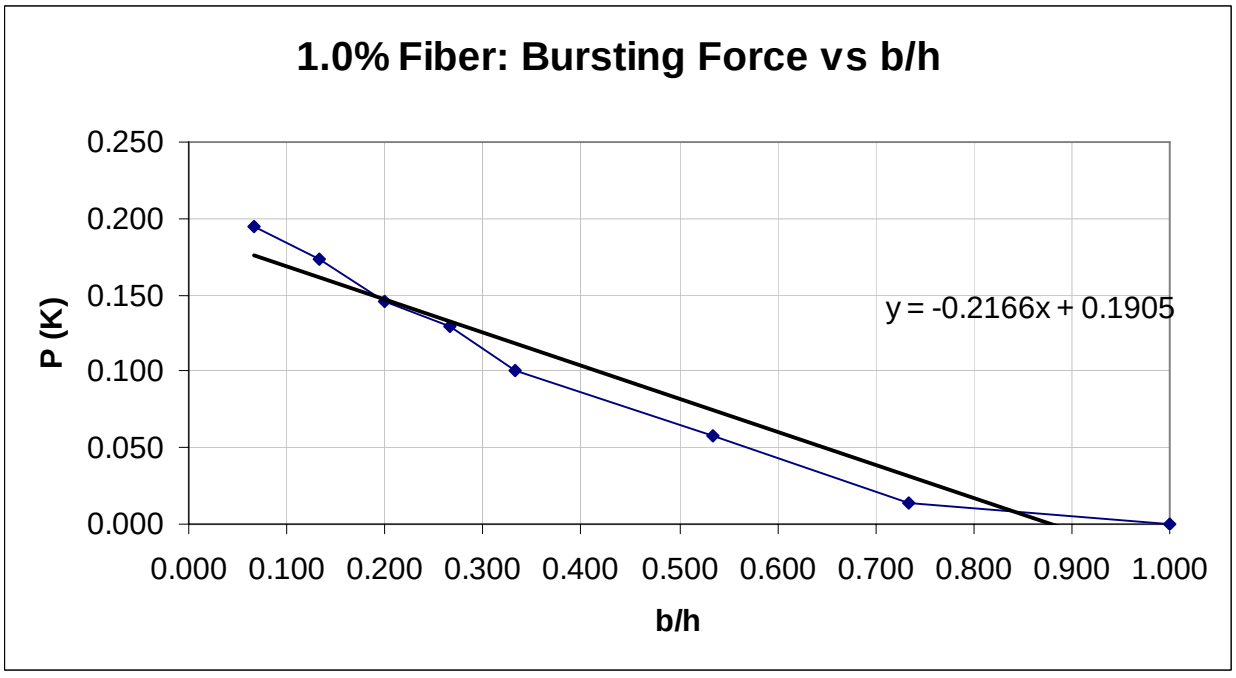

Figure 6-13: 1.0% Fiber Bursting Forces Versus b/h

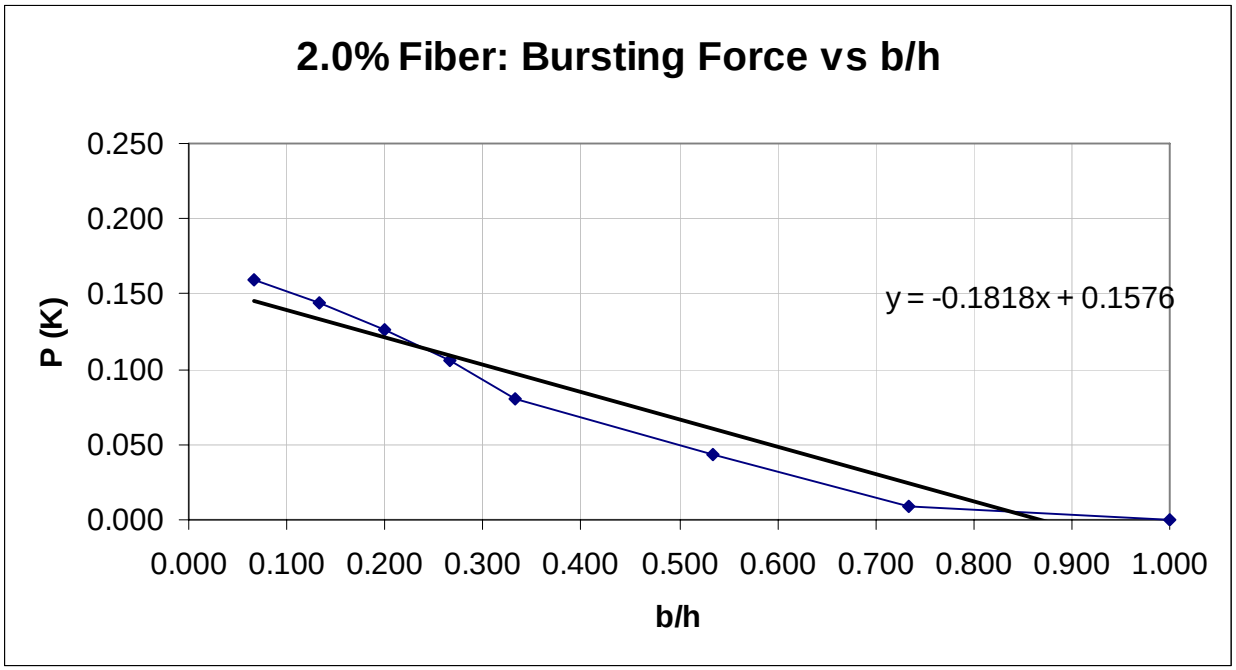

Figure 6-14: 2.0% Fiber Bursting Forces Versus b/h

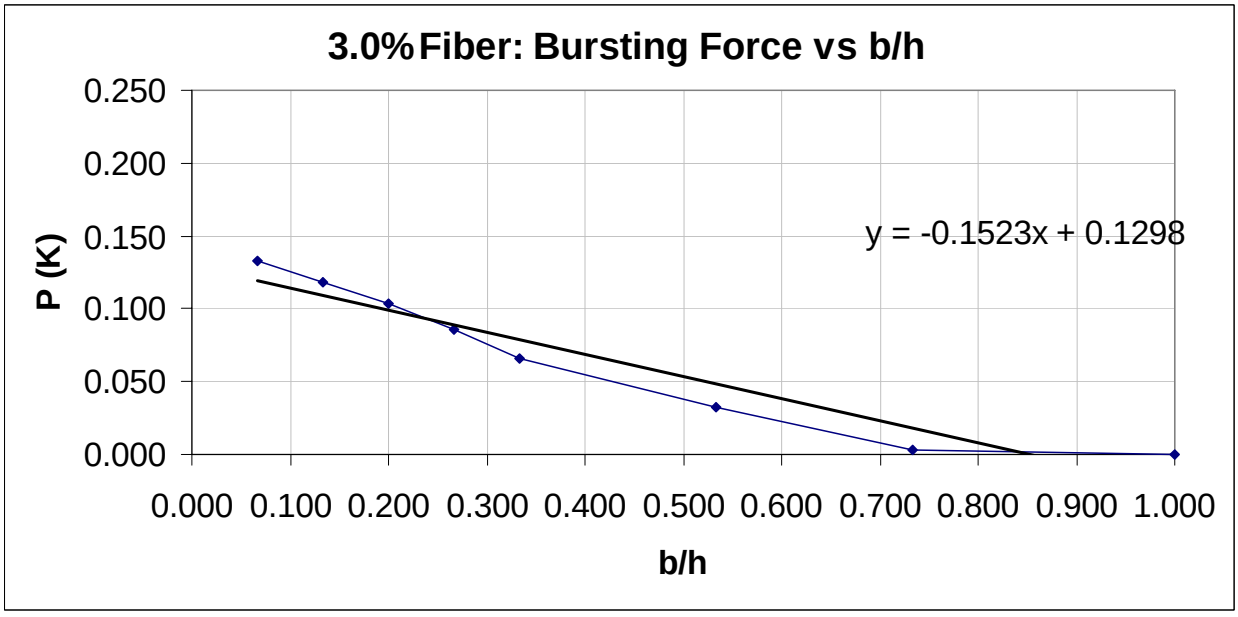

Figure 6-15: 3.0% Fiber Bursting Forces Versus b/h

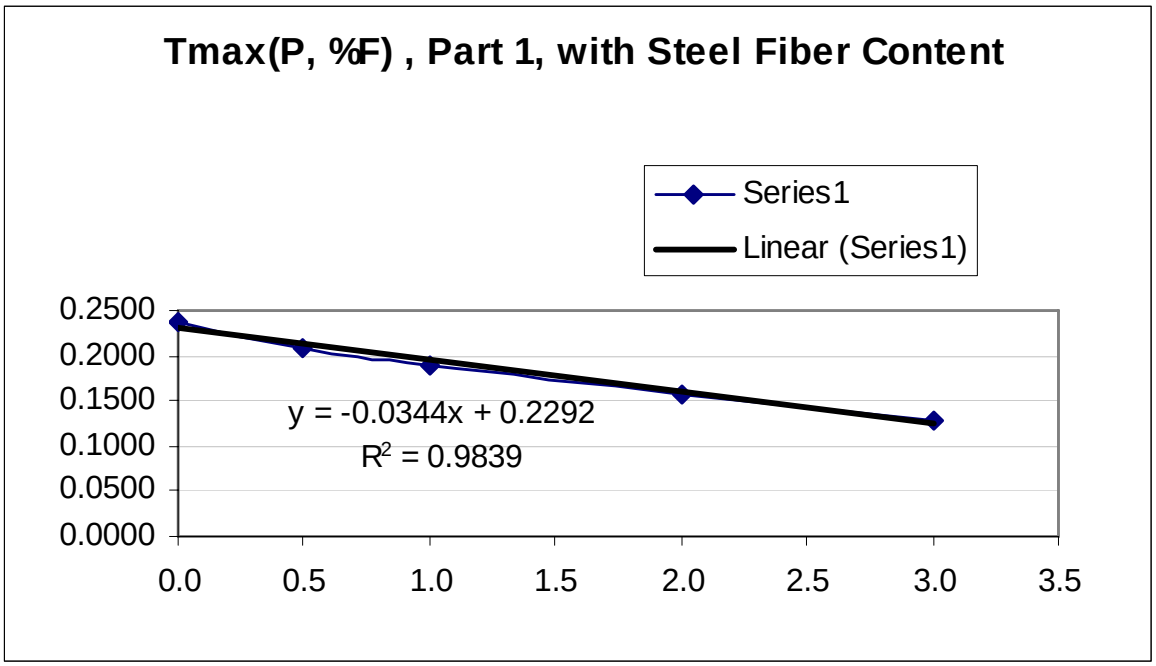

Figure 6-16: T_{max} (P), Part 1, Versus % Fiber

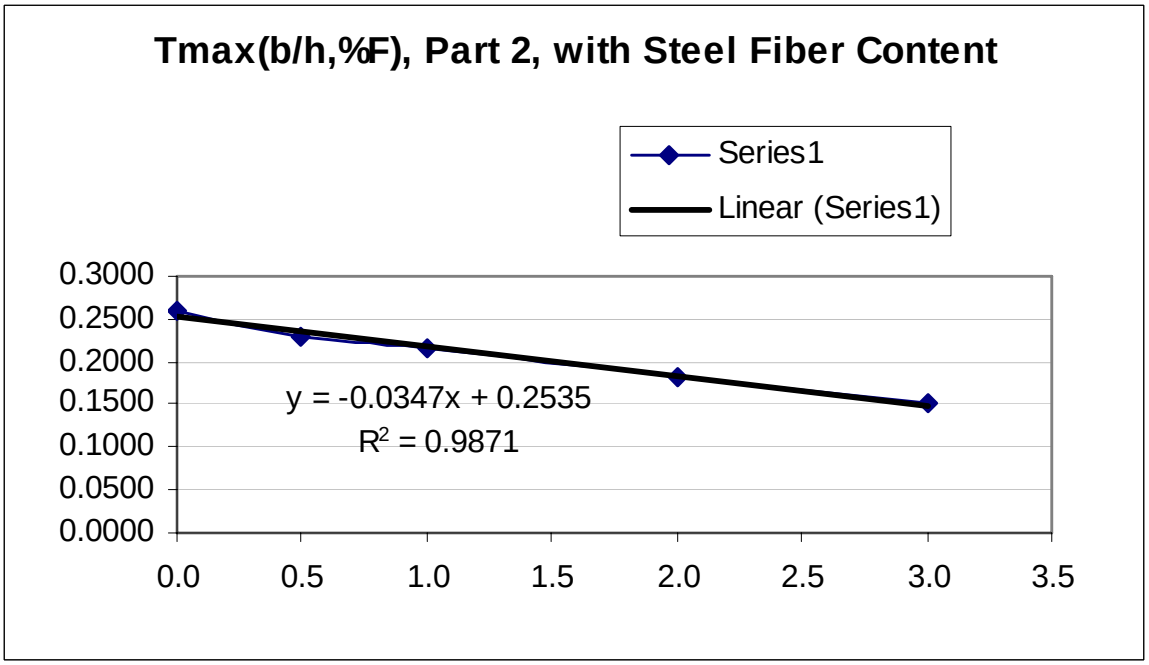

Figure 6-17: T_{max} (P, b/h), Part 2, vs. % Fiber

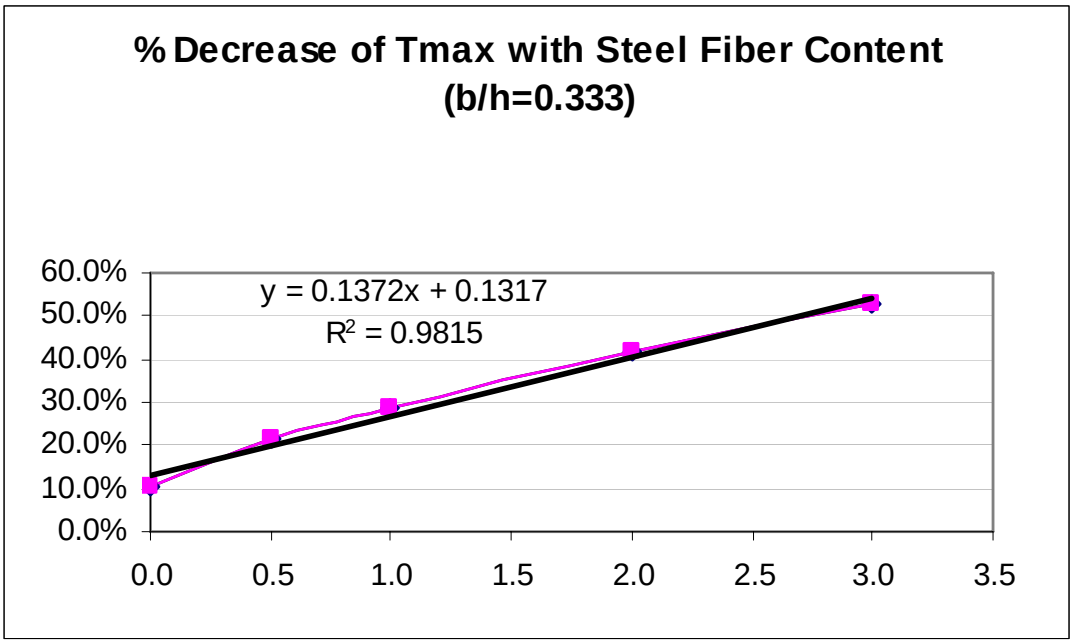

Figure 6-18: Percent Decrease of T_{max} with Steel Fiber Content

Next, considering the T_{max} equations obtained for each percentage of fiber, the equations were separated into two parts (Part 1 and Part 2). Plotting the coefficients versus fiber percentages for Part 1 and getting a best fit line for the curve to this part yields an equation relating T_{max} to the applied compressive load (tendon force, P) and the fiber percentage. Plotting the coefficients versus fiber percentages for Part 2 and obtaining the best fit line for the curve, yields an equation relating T_{max} to the b/h ratio and the fiber percentage. Then by adding the two equations for Part 1 and Part 2, an equation is obtained which relates T_{max} to the applied compressive force (P), the b/h ratio and the fiber percentage. The full equation (by adding Part 1 and Part 2), is as follows:

$$\mathbf{T_{max}=0.23\ P - 0.034\ P(\%F) - P\ (0.25)\ (b/h) + P(0.03)\ (b/h)(\%F)} \qquad \mathbf{6\text{-}1}$$

Using the equation determined for T_{max}, the T_{max} values can be computed and compared to both the AASHTO equation T_{max} and the T_{max} values computed by using the finite element results (Sx/h versus b/h plots). In Table 6.9, bursting force values are computed for b/h = 0.33 for fiber percentages ranging from 0.0% (no fiber) to 3.0%. Table 6-9 shows that the T_{max} values computed using the developed equation are on average 0.02% different from the values computed by determining the area under the curves of the Sx versus b/h plots for b/h = 0.333. The table also shows that by adding steel fibers in the concrete, the finite element results indicate that the maximum tensile force developed will be approximately 20% less for 0.5% fibers and approximately 54.3% less for 3.0% fibers.

By rounding the numbers in the equation to two decimal places, the equation proposed for computing the bursting force with consideration for both fiber percentage and b/h ratio becomes:

$$\mathbf{T_{max} = 0.23\ P\ [1\text{-}1.11(b/h)\text{-}0.15(b)+0.15(b/h)(F\%)]} \qquad \mathbf{6\text{-}2}$$

Table 6-10 shows T_{max} values computed by the proposed equation for various b/h ratios and fiber percentages. Table 6-10 and Table 6-11 show comparisons with the T_{max} values computed by the AASHTO equation and the new equation for various b/h ratios and two different equation coefficients (0.23 and 0.24). As shown by comparing the two tables, if a coefficient equal to 0.24 is used, the bursting forces calculated are more conservative and are almost always greater than the AASHTO values.

Table 6-8: Bursting Forces Comparison

	If Max b/h=1.0							
AASHTO:	A(P)(1-b/h) =	A(P)-(P)(B)(b/h)=			Tmax(P)		% AASHTO	% change in Tmax Decrease
FEM:	A(P)-B(P)(b/h) Assume P=1.0							
	% Fiber	A	B	b/h	Tmax	1/Tmax		
AASHTO	**0**	**0.25**	**0.25**	0.033	0.242	**4.1**	**100.0%**	0%
		0.25	**0.25**	0.067	0.233	**4.3**	**100.0%**	0%
		0.25	**0.25**	0.133	0.217	**4.6**	**100.0%**	0%
		0.25	**0.25**	0.200	0.200	**5.0**	**100.0%**	0%
		0.25	**0.25**	0.267	0.183	**5.5**	**100.0%**	0%
		0.25	**0.25**	0.333	0.167	**6.0**	**100.0%**	0%
		0.25	**0.25**	0.533	0.117	**8.6**	**100.0%**	0%
		0.25	**0.25**	0.733	0.067	**15.0**	**100.0%**	0%
FEM	0	0.2365	0.2601	0.033	0.228	**4.4**	**94.3%**	5.7%
		0.2365	0.2601	0.067	0.219	**4.6**	**93.9%**	6.1%
		0.2365	0.2601	0.133	0.202	**5.0**	**93.1%**	6.9%
		0.2365	0.2601	0.200	0.184	**5.4**	**92.2%**	7.8%
		0.2365	0.2601	0.267	0.167	**6.0**	**91.2%**	8.8%
		0.2365	0.2601	0.333	0.150	**6.7**	**89.9%**	10.1%
		0.2365	0.2601	0.533	0.098	**10.2**	**83.8%**	16.2%
		0.2365	0.2601	0.733	0.046	**21.8**	**68.6%**	31.4%
FEM	0.5	0.2077	0.2307	0.033	0.200	**5.0**	**82.8%**	17.2%
		0.2077	0.2307	0.067	0.192	**5.2**	**82.4%**	17.6%
		0.2077	0.2307	0.133	0.177	**5.7**	**81.7%**	18.3%
		0.2077	0.2307	0.200	0.162	**6.2**	**80.8%**	19.2%
		0.2077	0.2307	0.267	0.146	**6.8**	**79.7%**	20.3%
		0.2077	0.2307	0.333	0.131	**7.6**	**78.5%**	21.5%
		0.2077	0.2307	0.533	0.085	**11.8**	**72.6%**	27.4%
		0.2077	0.2307	0.733	0.039	**26.0**	**57.8%**	42.2%
FEM	1.0	0.1905	0.2166	0.033	0.183	**5.5**	**75.8%**	24.2%
		0.1905	0.2166	0.067	0.176	**5.7**	**75.5%**	24.5%
		0.1905	0.2166	0.133	0.162	**6.2**	**74.6%**	25.4%
		0.1905	0.2166	0.200	0.147	**6.8**	**73.6%**	26.4%
		0.1905	0.2166	0.267	0.133	**7.5**	**72.4%**	27.6%
		0.1905	0.2166	0.333	0.118	**8.5**	**71.0%**	29.0%
		0.1905	0.2166	0.533	0.075	**13.3**	**64.3%**	35.7%
		0.1905	0.2166	0.733	0.032	**31.6**	**47.5%**	52.5%
FEM	2.0	0.1576	0.1818	0.033	0.152	**6.6**	**62.7%**	37.3%
		0.1576	0.1818	0.067	0.145	**6.9**	**62.3%**	37.7%
		0.1576	0.1818	0.133	0.133	**7.5**	**61.6%**	38.4%
		0.1576	0.1818	0.200	0.121	**8.2**	**60.6%**	39.4%
		0.1576	0.1818	0.267	0.109	**9.2**	**59.5%**	40.5%
		0.1576	0.1818	0.333	0.097	**10.3**	**58.2%**	41.8%
		0.1576	0.1818	0.533	0.061	**16.5**	**52.0%**	48.0%
		0.1576	0.1818	0.733	0.024	**41.2**	**36.4%**	63.6%
FEM	3.0	0.1298	0.1532	0.033	0.125	**8.0**	**51.6%**	48.4%
		0.1298	0.1523	0.067	0.120	**8.4**	**51.3%**	48.7%
		0.1298	0.1523	0.133	0.109	**9.1**	**50.5%**	49.5%
		0.1298	0.1523	0.200	0.099	**10.1**	**49.7%**	50.3%
		0.1298	0.1523	0.267	0.089	**11.2**	**48.6%**	51.4%
		0.1298	0.1523	0.333	0.079	**12.7**	**47.4%**	52.6%
		0.1298	0.1523	0.533	0.049	**20.6**	**41.6%**	58.4%
		0.1298	0.1523	0.733	0.018	**55.2**	**27.2%**	72.8%

Table 6-9: T_{max} Comparison To AASHTO

	If Max b/h=1.0							
FEM	Tmax=	Part 1-Part 2						
FEM	Tmax=	0.2292P-0.0344P(%F) -P(0.2535(b/h)+P(0.0347(b/h)(%F)						
	Tmax=	0.2292P[1-1.1060(b/h)-0.1501(%F)+0.1514(b/h)(%F)]						
	Tmax	P	b/h	%F	%AASHTO	%Decease	%AASHTO	DIFF
					EQ		FEM	Q-S
AASHTO	0.167	1.0	0.3333	0.0	100.00%	0.00%	100.0%	0.00%
EQ	0.145	1.0	0.3333	0.0	86.82%	13.18%	89.9%	-3.06%
EQ	0.133	1.0	0.3333	0.5	79.97%	20.03%	78.5%	1.49%
EQ	0.122	1.0	0.3333	1.0	73.12%	26.88%	71.0%	2.14%
EQ	0.099	1.0	0.3333	2.0	59.42%	40.58%	58.2%	1.22%
EQ	0.076	1.0	0.3333	3.0	45.72%	54.28%	47.4%	-1.70%
							AVERAGE	0.02%
	Tmax=	0.23P[1-1.11(b/h)-0.15(%F)+0.15(b/h)(%F)]						
							FEM	DIFF
AASHTO	0.167	1.0	0.3333	0.0	100.00%	0.00%	100.0%	0.00%
EQ	0.145	1.0	0.3333	0.0	86.94%	13.06%	89.9%	-2.94%
EQ	0.133	1.0	0.3333	0.5	80.04%	19.96%	78.5%	1.56%
EQ	0.122	1.0	0.3333	1.0	73.14%	26.86%	71.0%	2.16%
EQ	0.099	1.0	0.3333	2.0	59.34%	40.66%	58.2%	1.14%
EQ	0.076	1.0	0.3333	3.0	45.54%	54.46%	47.4%	-1.88%
							AVERAGE	0.01%
	Tmax=	0.24P[1-1.11(b/h)-0.15(%F)+0.15(b/h)(%F)]						
							FEM	DIFF
AASHTO	0.167	1.0	0.3333	0.0	100.00%	0.00%	100.0%	0.00%
EQ	0.151	1.0	0.3333	0.0	90.72%	9.28%	89.9%	0.84%
EQ	0.139	1.0	0.3333	0.5	83.52%	16.48%	78.5%	5.04%
EQ	0.127	1.0	0.3333	1.0	76.32%	23.68%	71.0%	5.34%
EQ	0.103	1.0	0.3333	2.0	61.92%	38.08%	58.2%	3.72%
EQ	0.079	1.0	0.3333	3.0	47.52%	52.48%	47.4%	0.10%
							AVERAGE	2.51%

Table 6-10: T_{max} Considering 0.23 Factor

	Tmax=	0.23P[1-1.11(b/h)-0.15(%F)+0.15(b/h)(%F)]						
	Tmax	P	b/h	%F	%AASHTO	%Decease	%AASHTO	DIFF
					EQ	EQ	FEM	EQ-FEM
AASHTO	0.1667	1.0	0.3333	0.0	**100.00%**	0.00%	100.0%	0.00%
EQ	0.1449	1.0	0.3333	0.0	**86.94%**	13.06%	89.9%	-2.94%
EQ	0.1334	1.0	0.3333	0.5	**80.04%**	19.96%	78.5%	1.56%
EQ	0.1219	1.0	0.3333	1.0	**73.14%**	26.86%	71.0%	2.16%
EQ	0.0989	1.0	0.3333	2.0	**59.34%**	40.66%	58.2%	1.14%
EQ	0.0759	1.0	0.3333	3.0	**45.54%**	54.46%	47.4%	-1.88%
EQ	0.2216	1.0	0.033	0	**91.7%**	8.35%	94.3%	-2.62%
EQ	0.2130	1.0	0.067	0	**91.3%**	8.72%	93.9%	-2.65%
EQ	0.1960	1.0	0.133	0	**90.4%**	9.56%	93.1%	-2.70%
EQ	0.1789	1.0	0.200	0	**89.5%**	10.53%	92.2%	-2.77%
EQ	0.1618	1.0	0.267	0	**88.3%**	11.69%	91.2%	-2.85%
EQ	0.1449	1.0	0.333	0	**86.9%**	13.06%	89.9%	-2.94%
EQ	0.0939	1.0	0.533	0	**80.4%**	19.55%	83.8%	-3.38%
EQ	0.0428	1.0	0.733	0	**64.2%**	35.83%	68.6%	-4.47%
EQ	0.2049	1.0	0.033	0.5	**84.8%**	15.25%	82.8%	1.99%
EQ	0.1969	1.0	0.067	0.5	**84.4%**	15.62%	82.4%	1.95%
EQ	0.1810	1.0	0.133	0.5	**83.5%**	16.46%	81.7%	1.88%
EQ	0.1651	1.0	0.200	0.5	**82.6%**	17.43%	80.8%	1.79%
EQ	0.1492	1.0	0.267	0.5	**81.4%**	18.59%	79.7%	1.68%
EQ	0.1334	1.0	0.333	0.5	**80.0%**	19.96%	78.5%	1.56%
EQ	0.0859	1.0	0.533	0.5	**73.5%**	26.45%	72.6%	0.97%
EQ	0.0382	1.0	0.733	0.5	**57.3%**	42.73%	57.8%	-0.51%
EQ	0.1882	1.0	0.033	1.0	**77.9%**	22.15%	75.8%	2.01%
EQ	0.1808	1.0	0.067	1.0	**77.5%**	22.52%	75.5%	2.02%
EQ	0.1661	1.0	0.133	1.0	**76.6%**	23.36%	74.6%	2.05%
EQ	0.1513	1.0	0.200	1.0	**75.7%**	24.33%	73.6%	2.08%
EQ	0.1365	1.0	0.267	1.0	**74.5%**	25.49%	72.4%	2.12%
EQ	0.1219	1.0	0.333	1.0	**73.1%**	26.86%	71.0%	2.16%
EQ	0.0778	1.0	0.533	1.0	**66.6%**	33.35%	64.3%	2.37%
EQ	0.0336	1.0	0.733	1.0	**50.4%**	49.63%	47.5%	2.88%
EQ	0.1549	1.0	0.033	2.0	**64.1%**	35.95%	62.7%	1.34%
EQ	0.1486	1.0	0.067	2.0	**63.7%**	36.32%	62.3%	1.33%
EQ	0.1362	1.0	0.133	2.0	**62.8%**	37.16%	61.6%	1.29%
EQ	0.1237	1.0	0.200	2.0	**61.9%**	38.13%	60.6%	1.25%
EQ	0.1113	1.0	0.267	2.0	**60.7%**	39.29%	59.5%	1.20%
EQ	0.0989	1.0	0.333	2.0	**59.3%**	40.66%	58.2%	1.14%
EQ	0.0617	1.0	0.533	2.0	**52.8%**	47.15%	52.0%	0.86%
EQ	0.0244	1.0	0.733	2.0	**36.6%**	63.43%	36.4%	0.15%
EQ	0.1215	1.0	0.033	3.0	**50.3%**	49.75%	51.6%	-1.35%
EQ	0.1164	1.0	0.067	3.0	**49.9%**	50.12%	51.3%	-1.40%
EQ	0.1063	1.0	0.133	3.0	**49.0%**	50.96%	50.5%	-1.49%
EQ	0.0961	1.0	0.200	3.0	**48.1%**	51.93%	49.7%	-1.60%
EQ	0.0860	1.0	0.267	3.0	**46.9%**	53.09%	48.6%	-1.73%
EQ	0.0759	1.0	0.333	3.0	**45.5%**	54.46%	47.4%	-1.88%
EQ	0.0456	1.0	0.533	3.0	**39.0%**	60.95%	41.6%	-2.60%
EQ	0.0152	1.0	0.733	3.0	**22.8%**	77.23%	27.2%	-4.40%
							Average Diff	-0.07%

Table 6-11: T_{max} Considering 0.24 Factor

	Tmax=	0.24P[1-1.11(b/h)-0.15(%F)+0.15(b/h)(%F)]						
	Tmax	P	b/h	%F	%AASHTO	%Decease	%AASHTO	DIFF
					EQ	EQ	FEM	EQ-FEM
AASHTO	0.1667	1.0	0.3333	0.0	**100.00%**	0.00%	100.0%	0.00%
EQ	0.1512	1.0	0.3333	0.0	**90.72%**	9.28%	89.9%	0.84%
EQ	0.1392	1.0	0.3333	0.5	**83.52%**	16.48%	78.5%	5.04%
EQ	0.1272	1.0	0.3333	1.0	**76.32%**	23.68%	71.0%	5.34%
EQ	0.1032	1.0	0.3333	2.0	**61.92%**	38.08%	58.2%	3.72%
EQ	0.0792	1.0	0.3333	3.0	**47.52%**	52.48%	47.4%	0.10%
EQ	0.2312	1.0	0.033	0	**95.6%**	4.36%	94.3%	1.36%
EQ	0.2223	1.0	0.067	0	**95.2%**	4.75%	93.9%	1.32%
EQ	0.2045	1.0	0.133	0	**94.4%**	5.62%	93.1%	1.23%
EQ	0.1867	1.0	0.200	0	**93.4%**	6.64%	92.2%	1.12%
EQ	0.1689	1.0	0.267	0	**92.2%**	7.85%	91.2%	0.99%
EQ	0.1512	1.0	0.333	0	**90.7%**	9.28%	89.9%	0.84%
EQ	0.0980	1.0	0.533	0	**83.9%**	16.05%	83.8%	0.12%
EQ	0.0446	1.0	0.733	0	**67.0%**	33.04%	68.6%	-1.68%
EQ	0.2138	1.0	0.033	0.5	**88.4%**	11.56%	82.8%	5.67%
EQ	0.2055	1.0	0.067	0.5	**88.0%**	11.95%	82.4%	5.62%
EQ	0.1889	1.0	0.133	0.5	**87.2%**	12.82%	81.7%	5.51%
EQ	0.1723	1.0	0.200	0.5	**86.2%**	13.84%	80.8%	5.38%
EQ	0.1557	1.0	0.267	0.5	**85.0%**	15.05%	79.7%	5.22%
EQ	0.1392	1.0	0.333	0.5	**83.5%**	16.48%	78.5%	5.04%
EQ	0.0896	1.0	0.533	0.5	**76.7%**	23.25%	72.6%	4.17%
EQ	0.0398	1.0	0.733	0.5	**59.8%**	40.24%	57.8%	1.98%
EQ	0.1964	1.0	0.033	1.0	**81.2%**	18.76%	75.8%	5.40%
EQ	0.1887	1.0	0.067	1.0	**80.8%**	19.15%	75.5%	5.39%
EQ	0.1733	1.0	0.133	1.0	**80.0%**	20.02%	74.6%	5.38%
EQ	0.1579	1.0	0.200	1.0	**79.0%**	21.04%	73.6%	5.37%
EQ	0.1425	1.0	0.267	1.0	**77.8%**	22.25%	72.4%	5.36%
EQ	0.1272	1.0	0.333	1.0	**76.3%**	23.68%	71.0%	5.34%
EQ	0.0812	1.0	0.533	1.0	**69.5%**	30.45%	64.3%	5.26%
EQ	0.0350	1.0	0.733	1.0	**52.6%**	47.44%	47.5%	5.07%
EQ	0.1616	1.0	0.033	2.0	**66.8%**	33.16%	62.7%	4.13%
EQ	0.1551	1.0	0.067	2.0	**66.4%**	33.55%	62.3%	4.10%
EQ	0.1421	1.0	0.133	2.0	**65.6%**	34.42%	61.6%	4.02%
EQ	0.1291	1.0	0.200	2.0	**64.6%**	35.44%	60.6%	3.94%
EQ	0.1161	1.0	0.267	2.0	**63.4%**	36.65%	59.5%	3.84%
EQ	0.1032	1.0	0.333	2.0	**61.9%**	38.08%	58.2%	3.72%
EQ	0.0644	1.0	0.533	2.0	**55.1%**	44.85%	52.0%	3.16%
EQ	0.0254	1.0	0.733	2.0	**38.2%**	61.84%	36.4%	1.74%
EQ	0.1268	1.0	0.033	3.0	**52.4%**	47.56%	51.6%	0.84%
EQ	0.1215	1.0	0.067	3.0	**52.0%**	47.95%	51.3%	0.77%
EQ	0.1109	1.0	0.133	3.0	**51.2%**	48.82%	50.5%	0.64%
EQ	0.1003	1.0	0.200	3.0	**50.2%**	49.84%	49.7%	0.49%
EQ	0.0897	1.0	0.267	3.0	**49.0%**	51.05%	48.6%	0.31%
EQ	0.0792	1.0	0.333	3.0	**47.5%**	52.48%	47.4%	0.10%
EQ	0.0476	1.0	0.533	3.0	**40.7%**	59.25%	41.6%	-0.90%
EQ	0.0158	1.0	0.733	3.0	**23.8%**	76.24%	27.2%	-3.41%
							Average Diff	2.80%

6.5 Comparison of Test Results and Empirical Analysis

Table 6-12 compares the tension forces computed by the strut-and-tie method to the T_{burst} from the AASHTO equation and tension forces that are computed by the new equation proposed as a result of the finite element analysis. The strut-and-tie maximum tensile forces (the bursting forces) are 70% to 73% of the maximum values computed by the AASHTO equation for T_{burst} for the long side (a/h=0.22) of the anchorage Specimens.

6.6 Comparison of Finite Element Analysis and Empirical Analysis

From Table 6-12, the maximum tensile forces (the bursting forces) resulting from use of the new equation based upon the finite element results are 82% of the maximum values computed from the AASHTO equation for T_{burst} for all Specimen S1 load cases. For specimen S2 load cases, the maximum tensile forces (the bursting forces) resulting from use of the new equation based upon the finite element results are 84% of the maximum values computed from the AASHTO equation for T_{burst}. Thus, relative to the AASHTO equation values, the bursting forces which result for using the new equation are 16% to 18% lower. This suggests that due to the use of 0.5% fiber in the post-tensioned anchorage zone, it may be possible to provide 16% to 18% less bursting reinforcement (tension ties) than was required by the AASHTO code for the test specimens or anchorage zones with similar b/h ratios.

Table 6-12 Strut-And-Tie, AASHTO Equation, And New Equation Comparison

Specimen	Specimen ID	Load Test Results			Strut and Tie	AASHTO		NEW EQUATION		COMPARISONS				
		Total Load (K)	West Actuator P2 (K)	East Actuator P1 (K)	Tburst Tie Total (Kips) Long TL1 Load Test	Tburst Tie Total (Kips) Short TS1 Load Test	AASHTO Tburst2 Long a/h=0.22 TL2 Empirical	AASHTO Tburst1 Short a/h=0.33 TS2 Empirical	New Equation Long a/h=0.22 TL3 FEM	New Equation Short a/h=0.33 TS3 FEM	New Equation Long a/h=0.44	SNTI AASHTO LONG TI/TL2	SNTI NEW LONG TI/TL3	SNTI AASHTO SHORT TS/TS2	SNTI NEW SHORT TS/TS3	NEW/ AASHTO LONG TL3/TL2	NEW/ AASHTO SHORT TS3/TS2
	S1 Specimens																
1	S1-1	628	315	313	87	67	122	105	101	84	68	0.71	0.86	0.64	0.80	0.82	0.80
2	S1-2	794	389	405	109	85	155	132	127	106	86	0.70	0.85	0.64	0.80	0.82	0.80
3	S1-3	866	429	437	119	93	169	144	139	115	93	0.71	0.86	0.64	0.80	0.82	0.80
4	S1-4	999	500	499	138	107	195	167	160	133	108	0.71	0.86	0.64	0.80	0.82	0.80
5	S1-5	1000	503	498	138	107	195	167	160	133	108	0.71	0.86	0.64	0.80	0.82	0.80
6	S1-6	600	294	306	82	64	117	100	96	80	65	0.70	0.85	0.64	0.80	0.82	0.80
7	S1-7	677	338	339	93	73	132	113	109	90	73	0.71	0.86	0.64	0.80	0.82	0.80
8	S1-8	917	460	456	127	98	179	153	147	122	99	0.71	0.86	0.64	0.80	0.82	0.80
9	S1-9	869	436	433	120	93	169	145	139	116	94	0.71	0.86	0.64	0.80	0.82	0.80
10	S1-10	839	417	422	116	90	163	140	134	112	91	0.71	0.86	0.64	0.80	0.82	0.80
11	S1-11	706	352	354	97	76	138	118	113	94	76	0.71	0.86	0.64	0.80	0.82	0.80
12	S1-13	733	365	367	101	78	143	122	117	98	79	0.71	0.86	0.64	0.80	0.82	0.80
13	S1-14	996	496	499	137	107	194	166	160	133	108	0.71	0.86	0.64	0.80	0.82	0.80
	S2 Specimens																
14	S2-1	723	366	357	100	77	138	116	116	96	78	0.73	0.87	0.67	0.80	0.84	0.83
15	S2-2	557	278	279	77	60	106	89	89	74	60	0.72	0.86	0.67	0.80	0.84	0.83
16	S2-3	628	318	310	87	67	120	101	101	84	68	0.73	0.87	0.67	0.80	0.84	0.83
17	S2-4	674	333	341	93	72	129	108	108	90	73	0.72	0.86	0.67	0.80	0.84	0.83
18	S2-5	666	323	342	91	71	127	107	107	89	72	0.72	0.85	0.67	0.80	0.84	0.83
19	S2-6	568	288	280	79	61	108	91	91	76	61	0.73	0.87	0.67	0.80	0.84	0.83
20	S2-7	691	347	344	96	74	132	111	111	92	75	0.73	0.86	0.67	0.80	0.84	0.83
21	S2-8	748	372	376	103	80	143	120	120	100	81	0.72	0.86	0.67	0.80	0.84	0.83
22	S2-9	753	370	382	103	81	144	121	121	100	81	0.72	0.86	0.67	0.80	0.84	0.83
23	S2-10	654	328	326	90	70	125	105	105	87	71	0.72	0.86	0.67	0.80	0.84	0.83
24	S2-11	570	285	284	79	61	109	91	91	76	62	0.72	0.86	0.67	0.80	0.84	0.83
25	S2-12	750	375	375	104	80	143	120	120	100	81	0.72	0.86	0.67	0.80	0.84	0.83
26	S2-13	753	370	382	103	81	144	121	121	100	81	0.72	0.86	0.67	0.80	0.84	0.83
27	S1-14	646	326	319	90	69	123	103	104	86	70	0.73	0.86	0.67	0.80	0.84	0.83

6.7 Cost Comparison for Reinforced Concrete and Fiber Reinforced Concrete

In an effort to estimate whether the addition of steel fibers to post-tensioned anchorage zones of bridge segment will result in a significant cost change, the authors solicited information from the Florida Department of Transportation's Construction Estimates Section and several prestressed concrete manufacturers. In addition, the authors used material cost data and construction drawings from two bridge projects completed in Florida to consider cost effects. The results of these cost considerations are discussed in this chapter.

Only one concrete products manufacturer provided information as requested. Pomeroy Corporation supplied the cost information by considering the Manteca Box Girder project. This project consisted of 20-3' W xs3'7" H x 100' L box girders. Each box segment was approximately 24 CY of concrete. The following cost data is based upon using Novomesh 850 at a cost of $0.74 per lb and a dosage rate of 66 lb of per CY of concrete (0.5% fiber by volume): if the amount of black rebar is reduced by 50%, the cost of steel is reduced by 15% relative to the total materials costs. The concrete cost increases by 55% and is a 12.41% increase relative to total material costs. The labor cost is reduced by 12 to 20%. The total cost of materials decreases by 5.9%. The retail price decreases by 8%. These cost changes were dependent upon material costs prevailing in Summer 2007.

A representative of Unistress Corporation did not have any cost data to share but did speculate that adding fibers would result in an increase in costs due to the alteration in batching procedure. One steel fiber manufacturer did not readily supply material costs. A representative of another

fiber retailer suggested that adding steel fibers at the dosage rate 66 lb per cubic yard (0.5% fiber by volume) could result in a material costs increase of approximately $75.00 per cubic yard of concrete. A sales representative for Novomesh 850, stated that a 24 lb bag of the steel and polypropylene fiber blend costs approximately $20.00/ bag. So for 66 lbs per cubic yard, the cost of fibers would be approximately $60.00 plus tax. A representative of The Florida Department of Transportation's Estimating Section did supply cost data from a recent construction project, State Road No. 9 (I-95)/ SR9A (I-295) North Interchange. This project is located in Jacksonville, Florida.

Using the information obtained, the authors concluded that the addition of steel fibers to concrete and a 40% reduction of non-prestressed steel in the post-tensioned anchorage zone of bridge segment will not result in a significant change in the costs of bridge segments for a precast segmental superstructure. Based upon the calculations and cost considerations used only a 0.44% cost savings would result. However, a 40% reduction in non-prestressed reinforcement may not be feasible with other design requirements. For a reduction in steel of 36% or less, the use of fibers would result in an increase in material and labor costs based upon the cost assumptions made. The information considered to reach this conclusion is summarized in Table 6-13.

Table 6-13: Construction Cost Estimates For Precast Segmental Superstructure

Table 10.1: Construction Cost Estimates For Precast Segmental Superstructure With and Without Steel Fiber Reinforcement Sample Bridge Project: SR 9/SR9A Let in April 2007					
Item #	Item	Units	Quantity	Average Unit Price	Extended Price
	Without Steel Fibers:				
1	Concrete: Class V, Precast Segmental Superstructure	CY	7830.2	$1,324.50	$10,371,099.90
2	Steel: Reinforcing Steel-Superstructure	LB	1367927	$0.85	$1,162,737.95
3	Reinforcing Steel Labor Costs	LB	1367927	$0.32	$437,736.64
				Cost	$11,971,574.49
	With Steel Fibers & 40% Less Reinforcing Steel :				
1	Concrete: Class V, Precast Segmental Superstructure	CY	7830.2	$1,324.50	$10,371,099.90
2	Steel: Reinforcing Steel-Superstructure	LB	820756.2	$0.85	$697,642.77
3	Reinforcing Steel Labor Costs	LB	820756.2	$0.32	$262,641.98
4	Steel Fibers	CY	7830.2	$75.00	$587,265.00
				Cost	$11,918,649.65
				Cost Decrease	$52,924.84
				% Savings	0.44%
	With Steel Fibers & 36% Less Reinforcing Steel :				
1	Concrete: Class V, Precast Segmental Superstructure	CY	7830.2	$1,324.50	$10,371,099.90
2	Steel: Reinforcing Steel-Superstructure	LB	875473.28	$0.85	$744,152.29
3	Reinforcing Steel Labor Costs	LB	875473.28	$0.32	$280,151.45
4	Steel Fibers	CY	7830.2	$75.00	$587,265.00
				Cost	$11,982,668.64
				Cost Increase	-$11,094.15
				% Increase	-0.09%

Considering a 50% reduction in steel and the addition of 66 lb/CY of Novomesh fiber, Pomeroy Corporation estimated an 8% reduction in retail costs. Based upon a 40% reduction in steel, the author has estimated less than a 1% reduction in cost. Thus, it is possible that steel fibers can be added to post-tensioning anchorage zones without altering the costs of construction significantly. However, in addition to considering material and labor direct costs, a potential cost savings may be associated with time saving associated with installing less steel reinforcement. For instance, if the labor productivity rate for installing rebar (size no. 6 and larger) is 800-1000 lbs of steel per 8 hour day, then installing 40% less steel would save approximately 4377 to 5471 man hours.

6.7.1 Cost Comparison for Reinforced Concrete and Fiber Reinforced Concrete

As stated above it is possible to presume that reducing the amount of steel congestion in post-tensioning anchorage zone may have beneficial effects related to construction costs. When less steel exists in the post-tensioning anchorage zone, the potential is reduced for construction delays related to steel congestion. This could lead to significant dollar savings by the avoidance of construction delays and associated construction claims. Figure 6-19 and Figure 6-20 show examples of steel congestion in bridge segments.

Figure 6-19: Steel Congestion in Post-Tensioning Anchorage Zone

Figure 6-20: Close-up View of Steel Congestion in Post-Tensioning Anchorage Zone

Delays and associated costs that occurred on the Roosevelt Bridge project in Florida is one example of major construction costs related to steel congestion, construction delays and construction claims. The Roosevelt Bridge project was a high profile project constructed in

Stuart, Florida in the mid-1990. The project included the integral pier being cast integrally with box girder pier segments. Post-tensioned anchorage zones existed in the pier segments. Figure 6-21 shows a constructed pier segment. In Figure 6-22 a close-up picture of the top of pier rebar shows rebar spacing problems which occurred due to fabrication and construction tolerances.

Figure 6-21: Pier Segment of the Roosevelt Bridge

Figure 6-22: Roosevelt Bridge Pier Segment Reinforcing Steel with Fabrication Issues

Due to the design of the pier segment reinforcement and related construction tolerances, the contractor was unable to properly construct the integral pier. The vertical steel in the pier segment was difficult to fit into the forms and conflicted with the location of the longitudinal post-tensioning ducts in the bottom flange of the box girder. A section drawing of the fixed pier which shows the longitudinal ducts in the bottom flange is shown in Figure 6-23.

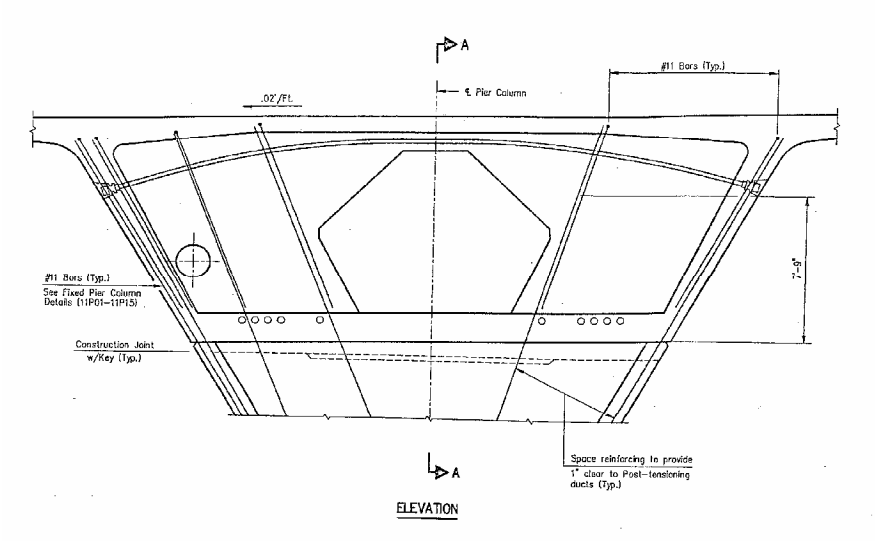

Figure 6-23: Cross-Section of Roosevelt Bridge Pier Segment

Since construction of the integral piers was on the critical path for the project, the difficulty with the rebar leads to work stoppage and construction delays. The solution to the problems involved bending the pier bars around a pin to reduce construction tolerances and improved rebar spacing. Figure 6-24 shows a cage of rebar that is being lifted in place in the pier form. As is visible in this photograph, the spacing of the pier rebar at the top is improved.

Figure 6-24: Reinforcing Steel Cage for A Pier Segment of the Roosevelt Bridge

It has been estimated that the total time delay on the Roosevelt Bridge project related to recognizing the problem, addressing the problem and making construction modifications to eliminate the problem was approximately six (6) months.

In the final analysis, the cost associated with the penalty for delay (approximately $20,000/day) and the payment for accelerating the project to get back on schedule resulted in a construction claim being paid to the contractor in the amount of approximately 6 to 7 million dollars. This was a major cost which was related to steel congestion and fabrication.

Avoiding such high expenditures due to construction problem will be beneficial to the Florida Department of Transportation. Thus, if the use of steel fiber reinforced concrete (SFRC) in the post-tensioned anchorage zones can reduce steel congestion in these zones, using SFRC may be very beneficial to the FDOT.

Source: Interview of Tom Andres, FDOT Structures Engineer, on March 28, 2008, Tallahassee, Florida.

CHAPTER 7

CONCLUSIONS AND RECOMMENDATIONS

7.1 Conclusions

An examination of the material test data and the finite element analysis revealed that using greater than 0.5% fiber by volume does not assure an increase in the average compressive strength of the concrete. For both Dramix and Novomesh fibers, the concrete with 1.0% fiber had lower average compressive strengths than the concrete with 0.5% fibers and the concrete with 0.75% fibers had approximately the same compressive strength as the concrete with 0.5% fibers. Just as was the case for the compressive strengths tests, the split tensile strength test results showed that using fiber percentages greater than 0.5% by volume did not guarantee higher tensile strengths. These results were based upon material tests on 6”x12” concrete cylinders.

Based upon the seven (7) batches cast with Helix, the following observations were made:

- If the concrete slump was very small, the compressive strength was low. As the Helix fiber percentage increased, there was a greater tendency for steel balls to develop in the mix.
- The formation of steel balls probably contributed to low compressive strengths.

Based upon the six (6) batches cast with Dramix fibers, the following observations were made:

- Using 0.75% and 1.0% fiber did not greatly improve the concrete compressive strength above similar mixes with much less fiber.
- While relatively high compressive strength and adequate slumps were achieved with 1.0% Dramix fiber, using fiber percentages greater than 0.5% was not necessary.
- Comparing concrete with Dramix fiber to the same concrete mix with Helix fiber showed that greater concrete slumps and compressive strengths were achieved for the concrete with Dramix fibers.

Based upon the seven (7) batches cast with Novomesh fibers, the following observations were made:

- Even with the variations in the concrete mixes, the compressive strength of the concrete containing Novomesh fibers had much less fluctuation than the Helix mixes and slightly less fluctuation that the Dramix mixes.
- Even with the variations in the concrete mixes, the compressive strength of the concrete containing Novomesh fibers was within 2% or greater than the design strength of 4000 psi.
- Using 0.75% and 1.0% fiber did not necessarily improve the concrete compressive strength above similar mixes with much less fiber.
- Given the variation in compressive strength, using more than 0.5% fiber may not be beneficial.

- Comparing concrete with Novomesh fiber to the same concrete mix with Helix fiber showed that greater compressive strengths were achieved for the concrete with Novomesh fibers.
- Comparing concrete with Novomesh fiber to the same concrete mix with Dramix fiber showed that greater concrete slumps and compressive strengths were achieved for the concrete with Dramix fibers.

Based upon all of the material tests, the following observations were made:

- For all batches of concrete (Batches 1 to 35) tested, the measured split tensile strengths for fiber reinforced concrete were less than the tensile strength computed from the AASHTO equation:

$$f'_t = 0.23 \sqrt{f'_c} \qquad 7.1$$

- For all cases except for cylinders with Helix fibers, the measured modulus was less than the AASHTO computed value. The modulus of elasticity for the Helix fiber reinforced concrete was 2% greater than the value computed using the AASHTO equation.
- According to the AASHTO LRFD Bridge Design Specifications (2007), the Poisson's ratio can be assumed to be 0.2 if physical tests are not conducted.
- The measured values for Poisson's ratio were 0.21, 0.22, 0.23 and 0.25 for plain concrete, Dramix fiber concrete, Helix fiber concrete and Novomesh fiber concrete, respectively
- For Batch 1 to 4, for all of the Helix cylinders except for the cylinders with 0.75% fiber, the modulus of rupture was greater than the AASHTO range. For the H0.36 cylinders

(0.36% fiber) the modulus of rupture was 919 psi which was 17% greater than the AASHTO value.

- For Anchorage Test Specimens S2 which had Dramix fibers (Specimens S2-2 to S2-5), the modulus of rupture was greater than the AASHTO range.
- For the Helix and Novomesh cylinders from the S2 Specimens, the modulus of rupture values was within the AASHTO range.
- There was less than a 10% difference in high and low modulus of rupture test values for three different fibers.
- Given the variation in compressive strength, using more than 0.5% fiber may not be beneficial.

Based upon all of the finite element analysis results, the following observation were made:

- The finite element analysis showed that using higher amounts of fiber reinforcement (0.75% and 1.0%) did not improve the anchorage zone performance much above the performance that could be achieved by using 0.5% fibers.
- Based upon the nine (9) different finite element (FE) models considered in this research for a box girder bridge segment, Johnson (2006) concluded that adding steel fibers at a percentage of 0.5% would be beneficial for the post-tensioning anchorage zone.
- The finite element analysis showed that using higher levels of fiber reinforcement (0.75% and 1.0%) did not improve the anchorage zone performance much above the performance that could be achieved by using 0.5% fibers.

Consideration of both S1 and S2 Specimens test results showed the following:

- Adding 0.5% steel fibers to the concrete mix without adding non-prestressed reinforcement in the local and general anchorage zones resulted in test specimens having load capacities that ranged from 77% to 134% of the load capacity of test specimens with plain concrete, 100% of the local zone reinforcement recommended by the anchorage manufacturer and 100% of the general zone reinforcement recommended by the approximate design method of the AASHTO code.
- Adding steel spiral along with the 0.5% steel fibers resulted in strength increases of up to 22%. However, for two specimens cast with Novomesh fibers (S1-11 and S2-11) the addition of spiral did not result in increase in strength instead a 13% to 17% decrease in strength resulted.
- Adding steel ties along with the 0.5% steel fibers resulted in strength increases of up to 32%.
- Even though the addition of 0.5% steel fibers did add up to 37% increase in strength to test specimens, steel spirals and steel ties are needed to prevent sudden failure due to punching shear at the anchors (in the local zone) and to prevent sudden failure due to bursting tension in the general zones.
- With 0.5% fibers by volume, 50% of steel spirals (recommended by PT anchor manufacturers) and 40% of steel ties (based upon AASHTO design guidelines) , the load capacities of the anchorage zone test specimens were from 92% to 159% the load capacity of the plain specimens with the recommend local and general zone reinforcement. Thus, the addition of steel fibers did increase the strength of the anchorage zone even with significant reductions in non-prestressed reinforcing steel.

- In addition, to improving the strength of the specimens, the addition of fibers (steel and steel with polypropylene fibers) resulted in smaller and few cracks developing of the surface of the test specimens. Thus, the use of fibers in PT anchorage zones may contribute to improvements in the durability of structural elements.

Based upon the maximum loads in the anchorage load tests, the strut-and-tie maximum tensile forces (the bursting forces) computed are 70% to 73% of the maximum values computed by the AASHTO equation for T_{burst}.

The following equation is proposed for computing the tensile bursting force in post-tensioning anchorage zones when steel fibers are used in the concrete. This equation considers both the percentage of steel fibers by volume and b/h ratio:

$$T_{max} = 0.23\ P\ [\ 1 - 1.11(b/h) - 0.15\ (F\%) + 0.15\ (b/h)\ (F\%)] \qquad 7.2$$

Where P = the maximum factored tendon force, h= the transverse dimension of the anchor zone, b= the width of the anchorage plate, and F%= the percentage of steel fiber by volume.

The strut-and-tie maximum tensile forces (the bursting forces) computed are 85% to 87% of the maximum values computed by the new equation proposed based upon the finite element results. Comparison of the bursting force values resulting from the new equation to the bursting tensile forces (T_{burst}) resulting from the AASHTO equation, shows that new equation values are 16% to

18% less than the AASHTO values. Thus, the experimental results suggest that the results computed the equation may be quite reasonable.

The maximum tensile forces (the bursting forces) resulting from use of the new equation based upon the finite element results are 82% of the maximum values computed from the AASHTO equation for T_{burst} for all Specimen S1 load cases.

For Specimen S2 load cases, the maximum tensile forces (the bursting forces) resulting from use of the new equation based upon the finite element results are 84% of the maximum values computed from the AASHTO equation for T_{burst}. Thus, relative to the AASHTO equation values, the bursting forces which result for using the new equation are 16% to 18% lower. This suggest that due to the use of 0.5% fiber in the test in the post-tensioned anchorage zone, it may be possible to provide 16% to 18% less bursting reinforcement (tension ties) than are required by the AASHTO code. According to the finite element analysis on the anchorage test specimens and the proposed equations, using higher percentages of steel fiber will lead to higher reductions in the bursting force. The percentage of reduction in the bursting force is related to the b/h ratio and the percentage of fibers. According to the proposed equation, with 3.0% fibers and b/h=0.733, there can be a 77.2% reduction in the tensile bursting force. More load tests are needed to verify the applicability of the new equation for fiber percentages greater than 0.5% fiber by volume.

Considering a 50% reduction in steel and the addition of 66 lb/CY of concrete (0.5% fiber by volume) Pomeroy Corporation estimated an 8% reduction in retail costs. Based upon a 40%

reduction in steel, the author has estimated less than a 1% reduction in cost. Thus, it is possible that steel fibers can be added to post-tensioning anchorage zones without altering the costs of construction significantly.

Comparison of experimental and analytical results showed that steel fibers can be added to concrete to increase the strength of post-tensioned anchorage zones and reduce the bursting and confinement mild reinforcement required in these zones. Research results suggest that the addition of steel fibers to concrete post-tensioned anchorage zones may result in labor cost savings and time savings but may not significantly change the overall project costs.

Based upon load test results, it was found that the addition of 0.5 percent steel fibers by volume to a post-tensioned concrete anchorage zone with an anchor plate width to transverse section depth ratio equal to 0.22 and 0.33 could lead to a 40 percent or more reduction in mild steel reinforcement (steel spiral and ties). The proposed equation was developed based upon finite element analysis results and takes into consideration the b/h ratio and the percentage of fibers in the concrete. Depending upon the b/h ratio and the percentage of steel fibers used in the concrete, the anchorage zone bursting forces computed by the proposed equation may be 15% to 77% less than bursting force values computed by the AASHTO code equation.

7.2 Recommendations

This research suggests that steel fibers can be used successfully to reduce steel congestion in the anchorage zone without decreasing the capacity of the member. Based upon this research, the authors recommend that 0.5% steel fiber by volume be used in the concrete. While greater

percentages of fiber may produce greater load capacity, this research showed that a greater percentage of fiber is not required to achieve the desired objective. It is recommend that confinement reinforcing (spirals) be used in the local zone and bursting steel (steel ties) be used in the general zone. However, the spacing of this steel can be increased above the current design recommendations and the current AASHTO recommendations for the approximate design method. Based upon the load test results for the parameters used in the test specimens, it was possible to double the tie spacing for the bursting reinforcement.

When designing post-tensioned anchorage zones with steel fibers, it is recommended that the newly proposed equation be used to take into consideration both the percentage of steel fibers and the bearing plate to transverse depth ratio. However, to provide greater confirmation that the proposed equation is applicable for steel fiber percentages greater than 0.5%, it may be necessary to load test specimens with greater than 0.5% steel fibers by volume. Also, It would also be beneficial to conduct long term durability tests on concrete specimens with steel fibers to verify that the strength of steel fiber reinforced concrete members do not become significantly weaker with time. This study did not include long term durability tests on anchorage test specimens.

BIBLIOGRAPHY

ACI Committee 544 (1998). Guide for Specifying, Proportioning, Mixing, Placing and Finishing Steel Fiber Reinforced Concrete, ACI 544.3R-93, American Concrete Institute.

ACI Committee 544 (1999). *Design Considerations for Fiber Reinforced Concrete*, ACI 544.4R-88), American Concrete Institute.

ACI Committee 544 (1999). *Measurement of Properties of Fiber Reinforced Concrete*, ACI 544.2R-89), American Concrete Institute.

ACI Committee 544 (2002). *State-of-the Art Report on Fiber Reinforced Concrete*, ACI 544.1R-96, American Concrete Institute.

Ahmed, A., (2001). Characterization of Steel Fiber And/Or Polymer Concrete Mixes and Applications to Slender Rectangular and I-Beams, Ph.D. Dissertation, University of Nevada.

Almansa, E. M. and Cavonas, M. F. (1997). "Mix Design of Steel Fiber Reinforced Concrete", Materiales De Construccion, Vol. 47, No. 247-248, Julio/Septiembre-Octubre/Diciembre.

Al-Saadoun, S.S. (1980). A Three-Dimensional Photoelastic Investigation of the Stress Distribution in the Anchorage Zones of Post-tensioned Beams, Master's Thesis, University of Petroleum & Minerals, Dhahran, Saudi Arabia.

American Association of State Highway and Transportation Officials (2007). *AASHTO LRFD Bridge Design Specification*, Customary U. S. Units, 4th edition, AASHTO: Washington, D.C.

American Concrete Institute, *Steel Fiber Reinforced Concrete*, Compilation 27.

American Concrete Institute, Synthetic And Other Non-Metallic Fiber Reinforcement Of Concrete, Compilation 28.

ASTM C31/C31M-03a,"Standard Practice for Making and Curing Concrete Test Specimens in the Field".

ASTM C39/C 39M-05,"Standard Test Method for Compressive Strength of Cylindrical Concrete Specimens."

ASTM C78-02,"Standard Test Method for Flexural Strength of Concrete (Using Simple Beam With Third-Point Loading)."

ASTM C138/C 138M-01a,"Standard Test Method for Density (Unit Weight), Yield, and Air Content (Gravimetric) of Concrete."

ASTM C143/C 143M-05a,"Standard Test Method for Slump of Hydraulic-Cement Concrete."

ASTM C157/C 157M-04,"Standard Test Method for Length Change of Hardened Hydraulic-Cement Mortar and Concrete".

ASTM C172,"Standard Practice for Sampling Freshly Mixed Concrete."

ASTM C173/C 173M-01,"Standard Test Method for Air Content of Freshly Mixed Concrete by the Volumetric Method".

ASTM C192/C 192M-05,"Standard Practice for Making and Curing Concrete Test Specimens in the Laboratory".

ASTM C293-02,"Standard Test Method for Flexural Strength of Concrete (Using Simple Beam With Center-Point Loading).

ASTM C469 -02,"Standard Test Method for Static Modulus of Elasticity and Poisson's Ratio of Concrete in Compression."

ASTM C512-02,"Standard Test Method for Creep of Concrete in Compression."

ASTM C1550-02,"Standard Test Method for Flexural Toughness of Fiber Reinforced Concrete (Using Centrally Loaded Round Panel).."

Banthia, N., "Toughness Performance of Hybrid (Steel + Polypropylene) Fiber Reinforced Concrete", Department of Civil Engineering, The University of British Columbia, Vancouver, Canada, V6T1Z4.

Barbosa, A. F. and Ribeiro, G. O. (1998). "Analysis of Reinforced Concrete Structures Using Ansys Nonlinear Concrete Model", *Computational Mechanics*, Barcelona, Spain.

Bayasi, Z., Gebman, M. J., and Hill. H. B., "Steel Fiber Reinforced Concrete Beam-Column Joint Test", http://kahuna.sdsu.edu/~sfrc/.

Bekaert (1998). "Dramix: The Properties of Dramix Steel Fiber Concrete", Editor, Nemegeer-Harelbeke, D. , N. V. Bekaert S.A.

Bernard, E. S. and Pircher, M. (2001). "The Influence of Thickness on Performance of Fiber-Reinforced Concrete in a Round Determinate Panel Test", *Cement, Concrete, and Aggregates*, CCAGDP, Vol. 23, No. 1, pp. 27-33.

Breen, J.E., Burdet, O., Roberts, C., Sanders, D., and Wollmann, G. (1994). *Anchorage Zone Reinforcement for Post-Tensioned Concrete Girders*, National Cooperative Highway Research Program Report 356, Washington D.C., pp. 204.

Burdet, O.L. (1990). *Analysis and Design of Anchorage Zones in Post-Tensioned Concrete Bridges*, Ph.D. Dissertation, The University of Texas at Austin.

Casanova, P. and Rossi, P. (1997). "Analysis and Design of Steel Fiber Reinforced Concrete Beams", *ACI Structural Journal*, September-October, pp. 595-602.

Chaallal, O., Thibodeau, S., Lescelleur, J., and Malenfant, P. (1996). "Steel Fiber or Conventional Reinforcement for Concrete Shearwalls?", *Concrete International*, American Concrete Institute, June, pp.39-42.

Collins, M. P. and Mitchell, D. (1991). *Prestressed Concrete Structures*. Englewood Cliffs: Prentice-Hall.

Cruso, B.., "Concrete Reinforcement: Nycon Fibers vs. Welded-Wire Fabric", Nycon/Reinforced Concrete (Form #020199), Nycon, Inc., Westerly, RI

Cucchiara, C., Lidia, L. M., Papia, M. (2004) Effectiveness of stirrups and steel fibres as shear reinforcement, Cement and Concrete Composites, Volume 26, Issue 7, pp 777-786.

Department of Structural Engineering and Materials, Technical University of Denmark, "Design of Steel Fiber Reinforced Concrete", RILEM TC 162-TDF: *Test and Design Methods for Steel Fiber Reinforced Concrete, Recommendations for Design of Steel Fiber Reinforced Concrete*.

Dilger, W. H. and Ghali, A. (1974). "Remedial Measures For Cracked Webs of Prestressed Concrete Bridges", *Journal – Prestressed Concrete Institute*, Vol. 19, No. 4, July/August, pp 76-85.

Dwarakanath, H.V. and Nagaraj, T.S. (1991). "Comparative Study of Predictions of Flexural Strength of Steel Fiber Concrete", *ACI Structural Journal*, November-December, pp. 714-719.

Dwarakanath, H.V. and Nagaraj, T.S. (1992). "Deformational Behavior of Reinforced Fiber Reinforced Concrete Beams in Bending", *Journal of Structural Engineering*, Volume 118, No. 10, November.

Florida Department of Transportation (1989). *Post-Tensioning Manual: A Guide to Post-Tensioning of Bridges*, Tallahassee: Florida Department of Transportation.

Franzen, T. (1992). "Shotcrete For Underground Support: A State-of–the-Art Report With Focus on Steel-Fiber Reinforcement", *Tunneling and Underground Space Technology*, Volume 7, Number 4, pp. 383-390.

Gaylord, Jr., E. H. and Charles G. N. (editors) (1990). *Structural Engineering Handbook*, 3 rd. Edition. New York: McGraw-Hill Publishing Company.

Gebman, M. (2001). Application of Steel Fiber Reinforced Concrete in Seismic Beam-Column Joints, Master's Thesis, San Diego State University.

Guerrini, G. L., Rosati, G., and Ragazzi, L., "Flexural Behavior of Prestressed Fiber Reinforced Concrete Bridge Beams".

Harajli, M. H., and Salloukh, K. A. (1997). *Effect of Fibers on development/ Splice Strength of Reinforcing Bars in Tension*, ACI Materials Journal, July-August, pp. 317-324.

Haroon, S. A. (2003). *Application of Fiber Reinforced Concrete in the End Zones of Precast Prestressed Bridge Girders*, Ph.D. Dissertation, Florida State University, FAMU-FSU College of Engineering.

Hengprathanee, S. (2004). *Linear and Nonlinear Finite Element Analyses of Anchorage Zones in Post-Tensioned Concrete Structures*, PH.D. Dissertation, Virginia Polytechnic Institute and State University.

Hsu, L. S. and Hsu, C.T. (1994). "Stress-Strain Behavior of Steel-Fiber High Strength Concrete Under Compression", *ACI Structural Journal*, July-August, pp. 448-457.

Hsu, C.T., He., R. L., and Ezeldin, A. S. (1992). "Load Deformation Behavior of Steel Fiber Reinforced Concrete Beams", *ACI Structural Journal*, November-December, pp. 650-657.

Huang, Ti (1959). An Experimental Study of Stresses In The End Blocks Of Post-Tensioned Prestressed Concrete Beams, Ph. D. Dissertation, The University of Michigan.

Jo, B., Byun, Y., and Tae, G. (2002). "Structural Behavior of Cable Anchorage Zones in Prestressed Concrete Cable-Stayed Bridge", *Canadian Journal of Civil Engineering*, 29:171-180.

Johnson, S. (2006). Analytical Modeling of Fiber Reinforced Post-Tensioned Concrete Anchorage Zones, Master's Thesis, Florida State University.

Junior, S. F. and Hanai, J. B. (1999). "Prestressed Fiber Reinforced Concrete Beams with Reduced Ratios of Shear Reinforcement", *Cement & Concrete Composites*, Vol. 21, No. 3, pp. 213-217.

Khajuria, A., Bohra, K. and Balaguru, P., "Long-Tern Durability of Synthetic Fibers in Concrete", SP 126-46, American Concrete Institute.

Libby, J. R. (1990). Modern Prestressed Concrete: Design Principles and Construction Methods, 4th edition. New York: Van Nostrand Reinhold.

Lin, T. Y. and Ned H. Burns (1981). *Design of Prestressed Concrete Structures*, 3 rd. Edition, New York: John Wiley & Sons.

Moens, J. and Nemegeer, D. (1991). "Designing Fiber Reinforced Concrete Based on Toughness Characteristics", *Concrete International*, November, pp. 38-42.

Natarajaa, M.C., Nagarajb, T.S., and Basavaraja, S. B (2005) Reproportioning of steel fiber reinforced concrete mixes and their impact resistance, Cem. Concr. Res. (35): 2350-2359.

Nawy, Edward G. (1996). *Prestressed Concrete: A Fundamental Approach*, 2nd ed. Upper Saddle River: Prentice-Hall.

Naaman, A. (1998). "New Fiber Technology", *Concrete International*, July, pp. 57-62.

Narayanan, R. and Darwish, I.Y.S. (1987). "Use of Steel Fibers As Shear Reinforcement", *ACI Structural Journal*, May-June, pp. 216-227.

Orabone, Bill (2007). Polytorx, e-mail from weo@healixfiber.com to Brenda Robinson.

Pacios, A. and Canovas, M. F. (1997). "Interface Study of Reinforced Concrete", *Materiales De Construccion*, Vol 47, no. 247-248, Julio/Septiembre-Octubre/Diciembre.

Podony, Jr., W. and Muller, Jean M. (1982). *Construction and Design of Prestressed Concrete Segmental Bridges*, John Wiley & Sons: New York.

Polytorx, Helix Product Profile, pp1-2.

Post-Tensioning Institute (1972). *Post-Tensioning Manual*, 4th edition, Phoenix: Post-Tensioning Institute.

Post-Tensioning Institute (1978). *Post-Tensioned Box Girder Bridge Manual*, Phoenix: Post-Tensioning Institute.

Post-Tensioning Institute (1978). *Precast Segmental Box Girder Bridge Manual*, Phoenix: Post-Tensioning Institute.

Ramakrishnan, V., Wu, G.Y., and Hosalli, G., "Flexural Behavior and Toughness of Fiber Reinforced Concretes", *Transportation Research Record 1226*, pp. 69-77.

Roberts, C. (1990). Behavior And Design Of The Local Anchorage Zone Of Post-Tensioned Concrete, M.S. Thesis, The University of Texas at Austin.

Roberts-Wollmann, C.L. (1994). *Load Transfer Test with Anchorage CS 5-31*, North Carolina University Structures Lab, September.

Roberts-Wollmann, C.L. and Breen, John E. (2000). "Design and Test Specifications for Local Tendon Anchorage Zones", *ACI Structural Journal*, November-December, pp. 867-875.

Sanders, D.H. (1990). *Design and Behavior of Post-Tensioned Concrete Anchorage Zones*, Ph.D. Dissertation, The University of Texas at Austin.

Sanguineti, Dante (2007). E-mail From Dante.Sanguineti@wgint to Brenda Robinson.

Shaaban, A. M. and Gesund, H. (1993). "Splitting Tensile Strength of Steel Fiber Reinforced Concrete Cylinders Consolidated by Rodding or Vibration", *ACI Materials Journal*, July/August 1993, pp. 356-369.

Shah, S. P., Sarigaphuti, M. and Karaguler, M.E. "Comparison of Shrinkage Cracking Performance of Different Types of Fibers and Wiremesh", ACI SP 142-1., pp. 1-59.

Soroushian, P, Mirza, F., and Alhozaimy, A. (1994). "Bonding of Confined Steel Fiber Reinforced Concrete To Deformed Bars", *ACI Materials Journal*, March-April, pp. 141-149.

Soroushian, P. and Bayasi, Z. (1987). "Prediction of Tensile Strength of Steel Fiber Reinforced Concrete: A Critique of the Composite Material Concept", *American Concrete Institute*, SP-105-4., pp. 71-84.

Soroushian, P. and Lee, C. (1990). "Tensile Strength of Steel Fiber Reinforced Concrete: Correlation with Some Measures of Fiber Spacing", *ACI Materials Journal*, November-December, pp. 541-546.

Swamy, R. N. and Al-Ta'an, Sa'ad A. (1981). "Deformation And Ultimate Strength In Flexure Of Reinforced Concrete Beams Made With Steel Fiber Concrete", *ACI Journal*, September-October, pp. 395-405.

Tan, K. H., Paramasivam, P., and Tan, K.C. (1994). "Instantaneous and Long-Term Deflections of Steel Fiber Reinforced Concrete Beams", *ACI Structural Journal*, July/August, pp. 384-393.

Vondran, G. L. (1991). "Application of Steel Fiber Reinforced Concrete", *Concrete International*, November, pp. 44-49.

VSL Corporation (1996). *VSL Post-Tensioning Systems*, Litho, Singapore.

VSL Corporation (2002). "VSL Post-Tensioning Systems", Website of VSL Structural Group.

VSL International LTD. *Detailing For Post-Tensioning*, 3 VSL Report Series, Bern, Switzerland.

Wafa, F. F., Hasnat, A. and Tarabolsi, O. F. (1992). "Prestressed Fiber Reinforced Concrete Beams Subjected to Torsion", *ACI Structural Journal*, May-June, 272-283.

Winter, G. and Nilson, A. H. (1979). *Design of Concrete Structures*, McGraw-Hill: New York, Ninth Edition.

Wollman, G.P. (1992). *Anchorage Zones in Post-Tensioned Concrete Structures*, Ph.D. Dissertation, The University of Texas at Austin.

Wollmann, G.P., and Roberts-Wollmann, C.L. (2000). "Anchorage Zone Design", Preprint of Chapter VIII, *Post-Tensioning Manual*, Sixth Edition, pp. 46.

Wollmann, G.P., and Roberts-Wollmann, C.L. (2000). *Anchorage Zone Design*, Post-Tensioning Institute.

Yazdani, N., Spainhour, L., and Haroon, S. (2002). *Application of Fiber Reinforced Concrete in the End Zones of Precast Prestressed Bridge Girders*, Florida Department of Transportation Report.

Yazdani, N., Tawfiq, K. (2004). "Post-Tensioned Bridge Girder Anchorage Zones Enhancement With Fiber Reinforced Concrete (FRC)", Proposal Submitted to the Florida Department of Transportation. FAMU-FSU College of Engineering, September.

Zellers, B., "Steel and Synthetic Fiber Blends", Steel/Synthetic Fiber Blends (Form #120102), Nycon, Inc., Westerly, RI.

Zellers, Robert (2004). "High Cost of Steel Not the Only Reason for Using Fibers as Shotcrete Reinforcement", Shotcrete, Fall , pp. 2-4.